

AMHYCO

Research and Innovation Action (RIA)

This project has received funding from the Euratom research and innovation programme 2014-2018 under Grant Agreement No 945057

Start date: 2020-10-01 Duration: 48 Months



Identification and Analysis of accidental sequences posing high H2/CO combustion risk (PWR-W, PWR-VVER, PWR-KWU)

Authors: Dr. Luis E. HERRANZ (CIEMAT), L.E. Herranz, J. Fontanet (CIEMAT)

AMHYCO - Contract Number: 945057

Project officer: PASSALACQUA Roberto

Document title	Identification and Analysis of accidental sequences posing high H2/CO combustion risk (PWR-W, PWR-VVER, PWR-KWU)
Author(s)	Dr. Luis E. HERRANZ , L.E. Herranz, J. Fontanet (CIEMAT)
Number of pages	142
Document type	Deliverable
Work Package	WP2
Document number	D2.2
Issued by	CIEMAT
Date of completion	2023-07-19 14:20:38
Dissemination level	Public

Summary

This D2.2 deliverable gathers the results of the analysis of sequences with high H2 and CO combustion risk for three types of pressurized water reactors (Western, Konvoi and VVER) in terms of those variables that better characterize the containment scenarios (i.e., Figures Of Merit, FOMs). As a result, a set of sequences are selected to be addressed in WP4 and some data are used for a better definition of WP3 experimental matrixes.

Α	n	n	r	O	V	al	

Date	Ву
2023-07-19 14:20:53	Dr. Luis E. HERRANZ (CIEMAT)
2023-07-20 08:29:16	Dr. Gonzalo JIMENEZ (UPM)



Enhancing H₂ & CO Combustion Risk Management

Research and Innovation Action

NFRP-2019-2020

D2.2 – Identification and analysis of accident sequences posing high H₂/CO combustion risk (PWR-W, PWR-VVER, PWR-KWU)

WP2 - Task 2.2-2.4

Date [10/07/2023]

Author(s): Luis E. Herranz, Joan Fontanet (CIEMAT)

<u>Contributors</u>: M. Braun (Framatome), A. Bentaib, A. Bleyer, L. Maas (IRSN), I. Kljenak, M. Leskovar (JSI), J. Hoffrichter, M.K. Koch, M. Müer (RUB), A. Iskra, O. Cherednichenko (LLC ENERGORISK), Luis Serra, Carlos Vázquez-Rodríguez (UPM)





Disclaimer

The content of this deliverable reflects only the author's view. The European Commission is not responsible for any use that may be made of the information it contains.

Table of Contents

1. Introduction	9
2. Selection criteria	10
3. Figures of merit	12
4. Results and discussion	13
4.1. Matrixes of sequences	13
4.2. PWR-W	16
4.2.1. Framatome 900 MWe & 1300 MWe with ASTEC (IRSN)	16
4.2.2. Westinghouse 700 MWe with MELCOR (JSI)	19
4.2.3. Westinghouse 1000 MWe with MELCOR (CIEMAT)	20
4.3. PWR-KWU	23
4.3.1. KONVOI 1300 MWe with AC ² (RUB)	23
4.3.2. KONVOI 1300 MWe with MELCOR (Framatome)	25
4.4. PWR-VVER	28
5. Application to other work packages	31
5.1. WP3: Experimental investigation	31
5.2. WP4: Full containment analysis	32
6. Conclusion	32
7. References	34
8. Annexes	36
List of Figures	
Figure 1. PWR accident sequences modelled (red: without PAR, black with PARs)	15
Figure 2. Containment nodalization for the PWR-W-1300	
Figure 3. Shapiro diagram for PWR-W-1300 simulations	
Figure 4. Gas composition in the main compartment of PWR-W-1300	
Figure 5. Containment pressure evolution for PWR-W-1300	
Figure 6. Containment nodalization for the PWR-W-700	

Figure 7. Shapiro diagram (left) and gas composition (right) for the PWR-W-700 MBLOCA	
sequence (with PARs)	20
Figure 8. Containment nodalization for PWR-W-1000	
Figure 9. Shapiro diagram of PWR-W-1000 simulations	
Figure 10. Gas composition in PWR-W-1000	
Figure 11. Containment nodalization for PWR-KWU-1300 used in AC ²	
Figure 12. Shapiro diagram for PWR-KWU	
Figure 13. Gas composition in PWR-KWU	
Figure 14. Containment nodalization for PWR-KWU-1300 used in MELCOR	
Figure 15. Shapiro diagram for PWR-KWU	
Figure 16. Gas composition for PWR-KWU	
Figure 17. Containment nodalization for the PWR-VVER-1000.	
Figure 18. Shapiro diagram of the PWR-VVER-1000	
Figure 19. Gas composition in PWR-VVER-1000	
Figure 20. PWR-W total H2 mass injected in the in-vessel phase	
Figure 21. PWR-W total H2 mass injected in the ex-vessel phase	
Figure 22. PWR-W total CO mass injected in the ex-vessel phase (in logarithmic scale)	
Figure 23. PWR-W H2 release rate peaks at in-vessel phase	
Figure 24. PWR-W H2 release rate peaks at ex-vessel phase	
Figure 25. PWR-W CO release rate peaks at ex-vessel phase	
Figure 26. PWR-KWU total H2 mass injected in the in-vessel phase	
Figure 27. PWR-KWU total H2 mass injected in the ex-vessel phase	
Figure 28. PWR-KWU total CO mass injected in the ex-vessel phase (in logarithmic scal	
Figure 29. PWR-KWU H2 release rate peaks at in-vessel phase (in logarithmic scale)	
Figure 30. PWR-KWU H2 release rate peaks at ex-vessel phase (in logarithmic scale)	50
Figure 31. PWR-KWU CO release rate peaks at ex-vessel phase	
Figure 32. Primary and secondary systems nodalization	
Figure 33. NPP containment nodalization	79
Figure 34. Detail of NPP containment nodalization	79
Figure 35: Containment pressure.	82
Figure 36: Heat transfer: melt - atmosphere/pool	82
Figure 37: Containment dome temperature.	
Figure 38: Hydrogen in RPV.	83
Figure 39: Hydrogen outside RPV.	84
Figure 40: H ₂ O fraction in containment dome	85
Figure 41: H ₂ fraction in containment dome	85
Figure 42: CO ₂ fraction in containment dome	86
Figure 43: CO fraction in containment dome.	87
Figure 44. Nodalization scheme of the containment	91
Figure 45, H- and CO generation in the SRLOCAL sequence	0.4

Figure 46. C	Containment pressure evolution in the SBLOCA-I sequence	94
Figure 47. C	Gas mole fraction of different components in the upper compartment for the	
SBLOCA-I s	equence	95
Figure 48. S	Shapiro diagram for the upper compartment in the SBLOCA-I sequence	95
Figure 49. C	Containment pressure evolution in the SBLOCA-II sequence	95
Figure 50. H	H2 and CO generation in the SBLOCA-II sequence	95
Figure 51. C	Gas mole fraction of different components in the upper compartment for the	
SBLOCA-II s	sequence	96
Figure 52. S	Shapiro diagram for the upper compartment in the SBLOCA-II sequence	96
Figure 53. C	Containment pressure evolution in the SBO sequence	97
Figure 54. H	H_2 and CO generation in the SBO sequence	97
Figure 55. C	Gas mole fraction of different components in the upper compartment for the SE	SO
sequence		97
Figure 56. S	Shapiro diagram for the upper compartment in the SBO sequence	97
Figure 57. F	H2 and CO generation in the LBLOCA sequence	98
Figure 58. C	Containment pressure evolution in the LBLOCA sequence	98
Figure 59. 0	Gas molar fraction of different components in the upper compartment for the	
LBLOCA sec	quence	99
Figure 60. S	Shapiro diagram for the upper compartment in the LBLOCA sequence	99
Figure 61.	Primary and secondary side nodalization in ATHLET(-CD)	102
Figure 62.	Containment nodalization in COCOSYS with PARs indicated	103
Figure 63.	SBO+PSD: Containment pressure (zone UKUPA);	106
Figure 64.	SBO+PSD: Containment temperature (zone UKUPA)	107
Figure 65.	SBO+PSD: Leakage masses from primary circuit (zone DHHKPB)	107
Figure 66.	SBO+PSD: Released gas masses from CCI (zones SUMPF and CAVITY)	108
Figure 67.	SBO+PSD: Atmosphere composition (zone DHHKPB)	
Figure 68.	SBO+PSD: Heterogeneity index	109
Figure 69.	SBO+PSD: Shapiro diagram (zone DHHKPB)	109
Figure 70.	SBLOCA+ECCS: Containment pressure (zone UKUPA)	
Figure 71.	SBLOCA+ECCS: Containment temperature (zone UKUPA)	110
Figure 72.	SBLOCA+ECCS: Leakage masses from PRZ (zone PKLB)	111
Figure 73.	SBLOCA+ECCS: Released gas masses from CCI (zones SUMPF and CAVITY)	111
Figure 74.	SBLOCA+ECCS: Atmosphere composition (zone PKLB)	112
Figure 75.	SBLOCA+ECCS: Heterogeneity index	112
Figure 76.	SBLOCA+ECCS: Shapiro diagram (zone PKLB)	113
Figure 77:	Representation of the reactor coolant system	116
Figure 78:	Nodalization of the KONVOI containment	
Figure 79:	Primary and secondary pressure	
Figure 80.	Containment pressure	
Figure 81:	Primary loop swell liquid level	126

Figure 82.	Molten corium-concrete interaction	126
Figure 83:	Progression of the core destruction between 6 h and 9 h	127
Figure 84.	Shapiro diagram for the large equipment rooms	128
Figure 85:	Shapiro diagram for the accessible rooms	128
Figure 86:	Shapiro diagram for other containment rooms	129
Figure 87:	Mass of H ₂ and CO within the containment	129
Figure 88. C	ontainment nodalization for PWR- VVER-1000 used in MELCOR (Red circles	marks
_	e compartment)	
List of	Tables	
Table 1. Con	nplete list of FOMs related with the different AMHYCO's work packages	14
Table 2. Rea	ctor type, code and nodalizations used in the sequences analyses by WP2 p	artners
Table 3. Ran	ges of boundary conditions at relevant times (transfer to WP3)	31
Table 4. PWI	R-W containment free volumes and scaling factors	37
Table 5. Mai	n compartments of containment model	80
Table 6. Tim	es of first important events	00
Table 7. Lim		80
	estone concrete composition (Humphries et al., 2021b)	
	estone concrete composition (Humphries et al., 2021b)n characteristics of containment compartments	89
Table 8. Mai		89 92
Table 8. Mai Table 9. Seq	n characteristics of containment compartments	89 92
Table 8. Mai Table 9. Seq Table 10. Ch	n characteristics of containment compartmentsuence definitions	
Table 8. Mai Table 9. Seq Table 10. Ch Table 11. Co	n characteristics of containment compartmentsuence definitionsronology of the main events.	89 92 93 res93
Table 8. Mai Table 9. Seq Table 10. Ch Table 11. Co Table 12. Flo	n characteristics of containment compartmentsuence definitionsronology of the main eventsmparison of combustible gases generation (kmol) for the analysed sequence	
Table 8. Mai Table 9. Seq Table 10. Ch Table 11. Co Table 12. Flo Table 13. C	n characteristics of containment compartmentsuence definitionsronology of the main eventsmparison of combustible gases generation (kmol) for the analysed sequence was paths opened between the RCS and the containment in the SBO sequence.	
Table 8. Mai Table 9. Seq Table 10. Ch Table 11. Co Table 12. Flo Table 13. Co Table 14. S	n characteristics of containment compartmentsuence definitionsronology of the main eventsmparison of combustible gases generation (kmol) for the analysed sequence paths opened between the RCS and the containment in the SBO sequence.	



Abbreviations and Acronyms

Acronym	Description
ECCS	Emergency Core Cooling System
FC	Fan Coolers
FCVS	Filtered Containment Venting System
FOM	Figure of Merit
IAEA	International Atomic Energy Agency
LBLOCA	Large Break Loss Of Coolant Accident
LOCA	Loss Of Coolant Accident
MBLOCA	Medium Break Loss Of Coolant Accident
MCCI	Molten Core Concrete Interaction
PAR	Passive Autocatalytic Recombiner
PSD	Primary Side Depressurization
PWR	Pressurized Water Reactor
RCS	Reactor Coolant System
RPV	Reactor Pressure Vessel
SA	Severe Accident
SBLOCA	Small Break Loss Of Coolant Accident
SBO	Station Black-out
WP	Work Package

Abstract

This D2.2 deliverable gathers the results of the analysis of sequences with high H₂ and CO combustion risk for three types of pressurized water reactors (Western, Konvoi and VVER) in terms of those variables that better characterize the containment scenarios (i.e., Figures Of Merit, FOMs). As a result, a set of sequences are selected to be addressed in WP4 and some data are used for a better definition of WP3 experimental matrixes.

Keywords

Combustion gases, SAMG, Safety, Risk Management, Accident modelling, Gases distribution

1. Introduction

Most of currently operating nuclear reactors use fuel claddings made up of different zirconium-based alloys. Zirconium itself is a highly reactive metal, which rapidly oxidizes. However, the oxide layer forming at the metal surface is very stable under normal plant conditions, preventing any further chemical attack of the cladding by water or steam.

During a severe accident (SA), though, the fuel reaches temperatures where oxygen can diffuse through this oxide layer, and thus, the fuel cladding is no longer protected from further oxidation. Thus, a redox-reaction starts to set in, reducing the present steam to hydrogen while oxidizing the zirconium to ZrO2.

At temperatures around 1500 K, the redox-reaction between Zr and steam speeds up exponentially. This not only causes a rapid increase in core temperatures, but also causes a rapid release of large amounts of hydrogen (H_2) by reducing the steam. Other in-core materials like steel or boron carbide (B_4 C) also oxidize at these conditions, but these materials contribute noticeably less to the overall hydrogen release. In case of Reactor Pressure Vessel (RPV) failure, the molten corium may fall into the reactor cavity and there start to interact with the structural concrete. This process is called molten corium-concrete interaction (MCCI). The resulting H_2O_v and CO_2 from the concrete thermal decomposition likely oxidize remaining metallic materials in the corium pool and, consequently, generate additional H_2 as well as carbon monoxide (CO), which is also a combustible gas.

The combustible gases released during the in-vessel as well as during the ex-vessel accident phase accumulate in the reactor containment. As pressurized water reactors have typically non-inert containments, sufficient oxygen is at least initially present that combustible mixture may form and may ignite. Depending on the combustion regime, such combustions may threaten the containment integrity by temperature loads, by quasi-static pressure loads in case of a slow combustion, by dynamic loads in case of a detonation. Evidences of energetic gas combustions in the course of a severe accident were gathered in the accident of Three Mile Island Unit 2 (TMI-2) (Sehgal 2012) and they were also observed in the reactor buildings of Units 1, 3 and 4 of the Fukushima Daiichi Nuclear Power Station (TEPCO 2015) (IAEA 2015).

The gas combustion risk during a severe reactor accident was already identified in the Wash1400 report (US-NRC 1975). And despite many efforts to analyse the formation and combustion of combustible gases, the in-containment combustion risk was still ranked as a high importance issue in EUROSAFE (Magallon et al. 2005) and, more recently, it was highlighted as a high-priority issue by the NUGENIA association (Manara et al. 2019). Consistently with these assessments, the

European Stress Tests report underlined the need to consider possible explosion hazards (ENSREG 2012) and one of the IAEA requirements for new reactor designs and for upgrading the existing ones refers to the practical elimination of dynamic phenomena leading to the loss of containment integrity (IAEA 2016). Such a significance has resulted in a number of research projects and expert groups activities, particularly launched after the Fukushima Daiichi accidents, as shortly compiled by Jiménez et al. (2022).

Significant progress has been achieved in recent European projects investigating combustion risk associated with severe accidents. Nonetheless, AMHYCO has noted the need of addressing representative conditions still barely explored, particularly during the ex-vessel phase of the accident, and use the findings to improve severe accident management guidelines, if necessary.

The objective of the AMHYCO work package 2 (WP2) is to identify bounding accident sequences in which the combustible gases (H₂ and CO) cause a risk for containment integrity. The simulations of different accident sequences with integral codes provide relevant estimations of the behaviour of the combustible gases in the containment. Therefore, one of the main tasks of this work package is the identification of criteria for the selection of the most challenging accident sequence regarding the gas combustion risk. Besides, the relevant data to be used in other AMHYCO's work packages are identified and stored in a scenario database. These related work packages are:

- WP3 (Experiments); WP2 is to provide the boundary conditions for supporting the definition of combustion and the PAR efficiency test matrix.
- WP4 (Full containment analysis); WP2 dictates the initial and boundary conditions for the generic containment modelling.

Given the current European nuclear reactor fleet, Tasks 2.2 to 2.4 have been defined to deal with the accident sequence simulation of three pressurized water reactor (PWR) designs: PWR-W (western), PWR-KWU, and PWR-VVER. Different sequences of these three reactor types are simulated with different codes and hypotheses, starting with the nodalization used. These simulations cover different initiating events and the involvement of diverse engineering safety features. Once completed, the sequences are evaluated based on several "in-containment" variables to feed into the selection criteria and the simulation data are gathered into the ad-hoc scenario database.

2. Selection criteria

In order to select accident sequences with the most challenging conditions for the containment integrity due to gas combustion, critical factors for combustion were identified and adopted as selection criteria. The final consensus for selection criteria (Herranz and Fontanet 2021) splits the relevant magnitudes into the in-vessel and ex-vessel phases of the accident.

For the in-vessel phase:

- High molar fractions of combustible gases (H₂ + CO) in control volumes whose conditions are within flammability limits.
- Large total mass of combustible gas $(H_2 + CO)$ within the containment.
- Fast combustible gas (H₂ + CO) release rates.
- High containment pressure.
- Qualitative assessment.
 - Some averaging required to smooth very short peaks.
 - The Shapiro diagram (Shapiro and Moffette 1957) was used in the absence of the correlation revision of WP1 and improvements that would be generated in the project.

For the ex-vessel phase:

- High molar fractions of combustible gases (H₂ + CO) in control volumes whose conditions are within flammability limits.
- Total mass of combustible gas (H₂ + CO).
- Qualitative assessment.
- High containment pressure.

The high molar fraction criteria must be understood as the sine-qua-non conditions since it gives a direct measure of the risk for the combustion of the gases. The Shapiro diagram will provide the flammability condition of the gas mixture during the sequence evolution. For practical purposes the gas mixtures is considered to deflagrate if the following molar fraction criteria are reached simultaneously.

- $X_{H2} + X_{CO} > 9 \text{ vol}\%$
- $X_{O2} > 5 \text{ vol}\%$
- X_{H2O} < 55 vol%

This criteria must be reached in large compartments (i.e., with big volume and with large amount of combustible gases). With this restriction, flammability conditions only in small compartments are not considered since deflagrations in these compartments will not represent a major threat for the containment.

The in-vessel phase is characterized by successive oxidation runaways, leading to high rates of hydrogen release into the containment. These periods can result in high local hydrogen concentration in the compartment of the release that will be progressively distributed to the adjacent compartments. These periods are also highly demanding for the operation of PARs, which could not recombine hydrogen at such a high rate as the inlet rate. The combustion risk of these runaway periods will be evaluated in case they represent a significant combustion risk regarding the whole containment. Nonetheless, regarding the whole sequences, these periods do not represent the highest combustion risk (i.e., the highest threat for the containment integrity) since either the gas concentration is not as high as for other periods in the sequence or a high concentration is reached only in small compartments for a relatively short period.

Finally, sequences with high pressure will be of interest since a slow combustion at a high pressure can also challenge the containment integrity. Besides, these sequences would need the actuation of mitigation measures, like FCVS, that would interact with the gas mixture in the containment.

3. Figures of merit

Based on the above criteria, and a suitable characterization of the combustion risk related variables, a set of variables has been chosen to describe the severe accident sequences simulated in WP2. This set of variables should meet three main objectives:

- To provide the necessary information to assess the potential combustion risk of the different sequences in a comparable way and to be able to make recommendations concerning the selection of the most representative sequences in WP2.
- To identify boundary conditions of scenarios to support the definition of test matrixes in the experimental work package (WP3).
- To provide all the necessary data for initial and boundary conditions to perform the full containment analysis in WP4.

As a whole, the variables hereafter will be referred to as figures of merit (FOMs). According to the selection criteria discussed above, the risk of the in-containment combustion would be associated with the atmosphere composition, combustible gases injection rate, and containment conditions (pressure and temperature). Therefore, the following variables have been selected:

- Gas molar fractions (H₂, CO, O₂, H₂O_v, CO₂, the N₂ one can be derived from the rest).
- Gas injection/generation rate into the containment (H₂, CO, H₂O_v, CO₂, H₂O₁).

- Enthalpy associated with the injection/generation rate into the containment (H₂, CO, H₂O_v, CO₂; H₂O₁).
- Temperature associated with the injection/generation rate into the containment (H₂, CO, H₂O_v, CO₂; H₂O₁).
- Containment pressure.
- Gas temperatures (representative compartments).
- Heterogeneity index (max. to min. ratio of combustible gases molar fraction). This index gives a way to quantify how much the gases are homogenized inside the specific containment during the sequence evolution.

Apart from these variables, in order to provide input to other project work packages (WP3 and WP4 – see section 5), magnitudes related to the combustible release rates, initial and boundary containment conditions, and other mass and energy sources are needed. Table 1 lists the complete set of selected FOMs together with the work package each of them is used in.

4. Results and discussion

4.1. Matrixes of sequences

Accident sequences with the potential to evolve in challenging combustion conditions were grouped for different PWR types:

- Western PWR (PWR-W). Different reactor sizes and variants are considered.
- Konvoi PWR (PWR-KWU).
- PWR-VVER.

Table 2 and Figure 1 show the different reactor types simulated by the different partners, the sequences analysed together with the code used, and the approaches used. It is important to highlight that the WP2 aims to identify sequences with high combustible associated risk and not to perform a thorough and comprehensive PSA level 2 analysis to consider all the potential sequences with high combustible gases concentration. Besides nodalization, hypotheses and approximations were diverse and specific for each plant simulation; some of the most relevant are listed below. In Table 2 is noted that containments are modelled with a moderate number of nodes ranging from 14 (PWR-900) to 30 (KWU-1300). In Figure 1 two different font colours have been used to distinguish simulations conducted with PARs included (black) from the ones with no PARs (red). All reactor designs have some sequences modelled without PARs, which will be found

the most challenging ones from the gas combustion perspective – which is not surprising as the PAR are installed for the task to suppress a containment challenge by combustible gases.

	WPs			
Figure of Merit	2	3.1	3.2	4
Gas molar fractions (H ₂ , CO, H ₂ O _v , CO ₂) in representative compartment	Yes	Yes	Yes	No
Gas injection/generation rates (H ₂ , CO, H ₂ O _v , CO ₂ ,H ₂ O _l) in each compartment	Yes	Yes	No	Yes
Enthalpy associated to the injection/generation rates into the containment $(H_2, CO, H_2O_v, CO_2, H_2O_l)$ in each compartment	Yes	Yes	No	Yes
Temperature associated to the injection/generation rate into the containment (H_2 , CO , H_2O_v , CO_2 ; H_2O_l)	Yes	No	No	Yes
Density of injected gases and water	No	No	No	Yes
Pressure difference between volume upwards and downwards of the break	No	No	No	Yes
Containment pressure	Yes	Yes	Yes	No
Gas temperature (representative compartment)	Yes	Yes	Yes	No
Heterogeneity index	Yes	No	No	No
Breach size	No	No	No	Yes
Power sinks/sources due to ESF	No	No	No	Yes
Power from MCCI due to radiation release to the gas mixture	No	No	No	Yes
Initial gas composition (each compartment)	No	Yes	Yes	Yes
Initial gas temperature (each compartment)	No	Yes	Yes	Yes
Initial surface, inner and outer, temperature (in each compartment)		No	No	Yes
Initial containment pressure		Yes	Yes	Yes
Initial amount of water in pools and on surfaces (each compartment)	No	No	No	Yes
Inter-compartment gas velocity (representative compartment and time)	No	Yes	No	No

Table 1. Complete list of FOMs related with the different AMHYCO's work packages

Partner	Reactor type	Code	Number of plant nodes	Number of cont. nodes
IRSN	PWR-900 (Framatome)	ASTEC v2.1	~160	14
IRSN	PWR-1300 (Framatome)	ASTEC v2.1	~160	18
JSI	PWR-700 (Westinghouse)	MELCOR 2.2	158	13
CIEMAT	PWR-1000 (Westinghouse)	MELCOR 2.2	157	19
Framatome	KWU-1300	MELCOR 2.2	69	30
RUB	KWU-1300	AC ² 2019.1	283	23
Energorisk	VVER	MELCOR v1.8.5	126	21

Table 2. Reactor type, code and nodalizations used in the sequences analyses by WP2 partners

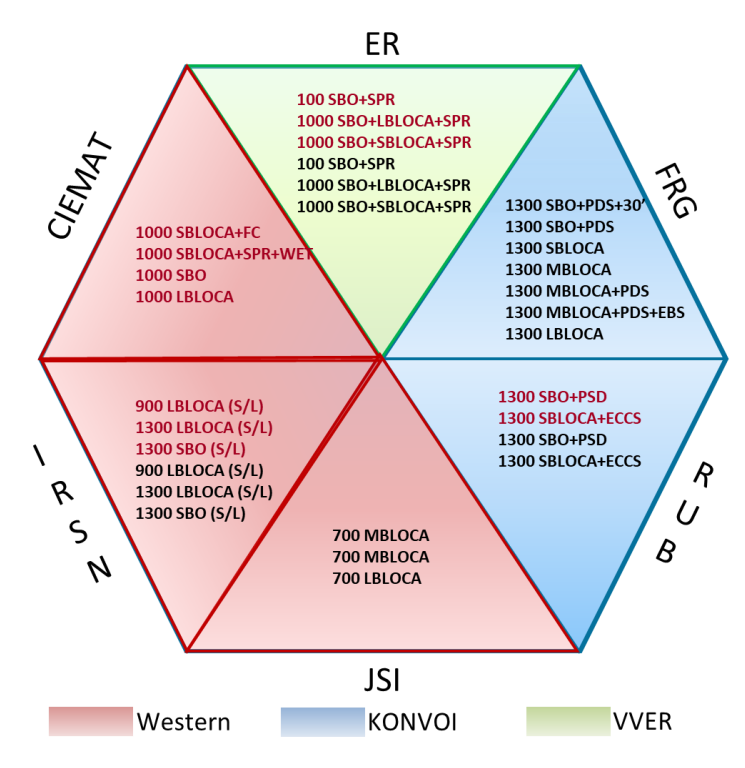


Figure 1. PWR accident sequences modelled (red: without PAR, black with PARs)

The main hypotheses and approximations used for the different plant designs can be summarised as follows. For PWR-W Framatome design:

- PWR-W-900 reactors have a single-wall containment building with a steel liner whereas the PWR-W-1300 reactors have a double concrete wall containment.
- Containment nominal leaks have been considered.

- After the RPV failure, in the LOCA sequences, the management strategy consists in spread of the corium, top water flooding and containment heat removal in the containment without venting.
- PARs have been considered.

For PWR-W Westinghouse design:

- No safety injection into the reactor coolant system (RCS) is available, except for accumulator's discharge.
- Availability of containment safety systems is sequence-dependent.
- A single-layer approach for the MCCI in the cavity pit with limestone concrete type (PWR-W-1000) has been adopted.

For the PWR-KWU reactor type:

- The four RCS loops have been clustered in two loops, one triple weighted and one single loop including the pressurizer.
- Generic siliceous concrete has been considered in RUB simulations, whereas Framatome uses a generic concrete composition with a bounding high carbonate content, enveloping all KONVOI plants.
- Radial melt through the biological shield and maintenance door is assumed after 45 cm concrete radial erosion, leading to a passive flooding of the core melt by water from the containment sump.
- RUB simulations split in-vessel and ex-vessel phases of the accidents; mass and enthalpy flow from the RCS to the containment were supplied from the former to the latter as boundary conditions for the ex-vessel simulation.

4.2. PWR-W

4.2.1. Framatome 900 MWe & 1300 MWe with ASTEC (IRSN)

As for the Framatome designs, IRSN simulated two SA sequences leading to the RPV failure and subsequent MCCI have been considered: a 12-inch hot leg LOCA and a SBO; the latter just in the case of PWR-W-1300. Particular attention has been paid to the late phase of the accident, particularly, to the concrete composition effect on the H₂ and CO generation. For this purpose, limestone and siliceous concretes have been modelled. In addition, the same sequences have been run with and without PARs to assess their impact on the accident scenario. Hence, a total of 12 sequences have been simulated.

Figure 2 shows the containment nodalization for the Framatome-1300 MWe design. The containment dome (marked with a red dot) is the volume where the largest mass of combustible gases eventually accumulates. Figure 3 depicts the simulated evolution of the gas composition in the dome of the containment during the identified accident sequences.

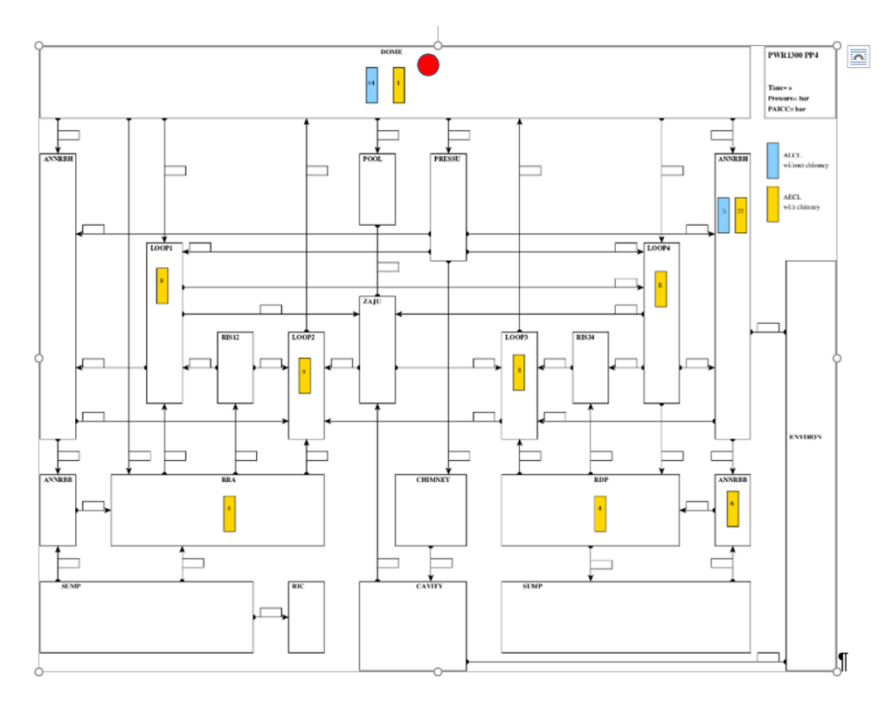


Figure 2. Containment nodalization for the PWR-W-1300

The most challenging conditions (i.e., those where the potential energetic events due to gas combustion are more likely) have been observed to prevail in the 1300 MWe reactor when no PARs are operational, and the reactor pit floor is made of siliceous concrete. Both the LOCA as well as the SBO sequences enter the flammability region in the Shapiro diagrams (Figure 3).

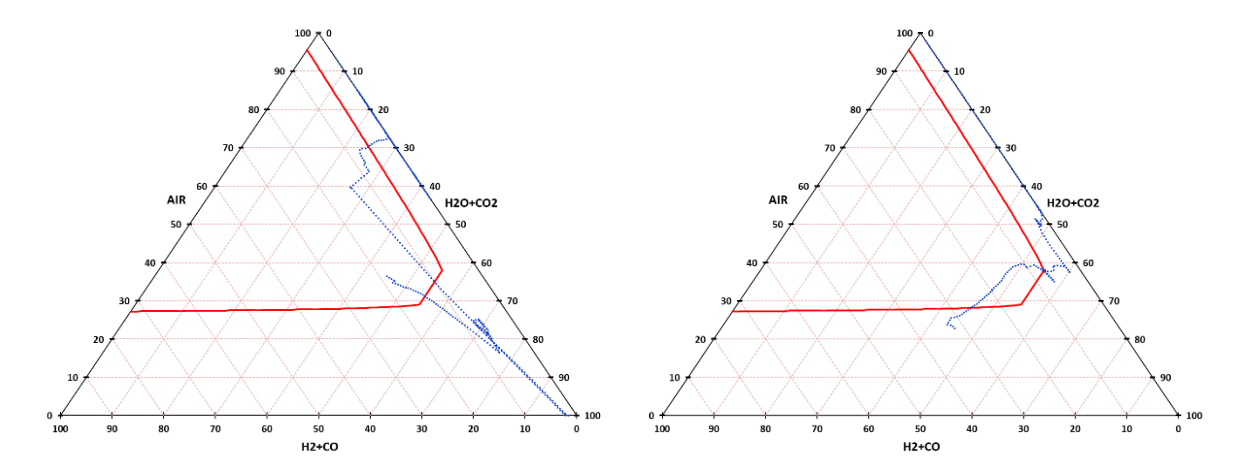


Figure 3. Shapiro diagram for PWR-W-1300 simulations. (Left: 12" LOCA, Right: SBO) without PARs

For the LOCA a flammable gas cloud fills the containment early in the sequence because of the in-vessel core oxidation. It leaves the flammability region during the ex-vessel phase because a high concentration of steam is reached as a side effect of the corium flooding by the sump water. At 86400 s (24 h), once the ultimate containment heat removal system is activated, the steam molar fraction in the dome decreases due to steam condensation (Figure 4) and, the containment atmosphere becomes flammable again (see Figure 3) and the combustible gases reach the maximum concentration at the end of the simulation.

The SBO sequences are characterized by a high release of steam into the containment in the invessel phase. Nonetheless, the amount of steam decreases along the ex-vessel phase and falls below the inerting threshold (55 vol% steam) after a few hours of the accident phase onset, while the amount of combustible gases keeps on monotonously increasing so that at \sim 45000 s the gas mixture reaches flammable conditions (Figure 4). Note that in the figure, vertical dotted line splits in-vessel and ex-vessel phases, whereas horizontal colour dotted lines indicate the thresholds mentioned above for O₂ (pink), combustible gas (orange) and steam (blue).

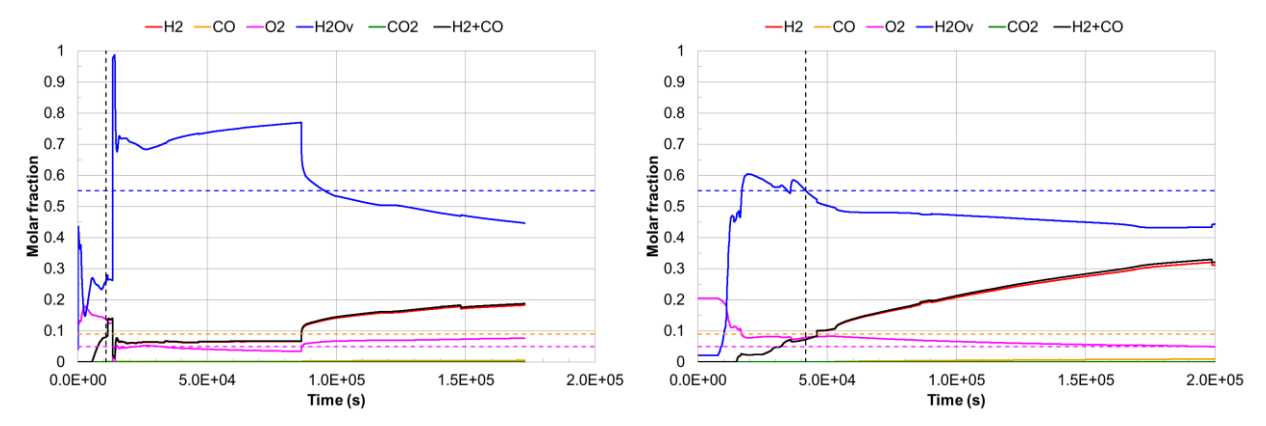


Figure 4. Gas composition in the main compartment of PWR-W-1300 (Left: 12" LOCA, Right: SBO) without PARs

The evolution of both these sequences lead to high pressure, around 5 bar (Figure 5). Whereas the LOCA shows the maximum value at 24 h, previous to the activation of the ultimate containment heat removal system, the SBO has its maximum pressure at the end of the simulation together with the maximum concentrations of the combustible gases.

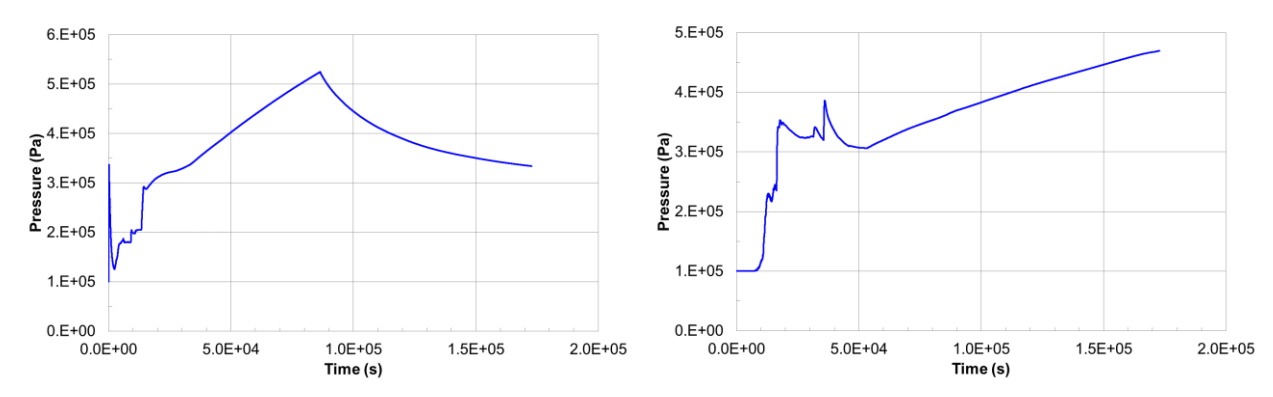


Figure 5. Containment pressure evolution for PWR-W-1300 (Left: 12" LOCA, Right: SBO) without PARs

4.2.2. Westinghouse 700 MWe with MELCOR (JSI)

For the PWR-W-700 design, JSI supplied full simulations with the MELCOR code for three SBO sequences, two of them with superimposed LOCA (pipe break sizes being 6-inch and 12-inch) have been simulated. In all these sequences, containment safety systems were supposed to be unavailable, and no safety injection has been assumed in the RCS, except for accumulators. In all the sequences, PARs have been considered, which results in a low combustion risk, as expected Containment nodalization considers 13 different compartments as shown in Figure 6 where the representative compartment is the upper compartment (marked with a red dot) as it constitutes the largest volume of the containment.

In the in-vessel phase of the SBO+6" LOCA, H₂ molar fractions never exceed 3.5 vol% and in the ex-vessel phase the high steam fraction keeps the containment inerted even if CO generation by MCCI increases the total combustible gas concentration above the considered flammability limit of 9 vol% (Figure 7). The high steam fraction in the evolution of these sequences also implies high containment pressure. The influence of the different initiating events is significant in the early phase of the simulated accidents. In later phases, the differences tend to vanish qualitatively and quantitatively.

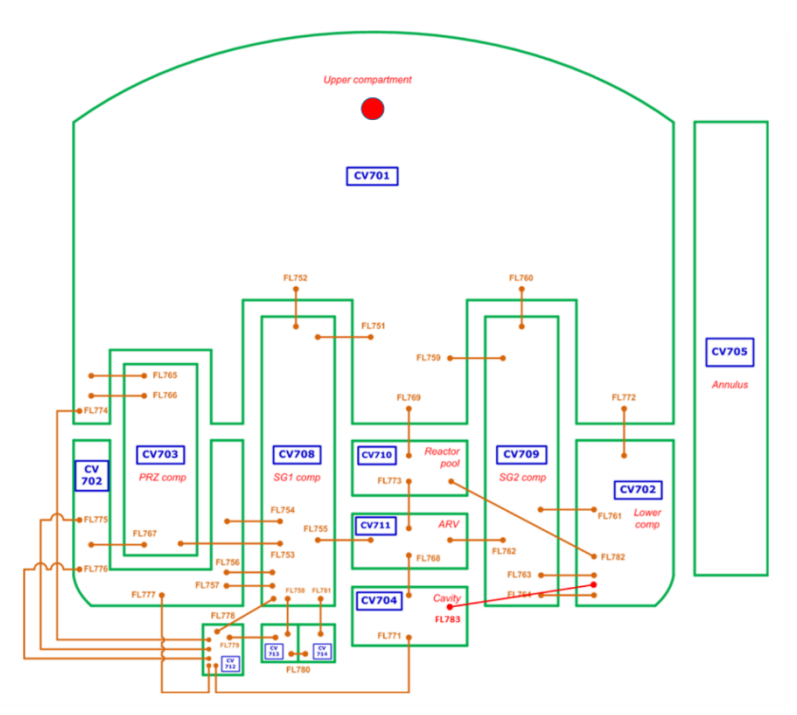


Figure 6. Containment nodalization for the PWR-W-700

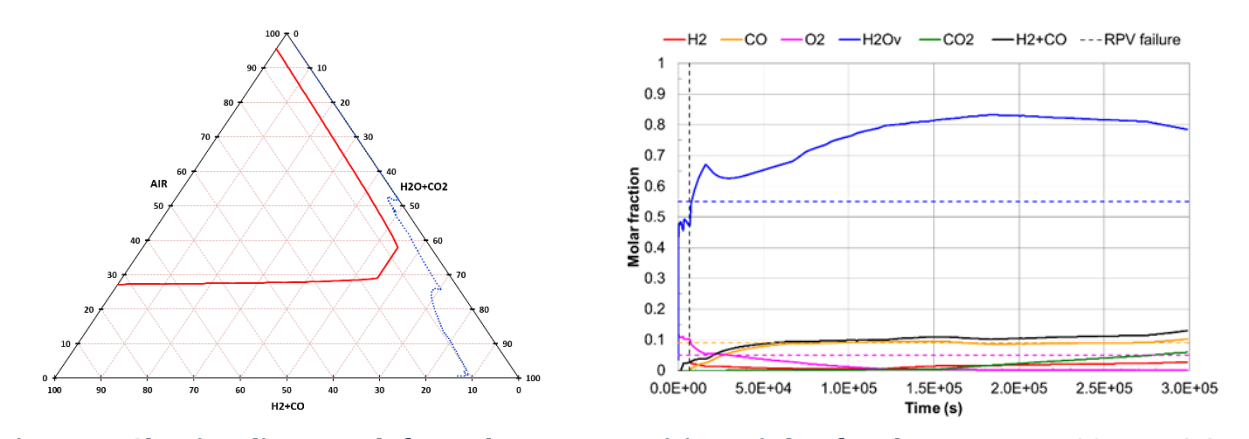


Figure 7. Shapiro diagram (left) and gas composition (right) for the PWR-W-700 MBLOCA sequence (with PARs)

4.2.3. Westinghouse 1000 MWe with MELCOR (CIEMAT)

Two types of sequences have been considered for this plant design: LOCA and SBO. The different pipe breaks sizes and accident management actions (fan coolers –FC; sprays and cavity flooding) considered, added it up to a total of four sequences analysed:

- 2-inch SBLOCA with fan coolers available.
- 2-inch SBLOCA with sprays on and cavity flooding.

- Double-ended guillotine LBLOCA with both sprays and fan coolers available.
- Station blackout (no safety system available).

All these sequences have been simulated without PARs. The containment nodalization, with 19 volumes, is shown in Figure 8, where the representative compartment for the combustible gases risk is the reactor service floor compartment (marked with a red dot).

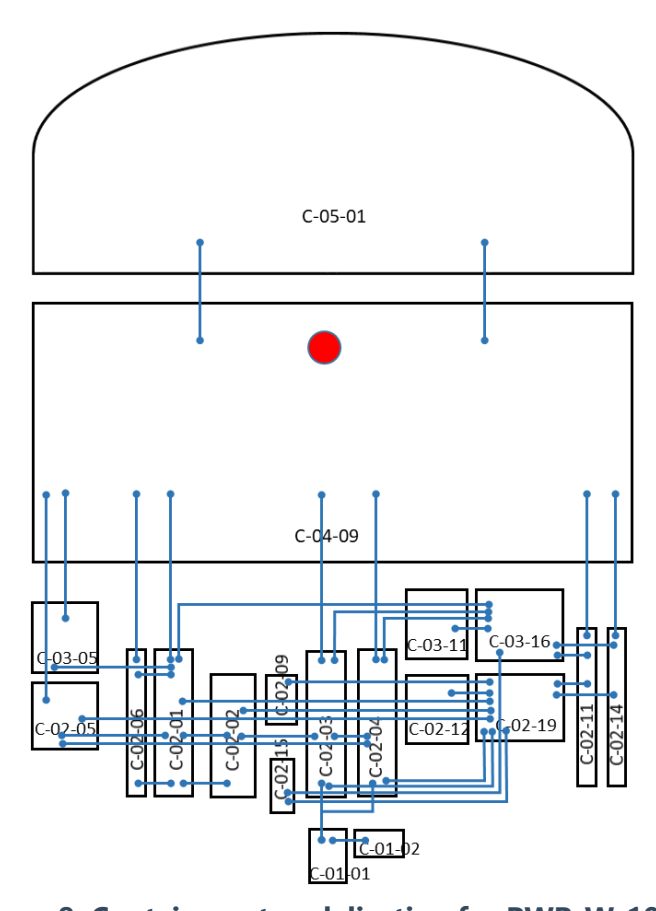


Figure 8. Containment nodalization for PWR-W-1000

In sequences with systems capable of condensing steam (i.e., fan coolers, sprays), a higher fraction of combustible gases has been observed. As a consequence, the two sequences which represent the highest risk associated with combustible gases are the 2" LOCA with fan coolers and the LBLOCA. Figure 9 shows the Shapiro diagrams of both of them, where deeper and longer lasting penetration within the flammability region is noted in the case of LBLOCA.

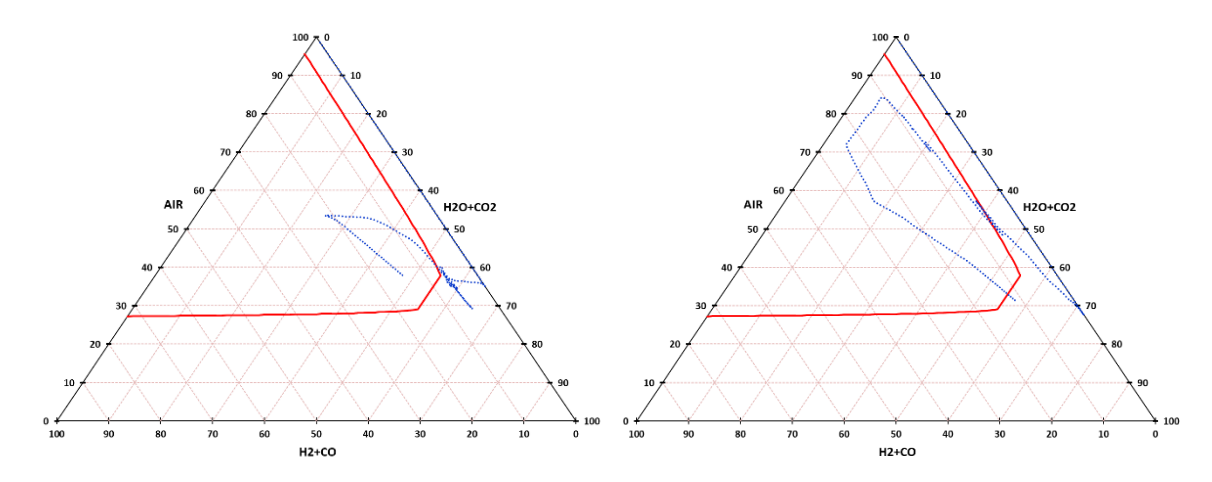


Figure 9. Shapiro diagram of PWR-W-1000 simulations (Left: SBLOCA with fan coolers; Right: LBLOCA with spray and fan coolers) without PARs

Both sequences lead to a high steam concentration at the beginning of the accident due to the steam release or the flashing of the water from the RCS. The sprays operation in the LBLOCA triggers a fast and large drop of steam content. Even though, for a short time the H₂ molar fraction reaches combustion limits at the end of the in-vessel phase (Figure 10). It is in the ex-vessel one, when further release of H₂ and CO from MCCI makes combustible gas mixture to attain molar fractions over 25 vol% at around 20000 s. The loss of efficiency in condensation when sprays turn into the recirculation operation mode and the generation of CO₂ eventually lead to a progressive dilution of such high combustible gas concentration in the long run of the sequence, but it still stands over the combustion limits.

For the SBLOCA sequence (Figure 10), the combustible gas mixture does not exceed the combustion threshold until CO is produced in the ex-vessel phase. This CO together with the effect of the fan coolers on steam content, makes total combustible gases molar fraction grow to higher than 20 vol% at about 30000 s. They stay that high until massive amounts of CO₂ are released and make combustible gas concentration decrease, although they reach the end of the calculation well over the threshold. The operation of the safety systems in the containment makes these sequences to evolve with a limited increase in pressure.

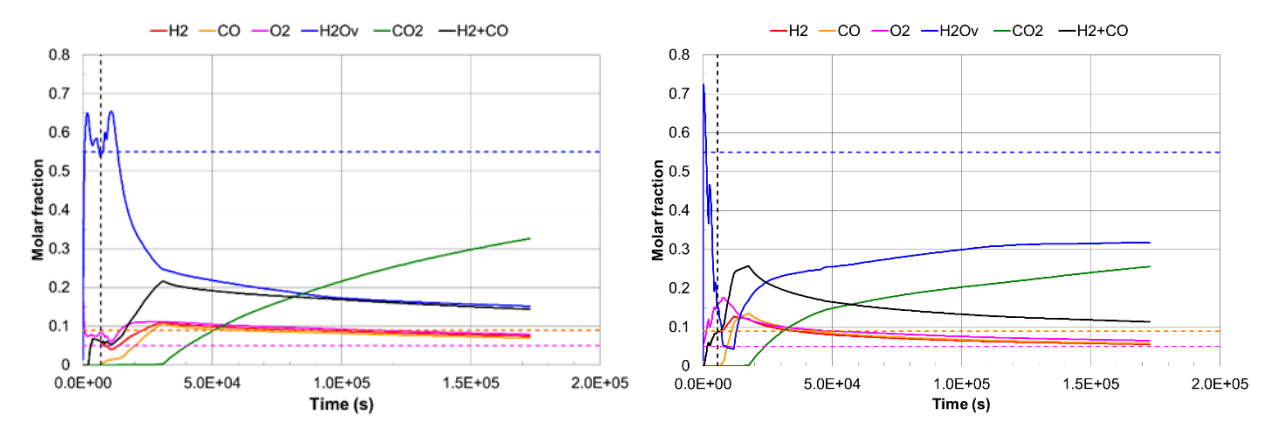


Figure 10. Gas composition in PWR-W-1000 (Left: SBLOCA with fan coolers, Right: LBLOCA;)

4.3. PWR-KWU

A number of sequences has been simulated for the Konvoi PWR design. As noted in Table 2, variability is not associated with reactor size, but with the analytical tools and the approaches used for the modelling: AC² and MELCOR.

4.3.1.KONVOI 1300 MWe with AC² (RUB)

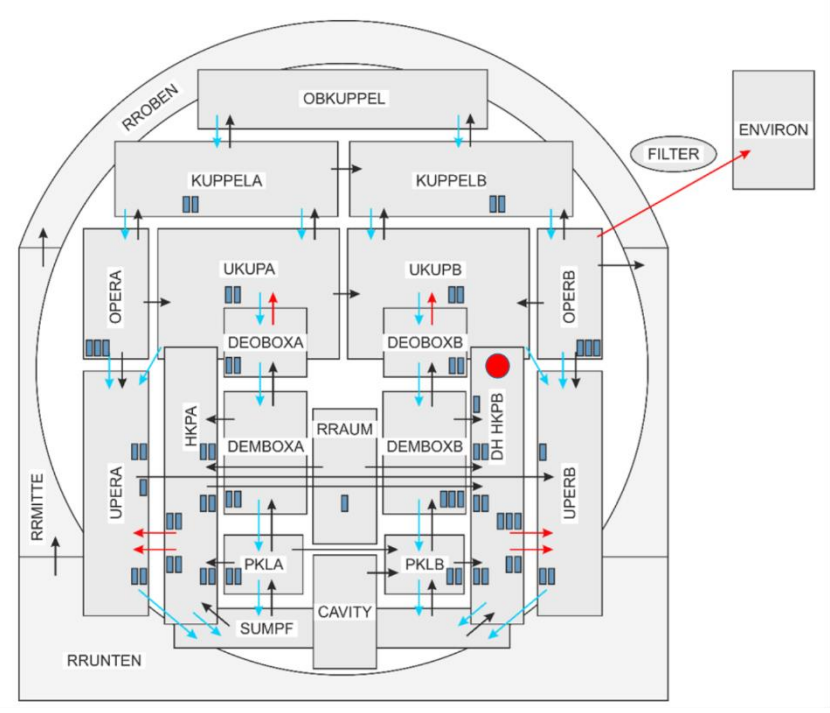


Figure 11. Containment nodalization for PWR-KWU-1300 used in AC².

From the pool of sequences that have been simulated by RUB with AC², the most challenging ones in terms of combustion risk have been a SBO with Primary Side Depressurization (SBO+PSD) and a LOCA (80 cm²) with a limited water injection by the extra borating system (SBLOCA¹+ECCS). Both of them have been modelled with and without PARs. Even though both sequences enter the flammable region of the Shapiro diagram (Figure 12) when PARs are assumed to fail, the SBLOCA+ECCS stays longer and reaches higher combustible gas concentration than the SBO+PSD.

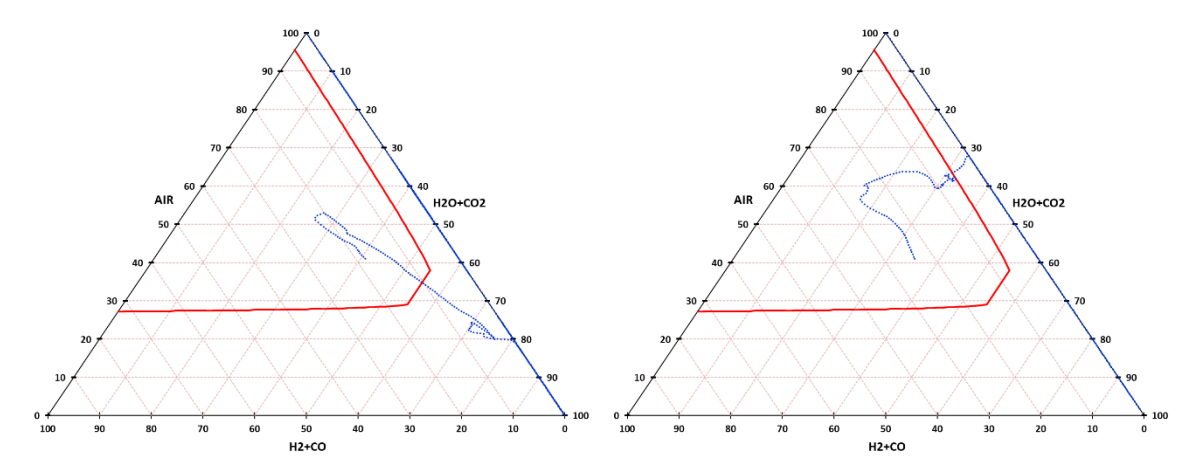


Figure 12. Shapiro diagram for PWR-KWU (Left: SBO+PSD; Right SBLOCA+ECCS) in case of PAR failure

As for atmosphere composition, in the SBO+PSD sequence the steam molar fraction reaches a value up to 100% in the considered compartment at nearly 10000 s in the in-vessel phase and progressively falls since the onset of the ex-vessel one, which causes the gas phase to move out of the inert region soon (Figure 13). Combustible gases build burnable fractions (over 9 vol%) early in the ex-vessel phase and builds up to values around 20 vol%, where they remain for long, despite cavity flooding at around 49000 s rises moderately the steam fraction again to value never exceeding 35 vol%. The evolution of the gas composition is not too different in SBLOCA+ECCS. Steam molar fraction peaks soon after the accident onset at nearly 1.0 and decreases progressively (Figure 13), while combustible gases enter the containment a few thousand seconds before the RPV failure and build up molar fraction which gets to around 25 vol% and states steady until the end of the sequence. Fast H₂ release in the in-vessel phase does not represent a significant risk for combustion because of the small accumulated mass amount. Like for the SBO+PSD sequence, the cavity flooding does not lead to inertization of the containment atmosphere.

 $^{^{1}}$ In this section the 80 cm 2 LOCA is identified as SBLOCA to preserve the initial nomenclature of RUB, the partner who performed the calculations

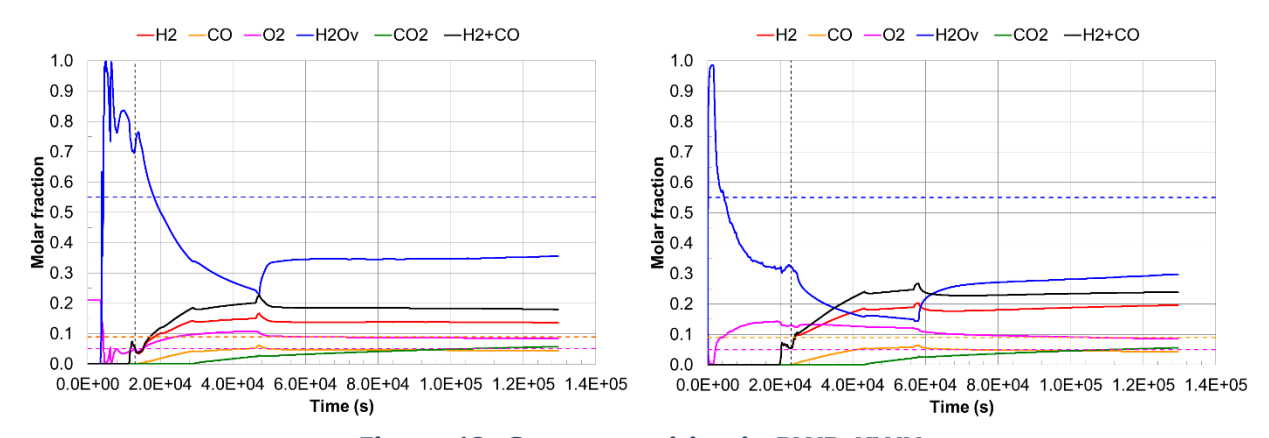


Figure 13. Gas composition in PWR-KWU (Left: SBO+PSD, Right: SBLOCA+ECCS) in case of PAR failure

4.3.2.KONVOI 1300 MWe with MELCOR (Framatome)

For the simulation of the KWU-type 1300 MWe "Konvoi" plants, Framatome GmbH supplied full-plant simulations with the MELCOR code. The used containment nodalization, with 30 compartments, is depicted in Figure 14. The zones that show the highest combustible gases molar fraction during the accident simulations are marked by red dots.

Due to the high reliability of Framatome PAR, on a best-estimate basis, the availability of PAR is considered in the simulations. A PAR system has the overall purpose to prevent the occurrence of large-scale combustion events, especially in the large containment compartments like the containment dome, which could endanger the containment integrity. A PAR system however cannot exclude the occurrence of locally flammable conditions within the containment, especially not close to the leakage location. At the leakage location of the reactor coolant system (RCS), nearly pure hydrogen can come in contact to the oxygen-containing containment atmosphere. Thus, the occurrence of locally flammable conditions is technically unavoidable. However, as long as these local combustions do not endanger the containment integrity, their possible occurrence is acceptable.

Based on these general PAR system operating principles, it is an expected behaviour that in the rather small control volumes of CV820 and CV825 (see Figure 14), which house the leakage location or are directly adjacent to the RCS leakage location, flammable conditions do occur. Thereby, the detection of such local combustible gas mixtures is closely linked to the level of detail of the containment nodalization. The fewer and thus larger control volumes are used, the more spatially averaged the simulation results become, the less likely local combustion zones are detected.

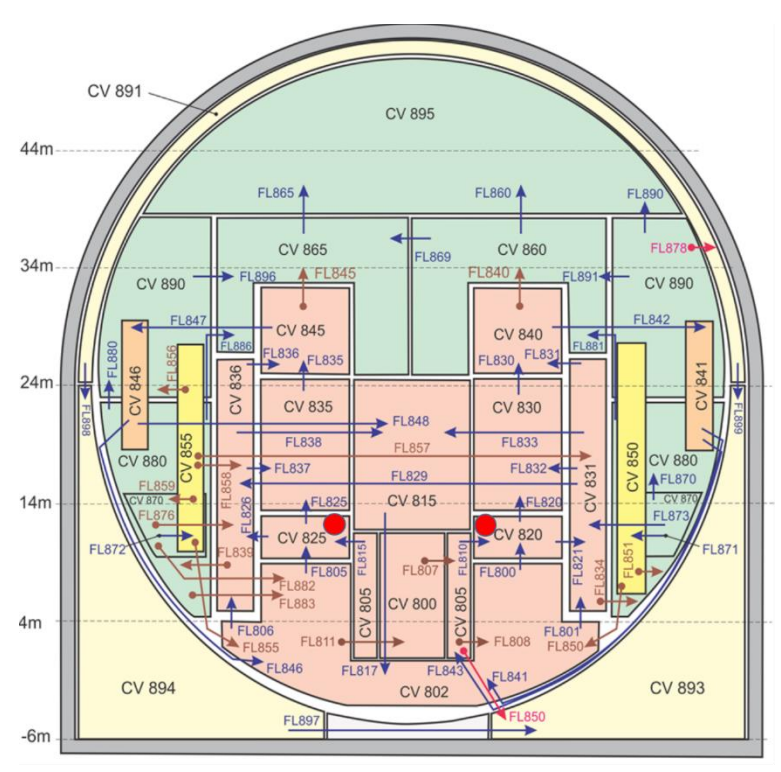


Figure 14. Containment nodalization for PWR-KWU-1300 used in MELCOR

The set of simulations performed with the MELCOR code in part correspond to the simulations with AC^2) and in part are other accident sequences. The accident sequences simulated are:

- SBO+PSD (at 650°C core outlet temperature);
- SBO+PSD (30 min. delayed);
- SBLOCA (5 cm²) with secondary cool-down of the steam generators and initial ECCS operation, but then failure of switching to sump recirculation
- MBLOCA ²(80 cm²) with secondary cool-down of the steam generators and initial ECCS operation, but then failure of switching to sump recirculation
- LBLOCA (380 cm²) with secondary cool-down of the steam generators and initial ECCS operation, but then failure of switching to sump recirculation
- MBLOCA (80 cm²) with only a small water injection (Extra Borating System), which is however insufficient to prevent core damage
- MBLOCA (80 cm²) without any water injection

 $^{^2}$ In this section the 80 cm 2 LOCA is named as MBLOCA to preserve the initial nomenclature of FRAMATOME, the partner who has performed the calculation.

More details of these simulations can be found in the annexes. From the entire set of simulations, the ones posing a higher combustion risk have been found to be the MBLOCA and the LBLOCA with the delayed accident progression due to the initially operating ECCS. This result is somewhat expectable as the delay of the core damage allows for partial condensation of the steam in the containment which was released from the blow-down of the reactor coolant system.

Mostly only the control volumes near the pipe leakage location show combustible conditions in the time interval of core oxidation causing a high hydrogen release rate, see Figure 15. In the long term, the PAR consume combustible gases as well as oxygen. Thus, the gas concentration shown in the Shapiro-diagram tends to reach <10% air in the long-term.

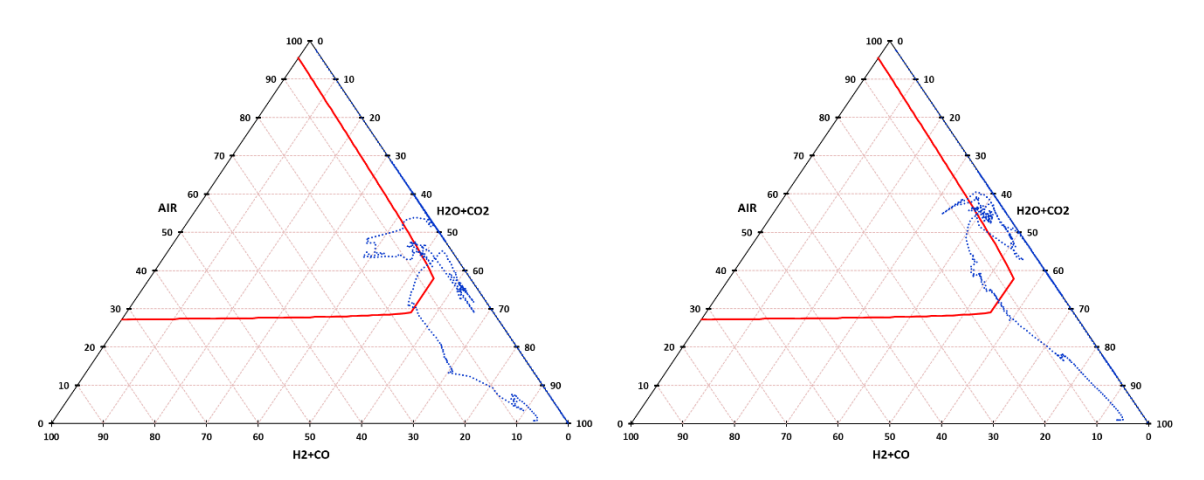


Figure 15. Shapiro diagram for PWR-KWU (Left: MBLOCA; Right: LBLOCA) with full PAR capacity

In the MBLOCA sequence, the fast H₂ release into the containment during the core oxidation phase leads to a hydrogen concentration close to the leakage of up to 18 vol%, see Figure 16. With progressing core damage, the hydrogen release rate decreases, and thus the convection within the containment leads to a reduction of the local hydrogen concentration. In parallel the PAR consume the hydrogen and the containment oxygen.

With RPV failure, the core melt, having a very high temperature, rapidly attacks the basemat concrete, releasing large masses of hydrogen and carbon monoxide, see Figure 16. In the phase of dry MCCI in the reactor pit, the combined combustible gas concentration reaches up to 15 vol% in the lower containment. However, at this point in time, the PAR already consumed a significant amount of oxygen from the containment atmosphere, thus the locally present ~5 vol% oxygen does no longer support large-scale combustion.

A basic assumption of the simulations for Konvoi plants is that after a certain grace period, the core melt will erode the so-called Biological Shield. After the penetration of this shield, the sump water passively floods the cavity. This results in a strong steam release at \sim 60 000 s, see Figure

16. This steam on one side leads to a rapid containment pressurization, and on the other side to an inertization of the containment, drastically reducing the concentration of combustible gases and O_2 . In overall terms, the LBLOCA scenario evolves faster but functionally similar to the MBLOCA scenario.

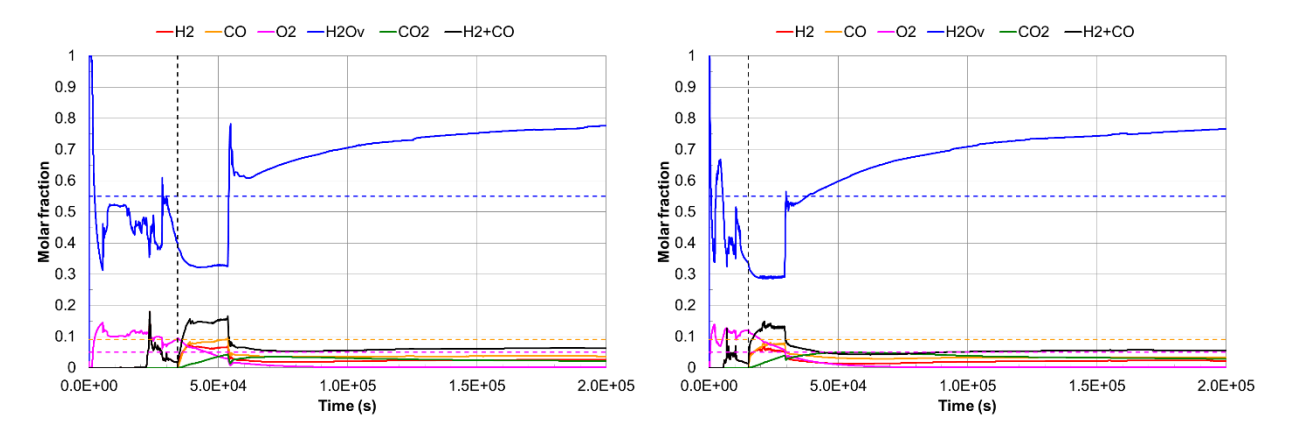


Figure 16. Gas composition for PWR-KWU (Left: MBLOCA; right: LBLOCA) with full PAR capacity

4.4. PWR-VVER

For the VVER design, three severe accident sequences have been simulated by Energorisk: SBO, 90 mm cold leg LOCA and double ended LBLOCA. For each sequence, the spray system has been activated at in-vessel or ex-vessel phase to assess their effect on the hydrogen and CO behaviour. Additionally, these sequences have been run with and without PARs. Hence, a total of 12 sequences have been calculated. The containment nodalization (Figure 17) considers 21 control volumes. The node labelled as CV-619 (*C-HALL*) is the largest compartment and is taken as the reference volume.

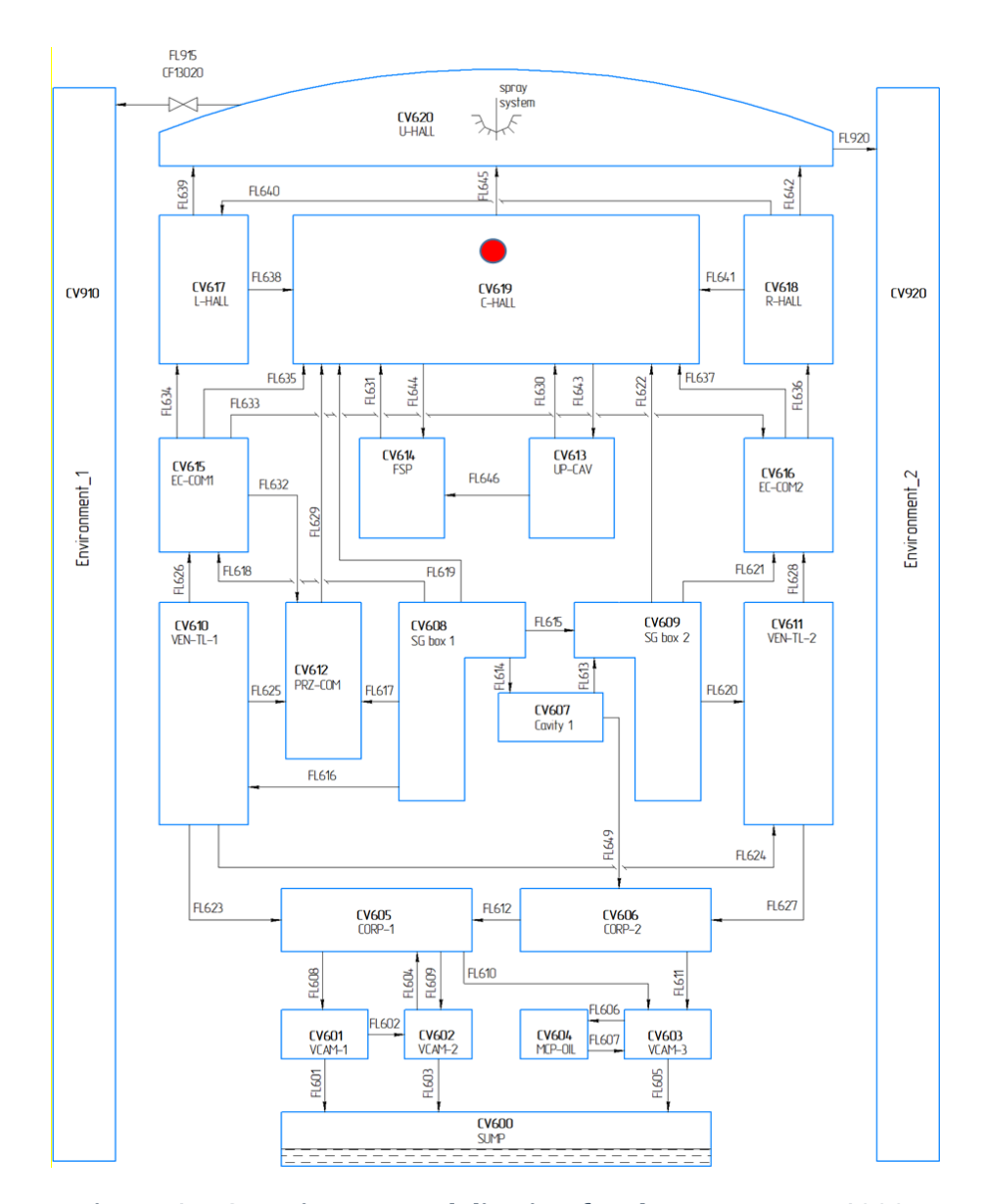


Figure 17. Containment nodalization for the PWR-VVER-1000.

Regarding the molar fraction of combustible gases the most challenging conditions are reached by the two SBO sequences, with the sprays activation in the in-vessel phase and in the ex-vessel phase. Figure 18 shows how the atmosphere composition in both sequences deeply enters into the flammability region of the Shapiro diagrams.

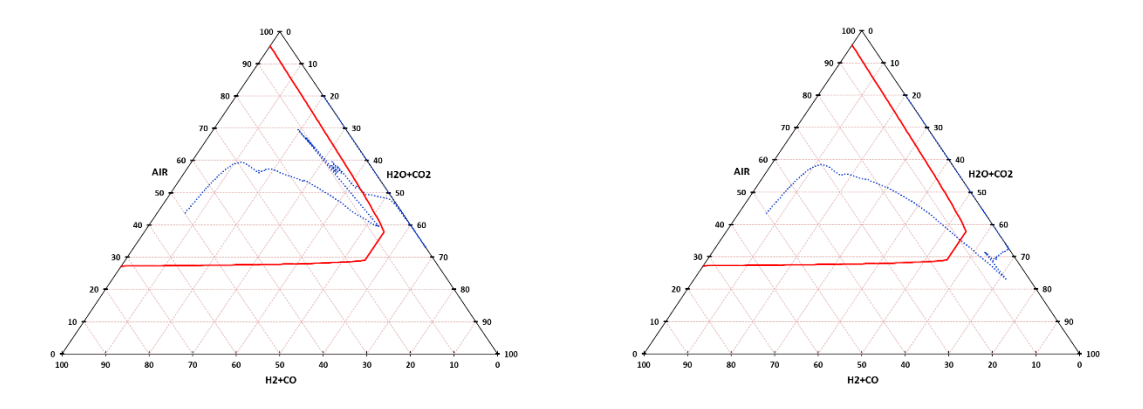


Figure 18. Shapiro diagram of the PWR-VVER-1000.

SBO with sprays activated during the in-vessel phase (left) and in the ex-vessel phase (right)

The SBO sequence triggers a fast rise of steam fraction in the reference compartment whereas the activation of sprays in the in-vessel phase lead to the decrease up to around the initial value (Figure 19). Later, at the RPV rupture, the steam in the containment rise again steeply. For a short period before the RPV rupture, the H₂ molar fraction reaches the deflagration criteria. During the ex-vessel phase the H₂ and CO accumulate at the same time that the steam content in the containment gradually decreases and as a consequence the total combustible gases (H₂+CO) molar fraction reaches values around 50 vol%. The evolution of the scenario with the sprays activated at the ex-vessel phase is very similar to the previous sequence. The main difference is that the decrease of the steam molar fraction is not observed in the in-vessel phase but in the exvessel phase (Figure 19).

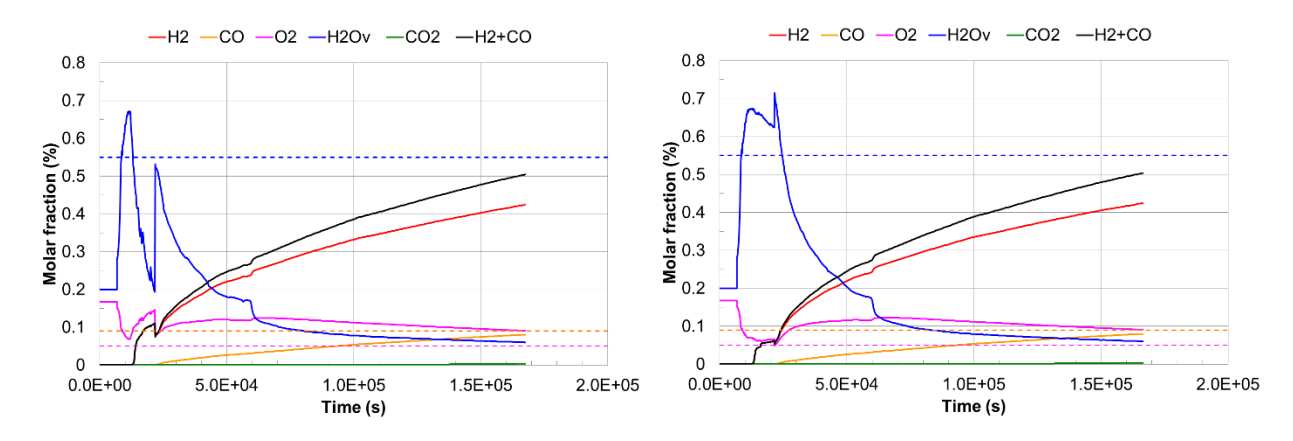


Figure 19. Gas composition in PWR-VVER-1000.

SBO with sprays activated during the in-vessel phase (left) and in the ex-vessel phase (right)

5. Application to other work packages

The database built in WP2 has important links to other work packages as it will provide important information of realistic conditions in a severe accident sequence for both the in-vessel and the ex-vessel phases of the accident.

5.1. WP3: Experimental investigation

The WP3 is divided into two main tasks, devoted to experimentation for combustion of $H_2/CO/H_2O_v$ mixtures and for PARs efficiency.

Data compiled in WP2 provide boundary conditions for the definition of the experimental matrix for both task in WP3. The simulated sequences data includes, when needed, the CO generation by the MCCI that help to build up a comprehensive set of experiments for both, H2/CO mixture combustion and PAR's recombination efficiency.

Data transferred to WP3 from WP2 includes time evolution for

- Gas molar fractions for H₂, CO, H₂Ov, CO₂
- Atmosphere pressure
- Gaseous temperature

in the compartments considered representative (Table 3). The combustible gases injection can be derived from the data.

	time	X _{H2}	Xco	X _{O2}	X _{H2Ov}	X _{CO2}	Р	Т
	(s)	(%vol)	(%vol)	(%vol)	(%vol)	(%vol)	(bar)	(K)
KWU-SBLOCA	25350	9.0	0.5	13.0	27.8	0.0	1.73	358.9
	58190	17.3	6.3	12.5	13.9	2.2	1.75	341.6
	129600	14.0	4.7	9.3	30.6	5.9	2.34	363.8
W1000-LBLOCA	7680	9.0	0.0	16.1	16.1	0.0	1.33	337.9
	20700	12.5	12.9	11.7	18.2	0.2	1.78	344.1
	172800	6.3	5.9	6.9	28.7	26.1	3.14	369.7
W1000-SBLOCA	16300	6.3	2.7	10.1	42.6	0.0	2.05	368.9
	30900	10.9	10.7	11.1	24.7	2.3	1.89	352.6
	172800	7.4	6.9	7.9	15.1	32.6	2.72	349.6
W1000-SBO	31700	6.7	2.3	7.3	55.6	0.2	3.16	401.9
	42700	9.5	8.0	7.3	47.1	0.4	3.06	396.7
	90000	8.2	7.5	6.1	37.4	17.7	3.26	402.5

Table 3. Ranges of boundary conditions at relevant times (transfer to WP3).

Data for four sequences have been transferred: the SBLOCA (20 cm²) with fan coolers, the double-ended guillotine LBLOCA, and the SBO for the PWR-W-1000 whereas for the PWR-KWU, the 80 cm² LOCA with limited water injection has been selected.

The LOCA sequences in PWR-W-1000 lead to ex-vessel conditions with similar molar fraction of H_2 and CO with high content of CO_2 . The SBO sequence presents similar trends but with a significant fraction of steam. The 80 cm² LOCA for the PWR-KWU has a H_2 fraction about four time higher than for CO, the H_2 release rate is higher and significantly delayed when compared with the PWR-W sequences.

5.2. WP4: Full containment analysis

The WP4, aimed to analyse the full containment response under different operation actions and/or safety systems actuation of sequences with high combustion risk, is directly related with the WP2. The results from WP2 are, in fact, the bases for the discussions held in WP4 concerning the set of sequences to be modelled in WP4.

Sequence evolution data will be used to define the initial and boundary conditions of the calculations to be carried out in WP4. Therefore, besides the initial temperature, pressure and gas composition of the different containment compartments, for each gas release into the containment is given its mass flow rate and temperature and the specific enthalpy. The effect of the different containment safety systems are also provided.

The objective of the WP4 to perform analysis of the full containment response under different operator actions and/or safety systems actuation in different scenarios makes that sequences of interest for WP4 would have different in-containment conditions. The following sequences have been selected:

- PWR-W: Double ended guillotine LOCA and SBO.
- PWR-KWU: 80 cm2 LOCA with limited water injection and the SBO with delayed PSD.
- PWR-VVER: SBO and the simultaneous LBLOCA+SBO with sprays activation in the exvessel phase.

6. Conclusion

Forty two severe accident sequences in PWR have been simulated with the purpose of identifying conditions under which combustion events might happen, with particular focus on H_2 and CO combustible mixtures during the ex-vessel phase of the accidents. The main outcomes from the work can be summarized as follows:

- The severe accident sequences that posed a higher risk of gas combustion (H₂ and CO) have been found to be SBLOCA (20 cm²) and LBLOCA, for PWR-W, LOCA (80 cm²) for PWR-KWU, and SBO with sprays for PWR-VVER.
- A key factor heavily conditioning sequence selection is the availability of safety systems. Their capability of condensing steam during the ex-vessel phase results in a boost of combustible gas molar fraction. In this respect, the partial restoration of sprays after a SBO can pose a threat to the containment integrity.
- As expected, the largest gas accumulation (as long as PARs are not modelled) is found in the ex-vessel phase. The composition of the concrete greatly influences the amount of released gas and the CO fraction.
- Whenever PARs are modelled, O₂ starvation in the ex-vessel phase makes gas composition exit the flammable region of the Shapiro diagram, even if the combustible gas fraction well exceeds 9 vol%. Even though a lack of oxygen prevents an in-containment combustion in the late phase of an accident, the hydrogen and carbon monoxide stored within the containment still represents a combustion risk in case a containment leakage occurs, as e.g. observed in the Fukushima Daiichi accidents or in case the gas comes in contact to environmental air, e.g. in a venting line. These combustion risks outside of the containment are currently not foreseen to be investigated within the AMHYCO project.
- The presence of a PAR system can significantly reduce the size and magnitude of possible combustible gas clouds within the containment. In the simulations of plants equipped with a PAR system, usually the full system capacity is considered. It may be of interest to investigate a partial PAR failure (e.g. by jet forces) or efficiency reduction of the PAR system (at least for plants where the employed PAR technology showed weaknesses in independent tests) within WP4.
- Cavity flooding overall reduces the in-containment combustion risk. The flooding at least partially quenches the core melt and thus reduces the release rate of combustion gases resulting from MCCI. Additionally, the strong release of steam during the quenching leads to a fast dilution of the combustible gases, reducing the respective concentrations. As disadvantage, however, the steam release also causes a rapid containment pressurization.
- Sequences evolving with high in-containment pressure normally do not imply a high risk for hydrogen and CO combustion because of the high steam concentration of these sequences, (e.g. SBO). Nonetheless they would be of interest to be considered in WP4 since they provide useful conditions to test the effect of FCVS or the potential

late recovery of safety systems (i.e., sprays and fan coolers) on the combustible gases behaviour.

Therefore, regarding the objective of both WP2 and WP4 the selected sequences to be simulated in WP4 have been:

• For PWR-W: The double ended LOCA simulated in PWR-W-1000

The SBO sequence simulated in the PWR-W-1300

For PWR-KWU: The 80 cm² LOCA with limited water injection by the EBS

SBO with delayed PSD

• For PWR-VVER SBO with sprays activation

LBLOCA + SBO with sprays activation

The next step of this investigation within AMHYCO, will be to fully characterize the scenarios (initial and boundary conditions) and transfer the information to AMHYCO WP3, to properly feed test matrices to investigate PAR performance and combustion of H₂ and CO mixtures, and to AMHYCO WP4, to benchmarking different approaches of containment analysis and to assessing the effect of different management actions. It is worth noting that the different containment free volume of the PWR-1300 compared with the reference PWR-1000 to be modelled in WP4 requires the scaling of the data provided for this sequence (Benteboula et al. 2011) as it is summarized in Annexe I.

7. References

Benteboula, S., A. Bentaib, A. Bleyer, and J. Malet. 2011. *ERCOSAM D-1.1. Scaling down Analysis from Real NPP Calculations*. ERCOSAM / WP1 / P1 / 2011-09 & RSN/DSR/SAGR/11-243. IRSN.

ENSREG. 2012. Peer Review Report. Stress Tests Performed on European Nuclear Power Plants.

Herranz, L. E., and J. Fontanet. 2021. AMHYCO: Milestone-2 Meeting Minutes. MS2.

IAEA. 2015. The Fukushima Daiichi Accident. Technical Volume 1/5: Description and Context of the Accident. Austria: IAEA.

IAEA. 2016. Considerations on the Application of the IAEA Safety Requirements for the Design of Nuclear Power Plants. IAEA-TECDOC-1791.

- Jiménez, G., L. E. Herranz, A. Bentaib, C. Nabiha, E. A. Reinecke, S. Kelm, M. Loeffler, M. Braun, C. Bratfisch, I. Kljenak, O. Sevbo, D. C. Visser, Z. Liang, and S. Balech. 2022. 'AMHYCO Project Towards an Enhanced Accident Management of the H2/CO Combustion Risk'. Brussels (Belgium).
- Magallon, D., A. Mailliat, J. M. Seiler, K. Atkhen, H. Sjövall, S. Dickinson, J. Jakab, L. Meyer, M. Buerger, K. Trambauer, L. Fickert, B. Raj Sehgal, Z. Hozer, J. Bagues, F. Martin-Fuentes, R. Zeyen, A. Annunziato, M. El-Shanawany, S. Guentay, C. Tinkler, B. Turland, and L. E. Herranz Puebla. 2005. 'European Expert Network for the Reduction of Uncertainties in Severe Accident Safety Issues (EURSAFE)'. *Nuclear Engineering and Design* 235(2–4):309–46. doi: 10.1016/j.nucengdes.2004.08.042.
- Manara, D., D. Jacquemain, J. P. Van Dorsselaere, P. D. Bottomley, M. Adorni, C. Journeau, Y. Pontillon, T. Lind, L. E. Herranz, F. Rocchi, A. Schaffrath, J. C. de la Rosa, S. Bechta, J. Duspiva, I. Kljenak, and P. Dejardin. 2019. 'Severe Accident Research Priority Ranking: A New Assessment Wight Years after the Fukushima Daiichi Accident'. in *Proceedings of the European Review Meeting on Severe Accident Research*. Prague (Czech Republic).
- Sehgal, Bal Raj, ed. 2012. 'Chapter 3 Early Containment Failure'. Pp. 185–306 in *Nuclear Safety in Light Water Reactors*. Boston: Academic Press.
- Shapiro, Z. M., and T. R. Moffette. 1957. *Hydrogen Flammability Data And Application To Pwr Loss-Of-Coolant Accident*. WAPD--SC-545, 4327402. doi: 10.2172/4327402.
- TEPCO. 2015. Evaluation of the Situation of Cores and Containment Vessels of Fukushima Daiichi Nuclear Power Station Units-1 to 3 and Examination into Unsolved Issues in the Accident Progression. Progress Report No. 3.
- US-NRC. 1975. Reactor Safety Study. An Assessment of Accident Risks in U. S. Commercial Nuclear Power Plants. Executive Summary: Main Report. [PWR and BWR]. WASH-1400-MR; NUREG-75/014-MR. Nuclear Regulatory Commission, Washington, D.C. (USA). doi: 10.2172/7134131.

8. Annexes

Annex I: Throughout analysis of the sequences regarding different criteria

Annex II: Individual report for the PWR-W900 and W1300 reactors (IRSN)

Annex III: Individual report for the PWR-W700 reactor (JSI)

Annex IV: Individual report for the PWR-W1000 reactor (CIEMAT)

Annex V: Individual report for the PWR-KWU reactor – AC2 model (RUB)

Annex VI: Individual report for the PWR-KWU reactor – MELCOR model (Framatome)

Annex VII: Individual report for the PWR-VVER reactor (Energorisk)

ANNEX I. Throughout analysis of the sequences regarding different criteria

I.1 PWR-W selection criteria

I.1.1 Selection based on total mass of combustible gases

Following the basis of the consensus regarding the criteria for selecting the most conservative sequences (Section 2. of deliverable D2.2.), a first study of the proposed transients has been carried out. This first classification gathers the total mass of combustible gas (H₂ + CO) within the containment during the whole duration of the sequences. The data has been collected by adding up the different sources of combustible gases in each type of containment. In the case of the PWR-W containments, a scaling factor has been applied to the total integrated mass for a coherent comparison among different containment types (Benteboula, Malet, and Bleyer 2015). Table 4 shows the scaling formula and factors together with the free volumes of the different PWR-W containments, being the PWR-W-1000 the reference one.

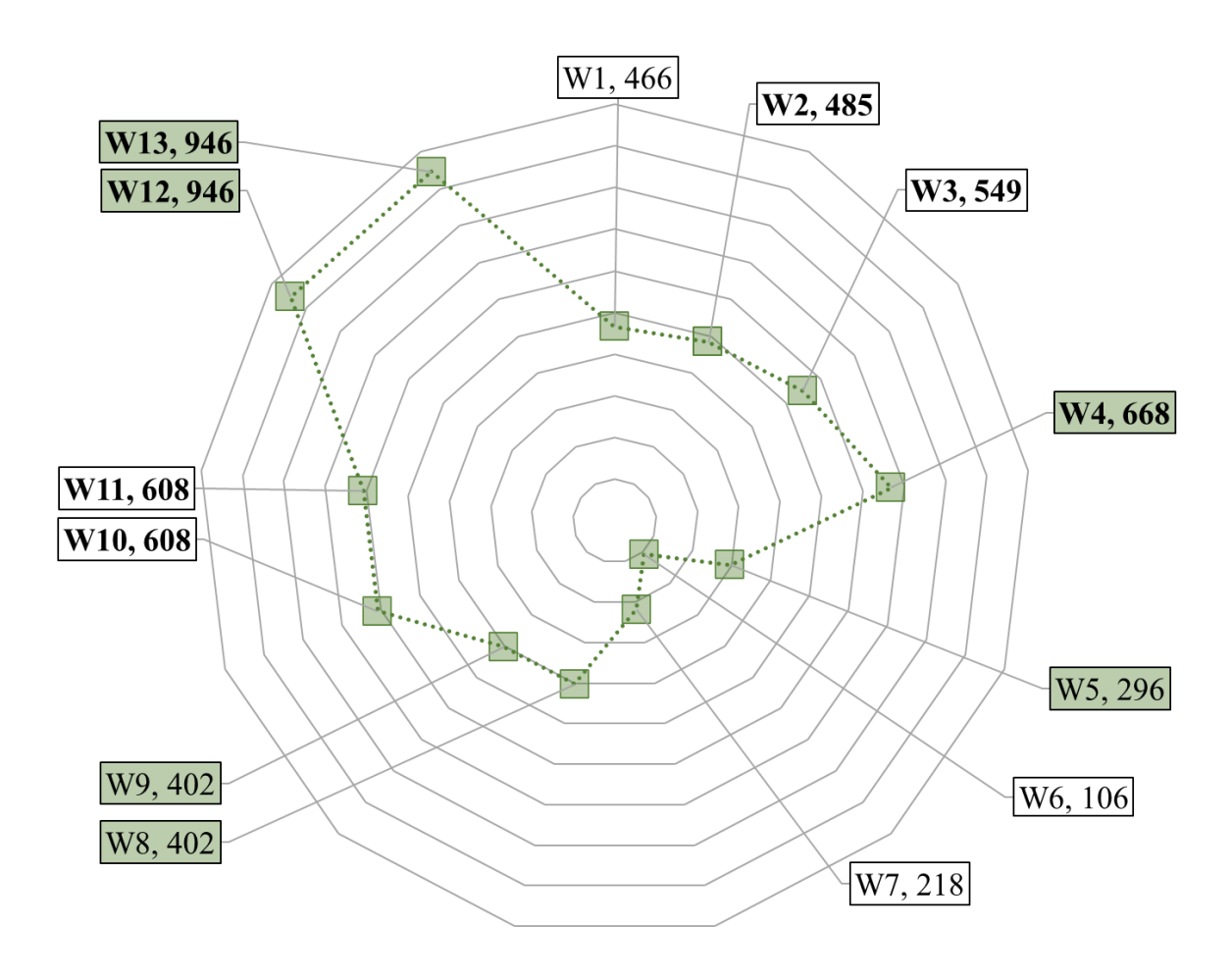
$$\lambda^3 = \frac{V_{PWR-W-1000}}{V_{PWR-W-xxx}}$$

	Free Volume (m3)	Scaling factor (-)
PWR-W-700	39822	1.15
PWR-W-900	48055	1.08
PWR-W-1000	61694	1
PWR-W-1300	71640	0.95

Table 4. PWR-W containment free volumes and scaling factors

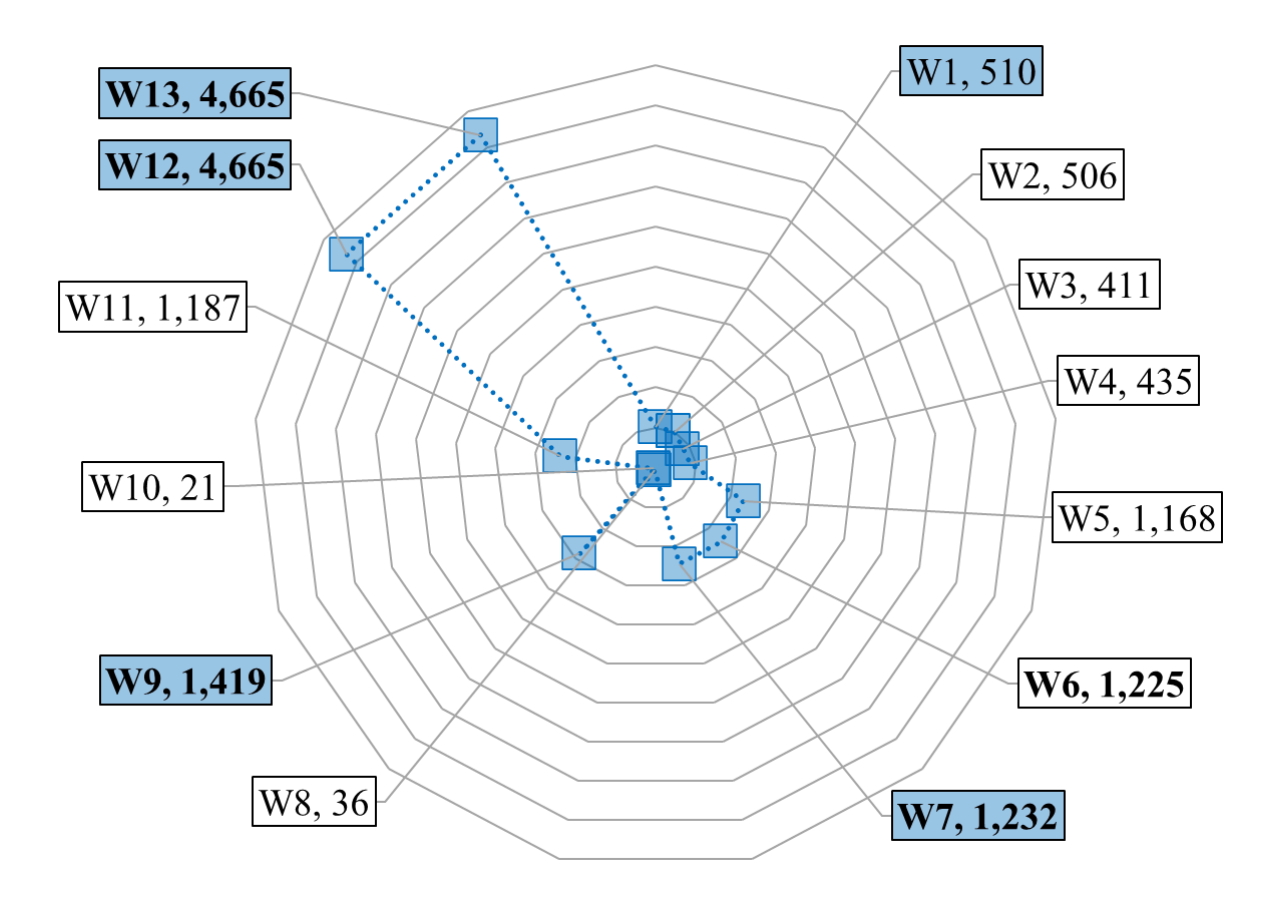
Also, for the cases with/without PARs as the single parametric variation, only the cases with PARs have been included in the classification since each pair of cases are identical in terms of combustible gas releases.

The data for the PWR-W sequences can be found in Figure 20 to Figure 22. There, the five sequences with the higher values of total integrated mass are highlighted in bold letters, while the most conservative sequence per type of reactor has its data label colored. The integrated masses are separated between in-vessel and ex-vessel phase.



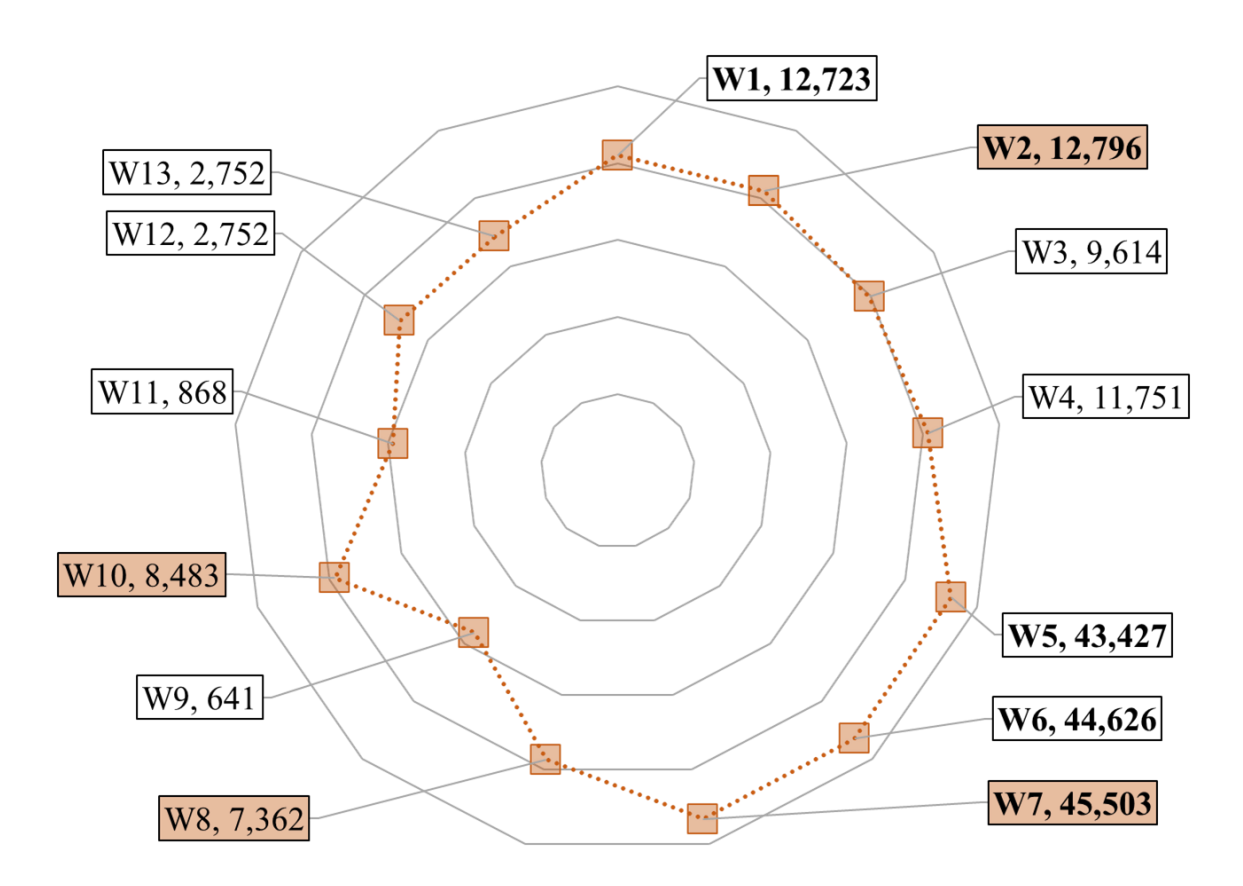
ID#	Sequence	Total integrated mass of H2 in-vessel phase (kg)
W1	1000_LBLOCA	466.3
W2	1000_SBLOCA_FC	484.5
W3	1000_SBLOCA_SPRAY	548.6
W4	1000_SBO	668
W5	700_SBO	296.5
W6	700_SBO_LBLOCA	106
W7	700_SBO_SBLOCA	218.4
W8 W9	900_LOCA	402.4
W10 W11	1300_LOCA	608.2
W12 W13	1300_SBO	945.9

Figure 20. PWR-W total H2 mass injected in the in-vessel phase



ID#	Sequence	Total integrated mass of H2 ex-vessel phase (kg)	
W1	1000_LBLOCA	509.8	
W2	1000_SBLOCA_FC	506.5	
W3	1000_SBLOCA_SPRAY	411.1	
W4	1000_SBO	434.8	
W5	700_SBO	1168	
W6	700_SBO_LBLOCA	1225	
W7	700_SBO_SBLOCA	1232	
W8	900_LOCA_limestone	35.51	
W9	900_LOCA_siliceous	1419	
W10	1300_LOCA_limestone	21	
W11	1300_LOCA_siliceous	1187	
W12	1300_SBO_limestone	4665	
W13	1300_SBO_siliceous	4665	

Figure 21. PWR-W total H2 mass injected in the ex-vessel phase



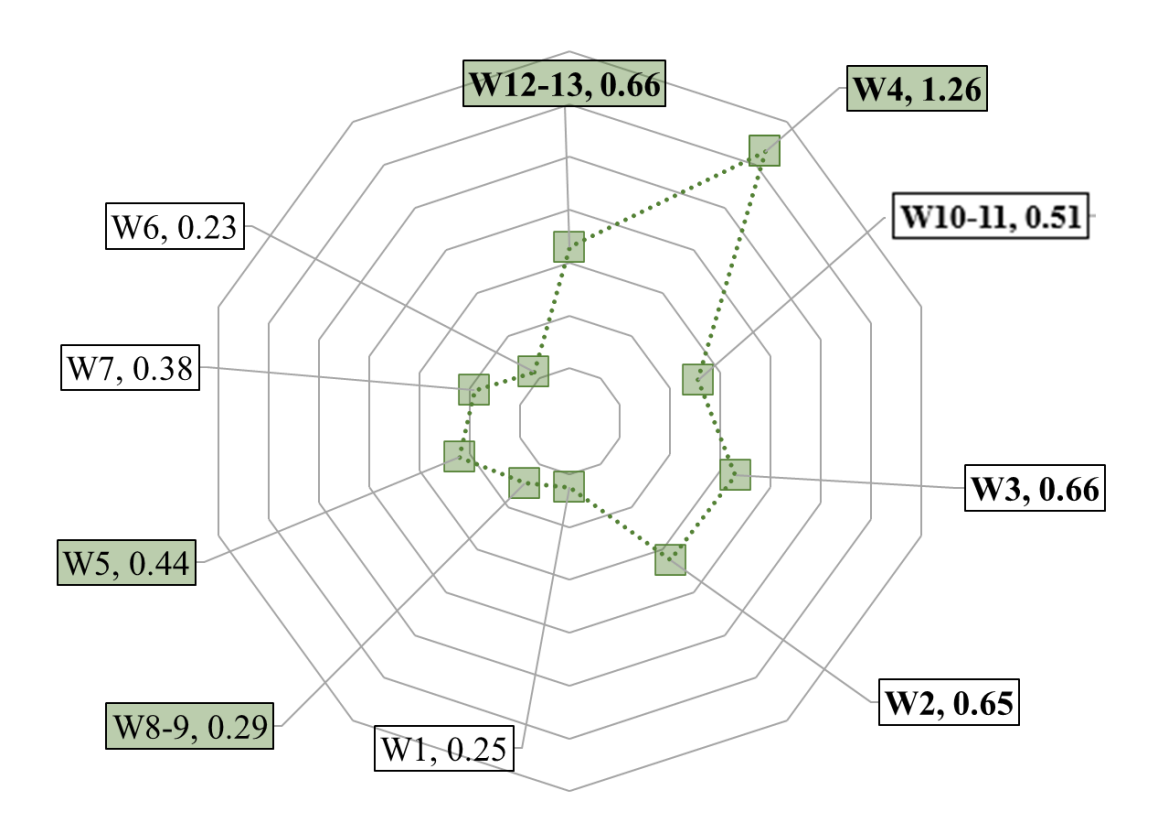
ID#	Sequence	Total integrated mass of CO ex-vessel phase (kg)
W1	1000_LBLOCA	12723
W2	1000_SBLOCA_FC	12796
W3	1000_SBLOCA_SPRAY	9614
W4	1000_SBO	11751
W5	700_SBO	43427
W6	700_SBO_LBLOCA	44626
W7	700_SBO_SBLOCA	45503
W8	900_LOCA_limestone	7362
W9	900_LOCA_siliceous	641
W10	1300_LOCA_limestone	8483
W11	1300_LOCA_siliceous	868
W12	1300_SBO_limestone	2752
W13	1300_SBO_siliceous	2752

Figure 22. PWR-W total CO mass injected in the ex-vessel phase (in logarithmic scale)

I.1.2 Selection based on fast releases of combustible gases

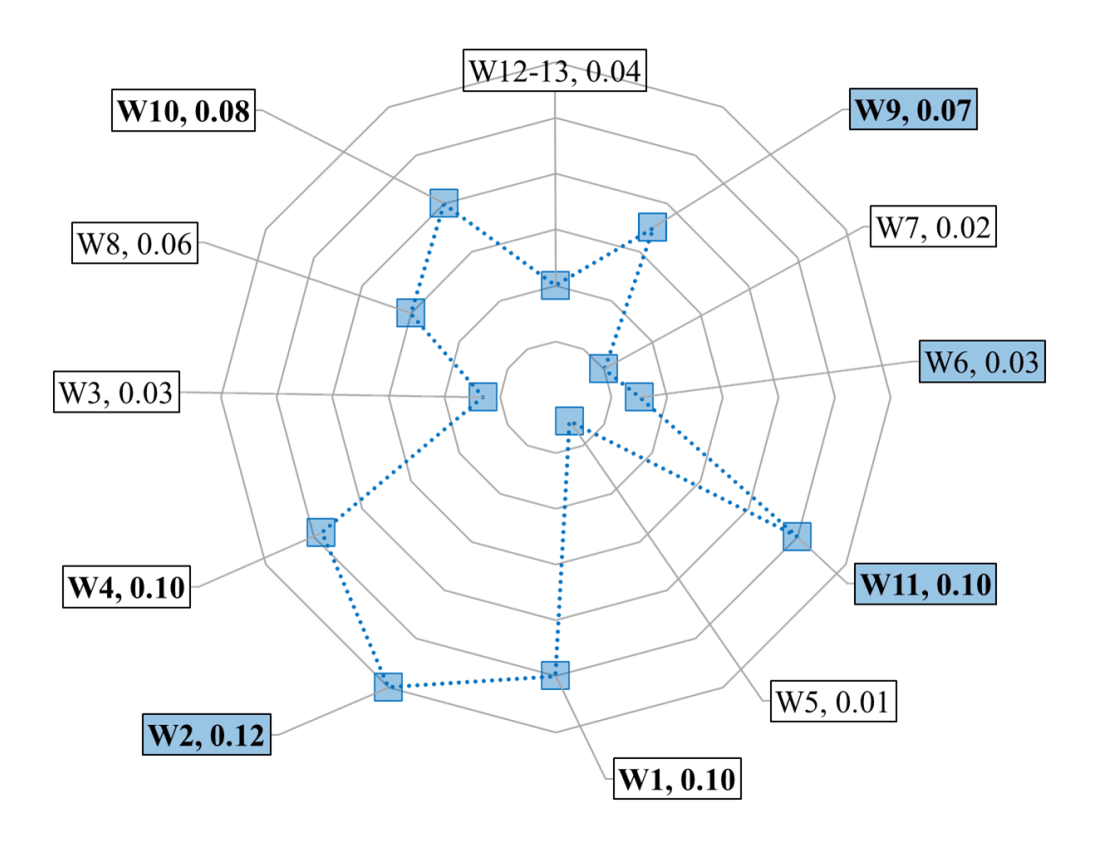
Another important criterion for the selection of the sequences is based on the effects that the kinetic of combustible gases release can have in the containment (Bentaib et al. 2010). Thus, a second classification of the proposed SA sequences has been carried out by calculating the maximum peaks of hydrogen release during the transients. The data has been interpolated with a piecewise constant scheme of 60 seconds. By obtaining the flow rates from an integral curve with a constant time frequency of 60 seconds, we avoid the selection of non-relevant peak values occurring during less than one second. The purpose is to identify releases fast enough to minimize the actions of the PARs, which don't have enough time to recombine all the combustible gases that are released to the containment at that point in time.

The data for the PWR-W sequences can be found in Figure 23 to Figure 25. There, the five sequences with the higher values of total integrated mass are highlighted in bold letters, while the most conservative sequence per type of reactor has its data label colored. Also, the order in which the values appear in the figures depends on the previous criterion; i.e., the sequences with the maximum values of total integrated mass, appear in a clockwise disposition in decreasing order. Moreover, the graphs distinguish between in- and ex-vessel phases for hydrogen and carbon monoxide.



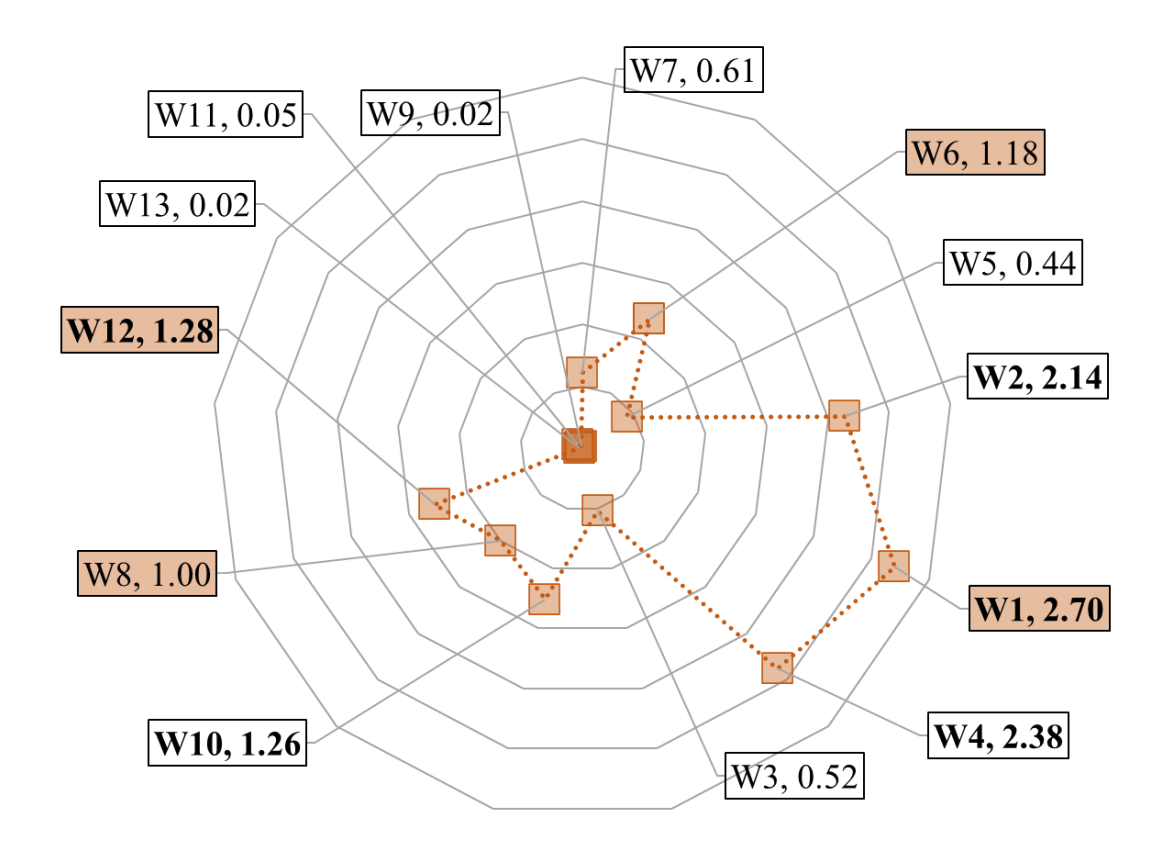
ID#	Sequence	Maximum in-vessel H2 release rate (kg/s)	Time of maximum H2 release rate (h)
W1	1000_LBLOCA	0.25	0.78
W2	1000_SBLOCA_FC	0.65	0.64
W3	1000_SBLOCA_SPRAY	0.66	0.72
W4	1000_SBO	1.26	3.55
W5	700_SBO	0.44	2.51
W6	700_SBO_LBLOCA	0.23	0.28
W7	700_SBO_SBLOCA	0.38	0.51
W8 W9	900_LOCA	0.29	0.98
W10 W11	1300_LOCA	0.51	1.65
W12 W13	1300_SBO	0.66	4.14

Figure 23. PWR-W H2 release rate peaks at in-vessel phase



ID#	Sequence	Maximum ex-vessel H2 release rate (kg/s)	Time of maximum H2 release rate (h)
W1	1000_LBLOCA	0.1	2.92
W2	1000_SBLOCA_FC	0.12	2.13
W3	1000_SBLOCA_SPRAY	0.026	1.97
W4	1000_SBO	0.097	8.29
W5	700_SBO	0.01	342
W6	700_SBO_LBLOCA	0.03	0.96
W7	700_SBO_SBLOCA	0.02	2.12
W8	900_LOCA_limestone	0.06	3.75
W9	900_LOCA_siliceous	0.07	3.6
W10	1300_LOCA_limestone	0.08	3.87
W11	1300_LOCA_siliceous	0.10	3.74
W12	1300_SBO_limestone	0.04	15.91
W13	1300_SBO_siliceous	0.04	15.91

Figure 24. PWR-W H2 release rate peaks at ex-vessel phase



ID#	Sequence	Maximum ex-vessel CO release rate (kg/s)	Time of maximum CO release rate (h)
W1	1000_LBLOCA	2.7	2.92
W2	1000_SBLOCA_FC	2.14	1.96
W3	1000_SBLOCA_SPRAY	0.52	4.87
W4	1000_SBO	2.38	8.29
W5	700_SBO	0.44	3.42
W6	700_SBO_LBLOCA	1.18	0.96
W7	700_SBO_SBLOCA	0.61	2.12
W8	900_LOCA_limestone	1	3.75
W9	900_LOCA_siliceous	0.02	3.6
W10	1300_LOCA_limestone	1.26	3.87
W11	1300_LOCA_siliceous	0.05	3.74
W12	1300_SBO_limestone	1.28	13.12
W13	1300_SBO_siliceous	0.02	15.91

Figure 25. PWR-W CO release rate peaks at ex-vessel phase

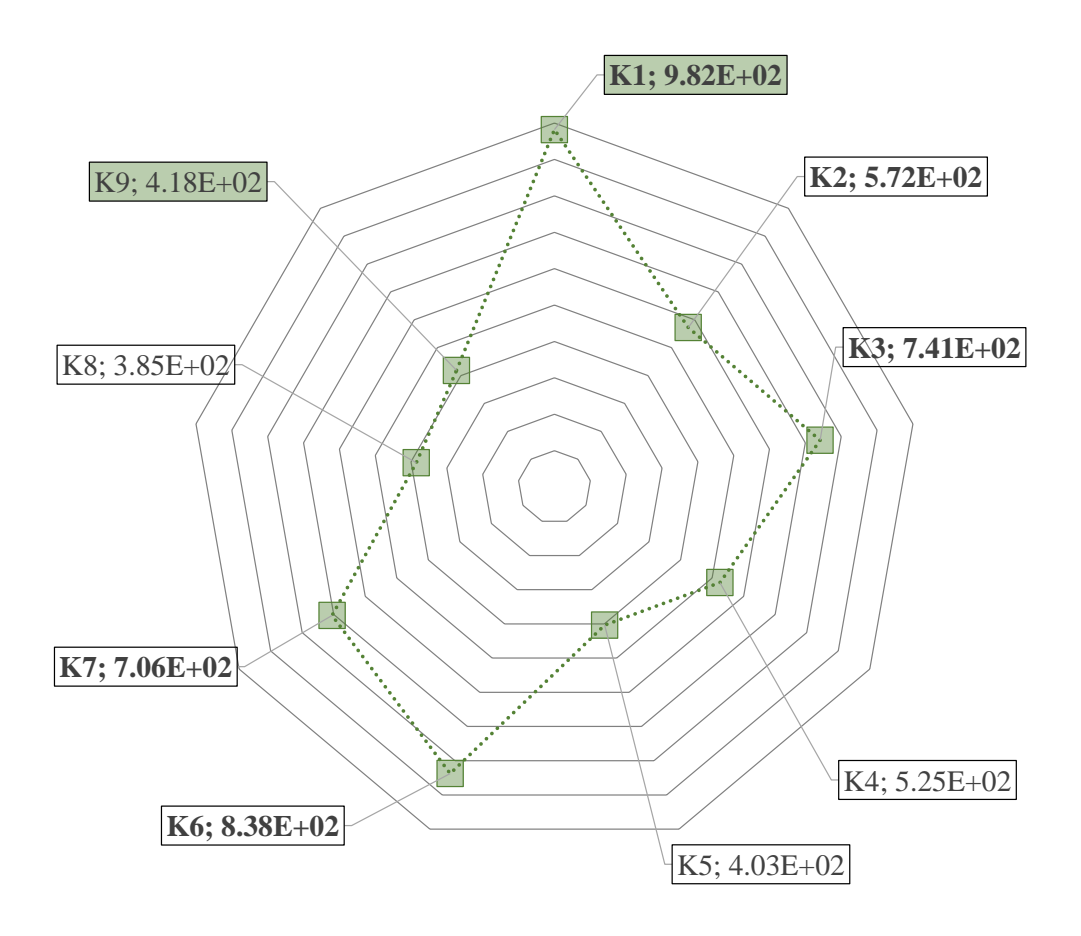
I.2 PWR-KWU selection criteria

I.2.1 Selection based on total mass of combustible gases

For this type of containment, the results have not been scaled. The data for the PWR-KWU sequences can be found in Figure 26 to Figure 28. There, the five sequences with the higher values of total integrated mass are highlighted in bold letters, while the most conservative sequence per type of reactor has its data label colored.

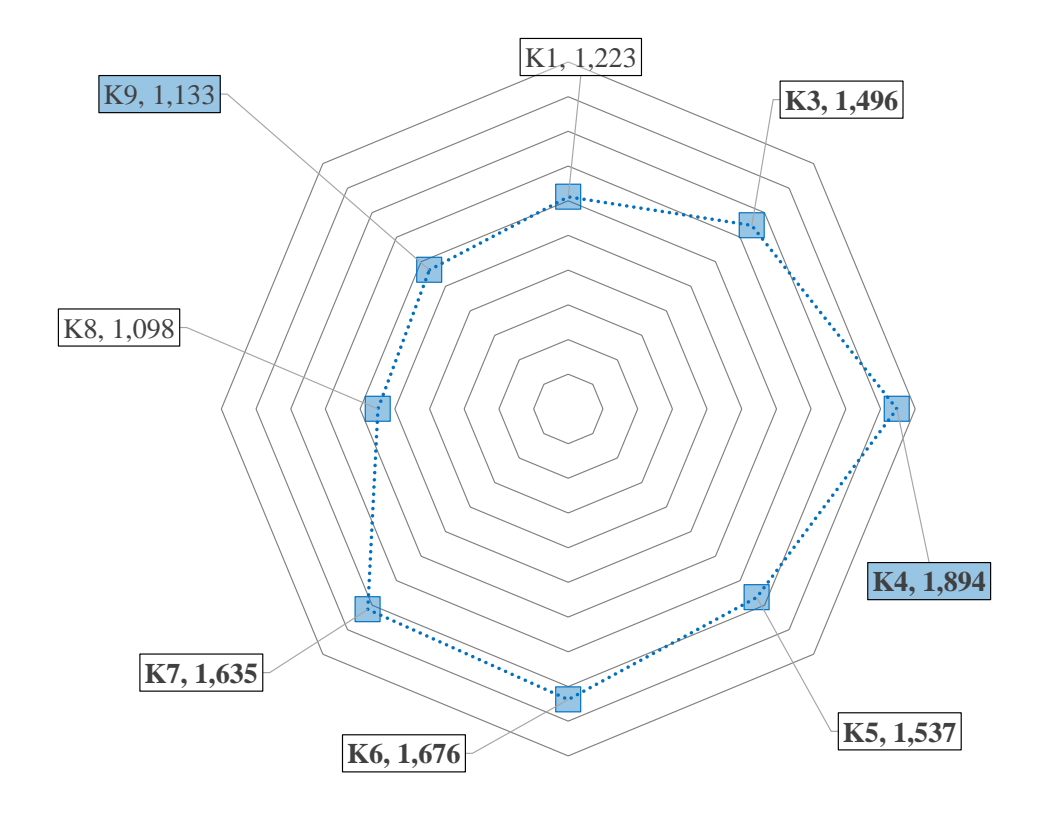
I.2.2 Selection based on fast releases of combustible gases

The data for the PWR-KWU sequences can be found in Figure 29 to Figure 31. There, the five sequences with the higher values of total integrated mass are highlighted in bold letters, while the most conservative sequence per type of reactor has its data label colored. Also, the order in which the values appear in the figures depends on the previous criterion; i.e., the sequences with the maximum values of total integrated mass, appear in a clockwise disposition in decreasing order. Moreover, the graphs distinguish between in- and ex-vessel phases for hydrogen and carbon monoxide.



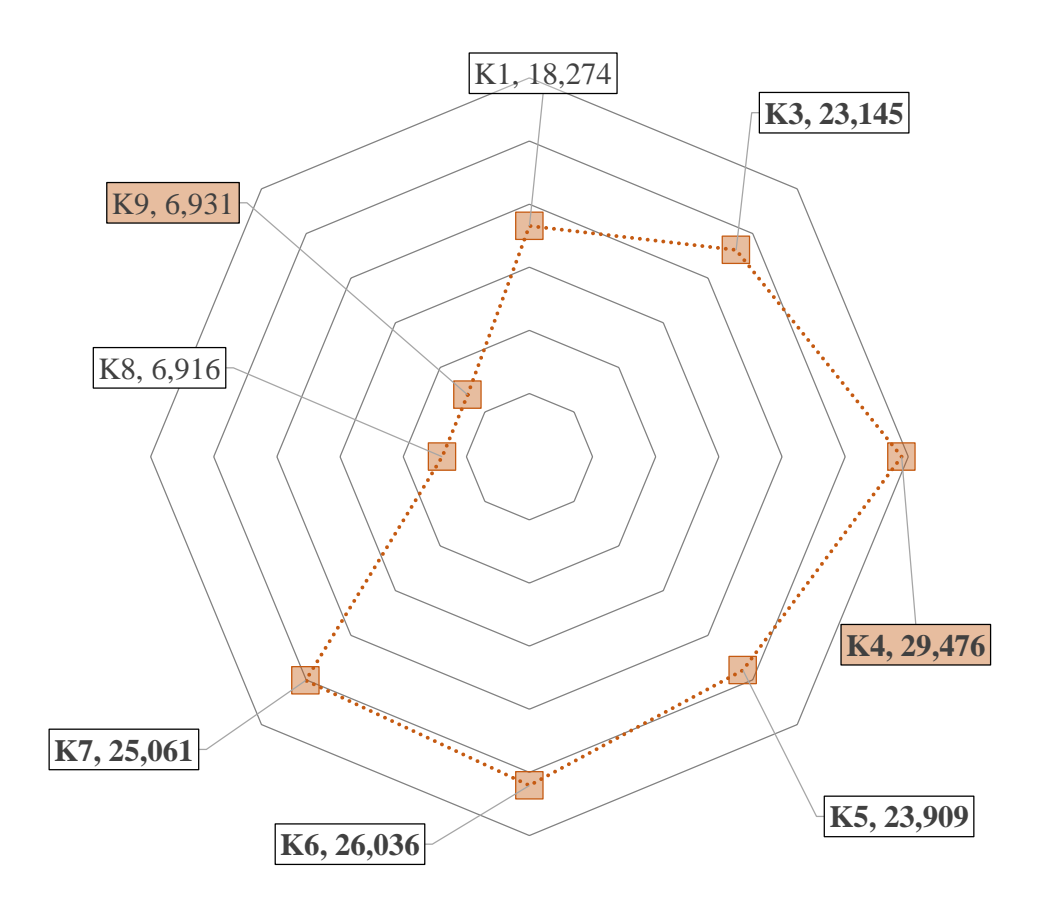
ID#	Sequence	Total integrated mass of H2 in-vessel phase (kg)
K1	FRAM_L05	982
К2	FRAM_L80c_onlyEBS	572
К3	FRAM_L80h	741.1
К4	FRAM_L80h_woSI	524.9
К5	FRAM_L380	403.4
К6	FRAM_SBO	837.6
К7	FRAM_SBO+30	705.5
К8	RUB_SBLOCA	385.31
К9	RUB_SBO	418.37

Figure 26. PWR-KWU total H2 mass injected in the in-vessel phase



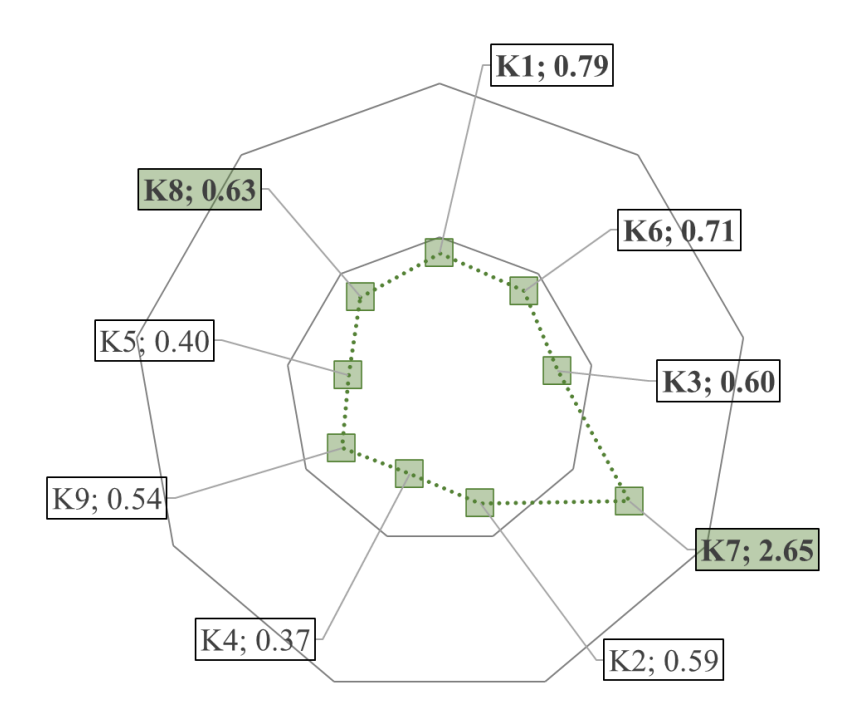
ID#	Sequence	Total integrated mass of H2 ex-vessel phase (kg)
K1	FRAM_L05	1222.5
К3	FRAM_L80h	1496
К4	FRAM_L80h_woSI	1894.2
К5	FRAM_L380	1536.5
К6	FRAM_SBO	1675.5
К7	FRAM_SBO+30	1634.5
К8	RUB_SBLOCA	1097.87
К9	RUB_SBO	1132.74

Figure 27. PWR-KWU total H2 mass injected in the ex-vessel phase



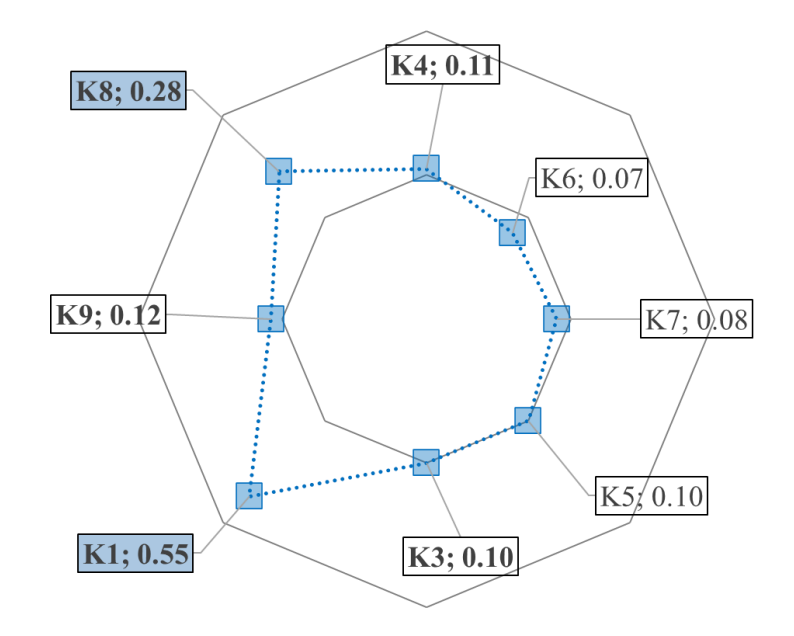
ID#	Sequence	Total integrated mass of CO ex-vessel phase (kg)
K1	FRAM_L05	18273.9
К3	FRAM_L80h	23145.3
К4	FRAM_L80h_woSI	29475.8
К5	FRAM_L380	23908.9
К6	FRAM_SBO	26036.4
К7	FRAM_SBO+30	25061.1
К8	RUB_SBLOCA	6916.4
К9	RUB_SBO	6930.5

Figure 28. PWR-KWU total CO mass injected in the ex-vessel phase (in logarithmic scal



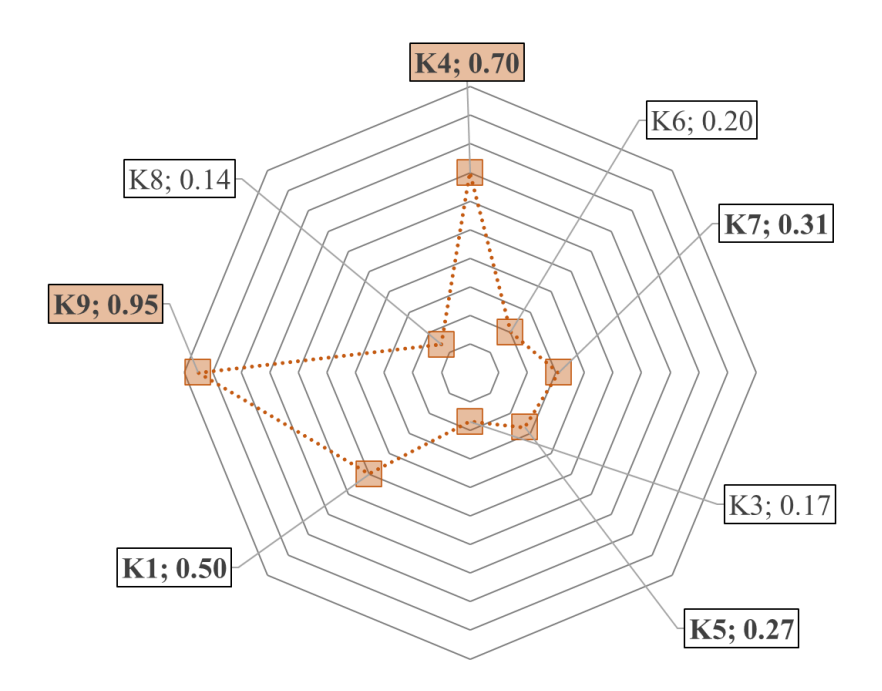
ID#	Sequence	Maximum in-vessel H2 release rate (kg/s)	Time of maximum H2 release rate (h)
K1	FRAM_L05	0.79	27.18
K2	FRAM_L80c_onlyEBS	0.59	1.6
К3	FRAM_L80h	0.6	6.45
К4	FRAM_L80h_woSI	0.37	1.63
K5	FRAM_L380	0.4	1.89
К6	FRAM_SBO	0.71	4.61
К7	FRAM_SBO+30	2.65	2.67
К8	RUB_SBLOCA	0.63	5.64
К9	RUB_SBO	0.54	3.23

Figure 29. PWR-KWU H2 release rate peaks at in-vessel phase (in logarithmic scale)



ID#	Sequence	Maximum ex-vessel H2 release rate (kg/s)	Time of maximum H2 release rate (h)
K1	FRAM_L05	0.55	27.27
К3	FRAM_L80h	0.1	14.94
К4	FRAM_L80h_woSI	0.11	7.8
K5	FRAM_L380	0.1	8.14
К6	FRAM_SBO	0.07	13.92
К7	FRAM_SBO+30	0.08	14.74
К8	RUB_SBLOCA	0.28	6.67
К9	RUB_SBO	0.12	4.32

Figure 30. PWR-KWU H2 release rate peaks at ex-vessel phase (in logarithmic scale)



ID#	Sequence	Maximum ex-vessel CO release rate (kg/s)	Time of maximum H2 release rate (h)
K1	FRAM_L05	0.5	27.69
К3	FRAM_L80h	0.17	10.14
К4	FRAM_L80h_woSI	0.7	3.42
K5	FRAM_L380	0.27	4.6
K6	FRAM_SBO	0.2	9.62
К7	FRAM_SBO+30	0.31	10.1
К8	RUB_SBLOCA	0.14	15.76
К9	RUB_SBO	0.95	7.27

Figure 31. PWR-KWU CO release rate peaks at ex-vessel phase

I.3 Conclusions

• For the **PWR-W containments**, the highest total integrated mass of hydrogen in the invessel phase has been found in the SBO sequences of the PWR-1000 and PWR-W 1300 containment types, while for the ex-vessel phase the highest amount of hydrogen is released at the SBO sequence of the PWR-1300 and in the LOCA of PWR-900. Regarding the total integrated mass of carbon monoxide released at the ex-vessel phase, the highest values correspond to the PWR-700 sequences and the PWR-W 1000 LOCAs.

Looking into the highest peak of combustible gases release rates, for the in-vessel phase the highest values of hydrogen appear at PWR-1000 & -1300 SBO, while for the ex-vessel phase they appear at the PWR-1300 LOCA and PWR-1000 SBLOCA_FC. In the case of the carbon monoxide, the highest values are present at PWR-1000 LBLOCA and SBO and PWR-1300 SBO.

The JSI sequences maximize the CO production. However, a qualitative assessment reveals that the larger productions are correlated with the longer transients (up to 300000 s) simulated by JSI. It should be considered that these transients' durations may be unaffordable for the calculation with 3D codes in WP4. Furthermore, the O₂ is already consumed at these late stages of the ex-vessel phase, with the corresponding limitation of the combustion risk.

Therefore, the most relevant cases might be the following:

- PWR-1000 LBLOCA, which has the largest production of combustible gases within the PWR-1000 sequences and with an ex-vessel phase starting way before other sequences (< 3h). This creates a scenario with a large concentration of combustible gases before the oxygen consumption related to the PARs operation.
- PWR-1300 SBO, which shows the highest values of hydrogen release both in the in-vessel and ex-vessel phases and the largest fast release.
- For the PWR-KWU containments, the highest total integrated mass of hydrogen in the in-vessel phase has been found in FRAMATOME's SBLOCA (L05) and SBO, while for the ex-vessel phase the highest amount of hydrogen is released at FRAMATOME's SBO and MBLOCA (L80h_woSI). Regarding the total integrated mass of carbon monoxide released at the ex-vessel phase, the highest values again correspond to FRAMATOME's SBO and MBLOCA (L80h_woSI).

Looking into the highest peak of combustible gases release rates, for the in-vessel phase the highest values of hydrogen concentration appear at FRAMATOME's SBLOCA and SBO+30, while for the ex-vessel phase they appear at FRAMATOME's SBLOCA and RUB's SBLOCA. In the case of the carbon monoxide, the highest values are present at RUB's SBO and FRAMATOME's SBLOCA.

Therefore, the most relevant cases are <u>FRAMATOME's SBO, MBLOCA (L80h woSI)</u>, and SBLOCA.

• For the **PWR-VVER containment**, the highest total integrated mass of H₂ and of total combustible gases (H₂ + CO) in the in-vessel phase has been found in the SBO with exvessel activation of sprays. Regarding the total integrated mass of combustible gases at the ex-vessel phase, the LBLOCA+SBO with PARs and sprays at ex-vessel phase, is the one showing the highest amount of combined H₂ and CO. Nevertheless, looking only to the CO generation at ex-vessel phase, the SBLOCA+SBO without PARs and sprays at in-vessel phase stands out, whereas for H₂ generation is again the LBLOCA+SBO but with sprays activated at the in-vessel phase. Adding up the in- and ex-vessel phases, data shows that indeed the SBO and SBLOCA sequences are the most relevant in terms of total generated mass of combustible gases. Regarding the molar fraction of combined H₂ + CO during the whole transients, the SBO sequences stand out as the most relevant. Finally, looking into the highest peak of combustible gases release rates, the LBLOCA+SBO (in- and ex-vessel spray activation) sequences are the ones showing higher values.

Therefore, the relevant sequences to study could be (in order of priority and in line with the hierarchy of selection criteria): the SBO sequences with spray activation at in-/ex-vessel stages without PARs and the SBLOCA+SBO with sprays activated in the in-vessel phase.

I.4 References

Bentaib, Ahmed, Cataldo Caroli, Bernard Chaumont, and Karine Chevalier-Jabet. 2010. 'Evaluation of the Impact That PARs Have on the Hydrogen Risk in the Reactor Containment: Methodology and Application to PSA Level 2'. Science and Technology of Nuclear Installations 2010:1–7. doi: 10.1155/2010/320396.

Benteboula, S., J. Malet, and A. Bleyer. 2015. 'EU-ERCOSAM PROJECT Scaling from Nuclear Power Plant to Experiments'. 12.

ANNEX II. Individual report for the PWR-W900 and W1300 reactors (IRSN)

II.1 Introduction

The objective of WP2 is to identify SA sequences leading to high H2/CO combustion risk. For that purpose, IRSN performed a set of simulations with the lumped-parameters code ASTEC V2.1 for two French PWR type reactors: 900 MWe reactors and 1300 MWe reactors (P'4 series).

Two SA sequences, leading to RPV failure and MCCI, have been considered: a 12 inch hot leg LOCA sequence for both type reactors, and a SBO sequence for 1300 MWe reactors only. Two types of concrete basemat (limestone and siliceous)³ have been considered, as the composition affects the hydrogen and carbon monoxide production during MCCI. The PARs installed in the containment have been considered. However, in order to assess their impact on the combustion risk, all the calculations have been repeated without PARs. Therefore, a total of 12 SA sequences are presented and analysed in this section.

II.2 Plant model

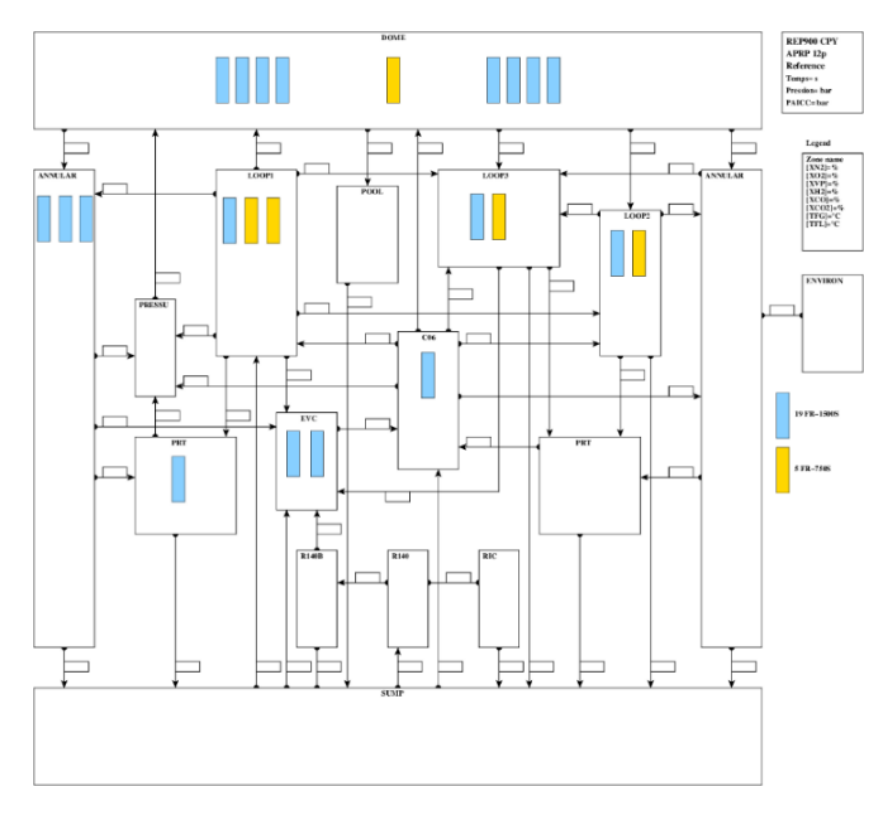
French 900 MWe PWR

900 MWe reactors have a single-wall containment building with a steel liner. The free volume of the containment is about 50 000 m³. The ASTEC nodalization for the containment is depicted in the figure below. The containment is divided in 14 zones, connected through 41 atmospheric junctions and 25 liquid junctions, and includes 195 wall structures. The 24 FRAMATOME type PARs installed in the containment (19 "FR-1500S" PARs and 5 "FR-750S" PARs) are modelled using the manufacturer correlation.

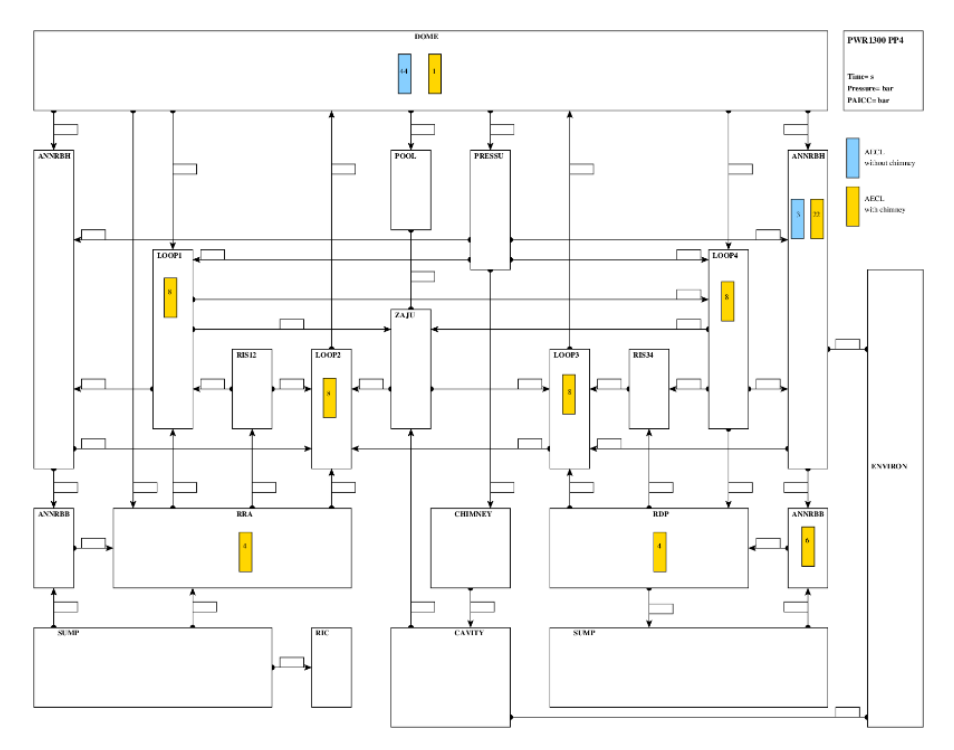
French 1300 MWe PWR

1300 MWe reactors (P'4 series) have a double concrete wall containment building. The free volume of the inner containment is about 70 000 m³. The ASTEC nodalization for the containment is depicted in the figure below. The containment is divided in 18 zones, connected through 49 atmospheric junctions and 37 liquid junctions, and includes 108 wall structures. The 116 AECL type PARs installed in the containment (66 with a chimney and 50 without chimney) are modelled using the manufacturer correlation.

³ Two representative concrete compositions (limestone and siliceous) have been selected for each reactor type (they differ slightly between the two reactor types).



ASTEC nodalization of the containment of a French 900 MWe PWR (PARs in blue and yellow)



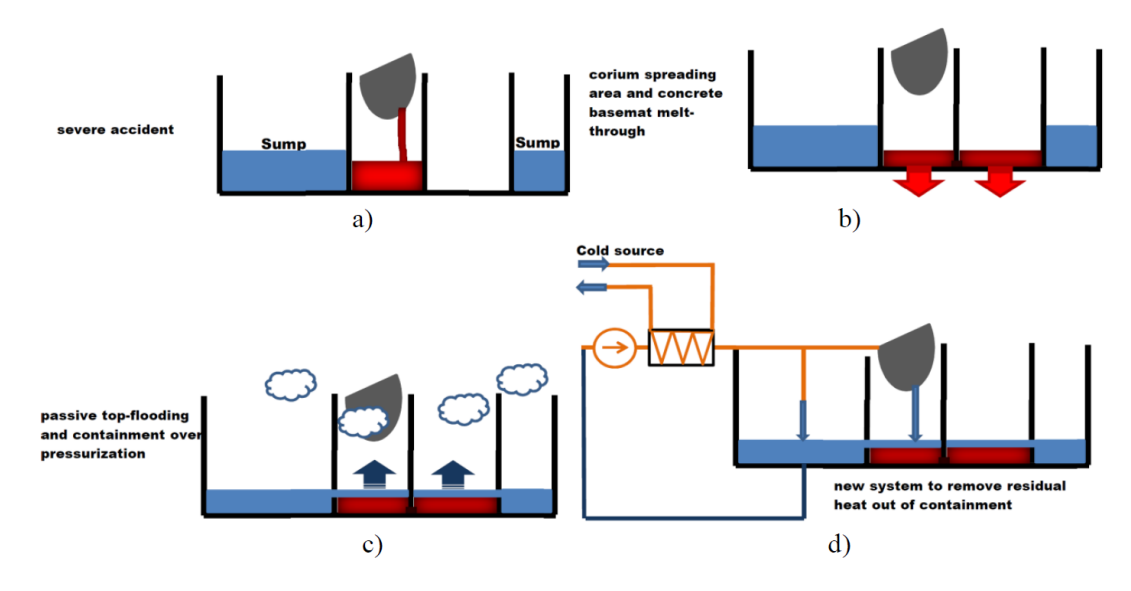
ASTEC nodalization of the containment of a French1300 MWe (P'4) PWR (PARs in blue and yellow)

II.3 Sequences description

900 MWe -12 inch hot leg LOCA

The scenario is initiated by a 12-inch break in the hot leg of loop 1. Afterwards, the main events are summarized in the table below. After the RPV failure, the strategy consists in stabilizing the corium in the dry vessel cavity and an adjacent area, flood it by the top and removing the heat from the containment without venting. The different phases are described in the figure below:

In-vessel phase	12 inch break in the hot leg of loop 1	0
	Spray system activation	
	Recirculation mode failure leading to the loss of safety injection and containment spray system	
	Beginning of severe accident	57 minutes
	RPV failure	2h50
Ex-vessel phase	Corium spreading in the reactor pit and the incore instrumentation room	
Corium flooding by the sump water		3h45
	Ultimate containment heat removal system activation by the Nuclear Action Force (FARN)	24 h



Schematic representations of different phases of stabilization of the corium: a) slump from vessel to dry cavity, b) spreading in dry cavity and dedicated adjacent room, c) top flooding of corium by water, d) ultimate residual heat removal [REF1]

1300 MWe -12 inch hot leg LOCA

The scenario is initiated by a 12 inch break in the hot leg of loop 1. Afterwards, the main events are summarized in the table below. After the RPV failure, the strategy consists in stabilizing the corium in the dry vessel cavity and an adjacent area, flood it by the top and removing the heat from the containment without venting.

In-vessel phase	12 inch break in the hot leg of loop 1	0
	Spray system activation	59 s
	Recirculation mode failure leading to the loss of safety injection and containment spray system	
	Beginning of severe accident	
	RPV failure	3h
Ex-vessel phase	Corium spreading in the reactor pit and the incore instrumentation room	
Corium flooding by the sump water Ultimate containment heat removal system activation by the Nuclear Action Force (FARN)		3h52
		24 h

1300 MWe - SBO

The SBO scenario is initiated by a loss of all offsite power. After the RPV failure, the corium spreads in the reactor pit only (no spreading in the adjacent area, no corium flooding and no ultimate heat removal system activation). The main events are summarized in the table below:

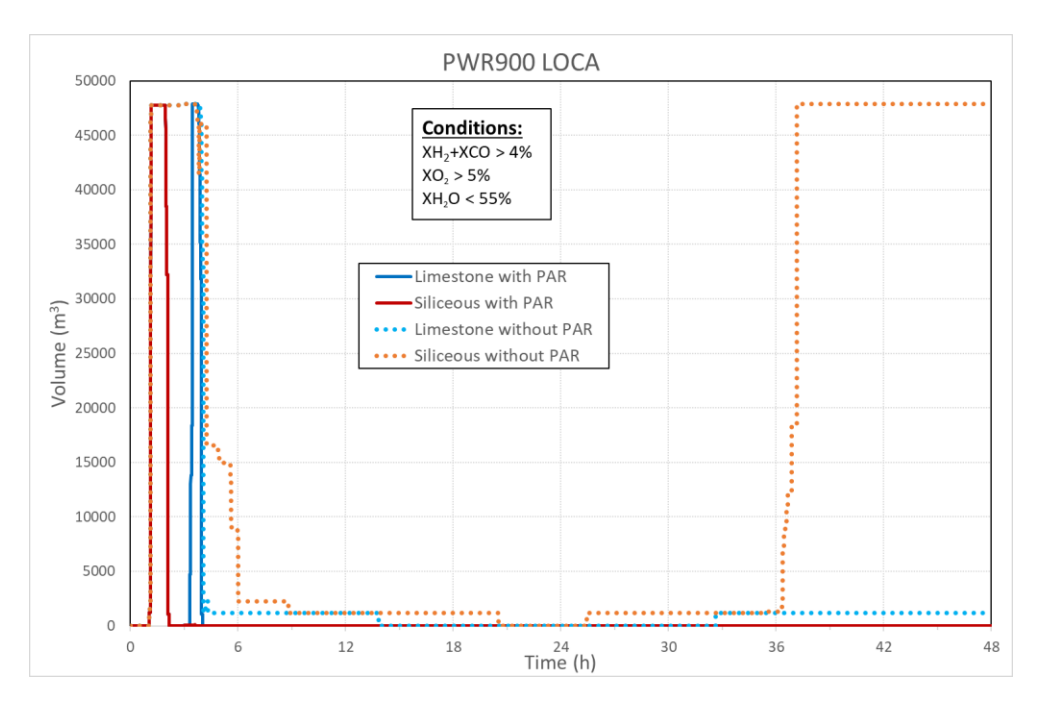
In-vessel phase	Loss of all offsite power	0
	Rupture of PRT (Pressure relief Tank) disks	2h26
	Pressurizer valves locked opened	4h33
	Accumulator tank discharge	4h46
	RPV failure	11h35
Ex-vessel phase	Corium spreading in the reactor pit only	

II.4 Results and discussion

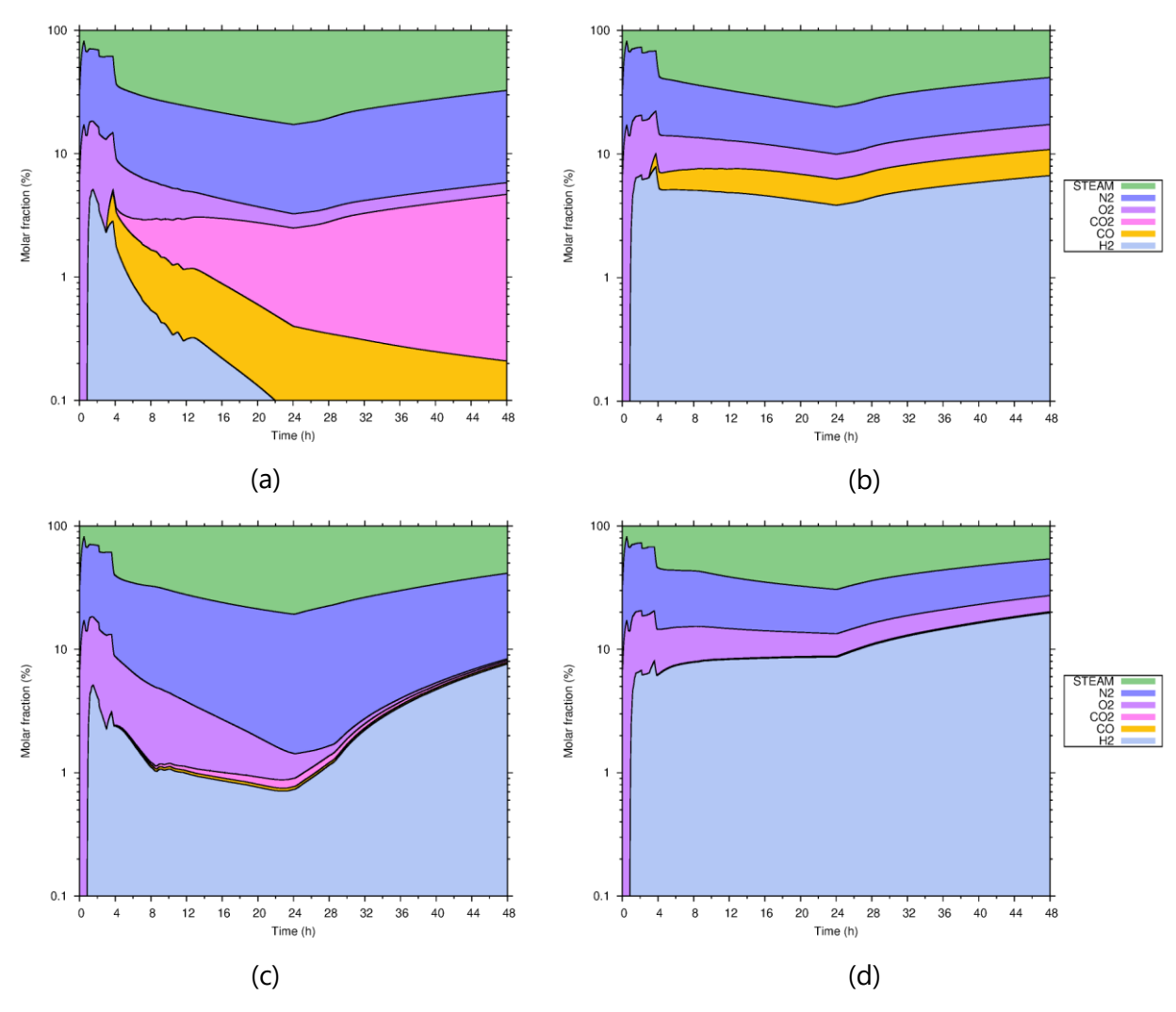
The flammable cloud volume, the gas composition in the dome compartment, and the gas composition on the Shapiro diagram for all the compartments are shown for the 12 simulations listed in the table below.

Simulation	Reactor type	Sequence	Basemat concrete	PARs number
1	900 MWe	12" HL LOCA	Limestone	24
2	900 MWe	12" HL LOCA	Limestone	None
3	900 MWe	12" HL LOCA	Siliceous	24
4	900 MWe	12" HL LOCA	Siliceous	None
5	1300 MWe	12" HL LOCA	Limestone	116
6	1300 MWe	12" HL LOCA	Limestone	None
7	1300 MWe	12" HL LOCA	Siliceous	116
8	1300 MWe	12" HL LOCA	Siliceous	None
9	1300 MWe	SBO	Limestone	116
10	1300 MWe	SBO	Limestone	None
11	1300 MWe	SBO	Siliceous	116
12	1300 MWe	SBO	Siliceous	None

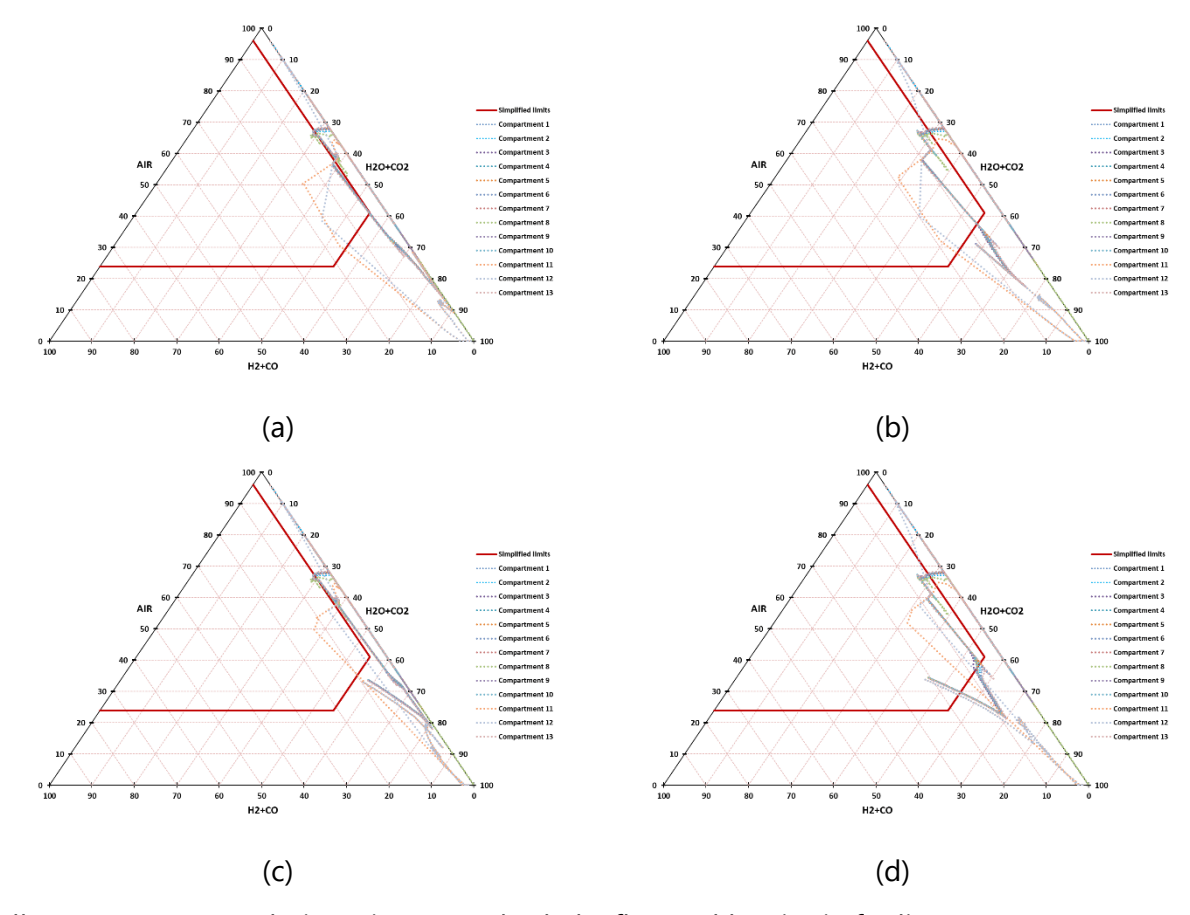
900 MWe -12 inch hot leg LOCA



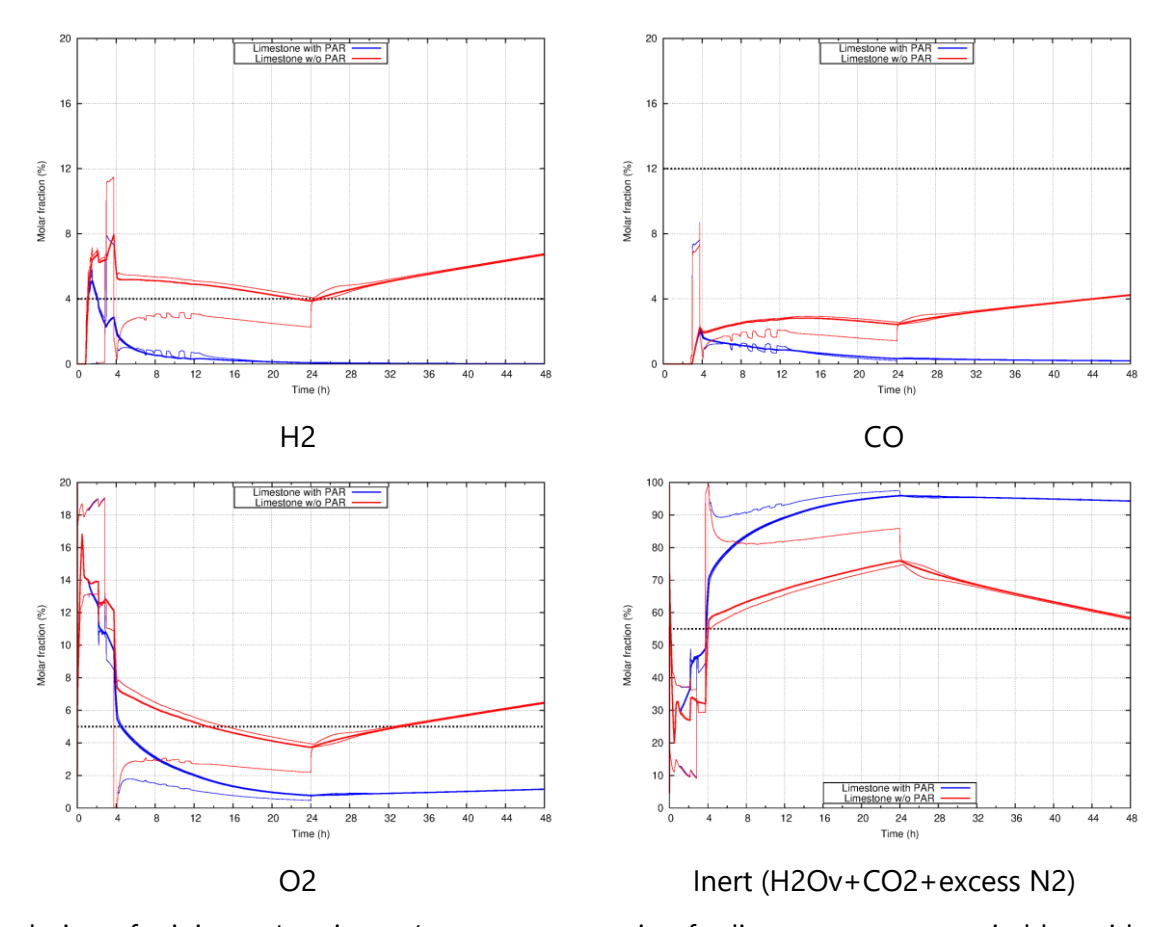
Flammable cloud volume evolution with limestone concrete (in blue) and siliceous concrete (in red), solid lines with PAR and dotted lines without PAR.



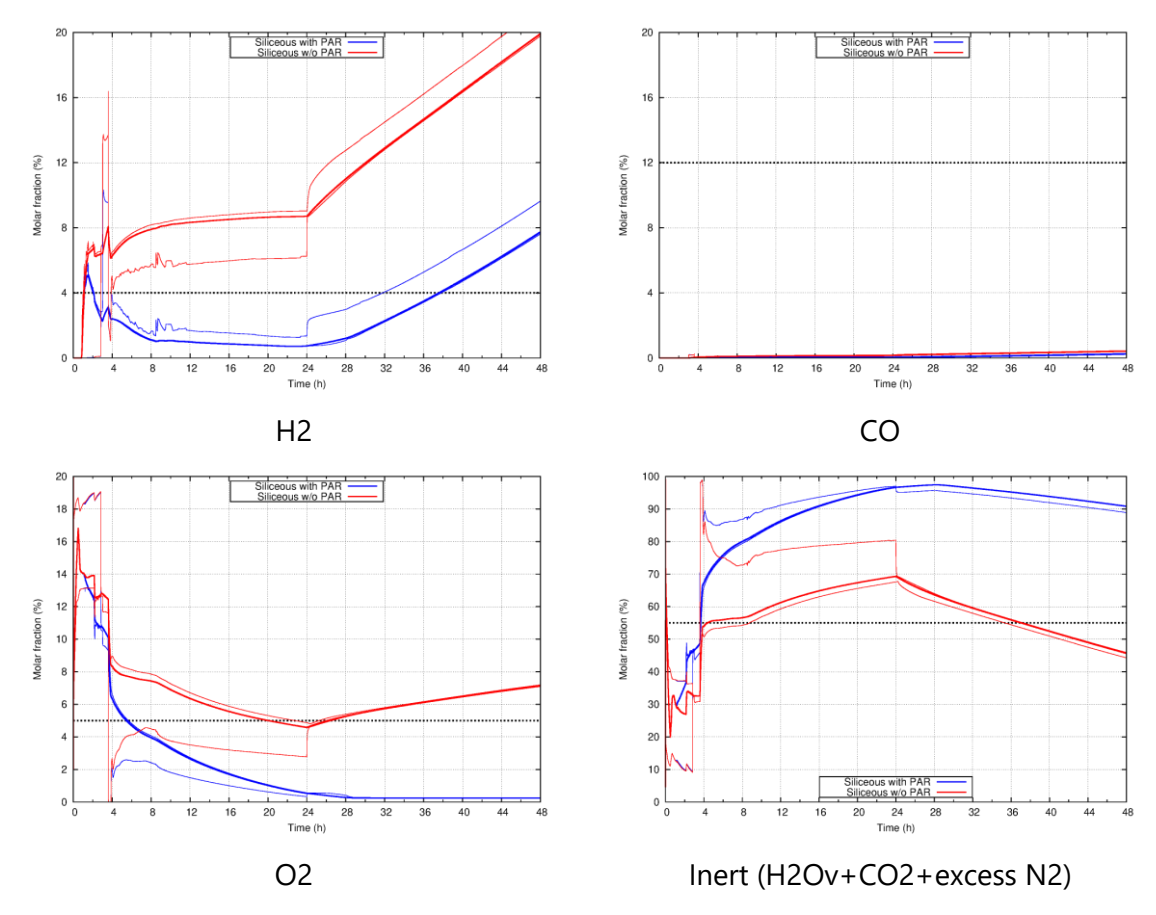
Gas composition in the dome compartment with limestone concrete (a) with PAR and (b) without PAR and siliceous concrete (c) with PAR and (d) without PAR



For all compartments evolution trigram to check the flammable criteria for limestone concrete (a) with PAR and (b) without PAR and for siliceous concrete (c) with PAR and (d) without PAR



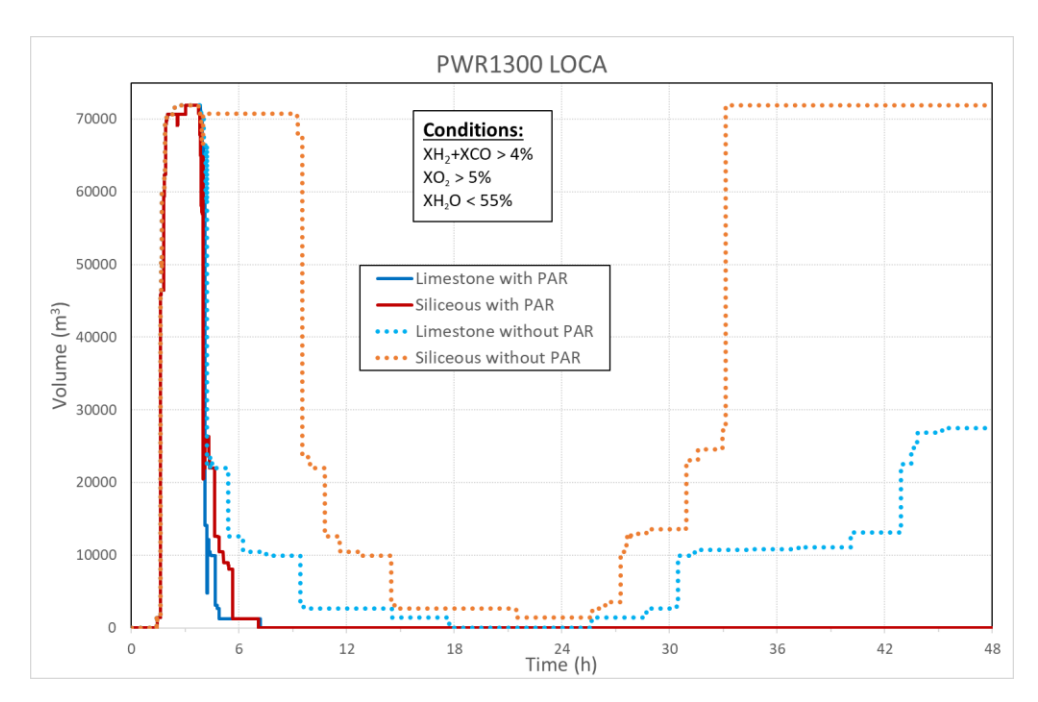
Evolution of minimum/maximum/mean concentration for limestone concrete, in blue with PAR, in red without PAR



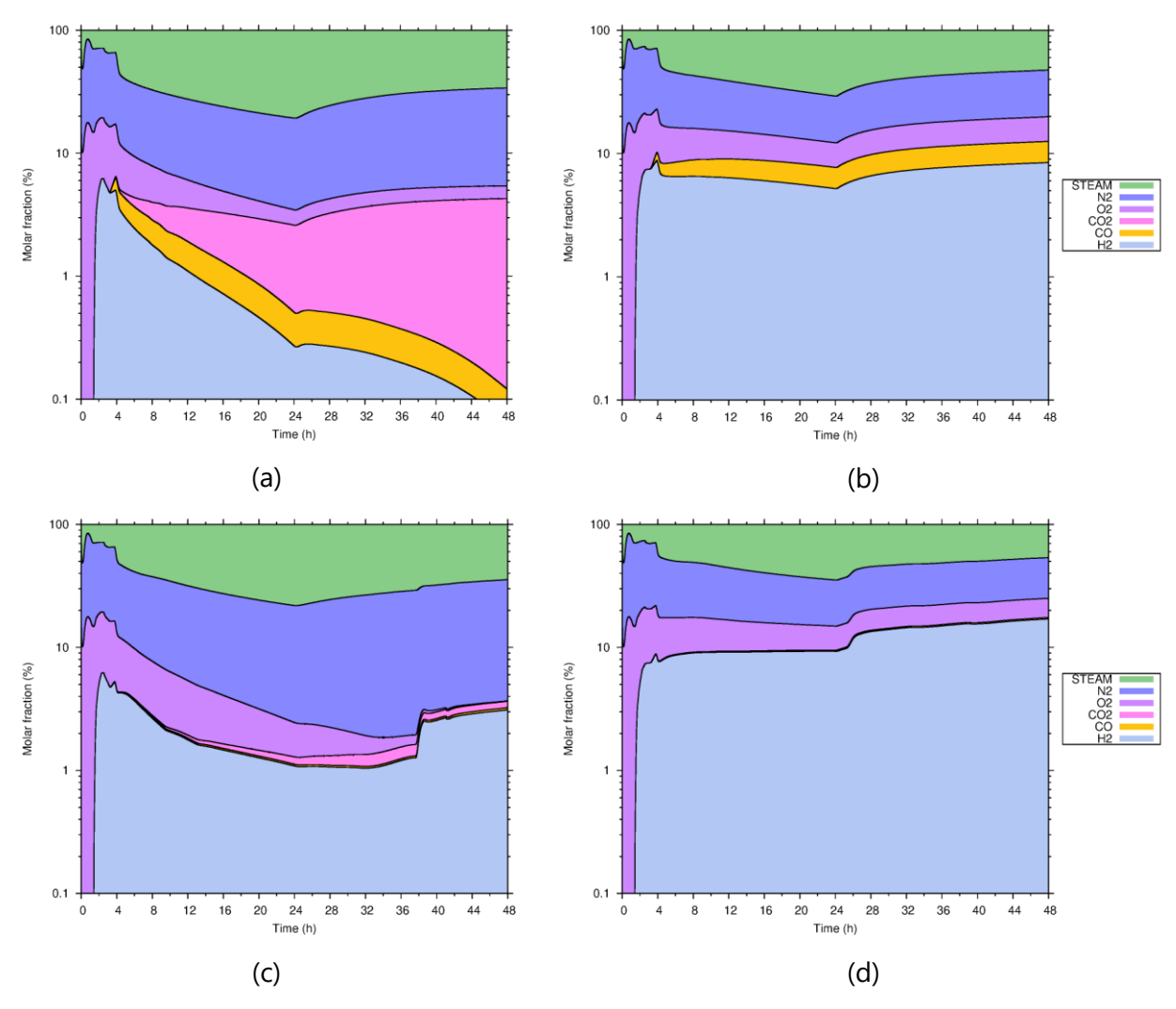
Evolution of minimum/maximum/mean concentration for siliceous concrete, in blue with PAR, in red without PAR

The 12" HL LOCA sequence has been repeated four times (two kinds of concrete, with and without PARs). A flammable cloud fills temporarily the containment at the beginning of the sequence for the 4 cases. Another flammable cloud fills the containment again during MCCI only for siliceous concrete without PARs.

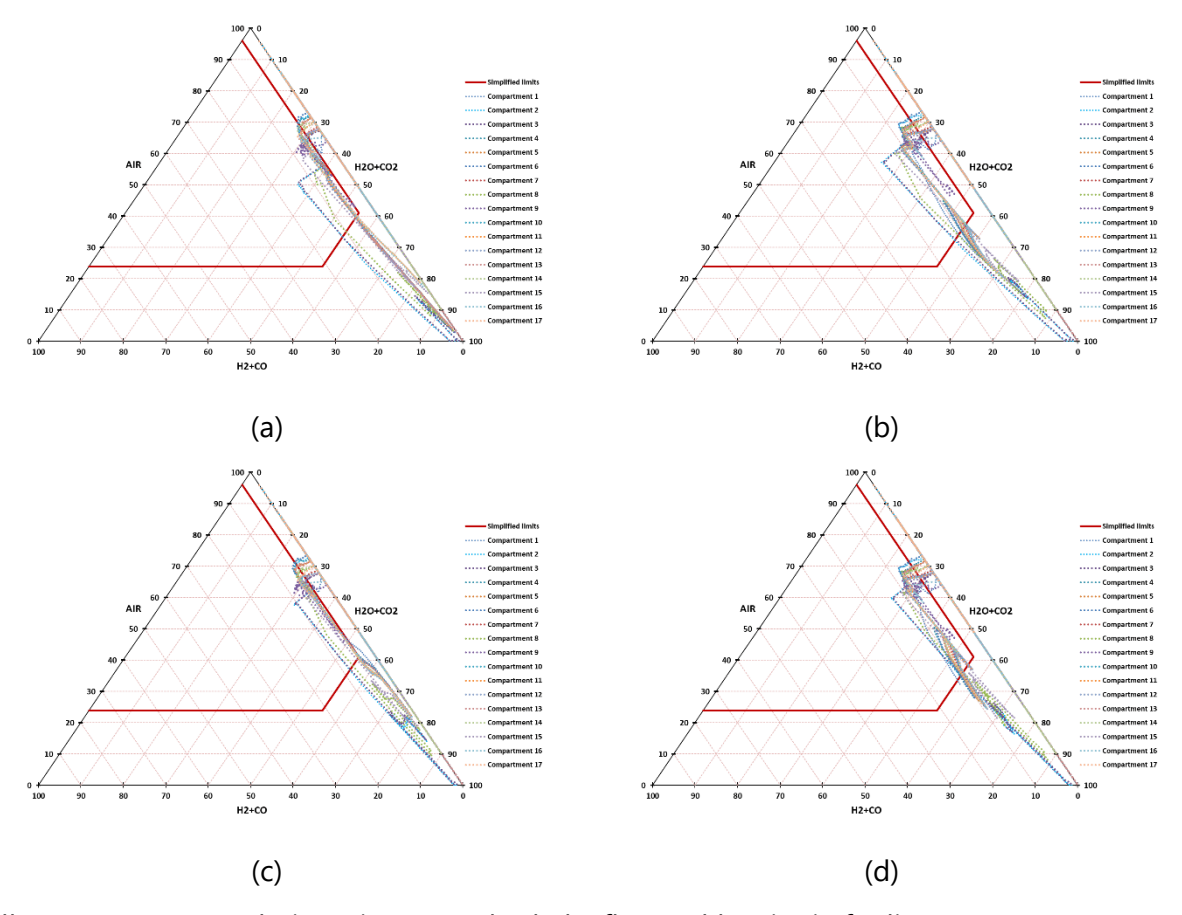
1300 MWe -12 inch hot leg LOCA



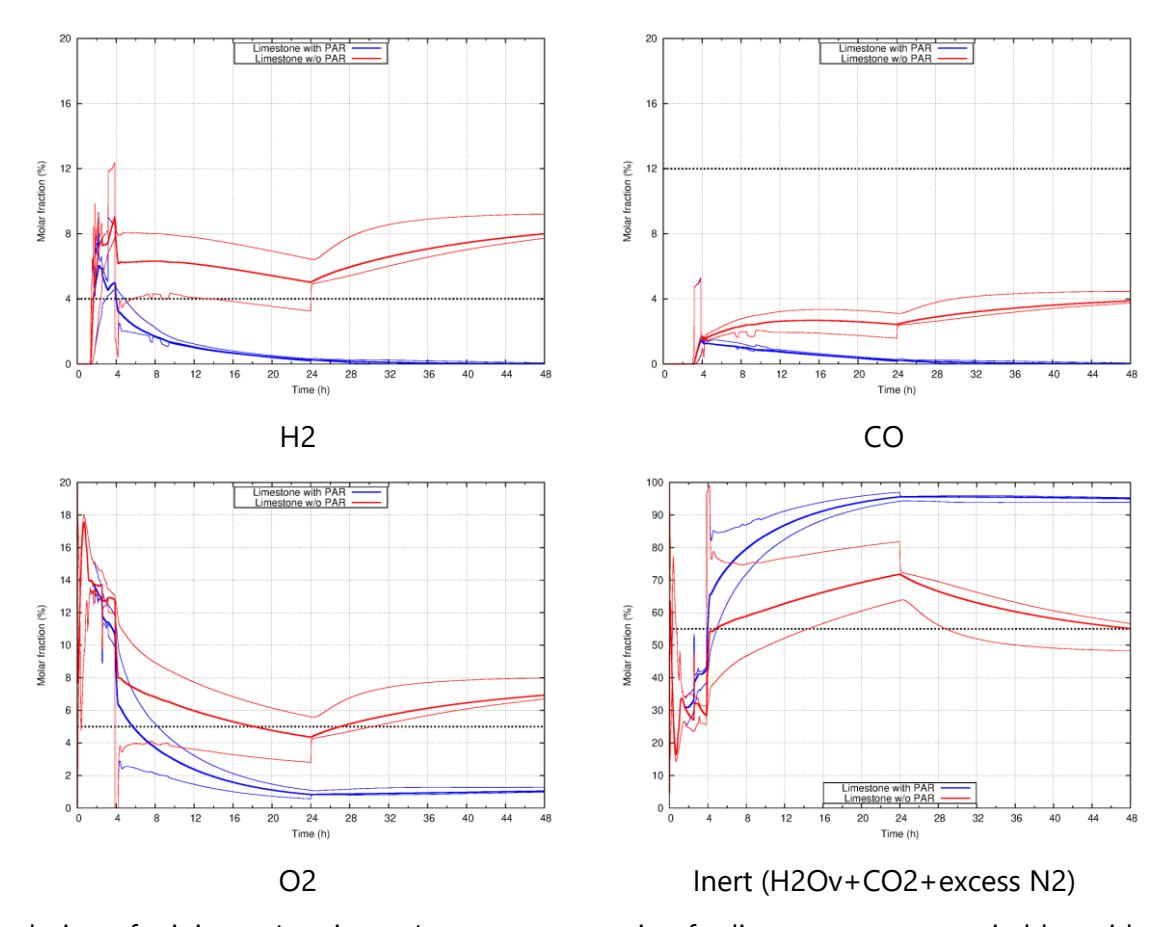
Flammable cloud volume evolution with limestone concrete (in blue) and siliceous concrete (in red), solid lines with PAR and dotted lines without PAR.



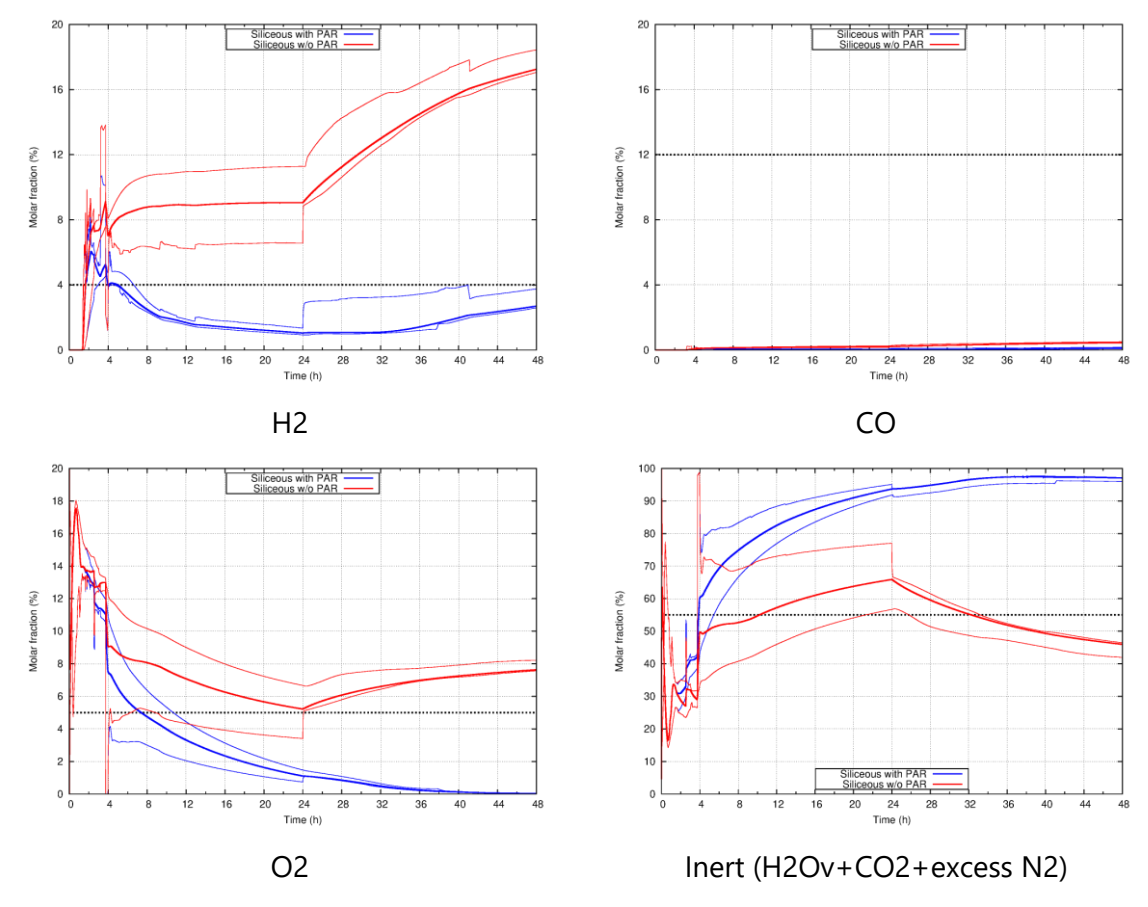
Gas composition in the dome compartment with limestone concrete (a) with PAR and (b) without PAR and siliceous concrete (c) with PAR and (d) without PAR



For all compartments evolution trigram to check the flammable criteria for limestone concrete (a) with PAR and (b) without PAR and for siliceous concrete (c) with PAR and (d) without PAR



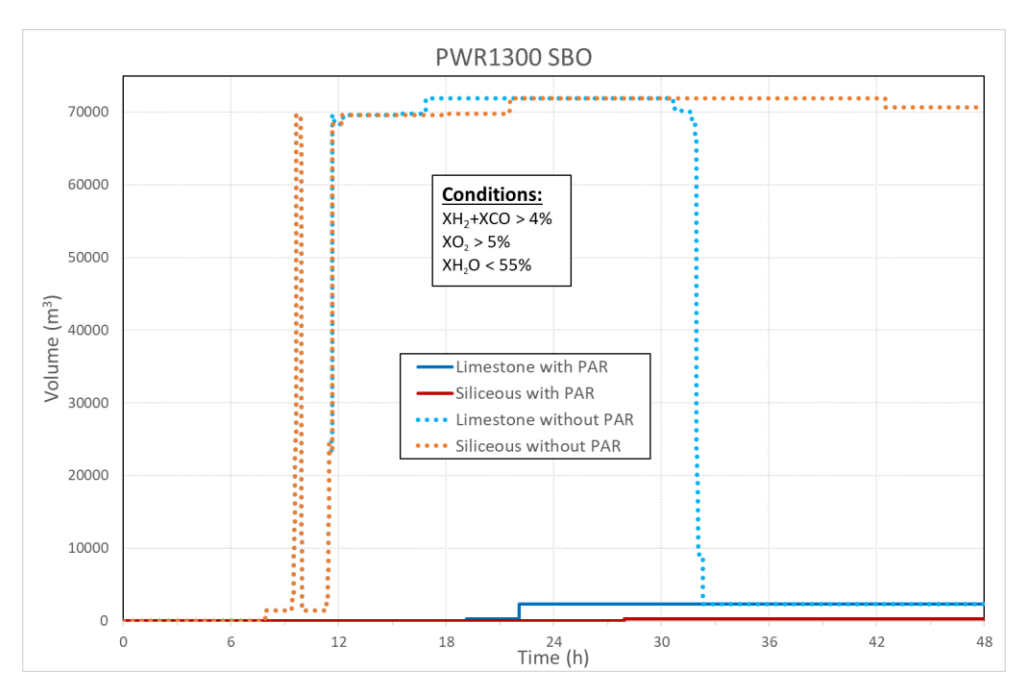
Evolution of minimum/maximum/mean concentration for limestone concrete, in blue with PAR, in red without PAR



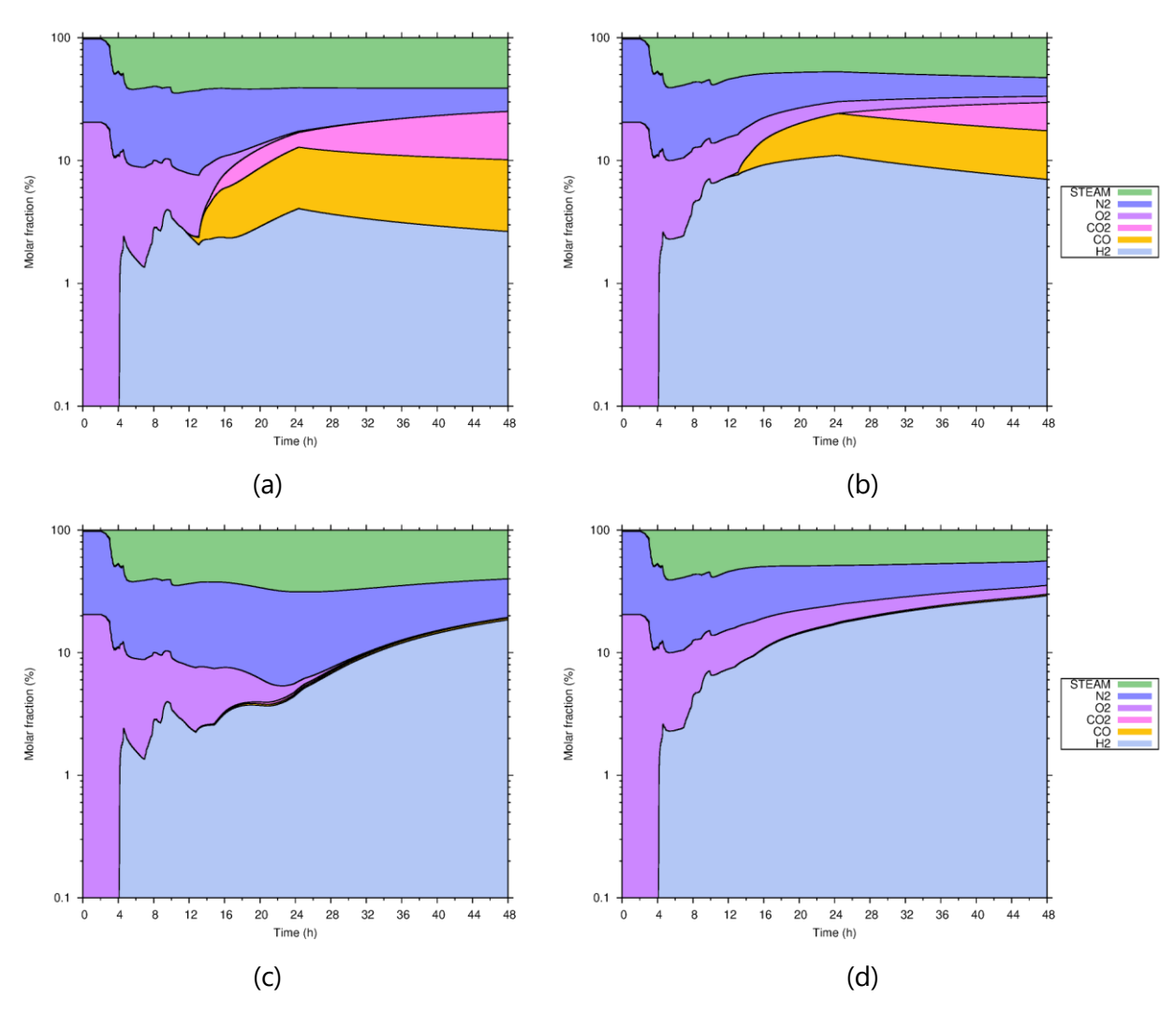
Evolution of minimum/maximum/mean concentration for siliceous concrete, in blue with PAR, in red without PAR

The 12" HL LOCA sequence has been repeated four times as well (two kinds of concrete, with and without PARs). A flammable cloud fills the containment at the beginning of the sequence for the 4 cases. It slowly vanishes without PARs, before to appear again. The flammable cloud is larger with siliceous concrete.

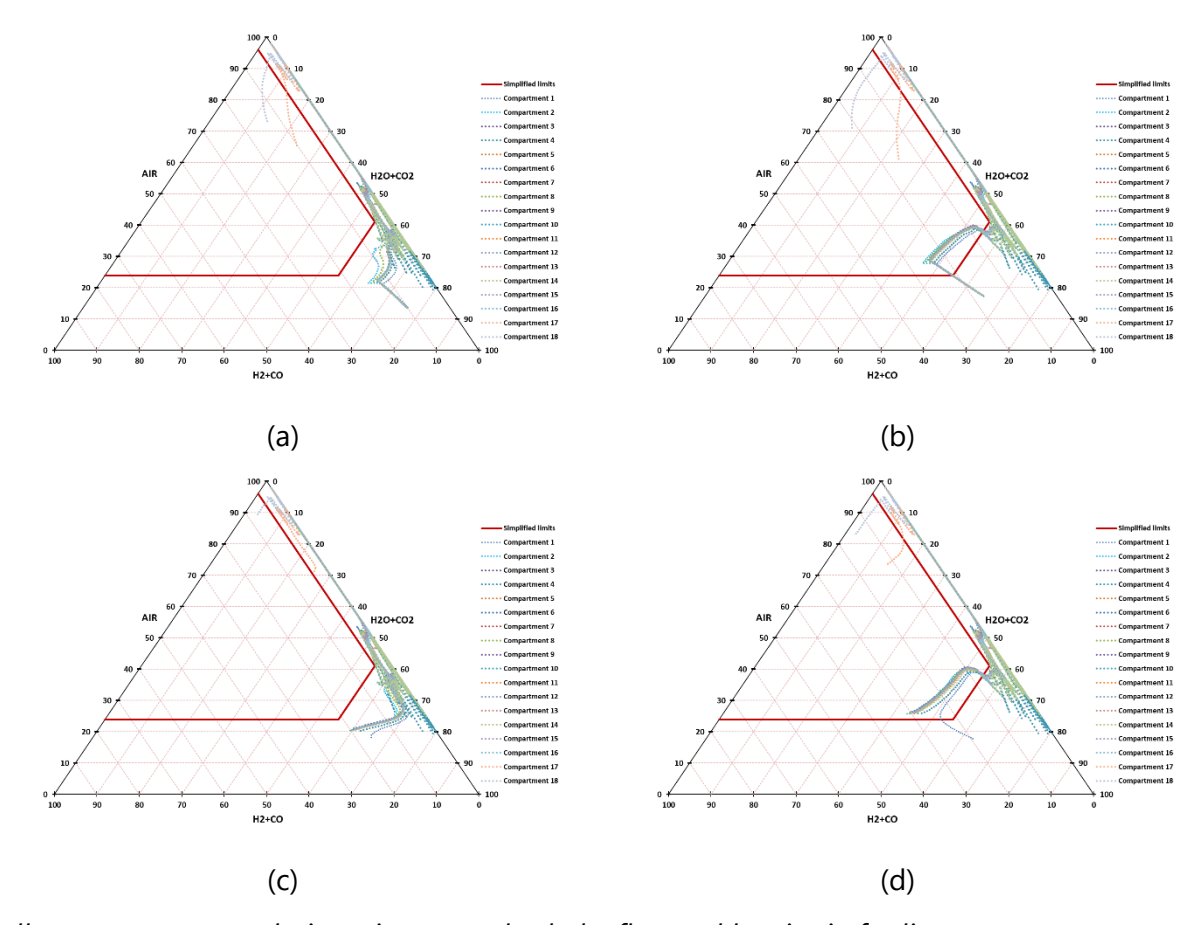
1300 MWe - SBO



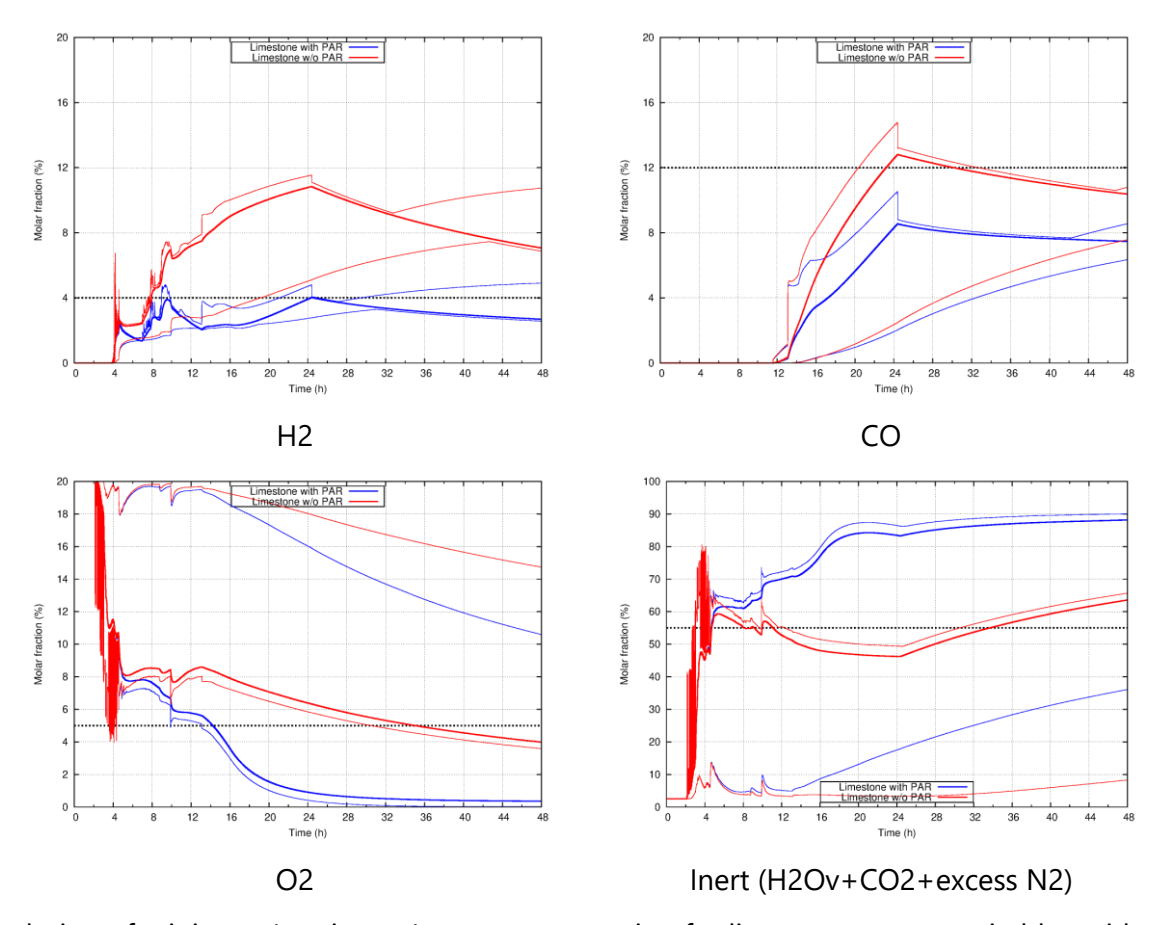
Flammable cloud volume evolution with limestone concrete (in blue) and siliceous concrete (in red), solid lines with PAR and dotted lines without PAR.



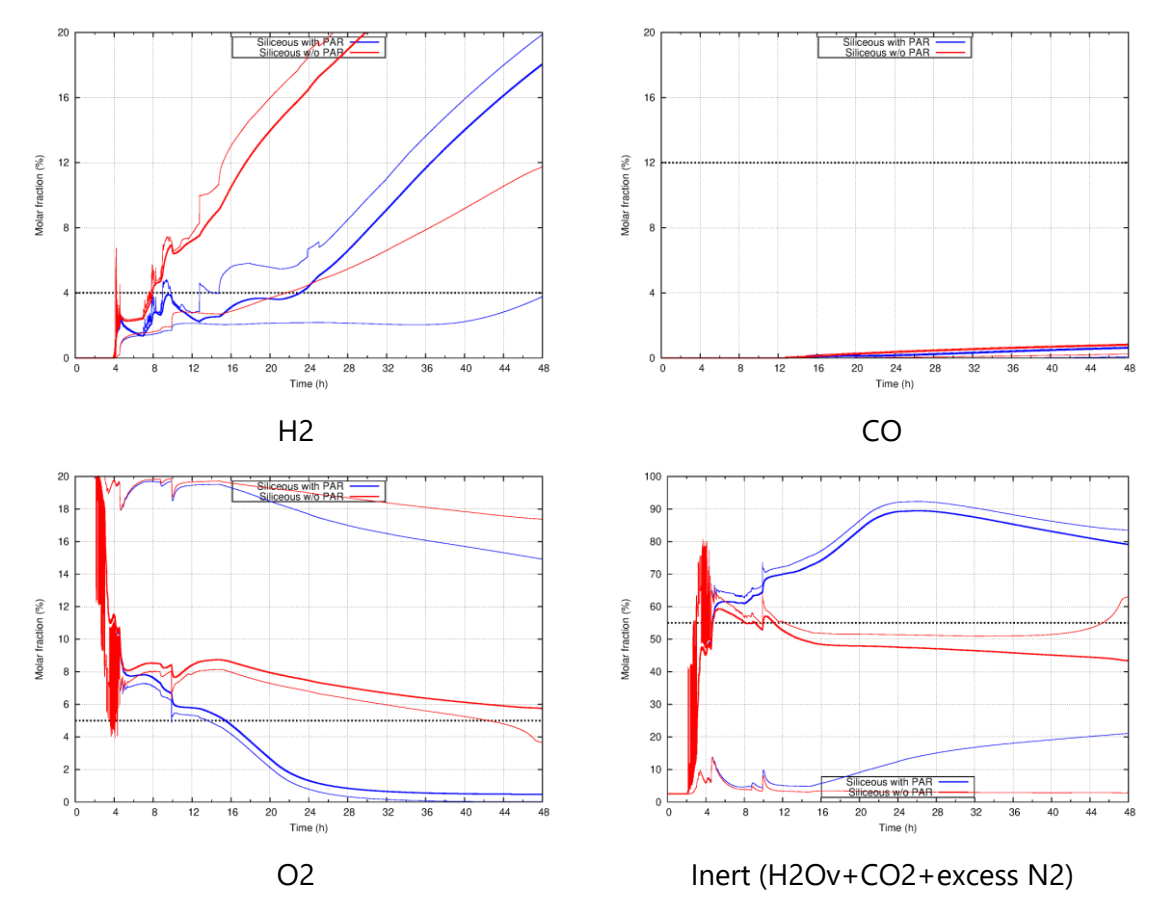
Gas composition in the dome compartment with limestone concrete (a) with PAR and (b) without PAR and siliceous concrete (c) with PAR and (d) without PAR



For all compartments evolution trigram to check the flammable criteria for limestone concrete (a) with PAR and (b) without PAR and for siliceous concrete (c) with PAR and (d) without PAR



Evolution of minimum/maximum/mean concentration for limestone concrete, in blue with PAR, in red without PAR



Evolution of minimum/maximum/mean concentration for siliceous concrete, in blue with PAR, in red without PAR

The SBO sequence has been repeated four times (two kinds of concrete, with and without PARs). A flammable cloud appears, and fills the containment, only without PARs. It vanishes faster with limestone concrete.

II.5 Main highlights

A set of 12 calculations have been performed by IRSN for the selection of relevant SA sequences in the frame of WP2. The main findings are listed hereafter:

- The type of concrete basemat has a strong impact on hydrogen and carbon monoxide production. Limestone concrete leads to high production of carbon monoxide but weak production of hydrogen, whereas siliceous concrete leads to very weak production of carbon monoxide but high production of hydrogen.
- The risk of combustion is higher for siliceous concrete.
- The use of PARs reduces strongly the time period with flammable clouds inside the containment.

II.6 Typical conditions in the containment during the exvessel phase

In addition, an analytical work has been performed to highlight the typical conditions in the containment during the ex-vessel phase. They are presented in the tables below for two concrete types (siliceous and limestone), without and with PAR operation. The hypotheses used to obtain the kind of mixture encountered are:

- Volume of a 1300 MWe (P'4 series) containment
- Initial mass of N2 conserved
- Initial mass of O2 conserved without PAR operation; reduction of 1/3 of O2 quantity with PAR operation (consumption of 700 kg of H2) during the in-vessel phase and the beginning of the ex-vessel phase
- Hydrogen molar fraction (XH2) representative of mixtures encountered during the exvessel phase without PAR operation; hydrogen mass reduction in accordance with PAR operation
- Carbon monoxide molar fraction (XCO) representative of mixtures encountered during the ex-vessel phase without PAR operation; no impact of PAR on the carbon monoxide mass at the beginning of the ex-vessel phase
- Temperature imposed to 100°C and 110°C
- Steam molar fraction (XVP) determined to have Psat(T)

• Lower flammability limit (LFL) <u>in air</u> for H2/CO mixture from Le Chatelier (4% for H2 and 12.5% for CO):

$$Lim_{H_2+CO} = \frac{X_{H_2} + X_{CO}}{\frac{X_{H_2}}{Lim_{H_2}} + \frac{X_{CO}}{Lim_{CO}}}$$

Typical conditions during the ex-vessel phase when considering no PAR operation

	Siliceous concrete type				Lir	nestone c	oncrete ty	pe	
Temperature (°C)	10	00	1	10	10	100		110	
Pressure (bar)	2.34	2.44	2.83	2.95	2.39	2.44	2.89	2.95	
XO2	10.2%	9.8%	8.7%	8.3%	10.0%	9.8%	8.5%	8.3%	
XH2	8.0%	12.0%	8.0%	12.0%	8.0%	8.0%	8.0%	8.0%	
хсо	0.0%	0.0%	0.0%	0.0%	2.0%	4.0%	2.0%	4.0%	
XN2	38.4%	36.7%	32.6%	31.2%	37.6%	36.7%	31.9%	31.2%	
XVP	43.4%	41.5%	50.7%	48.5%	42.5%	41.5%	49.6%	48.5%	
LFL	4.0%	4.0%	4.0%	4.0%	4.6%	5.2%	4.6%	5.2%	

Typical conditions during the ex-vessel phase when considering PAR operation and a consumption of 1/3 of the oxygen mass (non flammable mixture in grey)

	Siliceous concrete type				Lir	nestone c	oncrete ty	pe	
Temperature (°C)	100		1	10	10	100		110	
Pressure (bar)	2.10	2.20	2.58	2.71	2.15	2.20	2.64	2.71	
XO2	7.6%	7.2%	6.3%	6.0%	7.4%	7.2%	6.2%	6.0%	
XH2	1.3%	6.1%	2.4%	7.1%	1.5%	1.7%	2.6%	2.7%	
хсо	0.0%	0.0%	0.0%	0.0%	2.2%	4.4%	2.2%	4.4%	
XN2	42.8%	40.7%	35.7%	34.0%	41.7%	40.7%	34.8%	34.0%	
XVP	48.3%	46.0%	55.6%	52.9%	47.2%	46.0%	54.2%	52.9%	
LFL	4.0%	4.0%	4.0%	4.0%	6.7%	7.9%	5.8%	6.9%	

II.7 References:

[REF1] Romain Cozeret et al (IRSN), Improvement on 900 MWe NPPs in the occasion of the 4th 10-year periodic safety review on severe accident, EUROSAFE 2019.

ANNEX III – Individual report for PWR-W700 reactor (JSI)

III. 1 Introduction

The considered plant is a two-loop Westinghouse PWR of 2000 MWth and 700 MWe power. The following three accident scenarios were simulated:

- station black-out (SBO),
- station black-out with small-break loss-of-coolant accident (SBO + 6" SB LOCA),
- station black-out with large-break loss-of-coolant accident (SBO + 12" LB LOCA).

The rationale was to simulate accidents with very adverse conditions. For this reason, no active safety system was assumed to be available. Only the following passive systems were assumed to be available:

- accumulators,
- Passive Autocatalytic Recombiners (PARs),
- Passive Containment Filtered Venting System (PCFVS).

III.2. Plant model

III.2.1. Overview

The simulations were performed with the MELCOR 2.2 code, revision 15254.

The primary and secondary systems and the containment, including regulation systems and control volumes that represent boundary conditions, consist of 145 thermal-hydraulic control volumes, 197 flow paths and 149 heat structures (Figure 32).

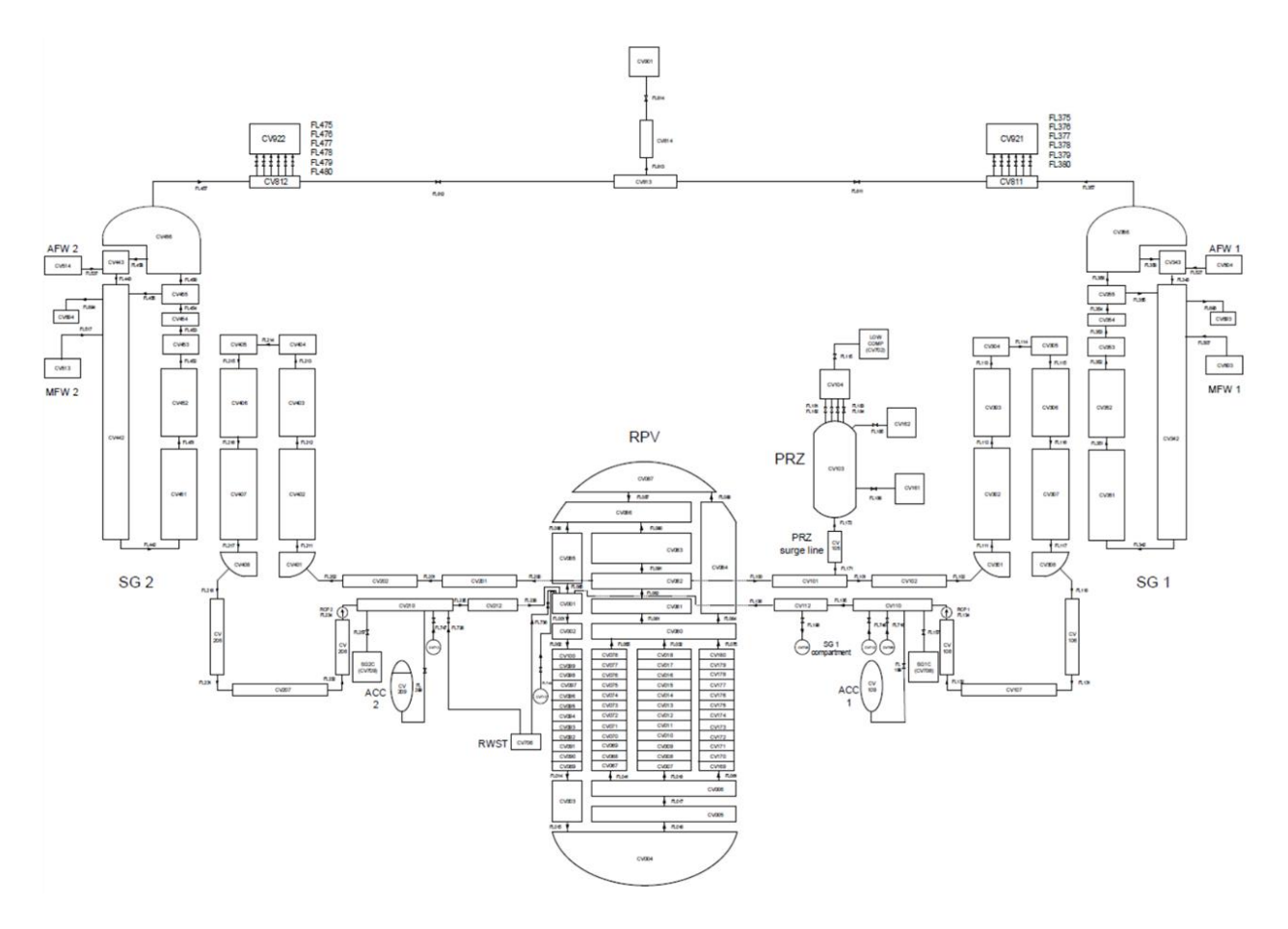


Figure 32. Primary and secondary systems nodalization.

III.2.2. Approximations and hypotheses

The usual approximations and hypotheses when simulating a severe accident with a system code were applied.

III.2.3. Containment nodalization

The NPP containment nodalization is presented in Figure 33, whereas Figure 34 shows some more detailed view around the reactor cavity with listed levels. The reactor pressure vessel is located in control volume CV711, and control volume CV704 presents the reactor cavity. The ventilation duct, denoted as flow path FL783, connects the reactor cavity CV704 with the containment lower compartment CV702. The ventilation duct opening is nearly 2.5 m above the floor of the containment lower compartment.

The rounded (for proprietary reasons) volumes of the main compartments of the containment nodalization are provided in Table 5.

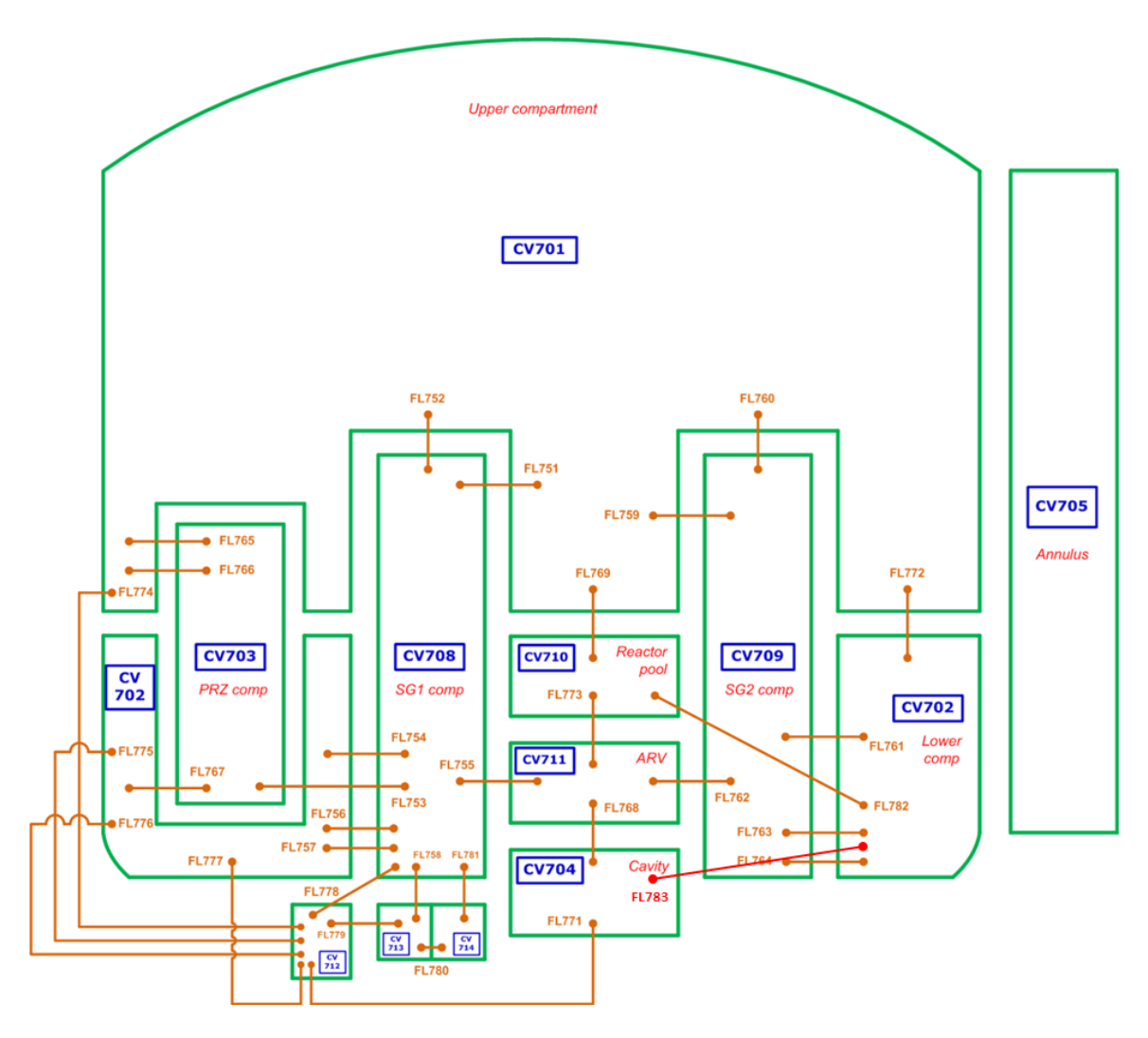


Figure 33. NPP containment nodalization.

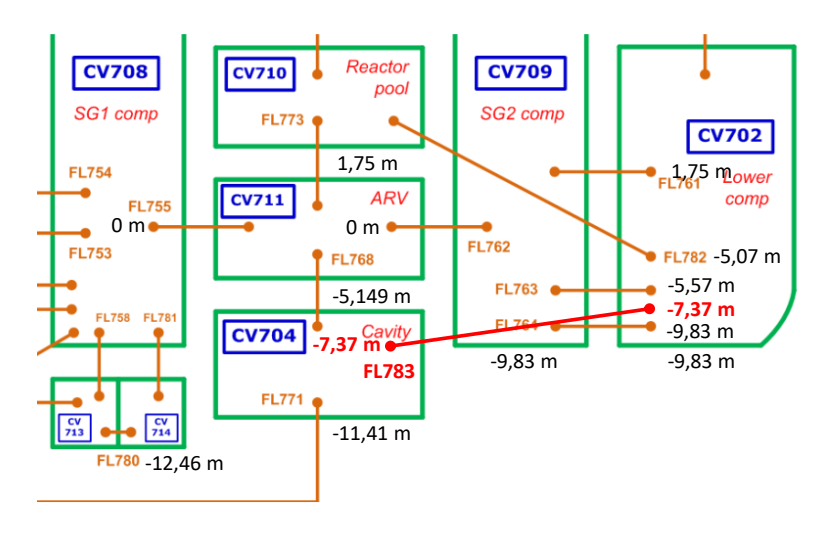


Figure 34. Detail of NPP containment nodalization.

Table 5. Main compartments of containment model.

Compartment	Volume (m³)
CV701	29·10³
CV702	6·10 ³
CV705	11·10³
CV708	1·10³
CV709	1·10³
CV710	1·10³

III.3. Sequences description

After the decrease of the RCS pressure, in the case of SB LOCA and LB LOCA, the first accumulator starts to inject water in the RCS, whereas the second accumulator is discharged into the containment due to the break at the connection to the RCS. In the case without LOCA, the inventory of the RCS is lost through the safety valves due to pressure increase caused by boiling.

When the core starts to heat up, the integrity of the fuel rods is lost and radioactive gases are released from the gap between the fuel pellets and the cladding. The core starts to melt and relocates to the RPV lower head which eventually fails. The molten core is released in the reactor cavity, where molten core concrete interaction (MCCI) starts.

The passive containment filtered venting system (PCFVS) has a rupture disc which breaks at a pressure of 6 bar. If the pressure inside the containment exceeds this value, the containment atmosphere is released into the environment through the filter till the setpoint of the containment relief valve closure of 4.1 bar is reached. The containment venting setpoint for the next containment relief valve openings is 4.9 bar.

The times of the core melting, RPV failure and first PCFVS opening are provided in Table 6. The simulation time was 300.000 s (approximately three and a half days).

Table 6. Times of first important events.

Event Cooperie	Time (s)				
Event \ Scenario	SBO	SBO+SB LOCA	SBO+LB LOCA		
Core melting	9632	2795	888		
RPV failure	12201	6420	3467		
PCFVS opening	81189	66257	72264		

III.4. Results and discussion

Figure 35 shows the pressure in the containment. The shape of the curves are the consequences of the functioning of the PCFVS, described in the previous section. When the pressure reaches the containment venting setpoint of 6 bars for the first opening of the containment relief valve, the pressure starts to decrease till it reaches the containment relief valve closing setpoint of 4.1 bar. Then the pressure starts to increase again till it reaches the containment venting setpoint of 4.9 bar for the next containment relief valve openings. The pressure then cycles between the two setpoints.

The availability of the PCFVS definitely causes a peculiar behaviour of the pressure that is not commonly observed in simulations. However, these results are more realistic, in the sense that such behaviour of the pressure would (presumably) be observed during an accident in the considered plant. Namely, although failure of active safety systems is commonly assumed, the failure of passive safety systems, of which the PCFVS is also part, is highly improbable.

Figure 36 shows the heat transfer rate between the core melt and the atmosphere/liquid pool. Although large differences may be observed in the beginning (with the highest values in the case of LB LOCA, as RPV failure in that case is the earliest, followed by lower values in the case of SB LOCA, as RPV failure in that case still occurs earlier than in the case of sole SBO), the rates in the late phases of the accident are very similar.

Figure 37 shows the containment atmosphere temperature. The temperature rises most of the time, which means that despite the high atmosphere temperature, the heat transfer through the containment walls is not sufficient to extract the entire residual heat from the molten core.

Figure 38 shows the hydrogen mass in the RPV. Again, one may observe the influence of the time of the RPV failure. That is, the final value of mass remains the lowest in the case of SBO+LB LOCA, where RPV failure occurs first, and the highest in the case of sole SBO, where RPV failure occurs last. This reasoning, but in reverse order, applies also to the hydrogen mass outside the RPV, shown in Figure 39. However, later into the transient, the hydrogen mass outside the RPV is almost equal in the cases of SB LOCA and LB LOCA, as the initial difference is compensated by different hydrogen generation rates during late MCCI. However, in the case of SBO, it appears that the hydrogen generation rate during late MCCI does not increase as in the case of SB LOCA.

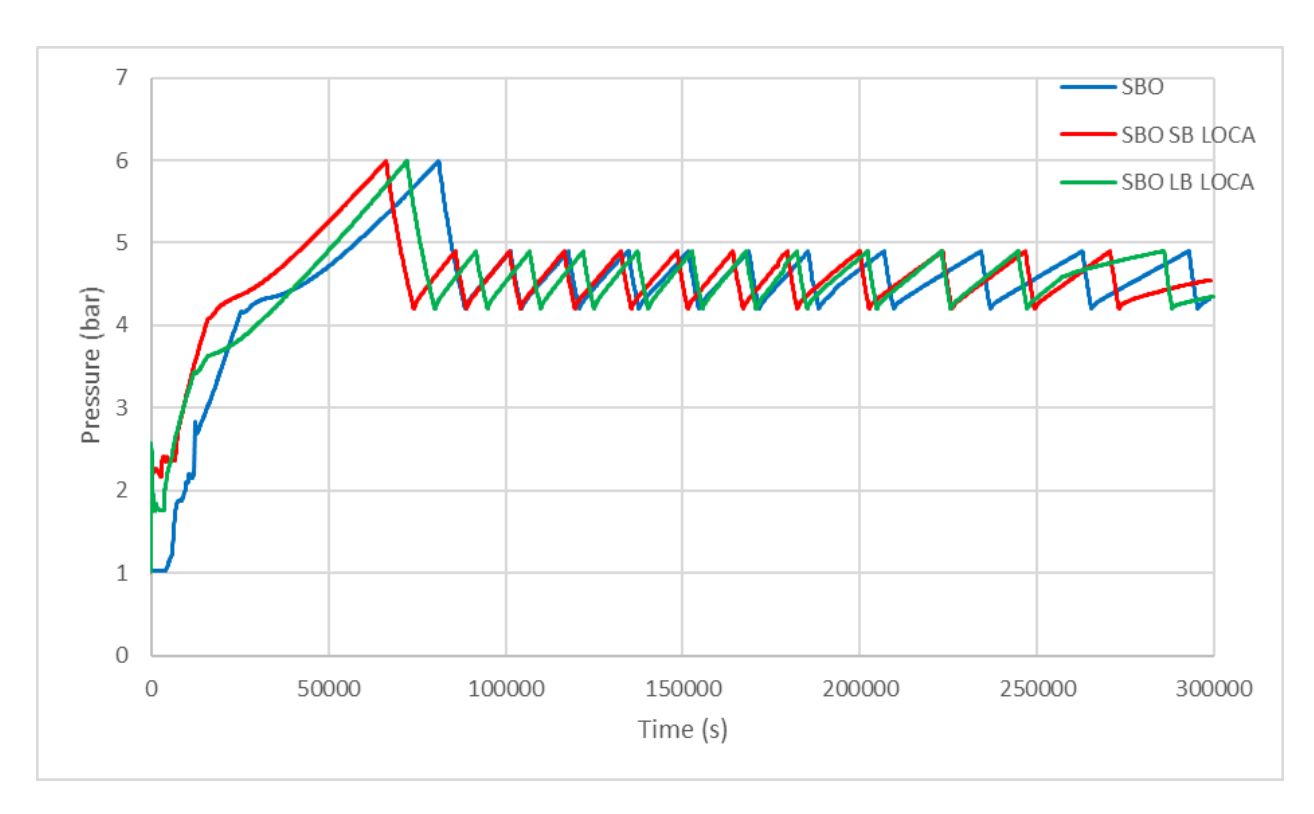


Figure 35: Containment pressure.

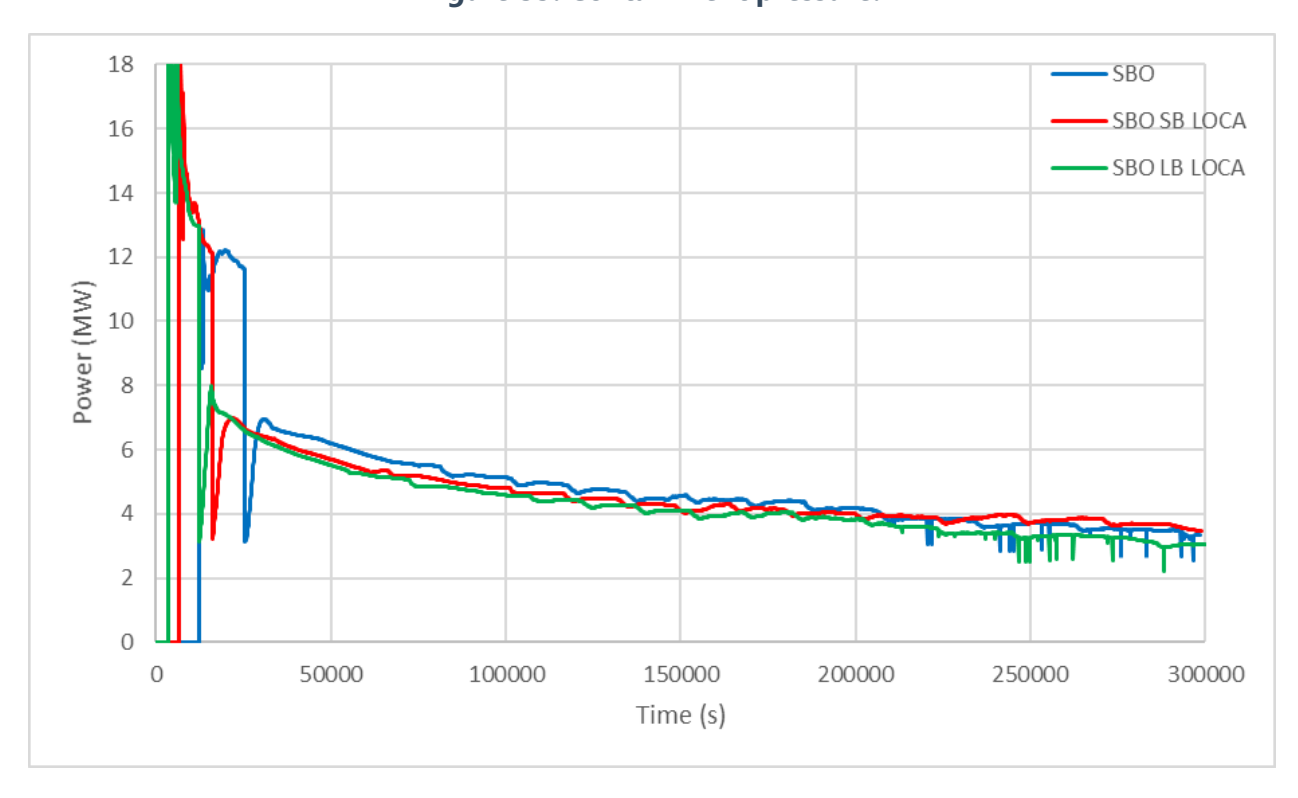


Figure 36: Heat transfer: melt - atmosphere/pool.

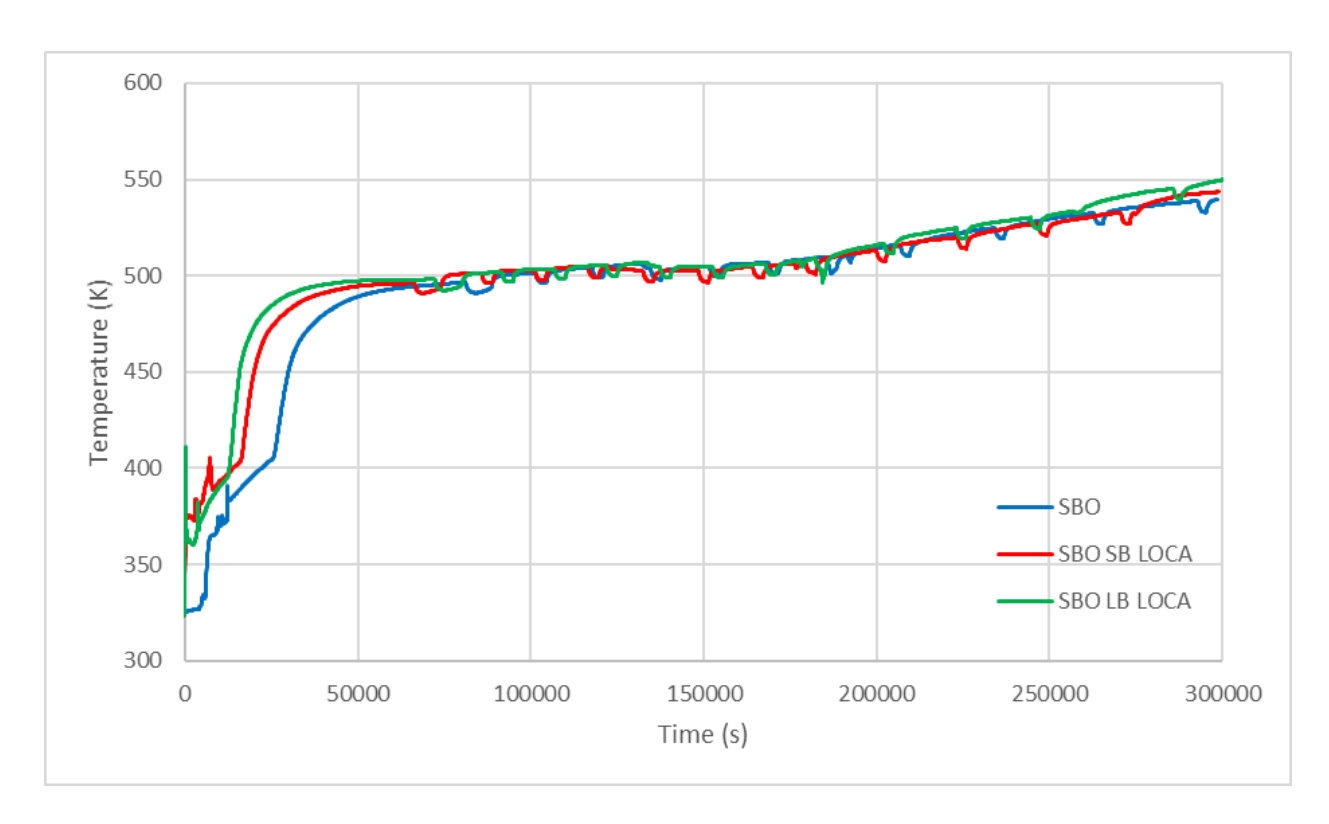


Figure 37: Containment dome temperature.

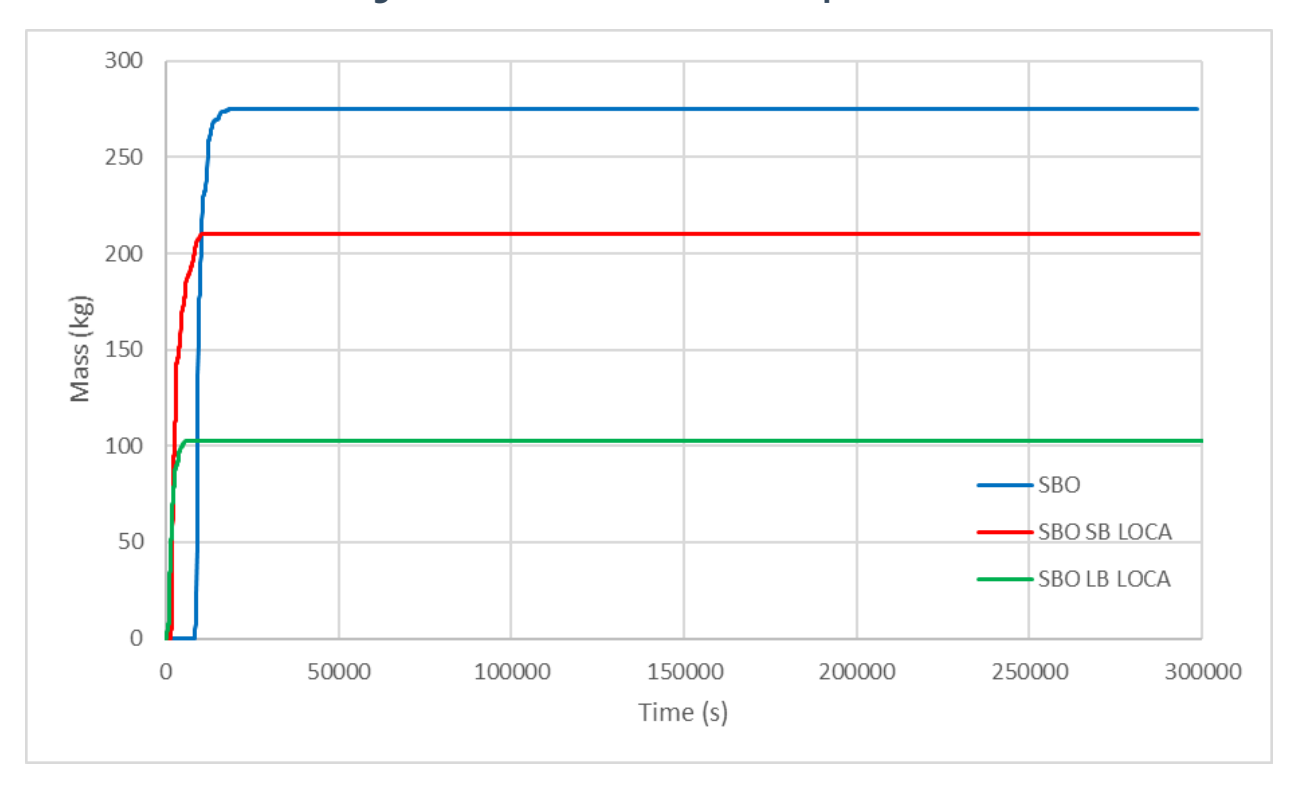


Figure 38: Hydrogen in RPV.

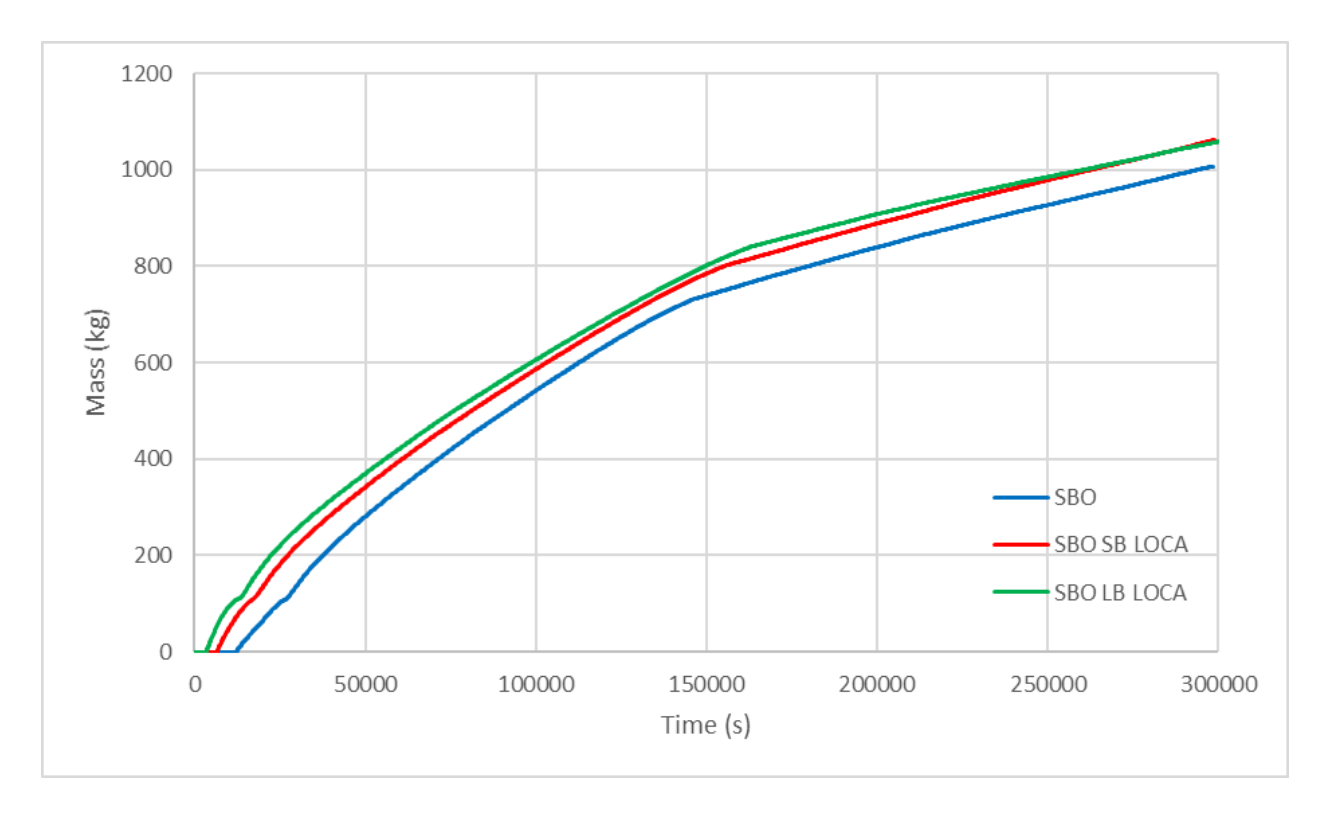


Figure 39: Hydrogen outside RPV.

Figure 40 shows the volume fraction of steam in the containment dome. Obviously, steam is the dominant gas component in the containment atmosphere. The initial and later increases are due to the release from the RCS. As in other observed quantities, the behaviour of the steam fraction exhibits large differences in the early phases of the accidents, but is very much similar in the later phases.

Figure 41 shows the hydrogen fraction in the containment dome. The highest value in the early phase in the case of SBO is related to the corresponding lowest value of steam fraction. The differences later into the accident are related to the hydrogen generation rates during late MCCI as well as the presence of different quantities of steam.

The essential feature is that the hydrogen fraction never reaches the value 0.035 (although it might eventually reach this value and even exceed it even later into the accident, but that is beyond the scope of the present simulations). As the commonly accepted minimum value of hydrogen fraction for the mixture to be flammable is 0.04, this means that the gas mixture in the containment dome is never flammable. Of course, this does not exclude the possibility, that the hydrogen fraction might exceed the limiting value 0.04 in some other compartment. However, the purpose of the simulations was to assess, whether flammability may be expected in the main part of the containment, and not to investigate eventual singularities.

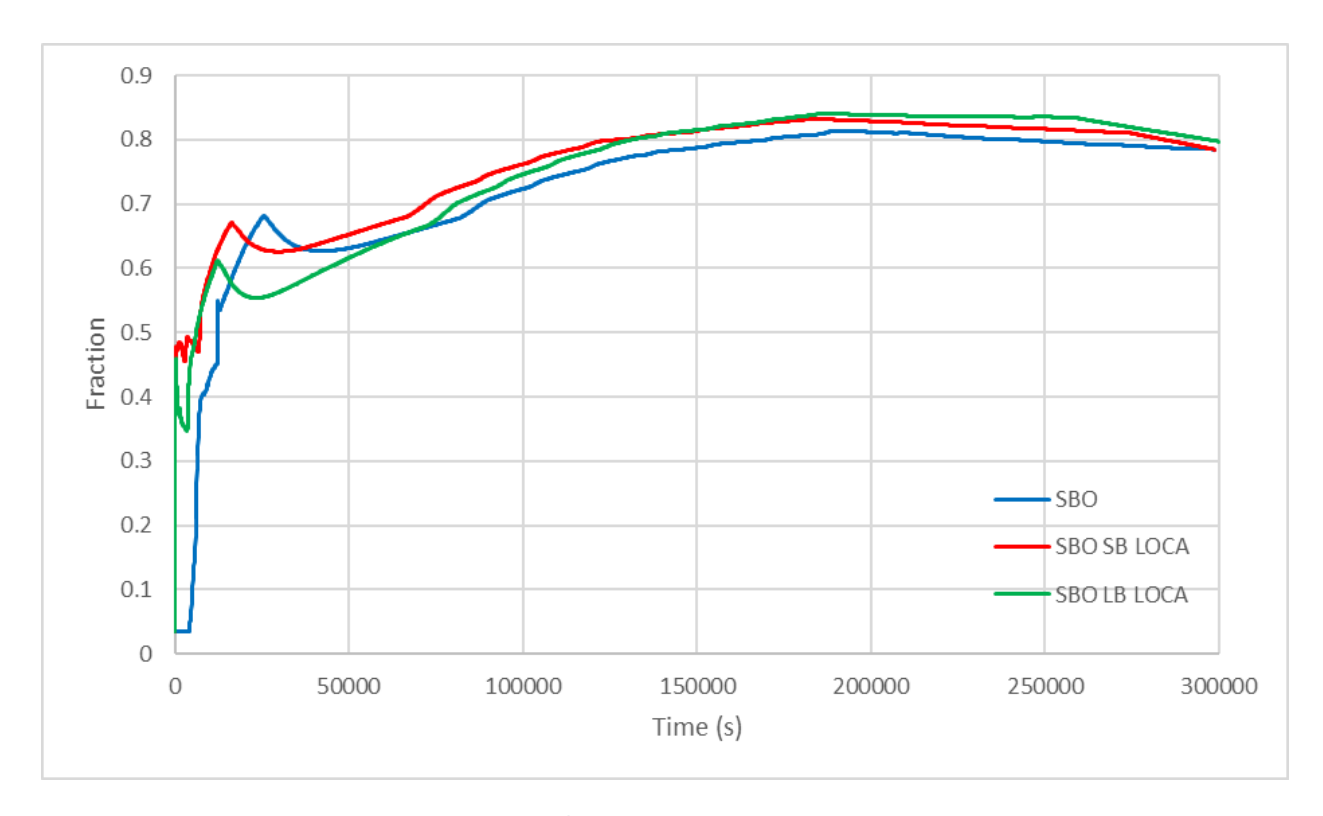


Figure 40: H₂O fraction in containment dome.

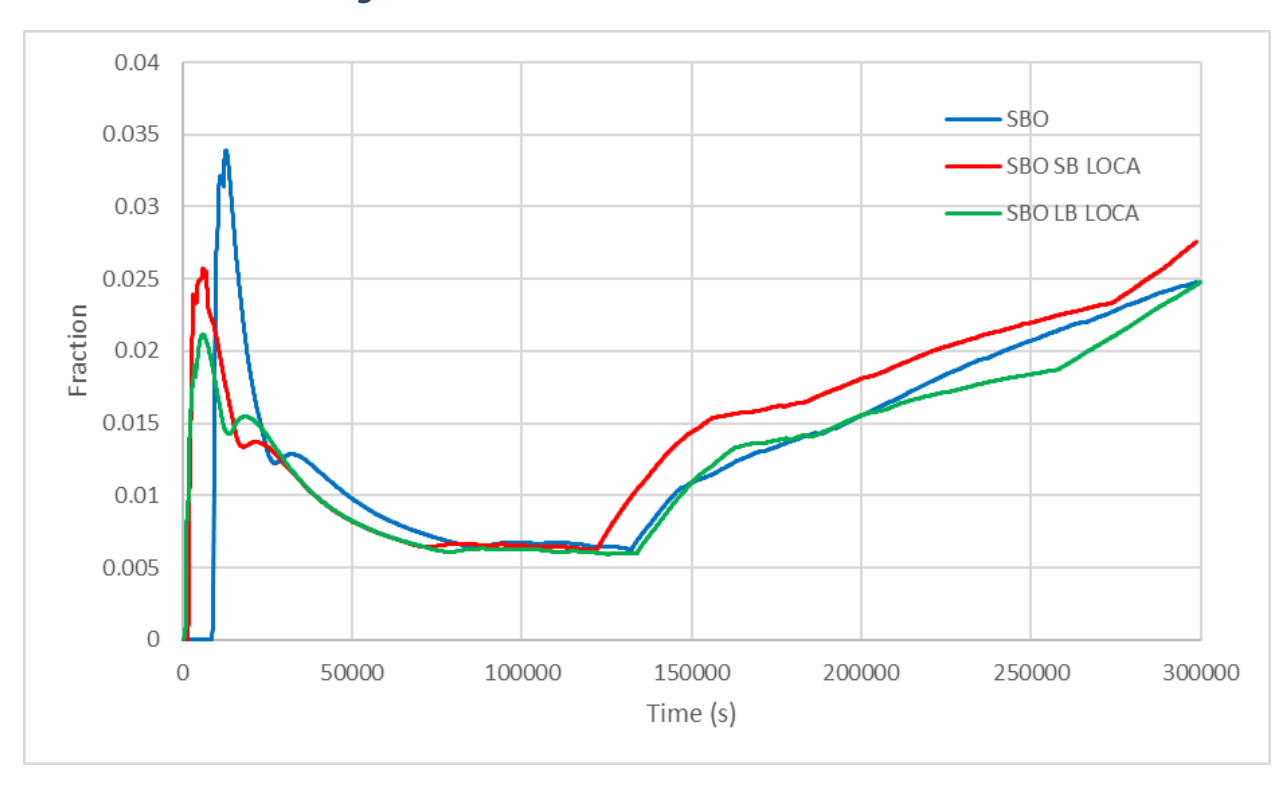


Figure 41: H₂ fraction in containment dome.

Figure 42 shows the CO_2 fraction in the containment dome. The generation of that gas is related to the later phase of MCCI, whereas the generation of CO, for which the fraction in the containment dome is shown in Figure 43, is related to the early phase of MCCI. The same comment about the representativity of the containment dome atmosphere, stated for hydrogen, is valid also for CO_2 and CO.

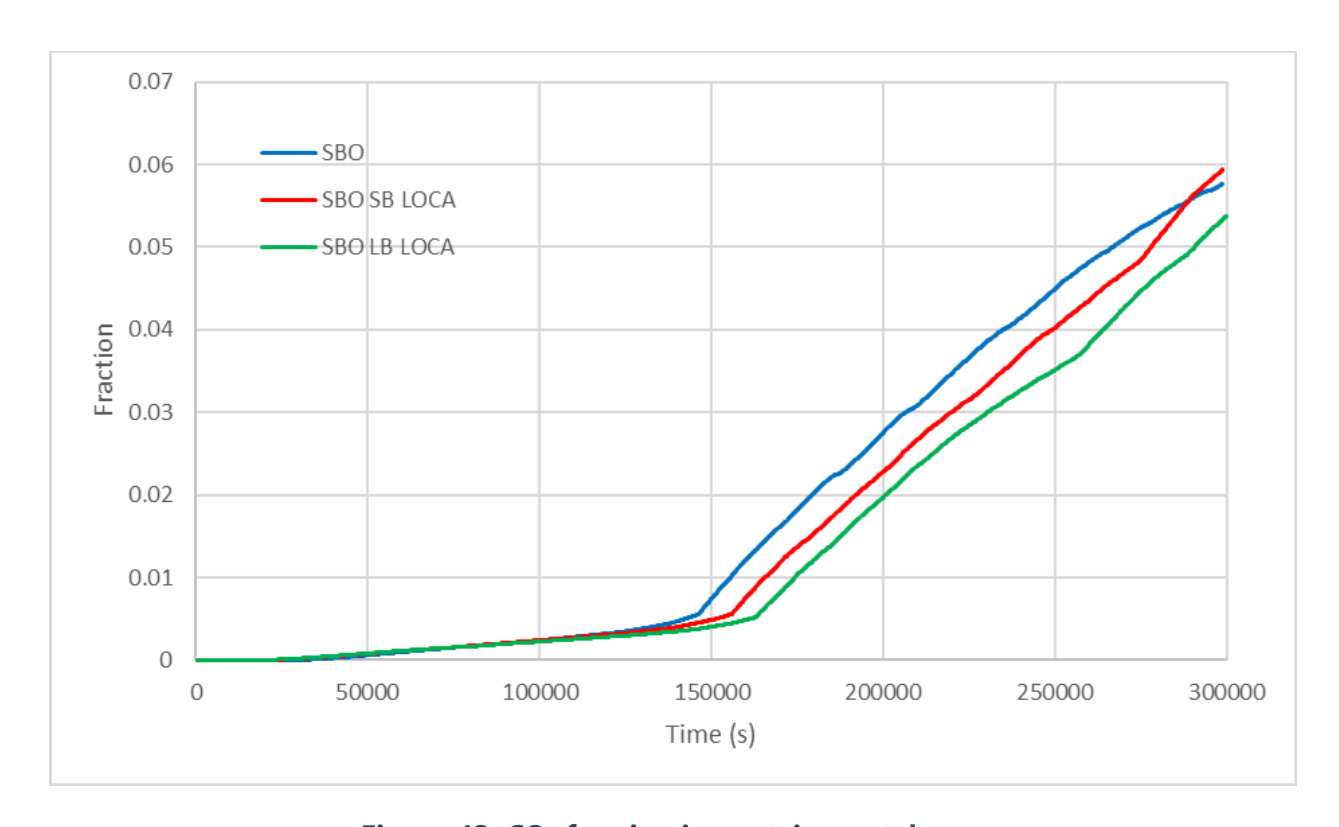


Figure 42: CO₂ fraction in containment dome.

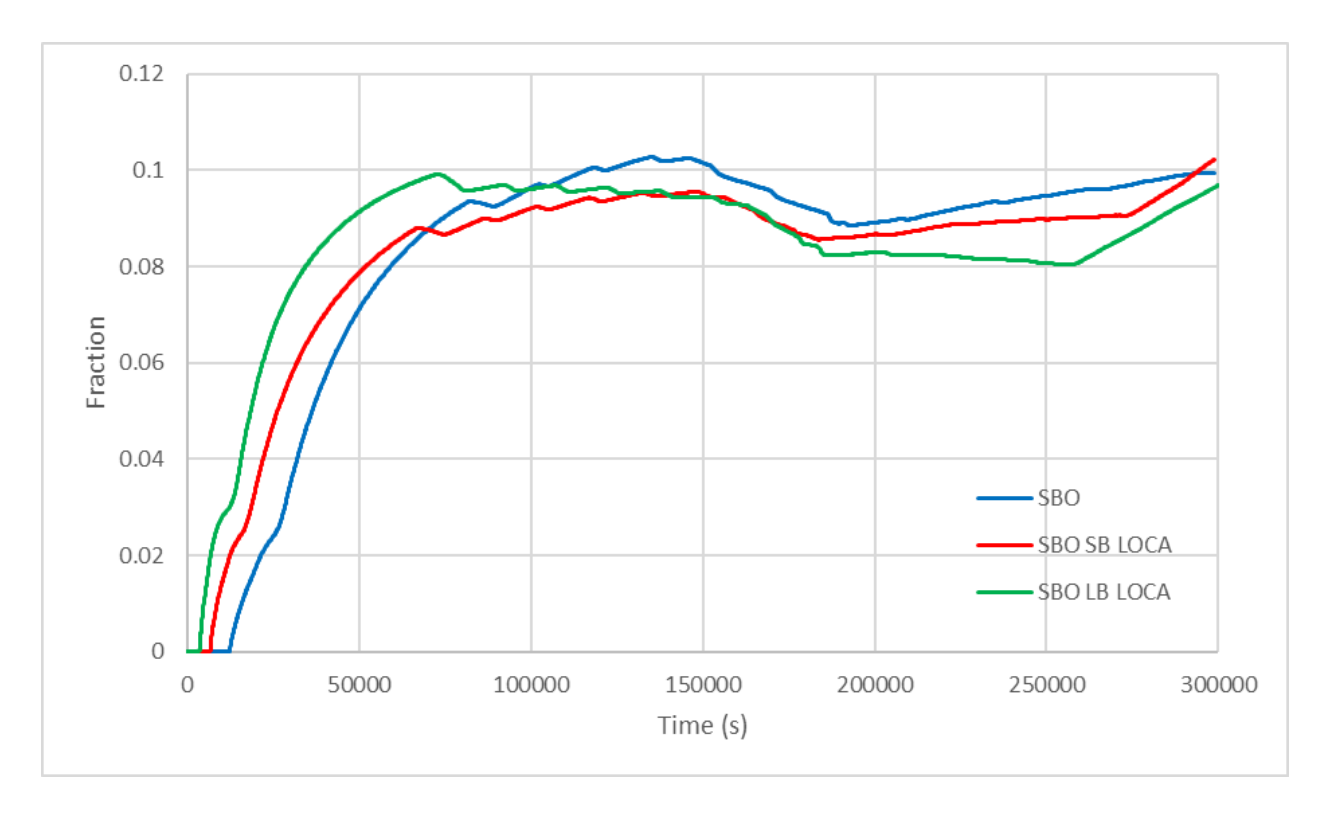


Figure 43: CO fraction in containment dome.

III.5. Main highlights

- Due to the Passive Containment Filtering Venting System, the pressure in the containment never reaches above 6 bar during the first increase and above 4.9 bar during later increases, so the integrity of the containment is not threatened (at least due to pressurization).
- The maximum hydrogen volumetric fraction in the containment dome is always below 0.035, so it is always below the commonly accepted flammability limit 0.04.
- The influence of the different initiating events (SBO, SBO + SB LOCA, SBO + LB LOCA) is strong in the early phases of simulated accidents. In later phases, differences tend to vane, mostly qualitatively but quantitatively as well.

ANNEX IV: Individual report for the PWR-W1000 reactor (CIEMAT)

IV.1 Introduction

In the event of a severe accident or Beyond Design Basis Accident (DBDA) in Light Water Reactors (LWR), hydrogen is produced by exothermal reactions of steam with overheated zirconium and stainless steel present inside the Reactor Pressure Vessel (RPV). This hydrogen eventually reaches the containment atmosphere through the primary circuit break or the pressurizer safety valves. Additionally, in case of vessel failure and subsequent slump of molten core into the cavity, more hydrogen and carbon monoxide can be generated by the reaction of gases coming out from the Molten Core-Concrete Interaction (MCCI) with the metallic materials in the corium. These combustible gases are distributed inside the containment by convective flows and interact with structures and systems, so that depending on the specific containment conditions their local concentration may become substantial and lead to flammable gas mixtures. The accidents in TMI-2 (Sehgal, 2012) and in Fukushima Daiichi (IAEA, 2015) confirmed that large amounts of hydrogen may be generated to the point of deflagration, which might impair containment and/or safequards in containment.

In the frame of the AMHYCO project (Jiménez et al., 2022), the workpackage-2 is devoted to the selection, for different containment plant designs, of the most representative sequences regarding combustible gases associated risk. The CIEMAT contribution of this workpackage consists of the simulation of four sequences in a PWR Westinghouse 1000 MW reactor with the MELCOR code.

IV.2. Plant model overview

IV.2.1.Overview

The modelled power plant is a 3-loop Westinghouse PWR 1000 MWe (2940 MWth) with a large and dry containment. The MELCOR v2.2-18019 code (Humphries et al., 2021a) is used to simulate the different accidental sequences.

The core and the Reactor Coolant System (RCS) are modelled following the recommendations of the SOARCA project (Ross et al., 2014). Each loop is modelled individually with 29 control volumes, (including the accumulator). The core consists of 5 channels in 5 axial nodes, plus the bypass. The vessel is completed with the downcomer, the lower plenum, and four nodes for the upper plenum. A total of 138 nodes define the primary and the secondary circuits.

In addition to the 82.6-tons of fuel (UO₂), in the core region there are a total of 23.2 tons of zirconium in the fuel cladding and about 44.8 tons of stainless steel in other metallic structures.

IV.2.2.Approximation and hypotheses

To enhance core degradation, only the hydro-accumulators are assumed to work as designed. So, each accumulator can inject 24.3 m³ into the primary loop through a flow path with a valve that opens if the pressure drops below 46 bar. All other injection safety system into the primary circuit is assumed to be unavailable.

In accidents with high pressure in the primary circuit (e.g. SBO), the pressurizer safety valves limit the pressure to 1.62 bar. These valves discharge steam and hydrogen into the pressurizer relief tank. The room housing the relief tank has been modelled separately to follow the hydrogen concentration in that particular location.

A single cavity region is defined in the model. Based on the CORCON-Mod3 model in MELCOR (Humphries et al., 2021a), the debris and molten materials falling into the cavity are assumed to be spread instantaneously over the cavity floor. The single-layer approach is used for the molten pool in the cavity. This approach implies that the materials present in the corium are completely mixed.

Generic, limestone type in the CORCON model has been selected for the concrete slab in the cavity (Table 7). No additional iron mass for the reinforcing bars has been modelled since no specific data are available.

Table 7. Limestone concrete composition (Humphries et al., 2021b)

Species	Mass fraction (%)
SiO2	35.80
TiO2	0.18
MnO	0.03
MgO	0.48
CaO	31.3
Na2O	0.082
K2O	1.22
Fe2O3	1.44
Al2O3	3.60
Cr2O3	0.014
CO2	21.154
H2O _{CHEM}	2.00
H2O _{EVAP}	2.70

Different safety systems of the containment are modelled:

- Fan coolers are installed in the containment dome and the total heat transfer coefficient is evaluated using the MARCH model (Humphries et al., 2021a), for which, the nominal fan cooler capacity (1.5·10⁷ W) and the rated conditions are specified in the input deck. Fan coolers are switched on at an in-containment pressure of 1.3 bar.
- Sprays nozzles discharge in the dome compartment at a constant flow rate of 0.134 m³/s and temperature of 293.15 K. The activation setpoint is at 1.7 bar in the containment. The injection mode is switched to recirculation once the RWST empties. In that case, the water source is taken from the containment sump (C-02-15 compartment).
- The cavity pit can be flooded by water injection at a constant flow rate of about 19 kg/s when the signal of 923.15 K at the core outlet is reached.

IV.2.3.Containment nodalization

The containment model consists in 19 nodes connected by flow path (Figure 44). The complete list of compartments together with their volumes is given in Table 8.

The annular regions surrounding the SGs and PRZ compartments are physically divided into two levels by a slab. Therefore, two flow paths must be defined for those compartments to each of the annular compartment levels. Similarly, for the connections between the different SGs and PRZ compartments the same division into levels have been kept. Some equipment compartments or stairwells also connect vertically the different levels of the containment.

Flow paths are defined from centre to centre of the connected volumes and the MELCOR's default values are used for the form and friction loss coefficients.

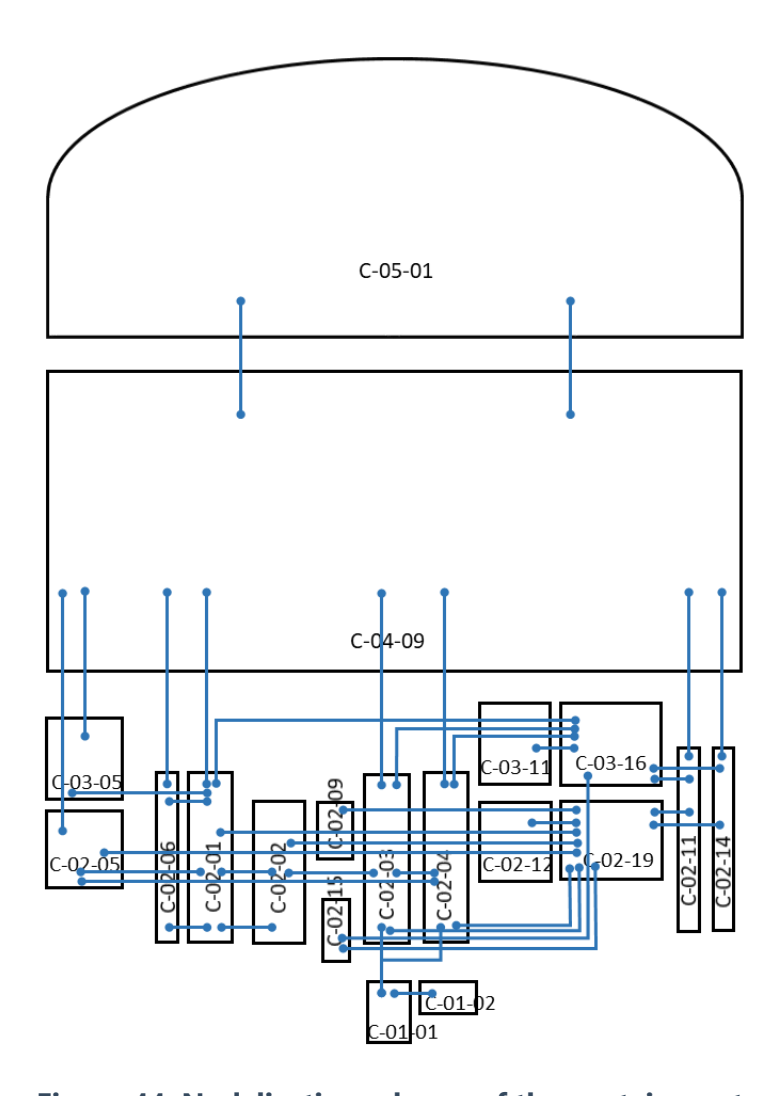


Figure 44. Nodalization scheme of the containment

IV.3. Sequences description

Four different sequences have been analysed (Table 9). The selection criteria have been: the significance in PSA level 2, the potential for combustible gases generation and the containment atmosphere conditions (both during the in-vessel and the ex-vessel phases). The LOCA sequences are characterized by the high amount of combustible gases in the ex-vessel phase with also a large amount of hydrogen in the in-vessel phase. The interest of the SBO lies in its similarity with the Fukushima accident and in its high core damage frequency.

Two Small Break LOCA in the cold leg have been simulated with different safety systems available in the containment (Table 9). A double-ended guillotine LOCA in the hot leg has also been simulated with both sprays and fan coolers actuating in the containment. Finally, the loss of power in the SBO prevents the activation of any safety system. All active injection systems into the

primary circuit are postulated to fail. This means that only the accumulators can inject their water inventory into the cold leg.

Table 8. Main characteristics of containment compartments

Compartment	Volume (m³)	MELCOR's name
Cavity	152.7	C-01-01
Adjacent room	216.4	C-01-02
SG-A	1206.5	C-02-01
SG-A (adjacent)	131.6	C-02-06
PRZ	580.9	C-02-02
SG-B	1778.6	C-02-03
SG-C	1878.1	C-02-04
Acces to RPV (inf)	207.1	C-02-05
PRZ tank	177.2	C-02-09
other rooms (inf)	470.3	C-02-12
Annulus (inf)	3472.6	C-02-19
Acces to RPV (sup)	1203.3	C-03-05
Other rooms (sup)	390.8	C-03-11
Annulus (sup)	2942.1	C-03-16
Upper	34965.0	C-04-09
Dome	16755.2	C-05-01
Containment sump	268.6	C-02-15
Stairswell	97.4	C-02-11
Stairswell	143.3	C-02-14

Table 9. Sequence definitions.

	SBLOCA-I	SBLOCA-II	SBO	LBLOCA
Auxiliary feed water	Off	Off	Off	Off
Safety injection	Off	Off	Off	Off
Containment sprays	Off	On	Off	On
Containment fan coolers	On	Off	Off	On
Cavity	Dry	Flooded ⁽¹⁾	Dry	Dry
Break diameter	5.05 cm (2")	5.05 cm (2")	_(2)	$DG^{(3)}$
Break location	Cold leg	Cold leg	_(2)	Hot leg

⁽¹⁾ cavity flooded as accident management

⁽²⁾ leakage from the main coolant pumps not considered

⁽³⁾ double guillotine

IV.4.Results and discussion

For all the sequences, the initial event is set at t = 0 s and the simulation evolves according to the sequence modelling (i.e., safety system's setpoints). Few seconds after the beginning of the accident, the scram occurs by low pressure in the primary. The chronology of main event during the accident evolution is listed in Table 10. Although time extend is not the same for all the sequences, the simulation cover the in-vessel and the ex-vessel phases in all the cases.

Table 10. Chronology of the main events.

Event	SBLOCA-I	SBLOCA-II	SBO	LBLOCA
Scram (s)	55	55	0.1	2.9
Fan coolers activation (s)	112	[-]	[-]	0.9
Sprays activation (s)	[-]	370	[-]	1.9
Cavity flooding activation (s)	[-]	1510	[-]	[-]
Switch sprays to recirculation (s)	[-]	12360	[-]	11961
Start of core uncovering (s)	863	860	6960	0.9
H ₂ generation onset (s)	1561	1570	9600	2.5
Total core uncovered (s)	1940	2740	10980	4320
Accumulator discharge (s)	2211	2220	12820	9.0
RPV rupture (s)	6945	6200	26400	6960

Regarding the combustible gases generation, the four sequences represent similar total amount at the end of the sequence (Table 11) although significant differences are observed in the generation in the in-vessel and the ex-vessel phases. Nonetheless, it is worth noting that low invessel generation is compensated in the ex-vessel phase due to the highest metal fraction present in the corium falling down into the cavity.

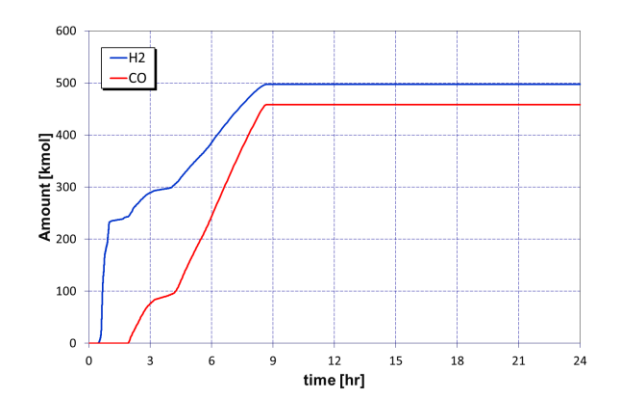
Table 11. Comparison of combustible gases generation (kmol) for the analysed sequences.

Gas	SBLOCA-I	SBLOCA-II	SBO	LBLOCA
Hydrogen (in-vessel)	255.6	294.7	341.9	247.3
Hydrogen (ex-vessel)	236.4	180.4	205.6	237.9
Carbon monoxide	458.0	343.3	420.5	456.2
TOTAL	950.0	818.1	968.0	941.4

IV.4.1.SBLOCA-I

The core degradation is produced at low pressure in the reactor vessel because of the inventory loss through the RCS breach. During the in-vessel phase, the containment pressure evolution is due to the opposing effects of the flow into the containment through the RCS breach and the fan coolers operation, which partially condense the steam into the containment. Both effects result in the pressure reaching a peak of 2.8 bar at ~3 h. At the ex-vessel phase, the generation of non-condensable gases and the reduced capacity of the fan coolers to further condensate steam lead to a slight but continuous rise in the pressure.

Figure 45 plots the H₂ and CO generated during the in-vessel and ex-vessel phases whereas Figure 46 plots the evolution of the in-containment pressure.



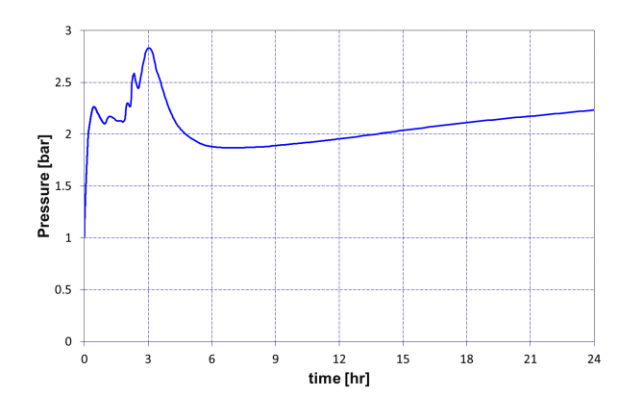
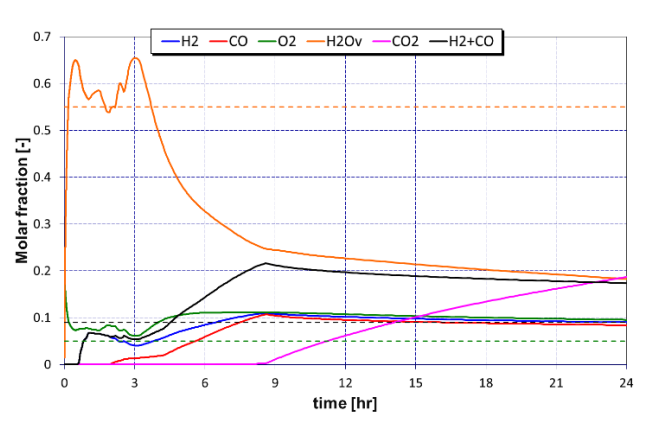


Figure 45. H₂ and CO generation in the SBLOCA-I sequence.

Figure 46. Containment pressure evolution in the SBLOCA-I sequence.

The high release of hydrogen in the in-vessel phase and later also CO in the ex-vessel phase leads to the accumulation of both gases in the containment. Besides, the operation of the fan coolers boots the combustible gases fraction, especially after 3 h after the accident beginning. As a consequence, the atmosphere mixture reaches flammability conditions. Figure 47 plots the atmosphere composition of the upper compartment as representative volume whereas. Figure 48 shows how the atmosphere reaches comes into the deflagration region in the Shapiro diagram.



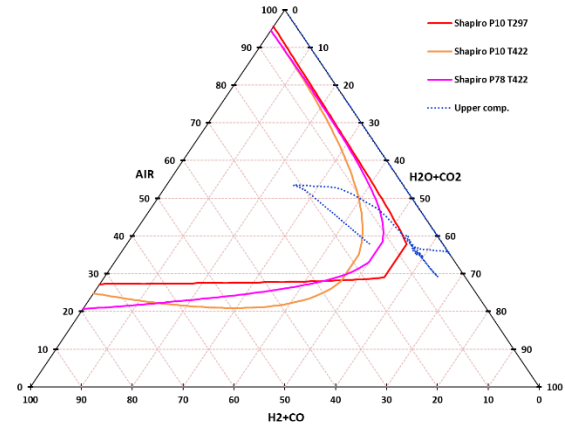
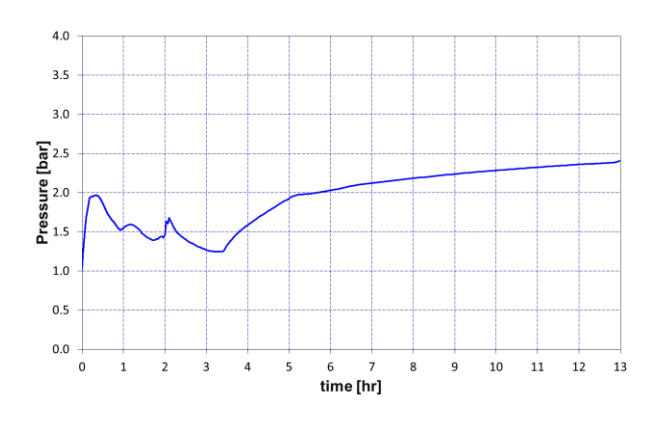


Figure 47. Gas mole fraction of different components in the upper compartment for the SBLOCA-I sequence.

Figure 48. Shapiro diagram for the upper compartment in the SBLOCA-I sequence.

IV.4.2.SBLOCA-II

The in-vessel evolution of this sequence is very similar to the evolution of the SBLOCA-I. Nonetheless, the activation of the sprays changes significantly the containment behaviour as they strongly limit the rise of the containment pressure (Figure 49) until the sprays are switched to the recirculation mode at \sim 3.4 h. The flooding of the cavity leads to a lower generation rate of H₂ and CO by MCCI (Figure 50) and a higher fraction of steam in the ex-vessel phase compared with the SBLOCA-I sequence.



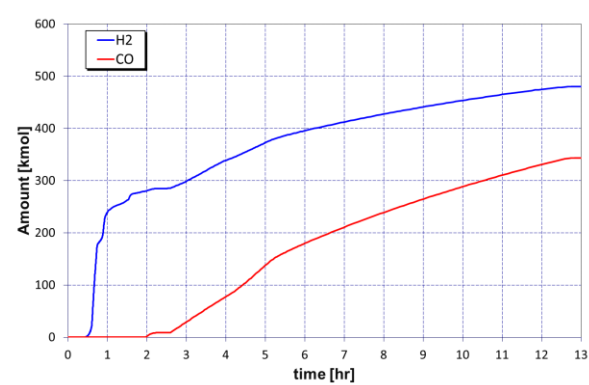


Figure 49. Containment pressure evolution in the SBLOCA-II sequence.

Figure 50. H2 and CO generation in the SBLOCA-II sequence.

At around 1 hour after the beginning of the accident, the total molar fraction of the combustible gas reaches 0.09 with the steam fraction low enough to do not inert the containment atmosphere.

During the ex-vessel phase, the combustible gases molar fraction even rises by the further gases generation (Figure 51). The Shapiro diagram (Figure 52) shows how the gas mixture becomes flammable.

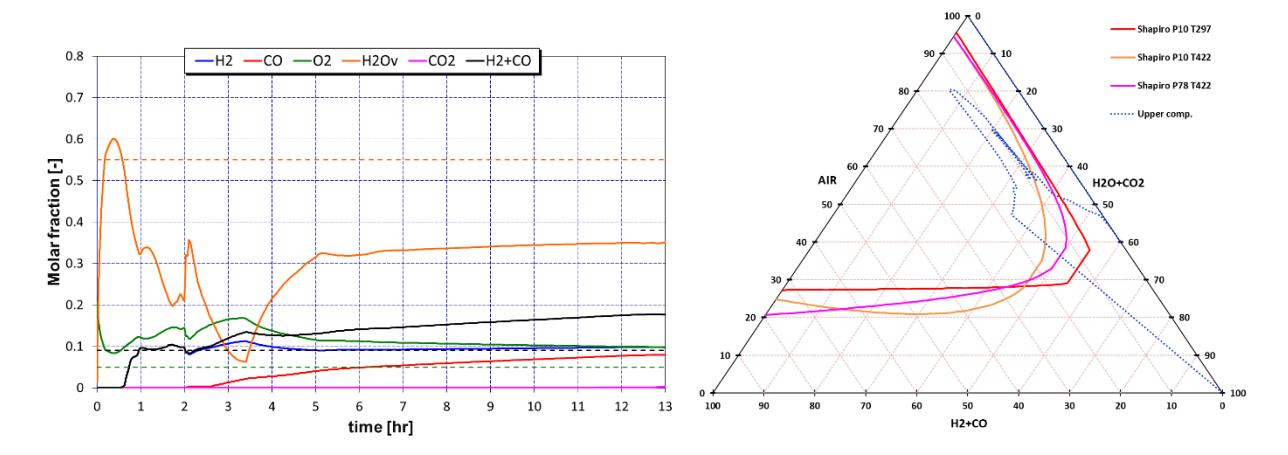


Figure 51. Gas mole fraction of different components in the upper compartment for the SBLOCA-II sequence.

Figure 52. Shapiro diagram for the upper compartment in the SBLOCA-II sequence.

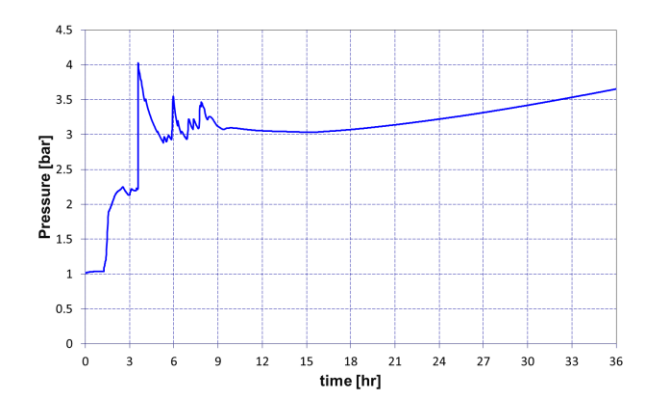
IV.4.3.SBO

In the SBO the pressure rise by steam release into the containment is not compensated by any safety system. Different paths to steam, and hydrogen, release into the containment open in the accident evolution (Table 12).

Table 12. Flow paths opened between the RCS and the containment in the SBO sequence.

Time	Break type	From	То
1.26 h	Disk rupture	Pressurizer tank	Pressurizer tank compart.
3.56 h	Pipe creep	Hot leg (loop 3)	SG-C compartment
7.33 h	Lower head failure	RPV lower plenum	Cavity

Pressure in the containment (Figure 53) peaks at 4 bar at the hot leg failure by creep, afterwards, it varies between 3 and 4 bar. The hydrogen generation begins at 2.7 h and the ex-vessel gases generation does not start until 7.7 h (Figure 54), notable delayed compared with the other sequences.



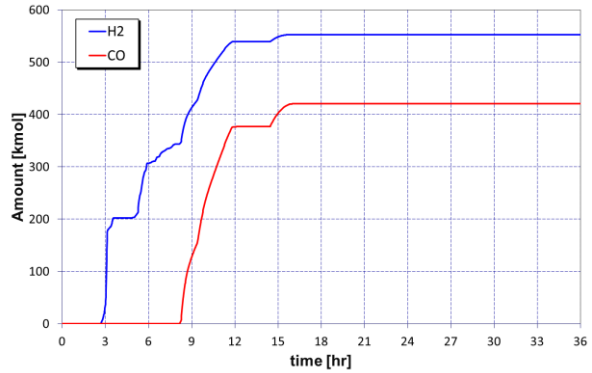
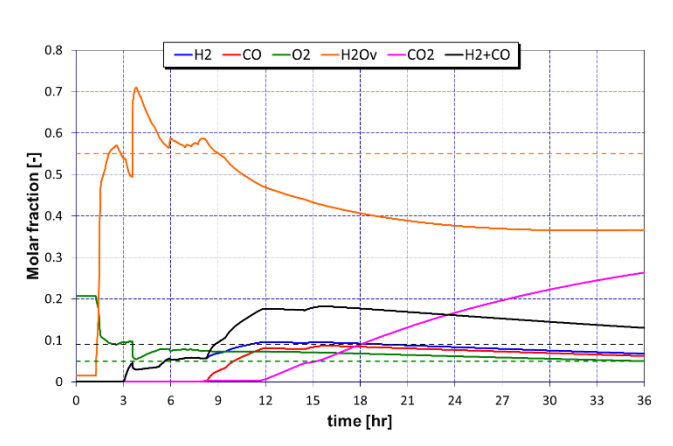


Figure 53. Containment pressure evolution in the SBO sequence.

Figure 54. H₂ and CO generation in the SBO sequence.

During most of the core degradation, the containment is inerted by high steam molar fraction. However, some minutes after the beginning of the ex-vessel phase, the accumulation of H_2 and CO yields the atmosphere mixture to reach flammable conditions (Figure 55 and Figure 56).



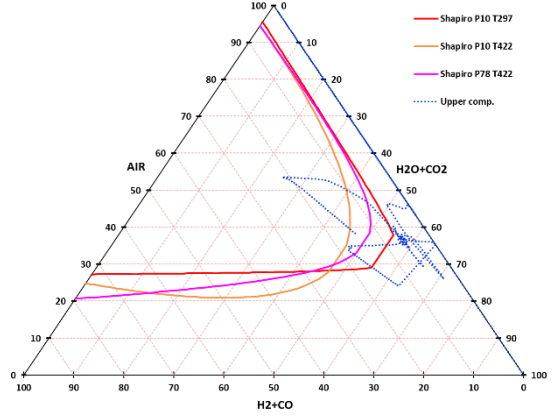


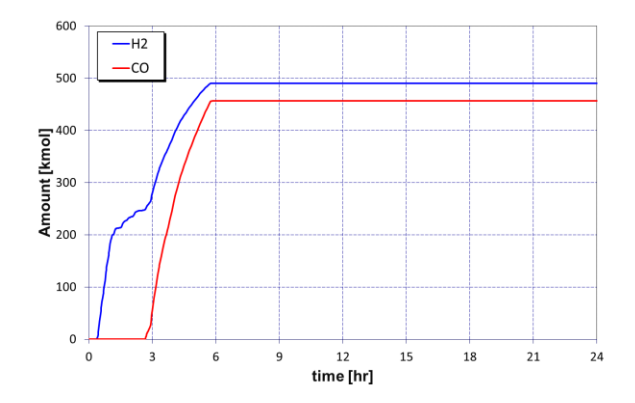
Figure 55. Gas mole fraction of different components in the upper compartment for the SBO sequence.

Figure 56. Shapiro diagram for the upper compartment in the SBO sequence.

IV.4.4.LBLOCA

Due to the fast uncovering and depressurization of the reactor vessel, the core degradation begins very early in the accident (Figure 57). The cladding oxidation onset is observed at 2.5 s after the beginning of the accident. The MCCI generation starts at 2.7 h and at about 6 h the corium in the cavity gets completely oxidized.

The large water and steam release through the RCS breach lead to a sudden peak of pressure (Figure 58). The activation of the containment safety systems (fan cooler and sprays) significantly reduces the pressure. Later, the generation of non-condensable gases by MCCI reverses this tendency. At around 3.3 h, the switch of sprays operation to the recirculation mode reduces their efficiency, and the steam molar fraction increases as so the pressure.



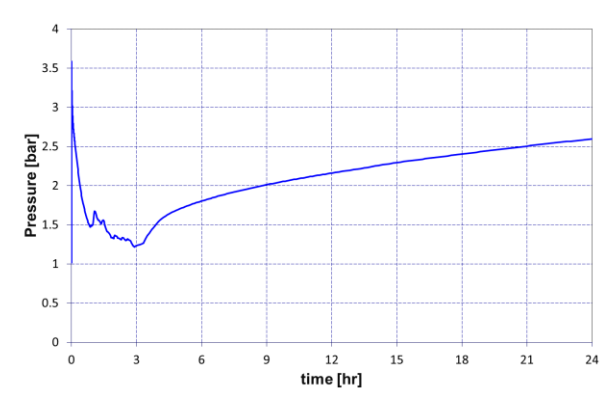


Figure 57. H2 and CO generation in the LBLOCA sequence.

Figure 58. Containment pressure evolution in the LBLOCA sequence

The high release of hydrogen in the in-vessel phase together with the important drop of steam molar fraction due to the actuation of the safety systems lead to reach flammable conditions at the end of the in-vessel phase (Figure 59). Later, in the ex-vessel phase, the further release of combustible gases leads them to reach a maximum value of \sim 0.25 at about 6 h. The subsequent CO₂ generation results in a certain dilution of the mixture (Figure 59). The Shapiro diagram (Figure 60) shows that the atmosphere mixture deeply comes into the deflagration region.

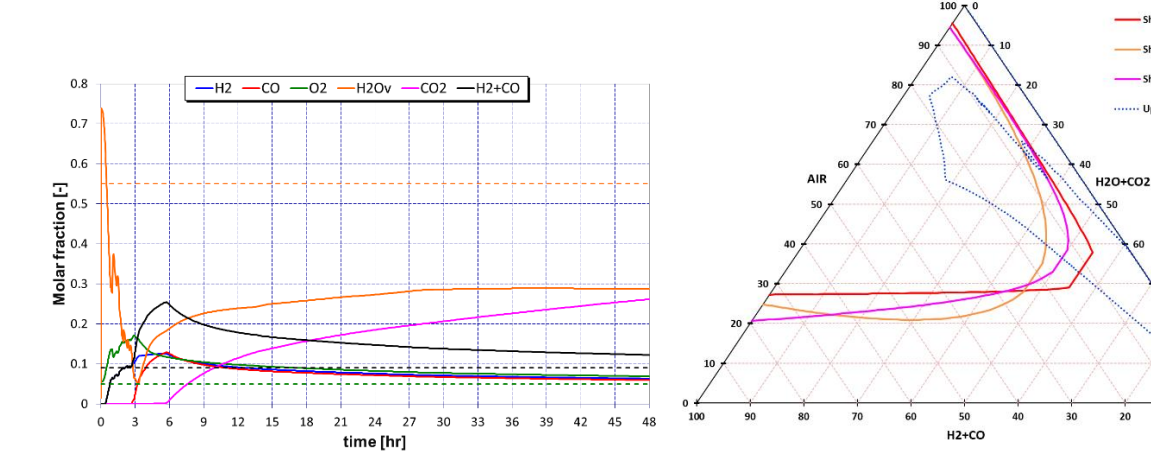


Figure 59. Gas molar fraction of different components in the upper compartment for the LBLOCA sequence.

Figure 60. Shapiro diagram for the upper compartment in the LBLOCA sequence.

IV.5. Main highlights

The hydrogen release into the containment is quite different in both types of sequences. For LOCA's hydrogen is released through the circuit breach whereas for the SBO the release path is more complex. The first release is produced to the PRZ tank and from it to the containment when the seals break. The creep of the hot legs depressurizes the primary circuit and the gas release, including H_2 , is through the estimated pipe rupture. Finally, the vessel's lower head failure lead to the remaining H_2 and the subsequent gas generation by MCCI.

The availability of safety systems is a key factor conditioning the combustion risk associated with each sequence. The capacity of safety systems to condensate steam, especially in the ex-vessel phase results in the rise of the combustible gas molar fraction in the atmosphere mixture.

All the sequences analysed in this work lead to flammable gas mixtures in the containment. The most challenging of them are the SBLOCA-I and the LBLOCA.

IV.6. References

Humphries, L.L., Beeny, B.A., Gelbard, F., Haskin, T., Louie, D.L., Phillips, J., Schmidt, R.C., Bixler, N.E., 2021a. MELCOR Computer Code Manuals Vol. 2: Reference Manual Version 2.2.18019 (No. SAND2021- 0241 O). Sandia National Laboratories, Albuquerque.

Humphries, L.L., Beeny, B.A., Gelbard, F., Haskin, T., Louie, D.L., Phillips, J., Schmidt, R.C., Bixler, N.E., 2021b. MELCOR Computer Code Manuals Vol. 2: Primer and Users' Guide. Version 2.2.18019 (No. SAND2021- 0252 O). Sandia National Laboratories, Albuquerque.

IAEA, 2015. The Fukushima Daiichi Accident. Technical Volume 1/5: Description and Context of the Accident. IAEA, Austria.

Jiménez, G., Herranz, L.E., Bentaib, A., Nabiha, C., Reinecke, E.A., Kelm, S., Loeffler, M., Braun, M., Bratfisch, C., Kljenak, I., Sevbo, O., Visser, D.C., Liang, Z., Balech, S., 2022. AMHYCO Project – Towards an Enhanced Accident Management of the H2/CO Combustion Risk. Presented at the The 19th International Topical Meeting on Nuclear Reactor Thermal Hydraulics (NURETH-19), Bussels (Belgium).

Ross, K., Phillips, J., Gauntt, R.O., Wagner, K.C., 2014. MELCOR Best Practices as Applied in the State-of-the-Art Reactor Consequence Analyses (SOARCA) Project (No. NUREG/CR-7008). Sandia National Laboratories.

Sehgal, B.R. (Ed.), 2012. Chapter 3 - Early Containment Failure, in: Nuclear Safety in Light Water Reactors. Academic Press, Boston, pp. 185–306. https://doi.org/10.1016/B978-0-12-388446-6.00003-4

ANNEX V. Individual report for the PWR-KWU reactor – AC² model (RUB)

V.1. Introduction

The report at hand describes simulations of hypothetical accident sequences in a generic 1,300 MW_{el} pressurized water reactor (PWR) of type Siemens KWU (KONVOI) conducted by Plant Simulation and Safety (PSS) at Ruhr-Universität Bochum (RUB) in the frame of working package two (WP2) in the AMHYCO project. Four in-vessel accident sequences are simulated using ATHLET and ATHLET-CD which are part of the code package AC² 2019.1 developed by Gesellschaft für Anlagen- und Reaktorsicherheit (GRS) gGmbH. Out of these four sequences, the two most limiting sequences regarding combustible gas release are selected as basis for ex-vessel simulations using COCOSYS (code package AC² 2019.1). For each of the two selected in-vessel simulations one COCOSYS simulation with fully functioning PARs and one simulation with complete PAR failure are performed.

V.2. Plant model

In the following paragraphs the plant model used for the simulations is described.

V.2.1. In-vessel nodalization

For the simulation of thermal-hydraulic processes and core degradation related phenomena within the accident sequences, ATHLET and ATHLET-CD from the code package AC² 2019.1 are used.

The simulated power plant is a generic four loop PWR Type KWU with 3,850 MW_{th} and 1,300 MW_{el}. In Figure 61 the primary and secondary side nodalization is shown. The four loops are modelled in two loops, one triple weighted and one single weighted loop including the pressurizer. The Utubes transfer the generated heat to the steam generators. The core itself consists of eight sections, six core channels, one bypass and one downcomer. In addition, the lower and upper plenum are modelled. After the degradation of up to 57,900 fuel rods and 1,465 control rods and the relocation to the lower plenum, the ATHLET-CD module AIDA is activated. AIDA simulates the corium inside the lower plenum as well as the degradation of the RDB wall and its failure, which is influenced by pressure difference, temperature, remaning wall thickness and corium mass.

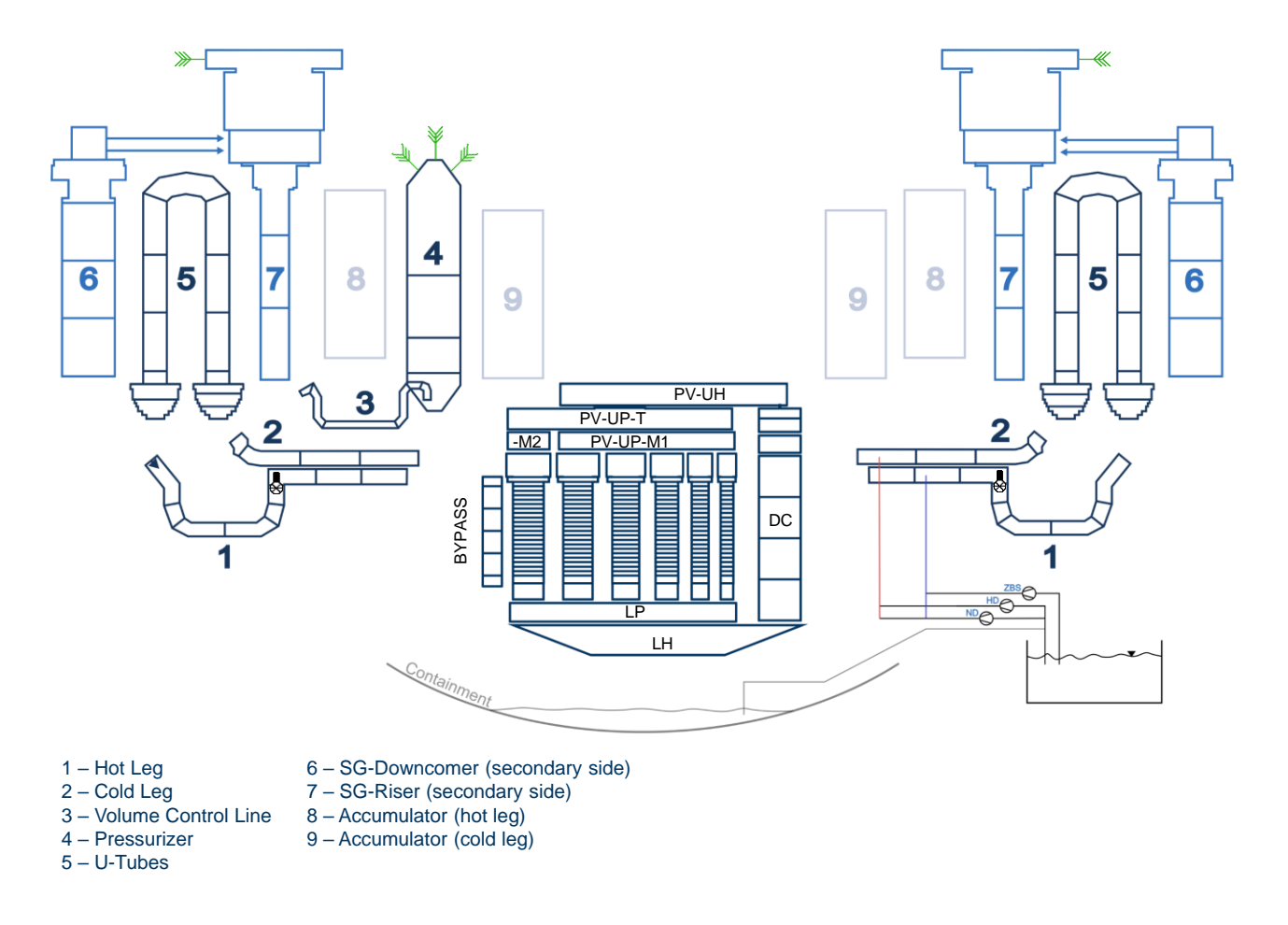


Figure 61. Primary and secondary side nodalization in ATHLET(-CD)

V.2.2. Approximations and assumptions

The power plant dataset contains several safety features. In case of a high-pressure accident the reactor coolant system (RCS) pressure is limited by the pressurizer safety valves to 160 bar. For a primary side depressurization (PSD) all three valves can be opened, when the core outlet temperature reaches 650 °C. In case of a pressure loss, for example due to a loss of coolant accident (LOCA) or a PSD, the eight passive hydro accumulators (HA) (one hot and one cold sided for each loop) can inject a water inventory of 30 m³ each to the RCS at a primary pressure of 26 bar. For reflooding scenarios four reflooding tanks with 1,560 t of water in total are modelled. Which safety systems are postulated to fail is defined within each sequence (see chapter 3).

The mass and enthalpy flow of water, steam, hydrogen and nitrogen from the leak (for the SBLOCA) or the safety relief valves and blow down valves (for the SBO) determined by the invessel simulation are taken as boundary condition for the ex-vessel simulation. Furthermore, the mass flow of corium from the RPV rupture to the cavity and the time dependent decay power are

taken as boundary condition for the simulation of corium concrete interaction (CCI). A radial melt through of the biological shield respectively the maintenance door is assumed after a radial erosion of 45 cm of concrete. A spreading of the melt to the sump and a sump water ingression into the cavity is assumed afterwards and modelled by a sump balance junction (SUMP_BAL). A generic siliceous concrete was selected for the simulation of CCI. The concrete composition is chosen in order to achieve a conservative result regarding the release of CO from CCI.

V.2.3. Containment nodalization

The containment nodalization shown in Figure 62 comprises 23 zones connected by junctions. These zones are listed in Table 13 with their corresponding volumes. The zones are connected by atmospheric junctions as well as drain junctions which allow water to flow to the sump compartment. Junctions of type RUPTURE are modelled for doors between compartments and for rupture discs (e.g. at the top of the steam generator housing). 57 passive autocatalytic recombiners (PARs) were modelled using the GRS_DIFF correlation for Framatome PARs and their distribution over the zones is indicated in the Figure 62. The main structures in the containment are modelled with their respective surface areas, thicknesses and materials. The heat transfer and condensation models CO1 and WWR are used.

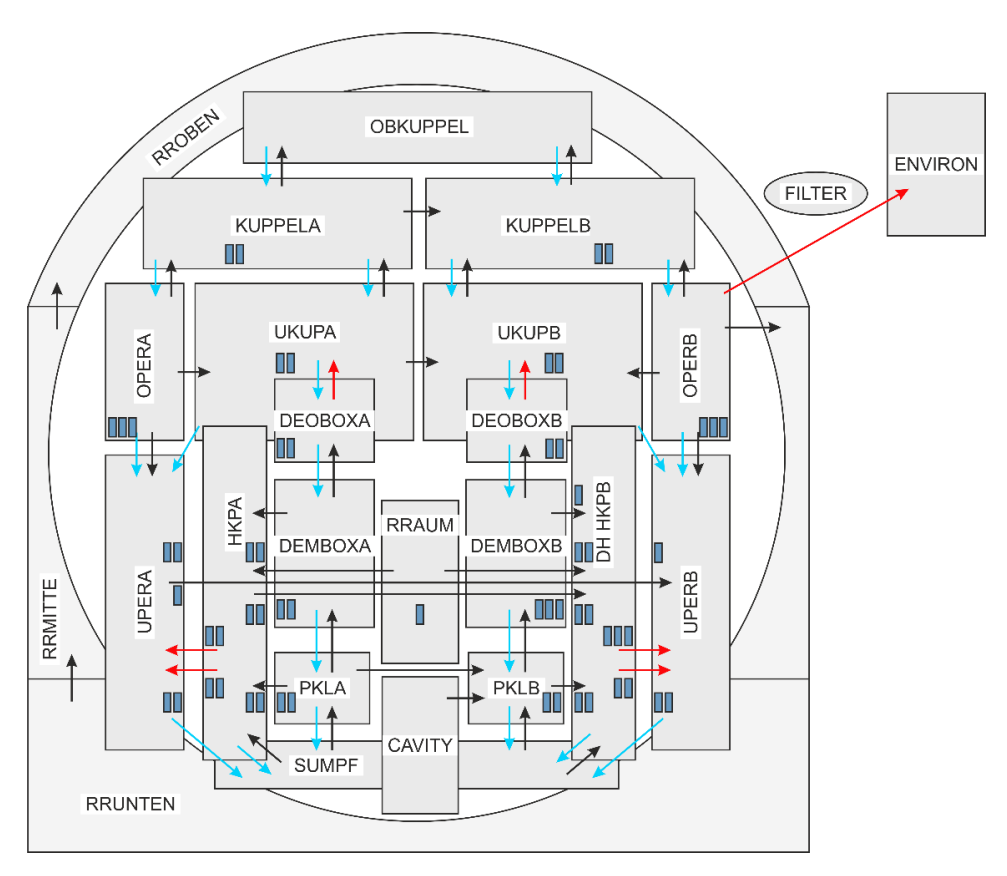


Figure 62. Containment nodalization in COCOSYS with PARs indicated

Zone	Volume [m³]	Zone	Volume [m³]
SUMPF	3858,0	RRAUM	640,0
PKLA	500,0	BEBECKEN	1665,0
PKLB	500,0	UKUPA	7038,0
НКРА	6096,0	UKUPB	7038,0
DHHKBP	5956,0	KUPPELA	5526,0
DEMBOXA	500,0	KUPPELB	5526,0
DEMBOXB	500,0	OBKUPPEL	2940,0
DEOBOXA	270,0	SPALT	147,0
DEOBOXB	270,0	RELTANK	38,0
UPERA	3889,0	CAVITY	143,0
OPERA	6719,0	RRUNTEN	21742,0
UPERB	3989,0	RRMITTE	14316,0
OPERB	6885,0	RROBEN	5664,0
	Table 13 Con	tainment Volumes	!

Table 13. Containment Volumes

V.3. Sequences description

For the in-vessel sequences, two scenarios with two different boundary conditions each are performed. One scenario is a postulated station blackout (SBO) with a postulated failure of grid and house load, station diesel and bunkered diesel. Only batteries remain available. Due to power loss and coolant pump failure the core starts to heat up. Following the coolant temperature, the primary pressure rises. When reaching 166 bar the pressurizer safety relief valve opens and closes alternating. In this scenario the pressure stays high until the reactor pressure vessel (RPV) fails. In the second sequence variation (SBO+PSD), the primary side depressurization takes places when the core outlet temperature reaches 650 °C. With the PSD start criterion three pressurizer safety valves open, causing a rapid pressure drop inside the primary coolant system. The pressure drop allows the accumulators to inject and therefore delays the RPV failure.

The other scenario is a small break loss of coolant accident (SBLOCA) with an 80 cm² leakage behind the main coolant pump in the cold leg of the pressurizer loop. In the first SBLOCA sequence, all active injection systems are postulated to fail. Only the accumulators can inject their inventory. In the second SBLOCA sequence (SBLOCA+ECCS) a limited injection is postulated to be available. When the waterlevel inside the pressurizer falls below 2.28 m the extra borating system with a small injection rate of 8 kg/s for every loop starts. Over a period of 9,000 s 72 t of water are slightly delaying the core uncovery process. For both SBLOCA sequences the secondary side pressure falls down to about 3 bar as a consequence of the available 100 K/h cooldown.

In all four sequences the sump recirculation is not available. Table 14 includes important events with related point of time for the four in-vessel sequences. The values for hydrogen and melt mass are captured at 30,000 s to include produced hydrogen after RPV failure also.

Due to the amount of produced hydrogen, melt and water mass transferred to the containment two sequences have been chosen for further ex-vessel simulations. As SBO+PSD and SBLOCA+ECCS have a comparable mass of hydrogen but a significant difference of water in the containment and to investigate the impact of inerting steam on flammability, these two sequences are used for ex-vessel simulations. For each of the two selected in-vessel simulations one COCOSYS simulation with fully functioning PARs and one simulation with postulated complete PAR failure are performed.

	SBO	SBO+PSD	SBLOCA	SBLOCA+ECCS
Event start	0 s	0 s	0 s	0 s
SCRAM		0 s	3 s	3 s
Start HA injection	-	6,635 s	18,293 s	1,747 s
Start ECCS	-	-	-	28 s
Start PSD	-	6,263 s	-	-
Start core degradation	6,390 s	10,909 s	14,492 s	19,180 s
Start relocation	7,509 s	12,223 s	15,951 s	20,663 s
RPV failure	7,942 s	13,491 s	17,176 s	23,451 s
Discharged melt mass to containment	106,264 kg	147,826 kg	145,242 kg	142,451 kg
Discharged water (Vapor+ Liquid) to containment	278,614 kg	531,809 kg	394,755 kg	447,613 kg
Generated H2	498 kg	617 kg	500 kg	588 kg

Table 14. Sequence events

V.4. Results and discussion

In the following the results of the ex-vessel simulations of the two selected sequences SBO+PSD as well as SBLOCA+ECCS are presented and discussed briefly.

V.4.1. Sequence SBO+PSD

During the SBO+PSD sequence the containment pressure peaks between 6,000 and 14,000 s at around 3.8 bar (cf. Figure 63) both for the simulation with fully operational PARs (left) and the simulation with postulated failure of PARs. The pressure then drops to 2 bar at around 47,000 s and rises again due to sump water ingression into the cavity and following steam production. The containment temperature (cf. Figure 64) also peaks between 6,000 and 14,000 s at around 140 °C. Due to the missing heat output from the PARs the temperature in the simulation with postulated complete failure of PARs remains about 10 to 20 °C below the temperature in the simulation with PARs from around 10,000 s up until the end of the sequence.

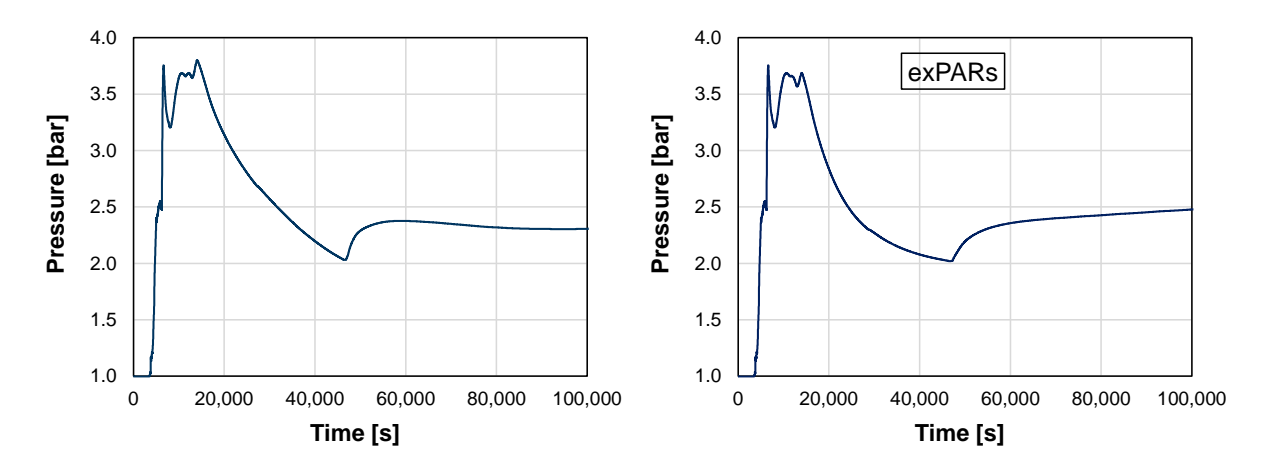


Figure 63. SBO+PSD: Containment pressure (zone UKUPA);
I.: Simulation with operational PARs, r.: Simulation without PARs

Figure 65 shows the mass transfer from the pressurizer relief tank to the containment (zone DHHKPB) over time. Figure 66 shows the gas release from CCI in zones CAVITY and SUMPF. In total around 900 kg H_2 and 6800 kg CO are released by CCI, the release rates only differ slightly between the simulation with and the simulation without PARs.

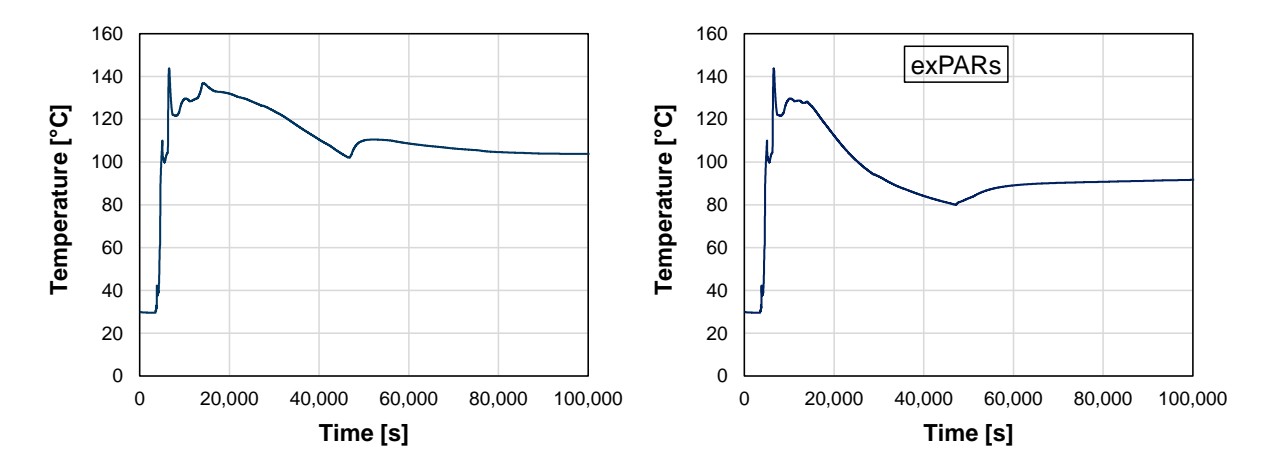


Figure 64. SBO+PSD: Containment temperature (zone UKUPA);
I.: Simulation with operational PARs, r.: Simulation without PARs

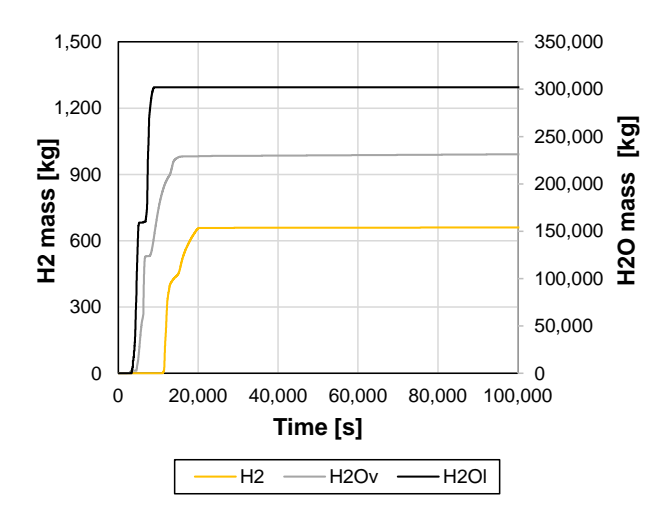


Figure 65. SBO+PSD: Leakage masses from primary circuit (zone DHHKPB)

The atmospheric composition for the zone identified to have the highest combustion risk (zone DHHKBP) is plotted in Figure 67. The steam (H_2O_v) concentration peaks at about 80 vol.% for both simulations and drops slowly to about 40 vol.% at 47,000 s. After that it peaks again at 60 vol.% due to the flooding of the cavity. The O_2 concentration drops to about 5 vol.% beginning with the mass transfer from the pressurizer relief tank to the containment at around 3600 s and remains there until 20,000 s for the simulation with operational PARs. The H_2 concentration peaks at 20,000 s with 6 vol.% and the CO concentration peaks at 27,000 s with around 3 vol.%. The O_2 , O_2 00 and CO concentrations subsequently decrease and at 60,000 s all three are below 1 vol.% for the simulation with operational PARs. In the simulation with postulated PAR failure the hydrogen concentration peaks at 16 vol.%, the CO concentration at 5 vol.% with O_2 availability between 7.5 and 11 vol.%.

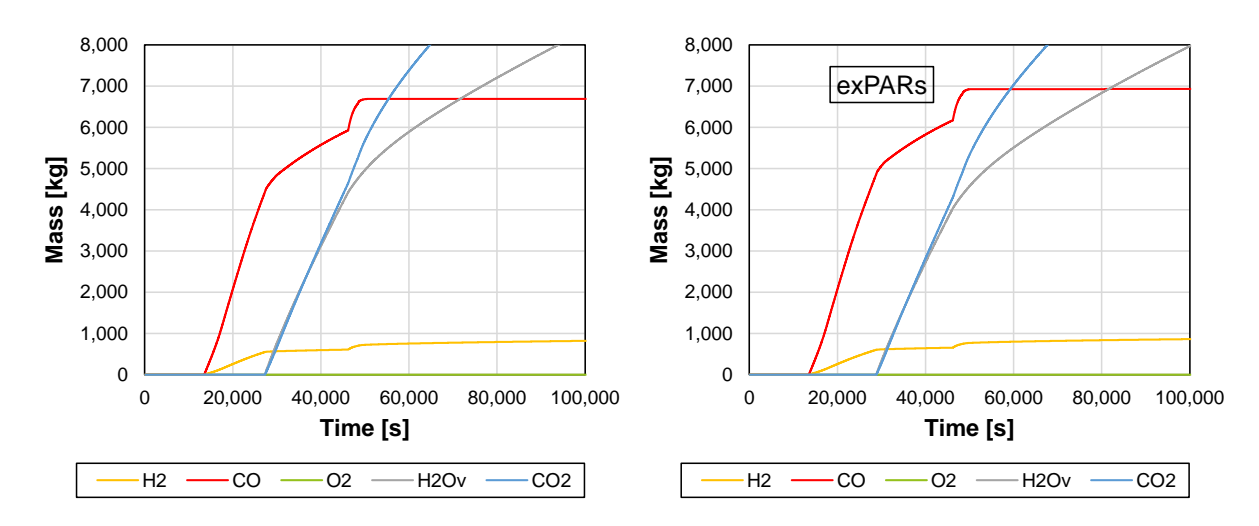


Figure 66. SBO+PSD: Released gas masses from CCI (zones SUMPF and CAVITY);
I.: Simulation with operational PARs, r.: Simulation without PARs

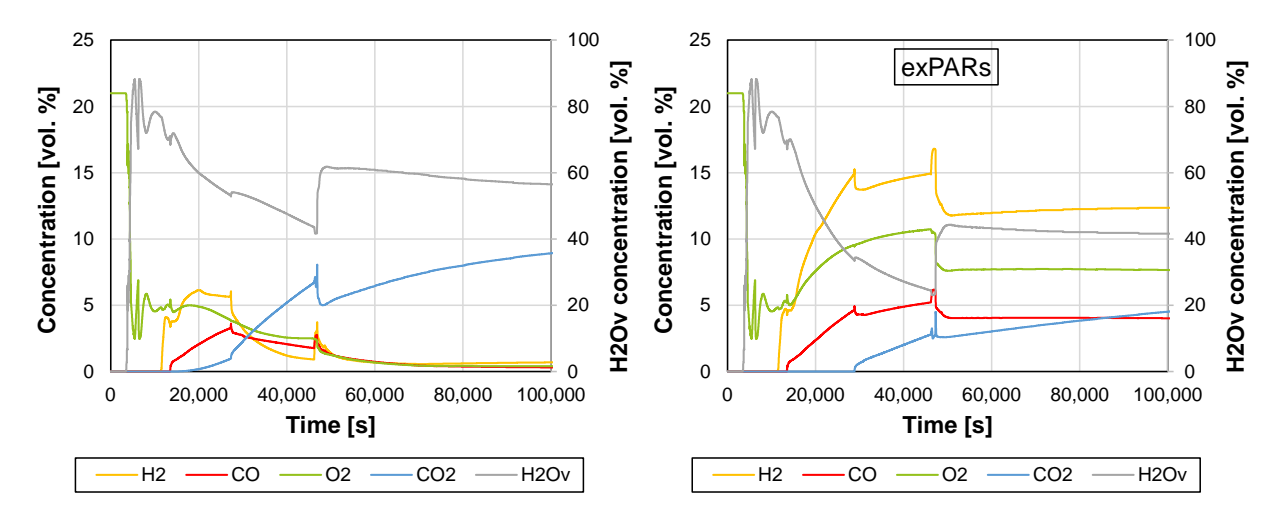


Figure 67. SBO+PSD: Atmosphere composition (zone DHHKPB);
I.: Simulation with operational PARs, r.: Simulation without PARs

The heterogeneity index shown in Figure 68 evolves similarly in the simulation with operational PARs and in the simulation with postulated PAR failure during the first 17,000 s of the sequence. After that they diverge noticeably. The heterogeneity index is determined by dividing the highest combined concentration of H_2 and CO by the lowest combined H_2 and CO concentration at any given time step.

In Figure 69 Shapiro diagrams for the zone with the highest combustion risk are plotted. For the simulation with PARs combustion criteria are not met due to a high concentration of inert components (steam, N₂ and CO₂). In the simulation with postulated failure of PARs combustible conditions are reached.

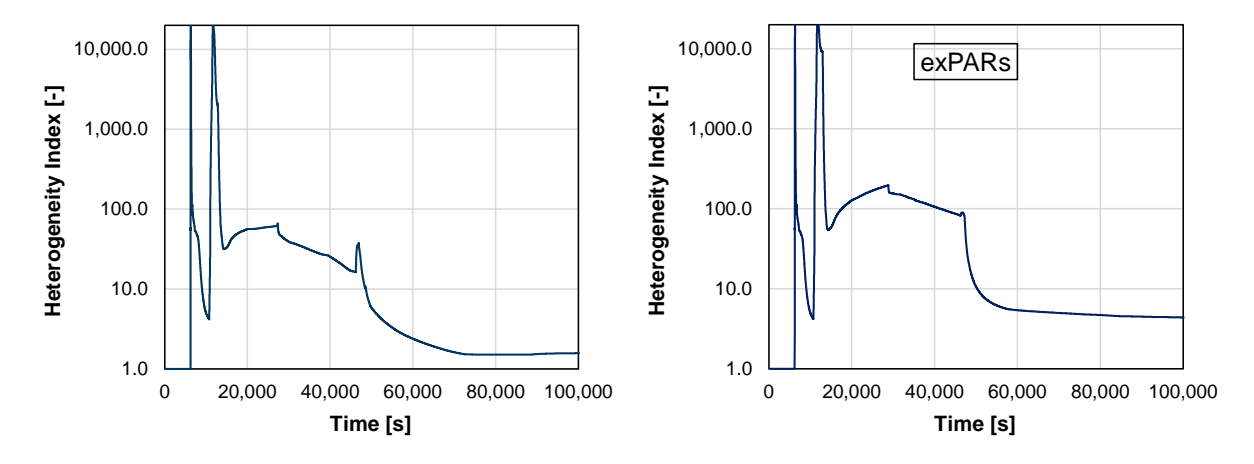


Figure 68. SBO+PSD: Heterogeneity index;
I.: Simulation with operational PARs, r.: Simulation without PARs

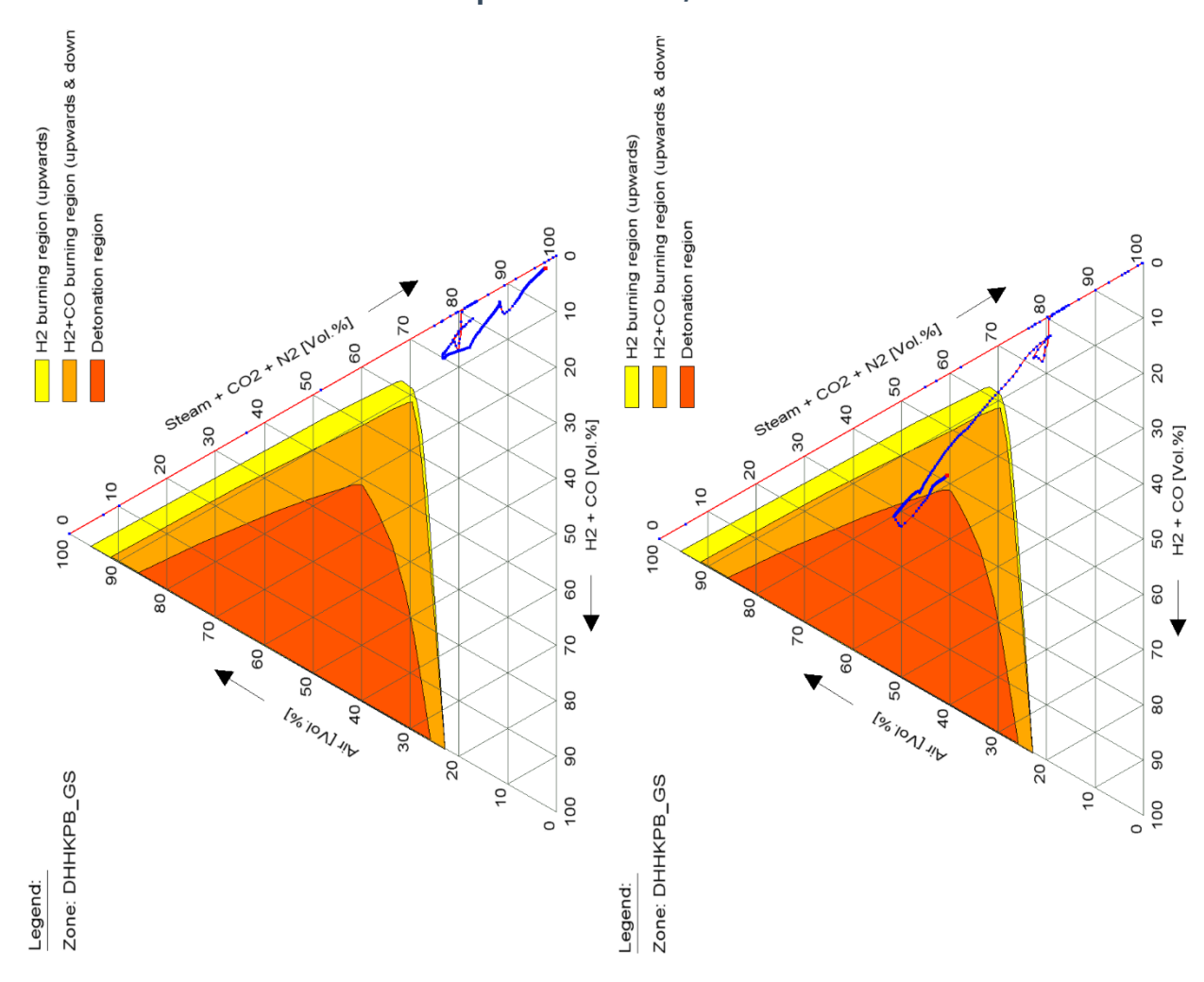


Figure 69. SBO+PSD: Shapiro diagram (zone DHHKPB);
I.: Simulation with operational PARs, r.: Simulation without PARs

V.4.2. Sequence SBLOCA+ECCS

The containment pressure (cf. Figure 70) peaks at about 2,000 s with 2.7 bar and subsequently drops to 1.6 bar at 20,000 s. Subsequently the pressure increases again due to the start of HA injection, RPV rupture and subsequent CCI. At 58,000 s another steep rise in containment pressure occurs due to sump water ingression into the cavity and following steam generation. The containment temperature (cf. Figure 71) peaks at 106 °C at 2,000 s and subsequently decreases up until the HA injection and RPV failure. In the simulation with postulated PAR failure the temperature remains significantly lower than in the simulation with active PARs after the onset of H_2 release to the containment (20,000 s).

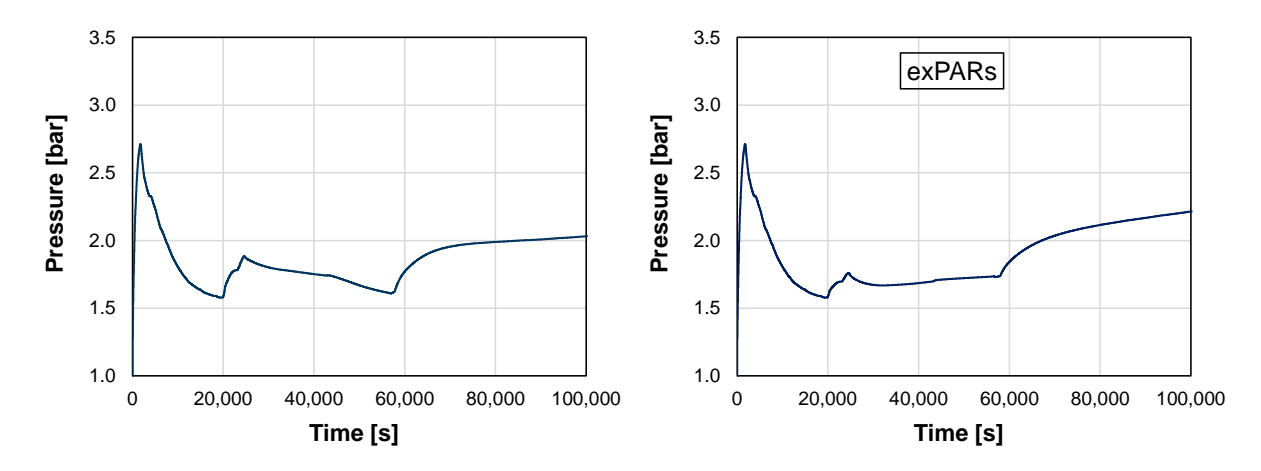


Figure 70. SBLOCA+ECCS: Containment pressure (zone UKUPA);
I.: Simulation with operational PARs, r.: Simulation without PARs

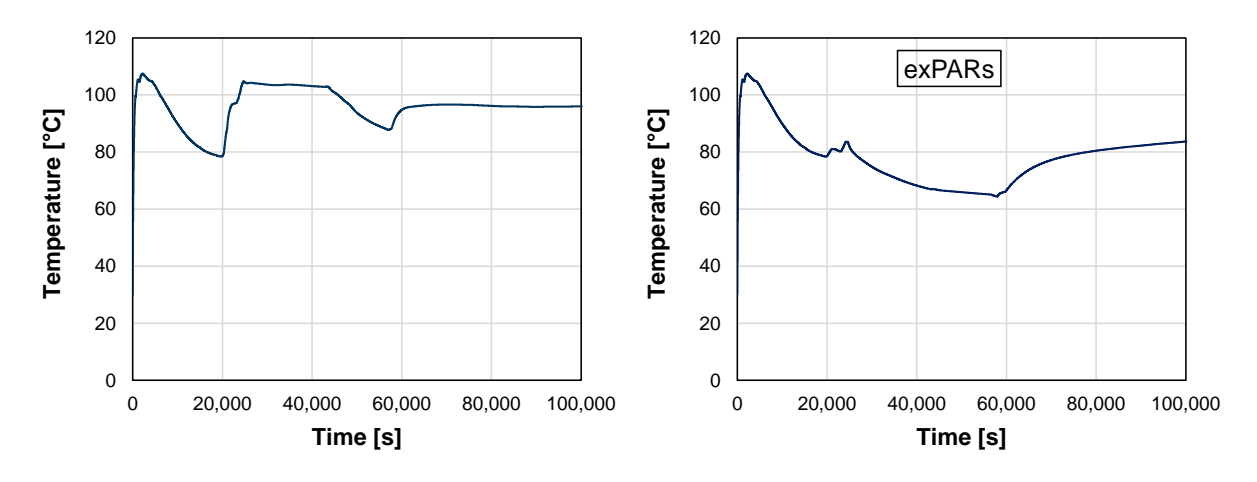


Figure 71. SBLOCA+ECCS: Containment temperature (zone UKUPA);
I.: Simulation with operational PARs, r.: Simulation without PARs

The released fluid masses from the primary circuit through the break to the containment are displayed in Figure 72. The released mass of H_2 is very similar to the SBO+PSD sequence. The released mass of liquid water (H_2O_1) is slightly higher than in case of the SBO+PSD sequence but the steam (H_2O_v) mass is significantly lower. Figure 73 shows the gas masses released by CCI. Approximately 7,000 kg of CO and 900 kg of H_2 are released.

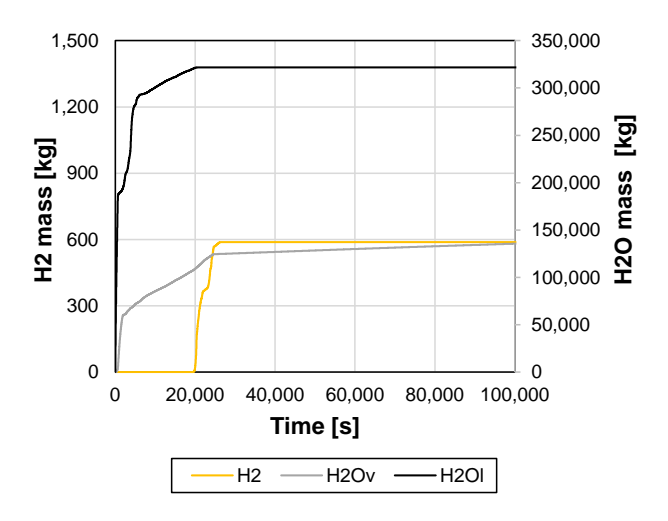


Figure 72. SBLOCA+ECCS: Leakage masses from PRZ (zone PKLB)

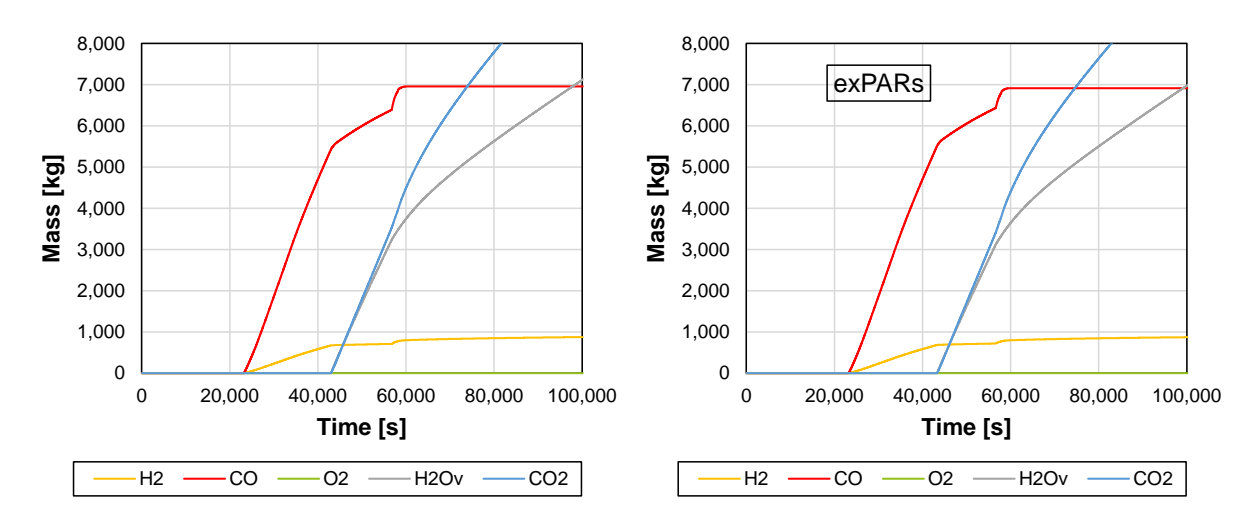


Figure 73. SBLOCA+ECCS: Released gas masses from CCI (zones SUMPF and CAVITY);
I.: Simulation with operational PARs, r.: Simulation without PARs

The atmospheric composition for the zone with the highest combustion risk is plotted in Figure 74. The steam concentration peaks at 100 vol.-% in the beginning with the leak opening. It subsequently drops to 42 to 33 vol.% between 10,000 and 50,000 s. In case of the simulation with operational PARs the H₂ concentration peaks at 22 vol.% but quickly drops to 5 to 10 vol.% between 20,000 and 40,000 s. In this time frame O₂ availability is between 5 and 12 vol.%. In case of the simulation with postulated PAR failure H₂, O₂ and CO are available throughout the whole

accident sequence with hydrogen concentration between 10 and 18 vol.% after 25,000 s. During the first 22,000 s of the sequence the heterogeneity index shown in Figure 75 evolves similarly in the simulation with operational PARs as in the simulation with postulated PAR failure. Subsequently they diverge noticeably with the latter sequence showing higher numbers than the former.

Figure 76 shows Shapiro diagrams for the zone with the highest combustion risk (PKLB). In contrast to the SBO+PSD simulation with operational PARs the Shapiro diagram for the SBLOCA+ECCS simulation with operational PARs shows fulfilled ignition criteria for a period of time. For most of the time the ignition criteria are fulfilled only for upwards burning. For the simulation with malfunctioning PARs selected detonation criteria are fulfilled.

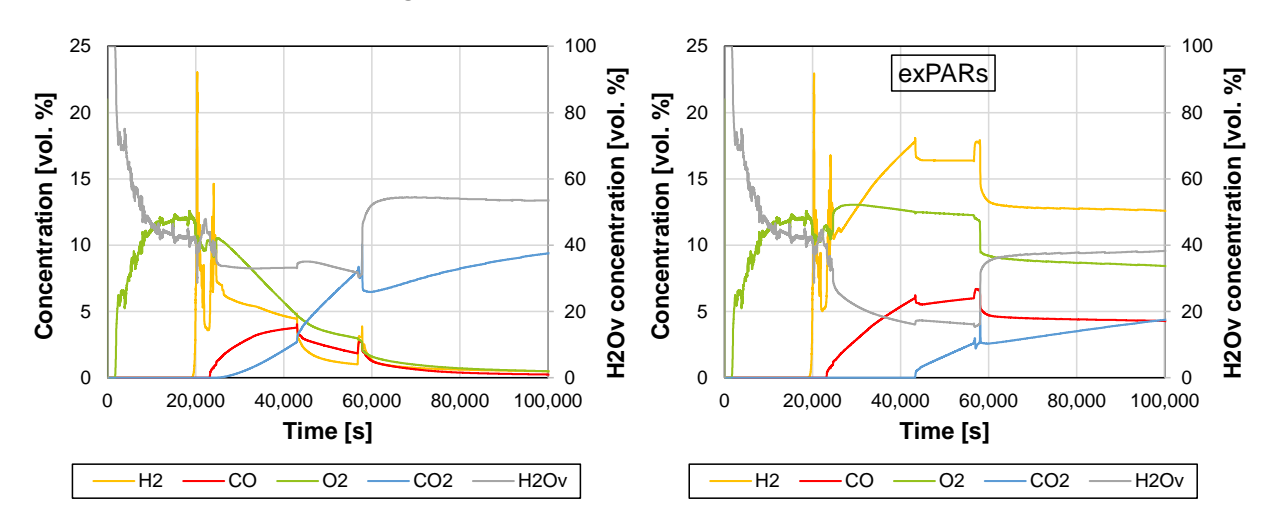


Figure 74. SBLOCA+ECCS: Atmosphere composition (zone PKLB);
I.: Simulation with operational PARs, r.: Simulation without PARs

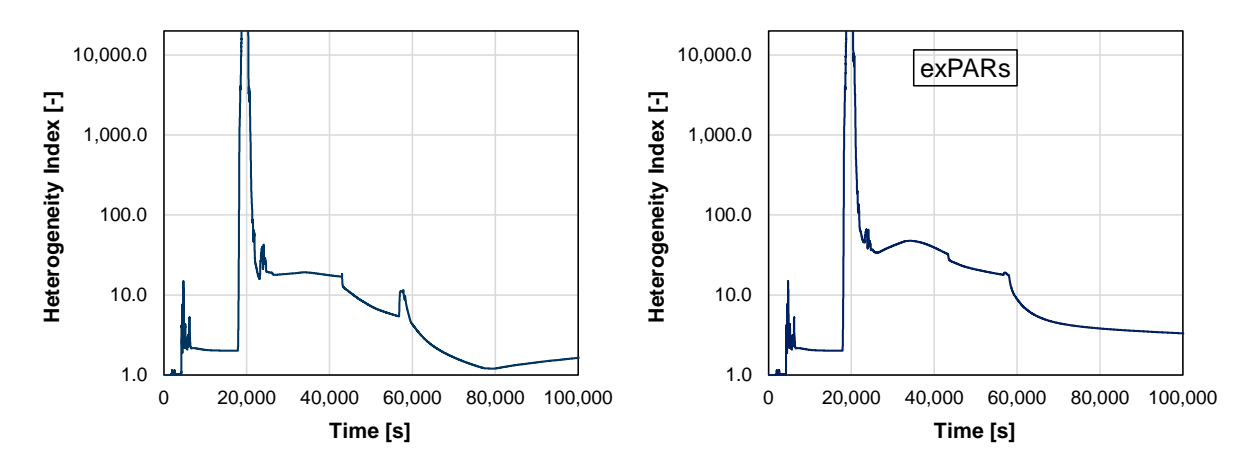


Figure 75. SBLOCA+ECCS: Heterogeneity index;
I.: Simulation with operational PARs, r.: Simulation without PARs

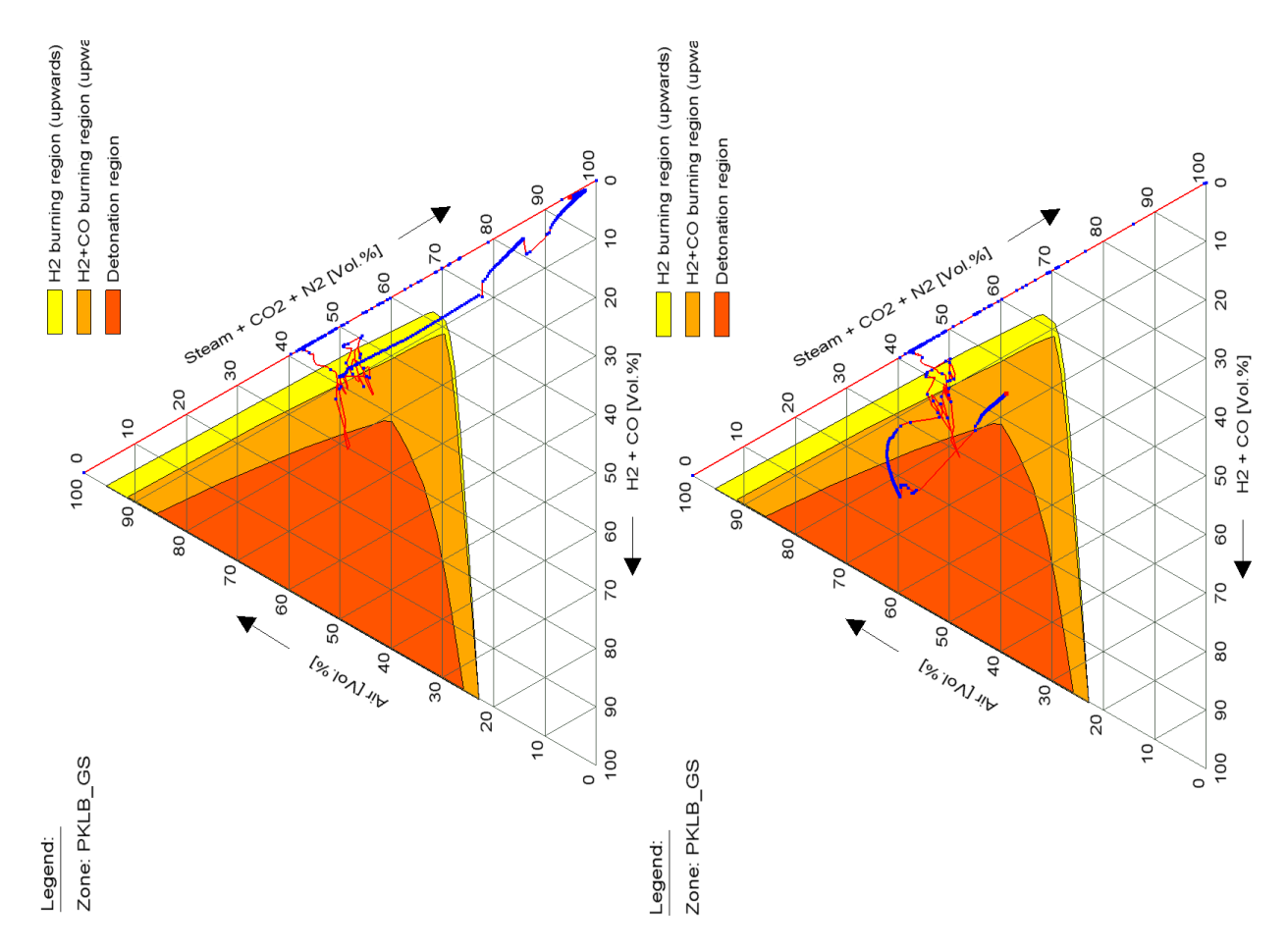


Figure 76. SBLOCA+ECCS: Shapiro diagram (zone PKLB);
I.: Simulation with operational PARs, r.: Simulation without PARs

V.5. Main highlights

The results of the conducted simulations indicate that of all conducted ex-vessel simulations the SBLOCA+ECCS sequence poses the highest combustion risk. The steam concentration in the containment during the phase with the highest concentration of combustible gases is lower than for the SBO+PSD sequence which leads to an ignitable atmosphere condition. This can at least partly be traced back to the fact that the H₂ and steam release from the primary circuit happen in a shorter timeframe while the release happens more or less at separate times in case of the SBLOCA+ECCS sequence. The higher released steam mass in case of the SBO also contributes to the lower combustion risk. The two sequences with postulated complete PAR failure both lead to ignitable atmosphere conditions but the time window for ignition is still bigger for the SBLOCA.

ANNEX VI. Individual report for the PWR-KWU reactor – MELCOR model (Framatome)

VI.1 Introduction

In the frame of Work Package 2 of the AMHYCO project, Framatome supplies simulations of hypothetical core damage accidents in the German pressurized water reactors (PWR) of the building line KONVOI. For this KONVOI plant design, a model for the severe accident simulation code MELCOR was developed by Framatome in the frame of the probabilistic risk assessments Level 2, and the introduction of severe accident mitigation guidelines (in German called "Handbuch mitigativer Notfallmaßnahmen").

The MELCOR plant model was originally created for the MELCOR Versions 1.8.x. To support the AMHYCO project, Framatome updated the MELCOR model to the currently used MELCOR Version 2.2.15254. Further, the small differences between the different KONVOI plants were reviewed, and the conservative bounding values for all KONVOI plants selected in the used MELCOR model.

In the MELCOR simulations, mostly the "best-practice" recommendations of Sandia National Laboratories are implemented. Also the optional Ag-In-Cd reactor poison release model is used. However, certain deviating choices were made based on experiences made by Framatome. The most pronounced adaptions are the re-definition of the RN-class 4 as volatile iodine, and the increase of the maximum void fraction sensitivity coefficient SC4407(11) to 0.7 (default is 0.4). Latter change is necessary to simulate the initial power operation state of the PWR steam generators.

This report uses an absolute pressure scale, if not separately noted otherwise. Further, only standard international (SI) units or directly derivative units like 1 bar = 1.E5 Pa are used. The unit [+m] refers to the absolute altitude in meters relative to the zero coordinate of the reactor building plus +6.00 m. This shift is necessary as MELCOR causes issues if the reactor pressure vessel (RPV) lower head has negative altitude.

VI.2. Framatome MELCOR Model Description

The KONVOI plants are four-loop light-water cooled PWR with a thermal power of 3850 MW. In the MELCOR model the Loop 2, where the pressurizer is attached and where a possible leakage location is assumed, is modelled individually, the other three loops are grouped together, see Figure 77. Note that in Figure 77 the core nodalization is not shown. Besides the primary and

secondary cooling systems, the MELCOR model also contains the containment (see Figure 78), the reactor building and auxiliary building, selected systems. These systems include operational ones like e.g. the nuclear ventilation, design-basis engineered safety features like the emergency core cooling system and extra borating system, and systems specific for the plant design extension conditions (DEC), i.e. the pressurizer depressurization system (PDS), passive autocatalytic recombiners (PAR) and the filtered containment venting system.

In a MELCOR simulation first the nominal power operation state is established and simulated for a considerable time, typically 1 h, to ensure that the accident simulation is not influenced by a simulation initialization transient. Then, at t=0, the initiating event happens, and the accident progression starts.

The KONVOI PWR were developed by Siemens KWU (nowadays Framatome GmbH). A significant difference of the KONVOI in comparison to other PWR worldwide is the usage of a free-standing spherical steel containment, resulting in a very high resistance to internal pressures. This steel containment is full protected against crashes of military aircrafts by a surrounding airplane crash shell. The airplane crash shell is made from reinforced concrete and has a thickness of 1.8 m. The space between the steel containment and the concrete shell is called the annulus.

The KONVOI containment is accessible by plant personnel during power operation. This allows for preventive maintenance during the entire fuel cycle and to prepare the reactor refueling before the plant enters the outage state. The outage time is additionally minimized by positioning the spent fuel pool inside the containment to minimize transport paths for fuel assembly handling. Therefore, the KONVOI plants have a very high power production availability. The accessibility is achieved by separating the containment into two main compartments, the large accessible rooms including the reactor floor, and the large equipment rooms (not accessible during power operation) housing the primary loop components. The accessible rooms and equipment rooms are separated by ventilation and radiation protection measures. In the nodalization picture in Figure 78 the accessible rooms are depicted in green, while the equipment rooms are shown in red. The blue room represent the spent fuel pool, the yellow rooms represent smaller compartments, and in orange the heating, ventilation, and air conditioning (HVAC) rooms for the equipment room recirculation cooling system are shown.

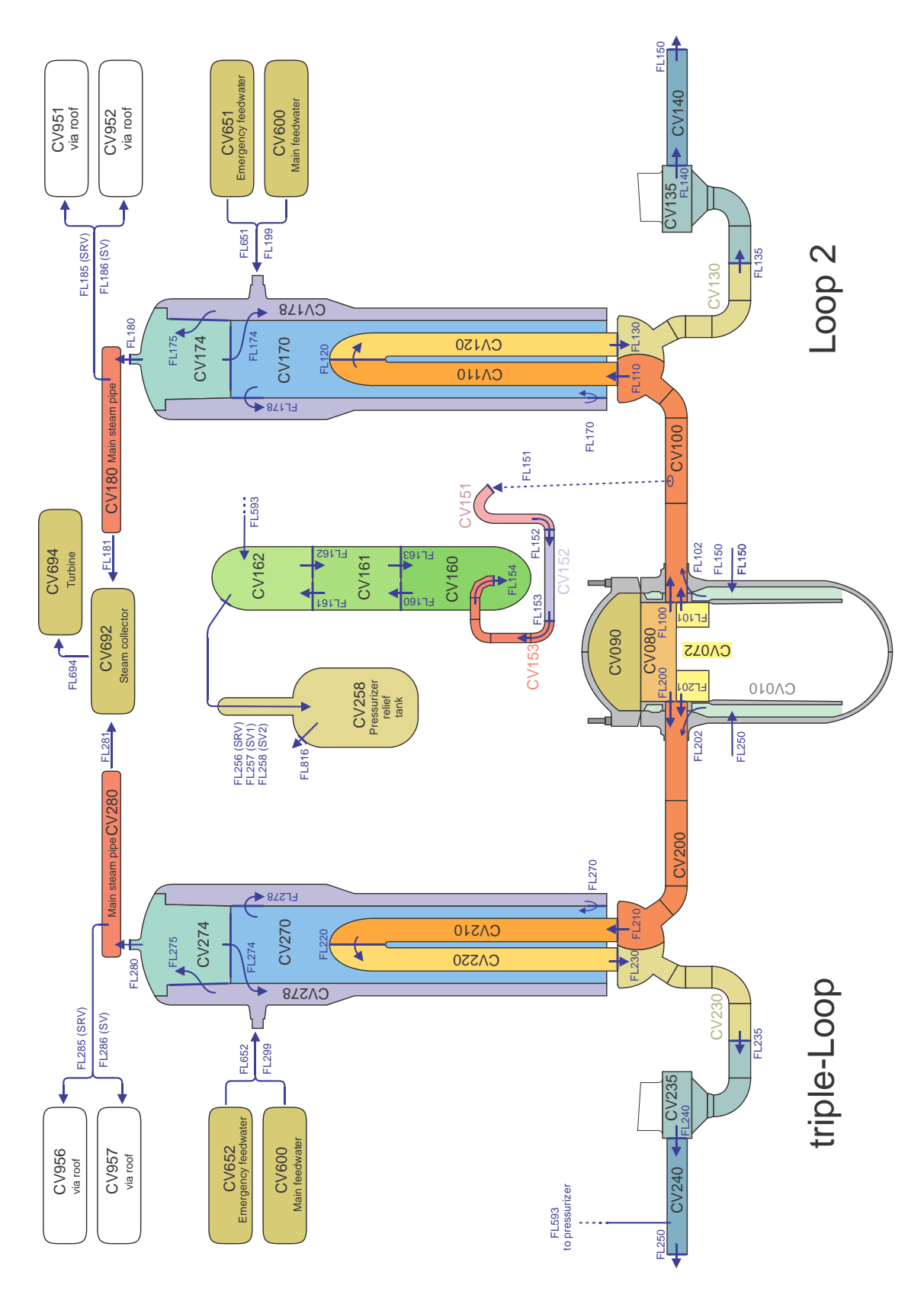


Figure 77: Representation of the reactor coolant system

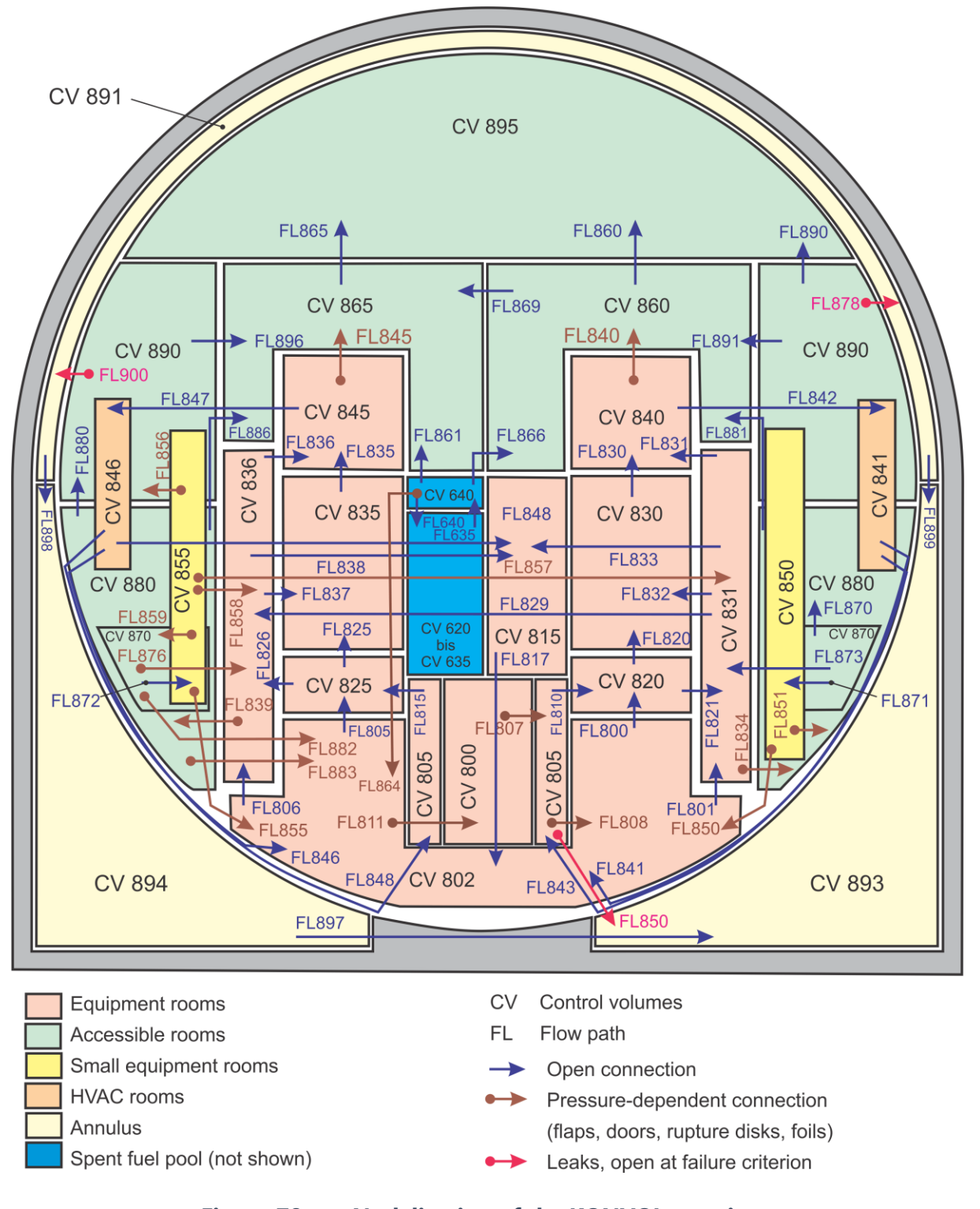


Figure 78: Nodalization of the KONVOI containment

In the event of a loss of coolant accident (LOCA) the entire volume of the containment is needed to contain the steam volume released by the primary loop. Thus, the ceilings on top of the steam generator towers are designed as flaps or rupture foils (depend on the specific KONVOI plant). These ceilings open at low differential pressures between 24 mbar and 48 mbar (depending on the specific plant). Thus, in case of a LOCA these ceilings open, and steam can be released from the equipment rooms into the accessible rooms. In the MELCOR model, these pressure equilibration ceilings are modelled as FL840 and FL845, see Figure 78. The degree of opening of these ceilings affect the gas convection within the containment, and thus, after start of the fast cladding oxidation in the reactor core, influence the risk for the formation of combustible gas clouds.

Several additional rupture foils or flaps are installed in the containment to prevent any excessive room pressures in case of a break of a high-energy pipe and to prevent the accumulation of condensed water in the respective rooms. Especially two flaps exist in the so-called channel (CV870) to drain water from the lower equipment rooms into the containment sump (CV802). Similar foil-devices ensure that the small equipment rooms (CV855) and the volume control system rooms (CV850) can drain always into the containment sump, where the emergency core cooling systems can re-inject the water back into the reactor coolant system.

In case of a RPV failure, the core melt slumps into the reactor pit (CV800). The KONVOI reactors employ the concept of a dry reactor pit to avert any possible thermal shocks of the RPV outer surface by getting in contract to cold water. Besides these design-basis accident considerations, this dry pit concept also excludes any possibility for an ex-vessel steam explosion in the event of a severe accident. The dryness of the pit is ensured by its narrow design and its water-tight outer boundary, isolating it from the surrounding containment sump (CV802).

When hot core debris gets in contact to concrete a so-called molten corium-concrete interaction (MCCI) occurs. The core melt chemically and physically decomposes the concrete and finally melts its constituent components. On one side this MCCI releases hydrogen and carbon monoxide into the containment atmosphere, on the other side it erodes the concrete in the reactor pit.

After a certain time period, it can be expected that the so-called Biological Shield surrounding the RPV gets penetrated by the MCCI. Thereafter water from the sump can rush into the pit, submerging the core melt, as well as melt may flow out of the pit into the containment sump.

The MELCOR model assumes that, after penetration of the Biological Shield, the water levels equilibrate between CV802/805/800, and the core melt level in the sump equals the melt level in the pit minus 30 cm. The 30 cm level step shall take into account the rather high viscosity of the core melt at this point in time on a best-estimate basis, making a perfect outflow highly unlikely.

Because of the confined geometry of the reactor pit, it can be expected that even after the penetration of the Biological Shield and the water inflow into the pit, the core melt remains non-coolable for a long time period. In contrast, the core melt which flow out of the pit into the sump spread there and gets rapidly cooled. The assumption of melt outflow from the pit into the sump therefore is optimistic with respect to the termination of MCCI, however, it is pessimistic with respect to the containment pressure buildup.

The AMHYCO project especially explores the behavior and distribution of combustible gases within the containment in the late phase of the accident. Therefore, the assumptions concerning the pit concrete are of high importance. The generation rates of hydrogen and carbon monoxide during the MCCI strongly depend on the content of water and carbonates respectively in the concrete composition. The water content of concrete is typically 4-5 mass% about half physically bound in pores and half chemically bound in hydroxides. The carbonate content however depends on the respective gravel uses in the concrete mix. For safety-related MELCOR simulations, the concrete of the KONVOI plants were sampled and chemically analyzed to make plant-specific MELCOR simulations. For the AMHYCO project, a generic concrete composition is used which has carbonate content enveloping all KONVOI plants. The used concrete mass composition is listed in Table 15. Thus, the carbon monoxide release ratio will be bounding high in the AMHYCO MELCOR simulations.

Table 15: Bounding concrete composition used in the AMHYCO project

45.62 3.19
2 10
3.19
10.93
3.28
17.94
1.00
0.91
2.82
1.27
1.09
11.93

VI.3. Performed Simulations

The AMHYCO project focuses on the mitigation of combustible gases within the containment of a nuclear power plant in case of severe accident with core damage. The main sources of combustible gases thereby are the core oxidation releasing hydrogen and, after RPV failure, a molten corium-concrete interaction (MCCI) releasing hydrogen and carbon monoxide. Additionally, smaller sources of combustible gases can be radiolysis, the presence of operational hydrogen due to the water chemistry of a PWR, and carbon monoxide release due to secondary smoldering fires within the containment under air starvation. Latter sources are however not included in the MELCOR code framework.

In the frame of Work Package 2 a series of simulations of hypothetical severe accident scenarios were numerically examined. That a nuclear incident like a pipe break can escalate into a nuclear accident, a series of redundant and diverse safety systems must be assumed to be not available. The failure combinations for the evaluated scenarios is shown in Table 16. The relative probability for such an initiating event and the conditional probability for a coinciding failure of several redundant and diverse safety systems was evaluated in the probabilistic risk assessments of the respective nuclear power plant. For the AMHYCO project, however, not necessarily the most likely accident sequences are evaluated. Instead, a mixture of typical accident sequences is simulated to give a global overview of possible accident progressions. Thereby, accident sequences were selected which are assumed to cause the highest conditional risk for an in-containment gas combustion.

All the KONVOI plants under consideration are equipped with Framatome PAR. In national as well as international tests, Framatome PAR have shown a very high reliability, and in prototypical experiments like e.g. in the PHEBUS FPT-3 test were outperforming all competitors. Thus, based on a probabilistic evaluation, a complete systematic failure of the Framatome PAR system occurring in parallel to a severe accident can be considered as practically eliminated⁴. Therefore, the PAR system is considered to be available for all scenarios in this chapter. Also the filtered containment venting system (FCVS), installed by Framatome in the KONVOI plants, is especially designed to be operated under severe accident conditions, i.e. the containment venting can be initiated manually, and the access paths and the operating station are radiation protected. Therefore, the failure of the FCVS is also considered as practically eliminated.

⁴ This statement is specifically made for a Framatome PAR system, and not a general statement, see e.g. the aforementioned PHEBUS FPT-3 test results.

To evaluate the maximum hydrogen combustion risk in the simulations, no spontaneous combustions of local gas clouds are allowed in the model. Smaller local combustions can be seen as beneficial as they accelerate the recombination of hydrogen and oxygen within the containment, in addition to the operation of the PAR, and thus reduce the risk for large-scale incontainment combustion events.

Table 16: Events and system availability for the simulated scenarios

Event	TLAP	TLAP	LOCA 80cm ²	LOCA 380cm ²	LOCA 5cm ²	LOCA 80cm ²	LOCA 80cm ²
Safety injection pumps	no	no	yes	yes	yes	no	no
Safety injection 3-way valves	no	no	no	no	no	no	no
Extra borating system	no	no	yes	yes	yes	yes	no
Primary depressurization	650°C +30 min	650°C	no	no	no	650°C	650°C
Steam generator feedwater	no	no	yes	yes	yes	yes	yes
Steam generator secondary cool-down	no	no	yes	yes	yes	yes	yes

Based on the hydrogen risk evaluation of these scenarios, the dominating scenario was evaluated (gray column in Table 16), which is discussed in detail in the following Chapter 0.

VI.3.1. Medium-break LOCA with Secondary Cool-down.

In this hypothetical accident sequence an 80 cm² leakage occurs at the connection of the safety injection system to the hot leg of the primary Loop 2 (the loop connected to the pressurizer). This safety injection pipe connects to the bottom of the hot leg, as it draws water from the primary loop in residual heat removal mode. This leakage location maximizes the loss of coolant from the primary loop.

Note that also cold-sided leakage was simulated as pre-work, however, the simulation showed no significant difference with respect to the in-containment hydrogen combustion risk in comparison to the hot-sided leakage.

The KONVOI plant has the regulatory requirement that the plant must be able to control an initiating event for the first 30 min autonomously without operator actions, thereafter manual

actions by the plant crew can be credited. The crew is not forbidden to already act within the first 30 min, however, to reduce the possible parameter space for the accident boundary conditions, in simulations the number of manual actions is minimized.

After the pipe break occurs (assumed at t=0 s in the simulation), primary coolant flashes into the large equipment rooms of the containment. The reactor protection system automatically detects the occurrence of a LOCA by falling primary pressure (see Figure 79), by falling liquid level in the pressurizer, or by pressure buildup in the containment (see Figure 80 Figure 80). After reaching respective set-points, the protection system initiates the reactor trip, the containment isolation, and start of the high-pressure safety injection pumps. These pumps draw water from the external flooding tanks and inject the water into the primary loop. Additionally, the steam generators automatic cool-down with a rate of 100 K/h gets started, see Figure 79. As in this accident scenario the secondary side is not impaired, the steam generators remain filled with water.

Caused by the assumed break size, the high-pressure pumps cannot stabilize the primary pressure. After the primary pressure dropped below 26 bar, the four accumulators attached to each primary loop hot leg, and four accumulators attached to the cold legs start injecting cold water passively into the primary loop. After the depletion of the hydro-accumulators after ~15 min, the primary pressure drops to ~10 bar. At this pressure, the low-pressure safety injection pumps are started, also drawing water from the external flooding tanks. The high-pressure pumps together with the low-pressure pumps can stabilize the primary pressure at ~10 bar, see Figure 79, without any uncover of the reactor core, see Figure 81.

After ~1.5 h, the external flooding tanks are empty. At this point in time, a 3-way valve would automatically switch in each redundancy the suction line of the emergency core cooling train from the respective external flooding tank to the containment sump. The water extracted from the containment would be cooled in the emergency core cooling systems, and re-injected into the reactor coolant loop. Thus, the LOCA would be automatically controlled by the emergency core cooling systems of the plant without the need of any human intervention.

To allow for an escalation of the nuclear incident into a nuclear accident with core damage, additional system failures must be assumed. The (overall unlikely but comparable) most likely failure mode of the safety injection system in a KONVOI plant is the failure of the 3-way valve switchover of the safety injection suction lines from the flooding tanks to sump recirculation mode (with a common-cause failure assumption). These valves are four-fold redundant but not diverse as e.g. the pumps or the power supply. Thus, after the flooding tanks are depleted, the injection stops. Any emergency operating actions like repairing the valves or injecting coolant into the reactor coolant system by other systems (e.g. extra borating system or volume control system) are not considered in the simulation as they would prevent the core damage.

With the stop of the active water injection, the primary pressure drops down to ~4 bar (see Figure 79), and the heat exchanger tubes in the steam generators fill with steam. As the steam generators were already cooled down to ~2 bar by the 100K/h automatic cool-down, a so-called reflux-condenser mode develops. In the RPV the coolant boils, releasing steam. This steam then gets condensed in the steam generators, and the condensate drains back along the bottom of the main coolant loops to the RPV. This reflux-condenser mode limits the amount of coolant lost via the pipe break, and thus elongates the overall accident progression.

In the simulation the RPV liquid level drops into the active core zone about 4 h after start of the accident, and after 6 h the core heated up sufficiently that the fast zirconium oxidation starts. Caused by the reflux-condenser mode, the atmosphere within the RPV contains steam to drive the core oxidation, resulting in a high hydrogen mass production inside the RPV of ~700 kg. The hydrogen produced by the core oxidation gets directly released via the pipe break location into the lower equipment rooms of Loops 1&2.

With 29 large (FR1-1500) PAR, four semi-large (FR1-750T) PAR, 21 medium sized (FR1-380T) PAR, and 4 small (FR1-320) PAR, the KONVOI PAR system has a nominal hydrogen recombination rate of 192 kg/h at norm conditions (1.5 bar-abs and 4 vol% hydrogen). Because of the consumption of the hydrogen by the PAR; the hydrogen mass within the containment peaks at ~350 kg during the core oxidation phase, see Figure 87.

The hydrogen release via the LOCA location, together with a relatively low amount of steam in the containment due to the secondary cool-down of the steam generators, lead to the short term formation of combustible gas mixtures in the lower regions of the large equipment rooms of the Loop 1 & 2 side, see Figure 84.

Note that the nodalization of the containment significantly affects the detection of combustible gas mixtures in the calculation. In lumped parameter codes it is always averaged over the entire control volume. Thus, when making the control volume, which contains the leakage location, smaller and smaller, the local hydrogen concentrations become higher and higher. That combustible gas concentrations are reached close to the leakage location is not unexpected.

While locally at the leakage location a combustible gas concentration is predicted, the large accessible rooms remain non-combustible, see Figure 85. Thus, even when considering an ignition of this gas cloud within the equipment rooms, which have no direct connection to the containment pressure boundary, it can be assumed that the respective pressure loads would not endanger the containment integrity.

In the time period between 6 h and 8 h the reactor core collapses into a debris bed and partially melts, see Figure 83. At ~8 h the core support plate fails, and the core debris slumps into the RPV

lower heat, starting to heat up the RPV bottom head. After ~9.5 h the RPV fails due to the heat impact.

After RPV failure, the core melt drops into the reactor pit where it starts eroding the basemat concrete, see Figure 82. The concrete decomposition releases steam and carbon dioxide. These gases get reduced by the metallic components of the melt to hydrogen and carbon monoxide respectively, which then get continuously released to the containment atmosphere. The MCCI releases about 100 kg hydrogen per hour, and about 2000 kg carbon monoxide per hour.

These gases are released with a temperature above their auto-ignition temperature. Thus, on a best-estimate bases, they would likely combust as a standing flame above the core melt. As mentioned previously, such spontaneous combustions are not considered in the simulation. Nevertheless, even without a spontaneous combustion, the PAR system within the containment is able to control the accumulation of the gases within the containment, see Figure 87. Only after the complete consumption of the oxygen within the containment, after ~24 h, the PAR stop operating, and the hydrogen and carbon monoxide masses within the containment start to continuously increase. Without any oxygen, however, there is no longer any in-containment combustion risk.

The secondary cool-down of the steam generators condenses a lot of steam inside the primary circuit, and thus reduces the amount of steam released to the containment. This lack of steam is detrimental concerning the containment flammability risk, but it also reduces the pressure buildup within the containment, see Figure 80. Thus, it causes an elongation of the grace period until the containment would reaches its design pressure limits and pressure-limitation emergency actions would be needed like e.g. an FCVS operation beyond 48 h after start the accident.

This scenario has the unique identifier string "L80h.100K". Every plot for this scenario is marked with this identifier for quality assurance.

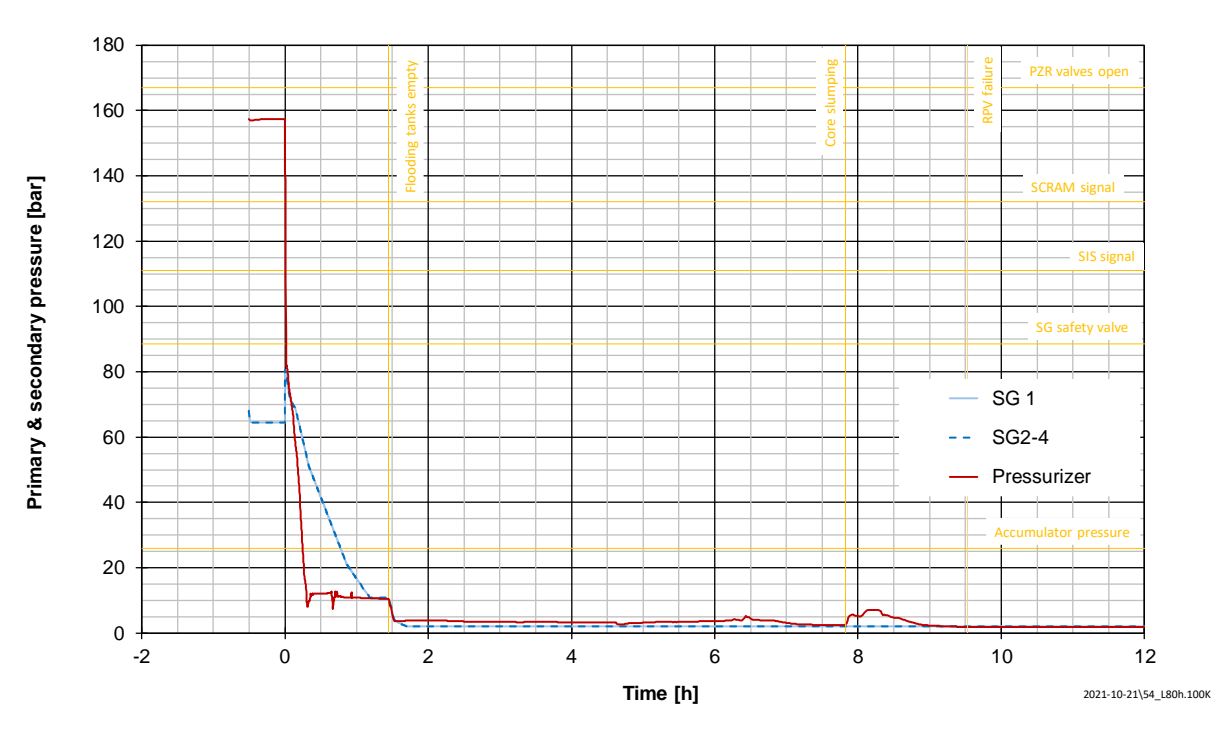


Figure 79: Primary and secondary pressure

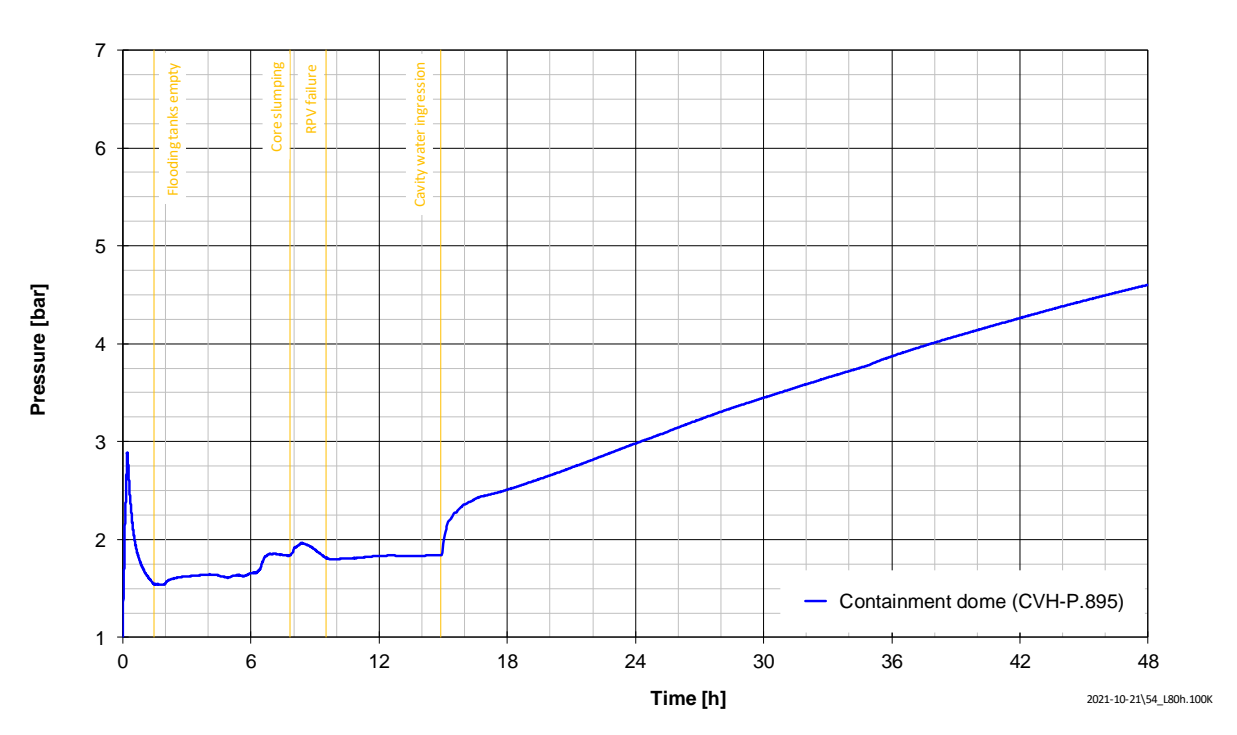


Figure 80. Containment pressure

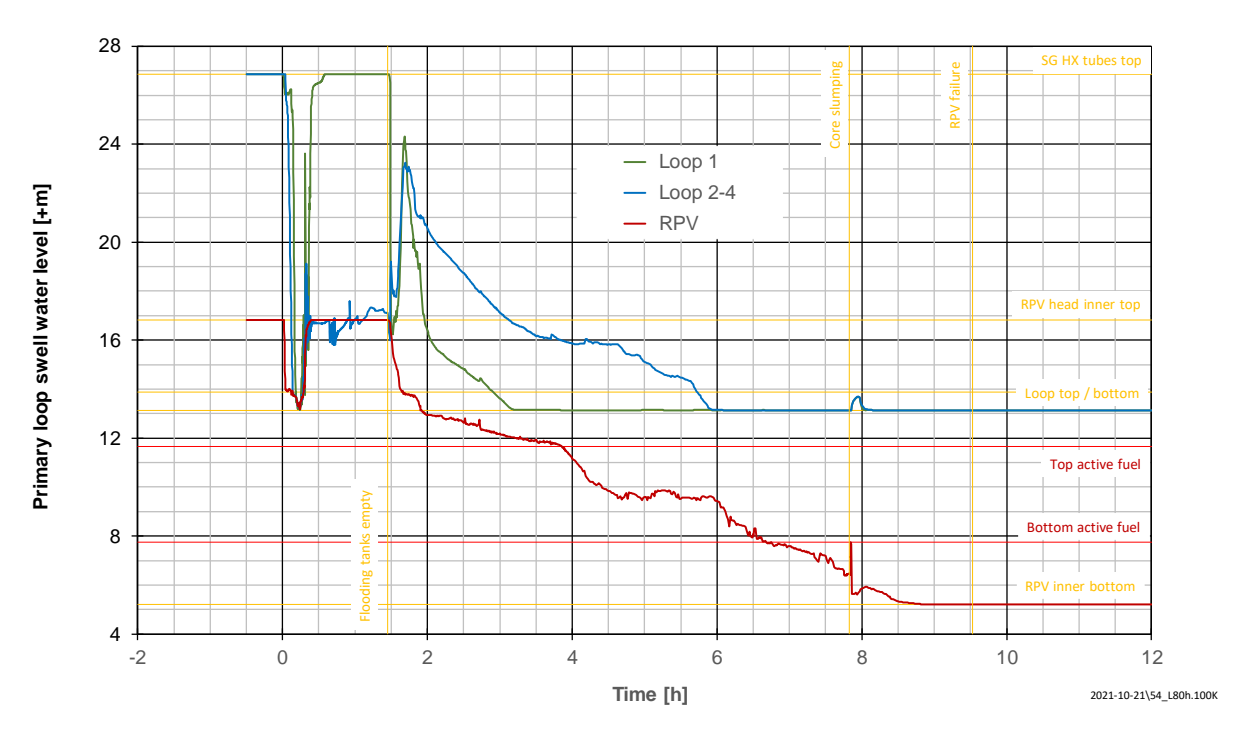


Figure 81: Primary loop swell liquid level

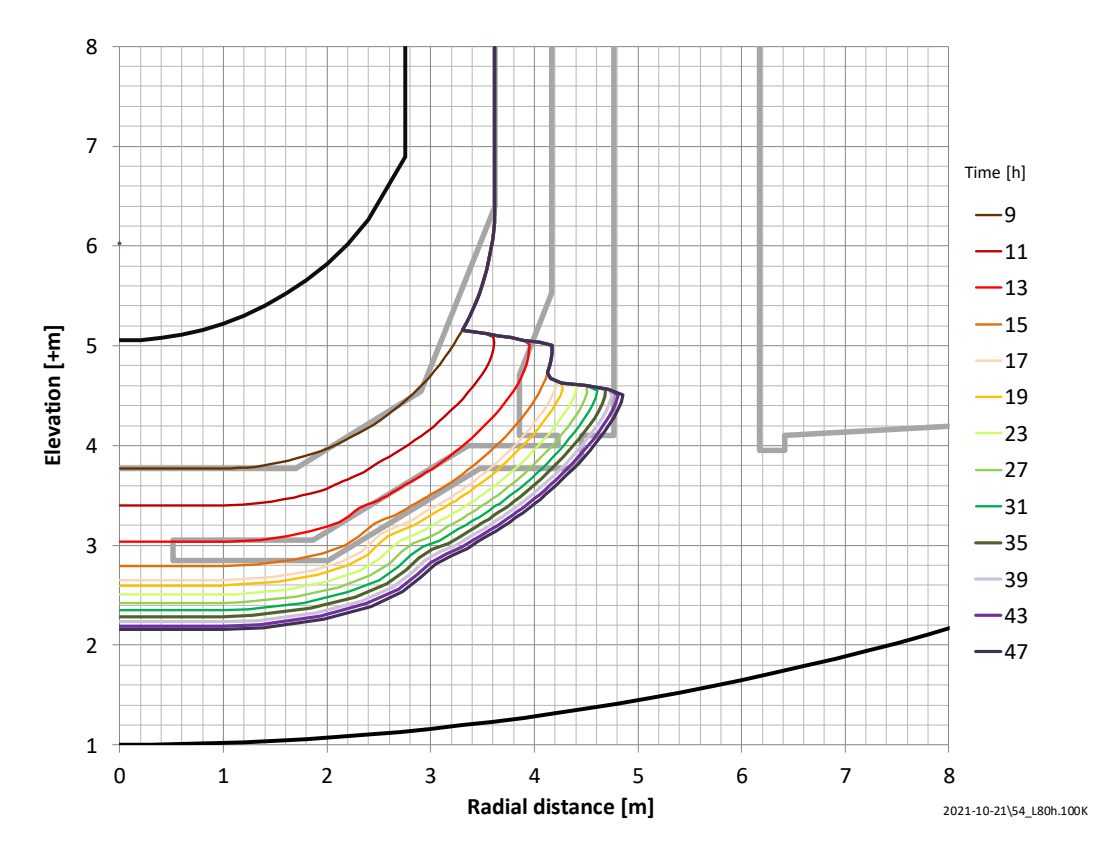


Figure 82. Molten corium-concrete interaction

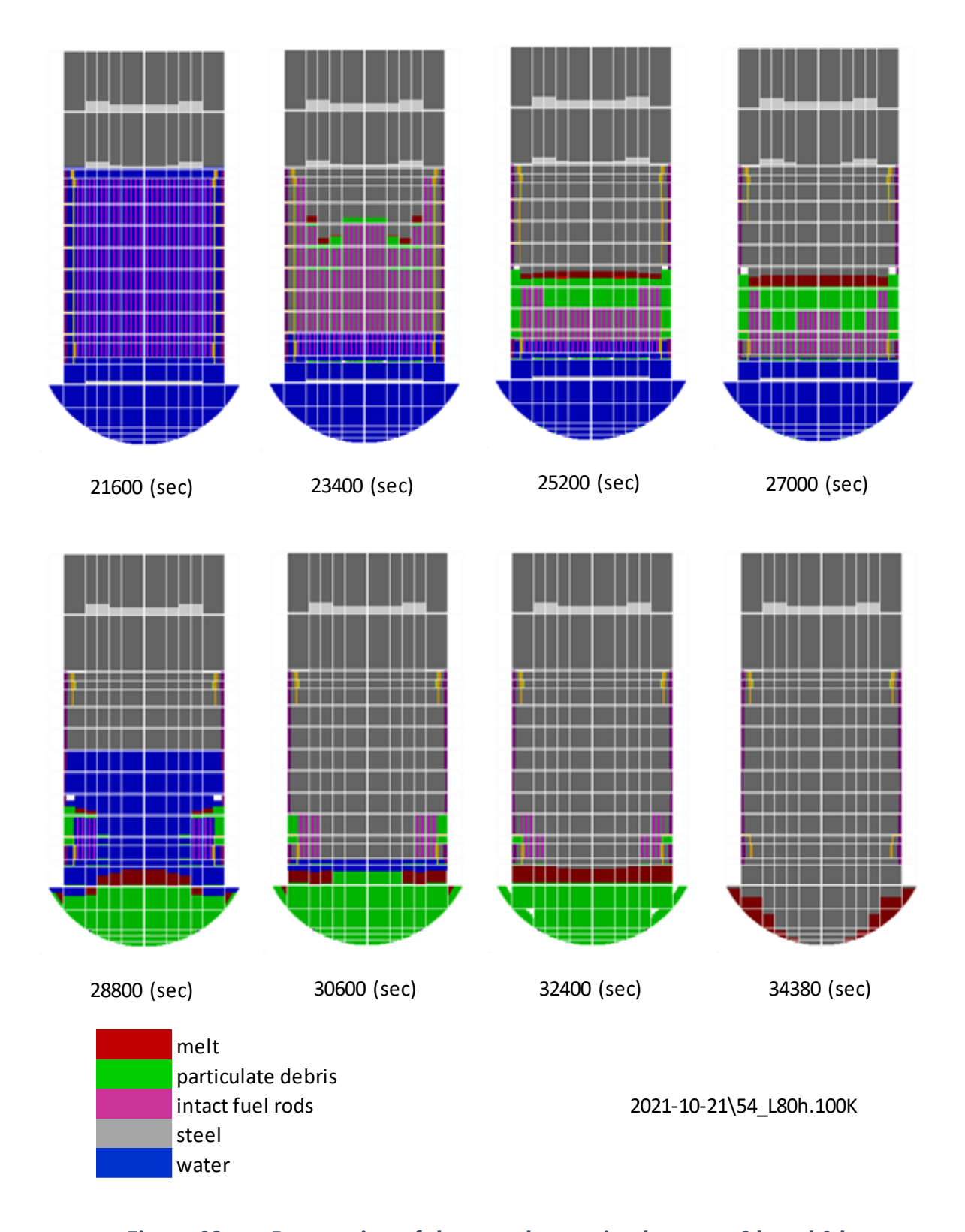


Figure 83: Progression of the core destruction between 6 h and 9 h

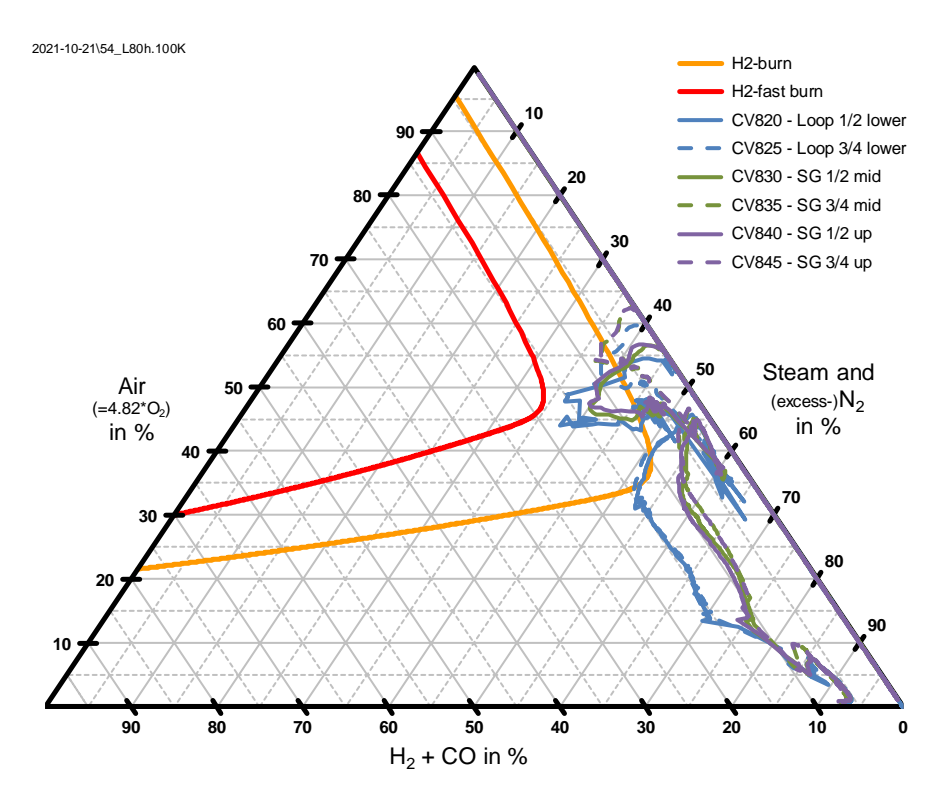


Figure 84. Shapiro diagram for the large equipment rooms

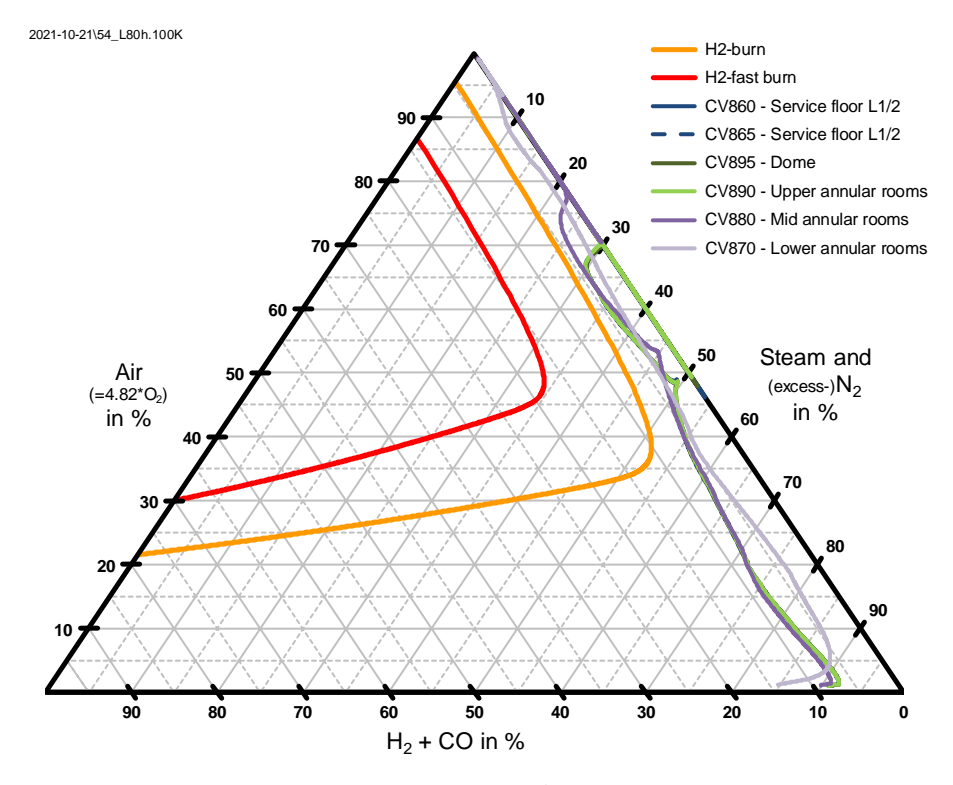


Figure 85: Shapiro diagram for the accessible rooms

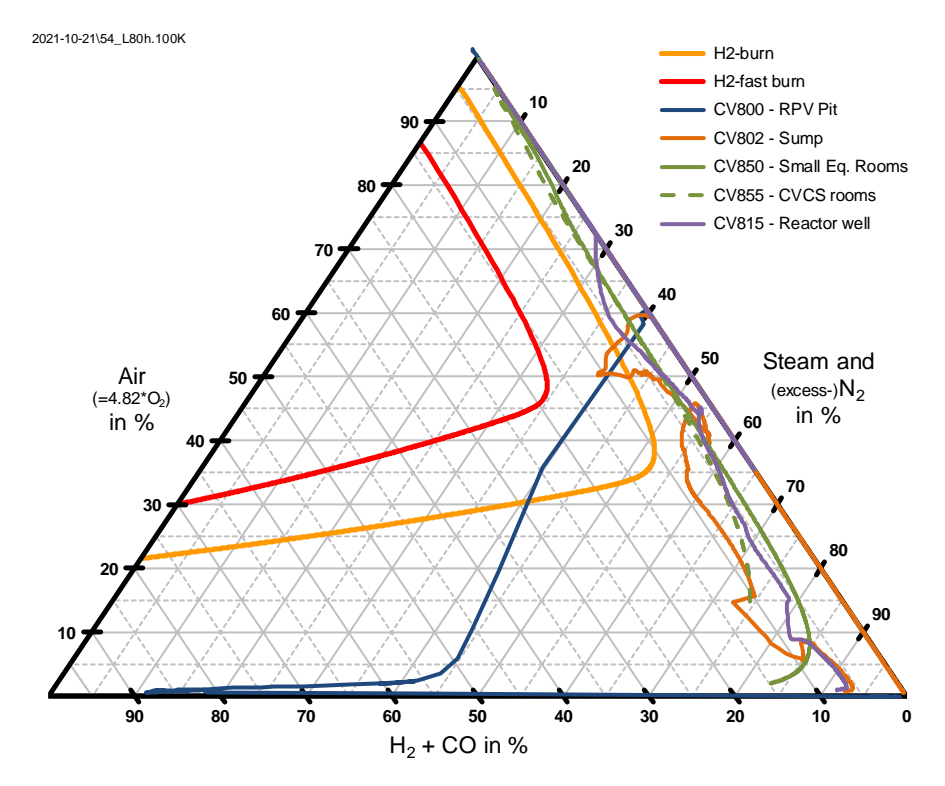


Figure 86: Shapiro diagram for other containment rooms

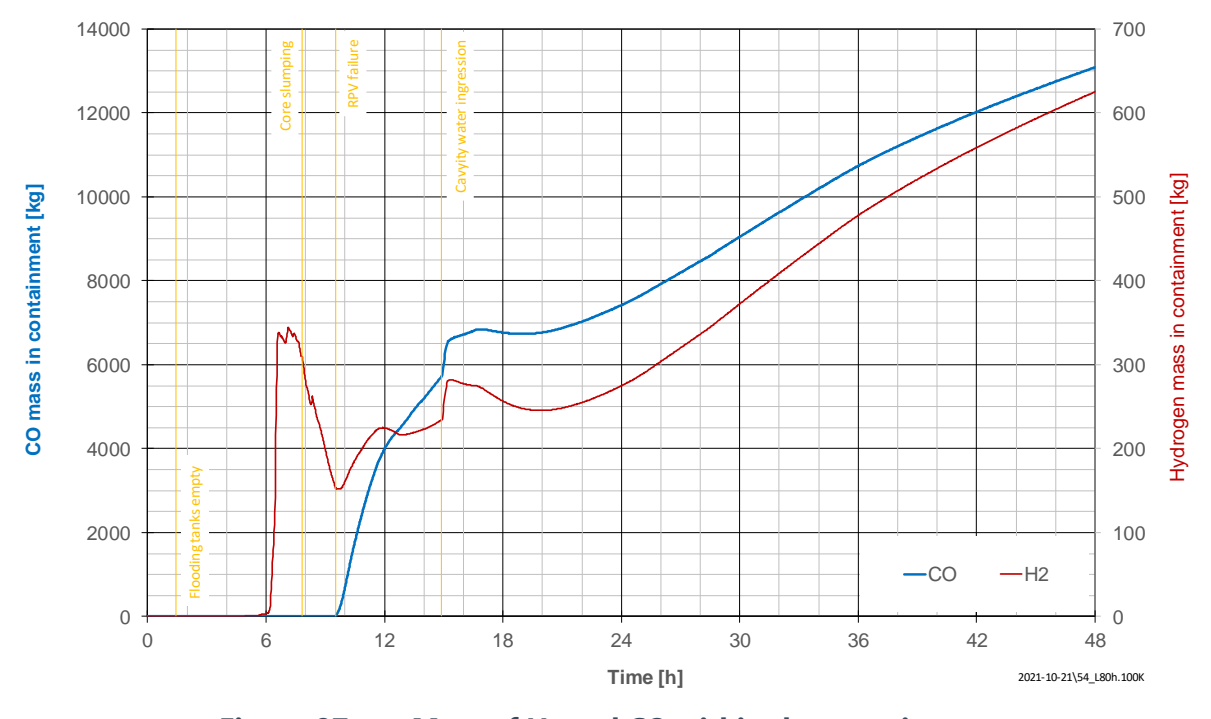


Figure 87: Mass of H₂ and CO within the containment

ANNEX VII. Individual report for the PWR-VVER reactor (Energorisk)

VII.1. PWR VVER

Several sequences has been simulated for the VVER-1000 V320 PWR design. As noted in Table 2, variability is not associated with reactor size, but with the analytical tool and the approach used for the modelling: MELCOR.

VII.1.1. MELCOR (Energorisk LLC, MELCOR 1.8.6)

The containment nodalization, with 20 control volumes, is depicted in Figure 88. Control volumes CV617 – CV620 represent upper big volume of the reactor hall. The accumulation of combustible gases in a large volume poses a threat to the integrity of the containment. The dangerous predicted combustible gases molar fractions are accumulated in the largest control volume CV619 of the reactor hall.

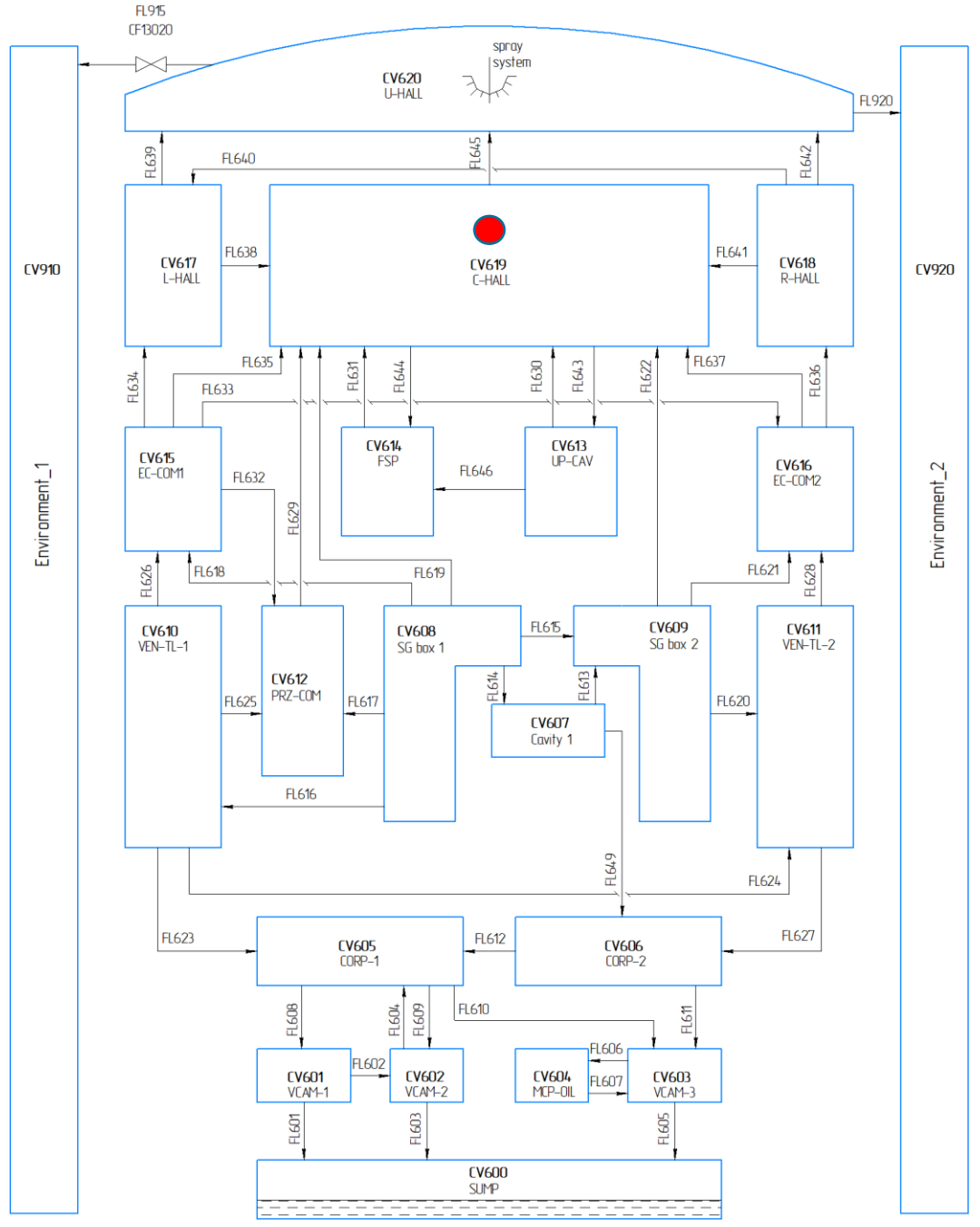


Figure 88. Containment nodalization for PWR- VVER-1000 used in MELCOR (Red circles marks the reference compartment)

Three SA sequences leading to the RPV failure and subsequent Corium-Concrete Interaction (CCI) have been considered: SBO, 90 mm cold leg LOCA and double ended large break LOCA. Spray system have been activated at in-vessel and ex-vessel stage to assess impact on hydrogen and CO concentration in containment compartment. In addition, these sequences have been run with and without PARs. Hence, a total of 12 sequences have been simulated:

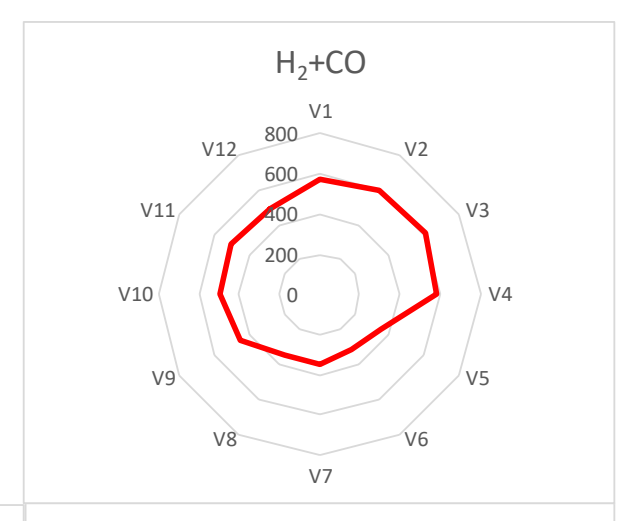
- V1 SBO without PARs, sprays activation in-vessel
- V2 SBO with PARs, sprays activation in-vessel
- V3 SBO without PARs, sprays activation ex-vessel
- V4 SBO with PARs, sprays activation ex-vessel
- V5 LBLOCA + SBO without PARs, sprays activation in-vessel
- V6 LBLOCA + SBO with PARs, sprays activation in-vessel
- V7 LBLOCA + SBO without PARs, sprays activation ex-vessel
- V8 LBLOCA + SBO with PARs, sprays activation ex-vessel
- V9 SBLOCA with diameter 90 mm + SBO without PARs, sprays activation in-vessel
- V10 SBLOCA with diameter 90 mm + SBO with PARs, sprays activation in-vessel
- V11 SBLOCA with diameter 90 mm + SBO without PARs, sprays activation ex-vessel
- V12 SBLOCA with diameter 90 mm + SBO with PARs, sprays activation ex-vessel

VII.1.2. Scenario selection based on total mass of combustible gases generated in COR at in-vessel phase

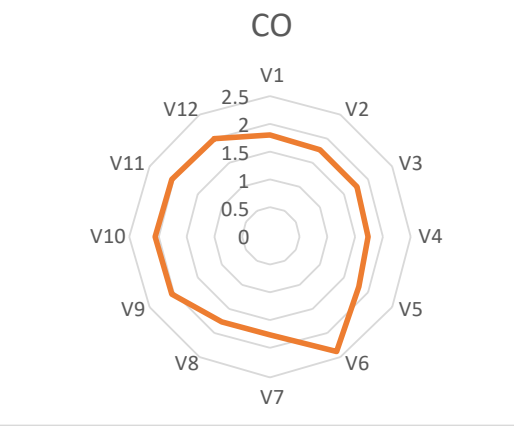
Variant of the most conservative scenarios selection based on total mass of combustible gases generated in COR at in-vessel phase of severe accident (Criteria #1). Scenarios with the largest mass of gases generated are in bold.

Mass of H2, CO and H2+CO generated at the end of run (COR in-vessel)

ID#	H2, kg	CO, kg	H2+CO, kg
V1	575.593	1.78406	577.37706
V2	598.152	1.78405	599.93605
V3	605.091	1.75878	606.84978
V4	583.192	1.74183	584.93383
V5	352.116	1.80344	353.91944
V6	313.391	2.36032	315.75132
V7	345.659	1.75218	347.41118
V8	346.129	1.75231	347.88131
V9	451.555	2.03781	453.59281
V10	490.784	2.03781	492.82181
V11	504.736	2.01591	506.75191
V12	485.24	2.01591	487.25591
	605.091	2.36032	606.84978





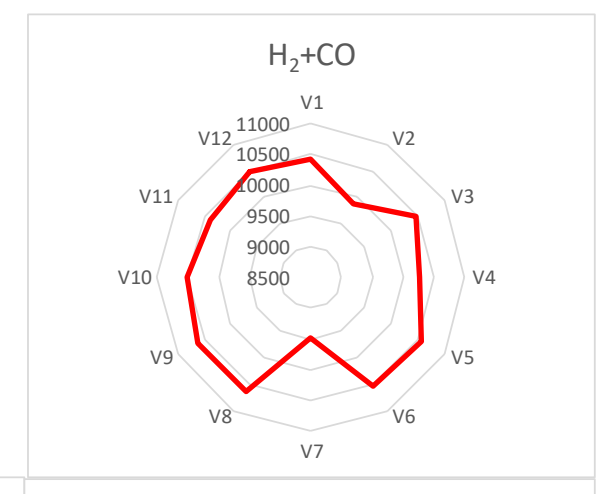


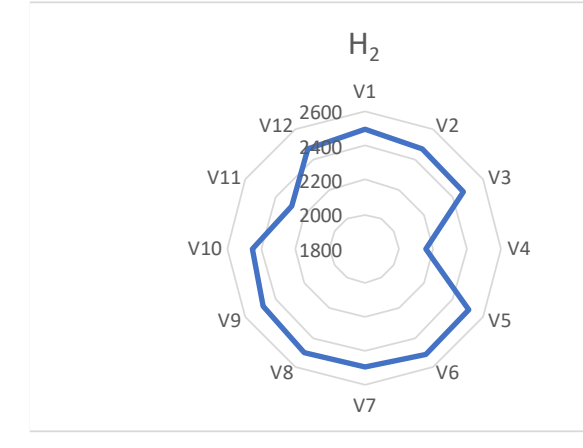
VII.1.3. Scenario selection based on total mass of combustible gases generated in CAV at ex-vessel phase

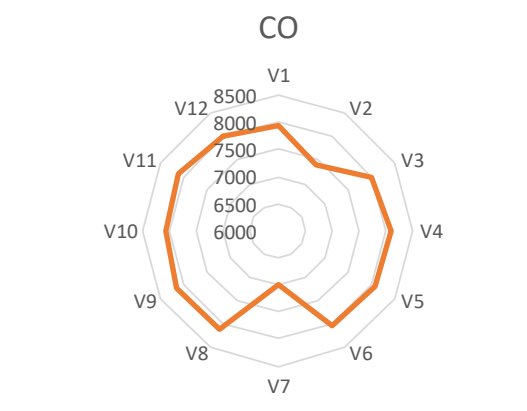
Variant of the most conservative scenarios selection based on total mass of combustible gases generated in CAV at ex-vessel phase of severe accident (Criteria #2). Scenarios with the largest mass of gases generated are in bold.

Mass of H2, CO and H2+CO generated at the end of run (CAV ex-vessel)

ID#	H2, kg	CO, kg	H2+CO, kg
V1	2495.87	7938.38	10434.25
V2	2476.9	7393.37	9870.27
V3	2466.2	8000.25	10466.45
V4	2160.58	8105.54	10266.12
V5	2508.74	8062.23	10570.97
V6	2516.26	8032.7	10548.96
V7	2491.94	6992.43	9484.37
V8	2502.72	8118.21	10620.93
V9	2475.82	8141.81	10617.63
V10	2451.5	8063.86	10515.36
V11	2285.84	8099.45	10385.29
V12	2467.78	8021.45	10489.23
	2516.26	8141.81	10620.93





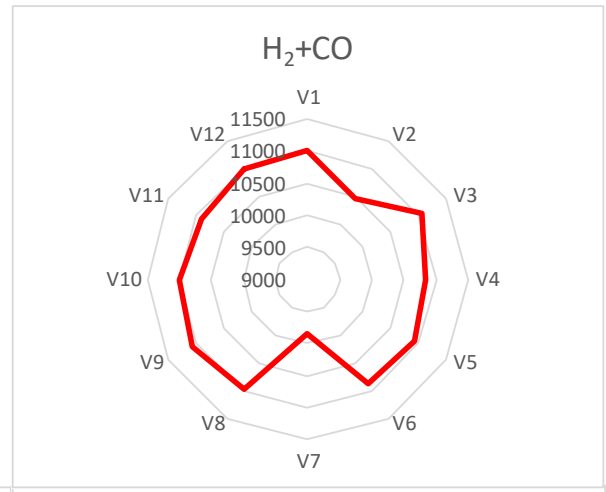


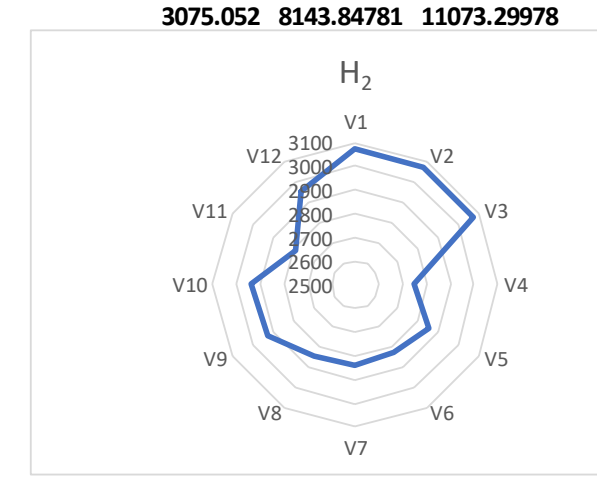
VII.1.4. Scenario selection based on total mass of combustible gases generated in scenario

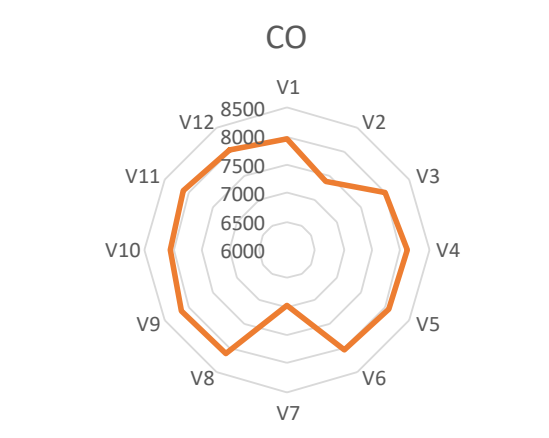
Variant of the most conservative scenarios selection based on total mass of combustible gases generated in scenario (Criteria #3). Scenarios with the largest mass of gases generated are in bold.

Mass of H2, CO and H2+CO generated at the end of run

H2, kg	CO, kg	H2+CO, kg
3071.463	7940.16406	11011.62706
3075.052	7395.15405	10470.20605
3071.291	8002.00878	11073.29978
2743.772	8107.28183	10851.05383
2860.856	8064.03344	10924.88944
2829.651	8035.06032	10864.71132
2837.599	6994.18218	9831.78118
2848.849	8119.96231	10968.81131
2927.375	8143.84781	11071.22281
2942.284	8065.89781	11008.18181
2790.576	8101.46591	10892.04191
2953.02	8023.46591	10976.48591
	3071.463 3075.052 3071.291 2743.772 2860.856 2829.651 2837.599 2848.849 2927.375 2942.284 2790.576	3071.463 7940.16406 3075.052 7395.15405 3071.291 8002.00878 2743.772 8107.28183 2860.856 8064.03344 2829.651 8035.06032 2837.599 6994.18218 2848.849 8119.96231 2927.375 8143.84781 2942.284 8065.89781 2790.576 8101.46591





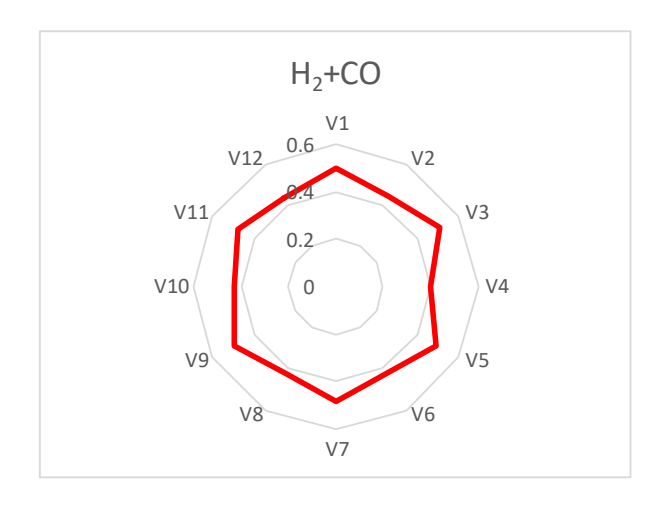


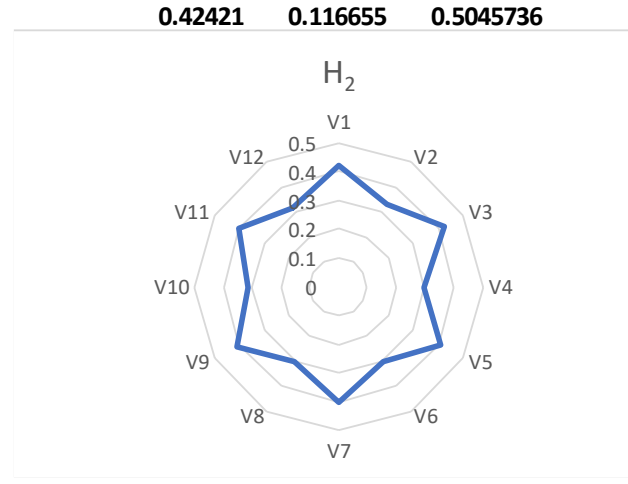
VII.1.5. Scenario selection based on mole fraction of combustible gases in the reference compartment

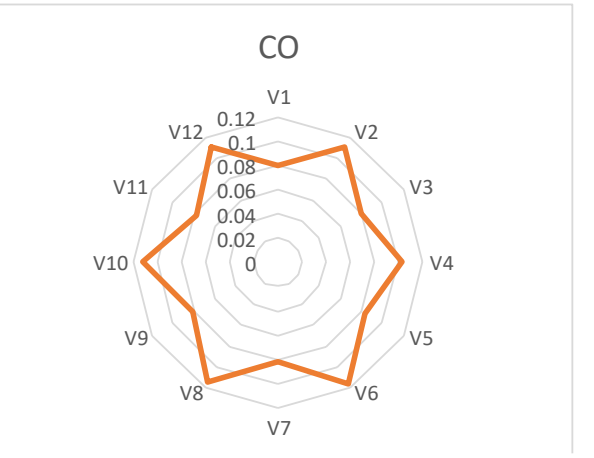
Variant of the most conservative scenarios selection based on mole fraction of combustible gases in the reference compartment (Criteria #4). The reference compartment is represent the largest control volume CV619 in the upper part of containment. Scenarios with the largest mole fraction of combustible gases in the reference compartment are in bold.

Mole fraction of H2, CO and H2+CO at the end of run in CV619

ID#	H2, -	CO, -	H2+CO, -
V1	0.424055	0.0805186	0.5045736
V2	0.334798	0.109837	0.444635
V3	0.42421	0.0797907	0.5040007
V4	0.294683	0.103259	0.397942
V5	0.40841	0.083498	0.491908
V6	0.304616	0.116655	0.421271
V7	0.404976	0.0829049	0.4878809
V8	0.304533	0.115074	0.419607
V9	0.412373	0.0813394	0.4937124
V10	0.318416	0.111376	0.429792
V11	0.404724	0.0772069	0.4819309
V12	0.318106	0.11139	0.429496







VII.1.6. Scenario selection based on combustible gases speed generation

Variant of the most conservative scenarios selection based on combustible gases speed generation in COR and CAV (Criteria #5). Scenarios with the largest combustible gases speed generation are in bold.

Maxima	al speed of H2 a	nd CO generat	ion	
ID#	H2(in), kg/s	H2(ex), kg/s	CO(ex), kg/s	
V1	0.440947		0.242222	CO(cv)
V2	0.440437	0.0787926	0.250455	CO(ex)
V3	0.631935	0.0821004	0.260972	V1 0.6
V4	0.547203	0.0794955	0.252691	V12 0.5 V2
V5	0.423922	0.141183	0.449087	V11 0.4 V3
V6	1.0093	0.154606	0.491911	V11 0.3 0.2
V7	0.468796	0.161943	0.515289	0.1
V8	0.481672	0.175265	0.557624	V10 (((0)) V4
V9	0.327748	0.118199	0.376177	
V10	0.285392	0.129768	0.412815	V9 V5
V11	0.313616	0.111791	0.355581	
V12	0.282571	0.157755	0.501908	V8 V6
	1.0093	0.175265	0.557624	V7
		$H_{2(in)}$		H _{2(ex)}
		\/1		V1
	V1	1.5	V2	V12 0.2 V2
	/	1		0.15
	V11	0.5	V3	V11 0.1 V3
			\ \	V10 0.05 V4
	V10 () V4	V10 0 V4
	,,,		/ / /	V9 V5
	V9		V5	V
	V	/8	V6	V8 V6
		V7		V7

VII.1.7. Conclusions

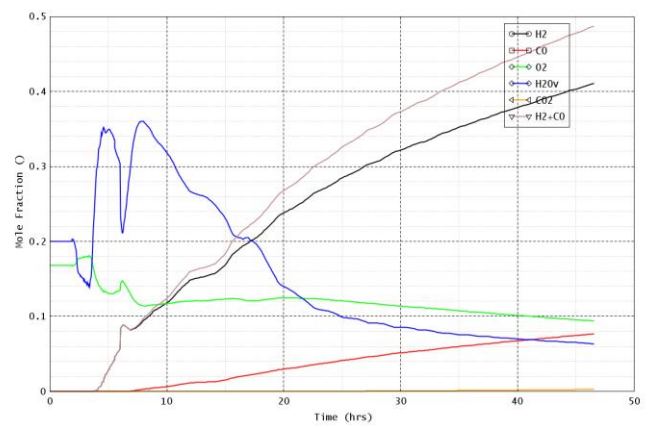
Based on the results of the performed SA analyses for the VVER-1000 V320 PWR design, it can be concluded that the restoration of the performance of one channel of the sprinkler system in case of accidents with a complete blackout of the power unit poses a threat to the integrity of the containment, regardless of the performance of the hydrogen recombiners. In case of large leaks of the primary circuit with a power unit blackout, the most rapid accumulation of hazardous concentrations of combustible gases in the containment occurs.

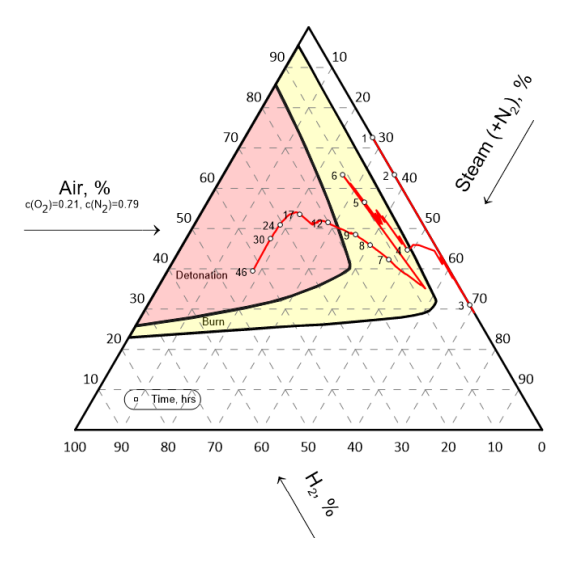
Selected scenarios:

- V6 LBLOCA + SBO with PARs, sprays activation in-vessel
- V8 LBLOCA + SBO with PARs, sprays activation ex-vessel

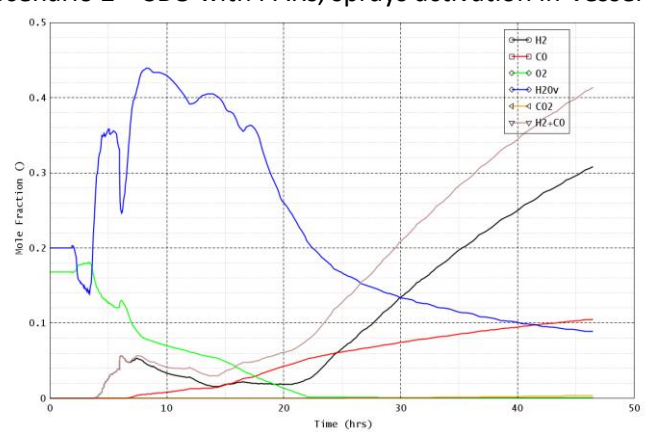
Plots of main parameters:

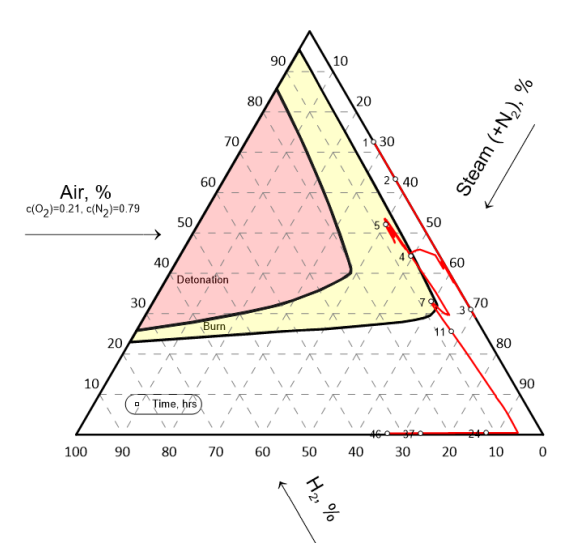
Scenario 1 – SBO without PARs, sprays activation in-vessel



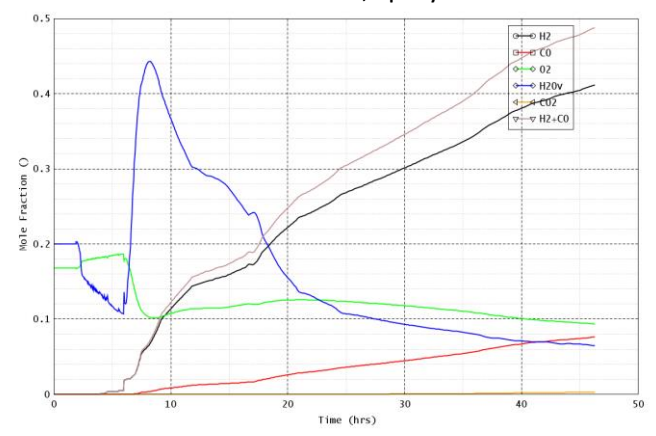


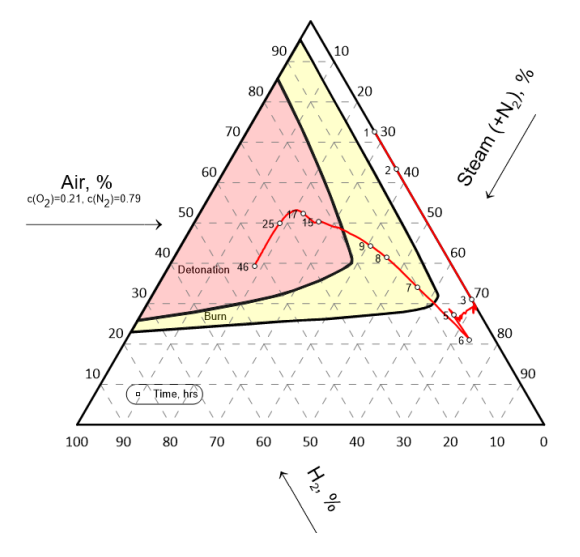
Scenario 2 – SBO with PARs, sprays activation in-vessel



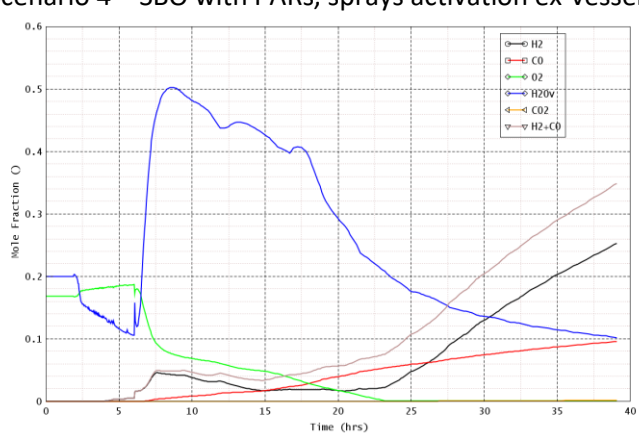


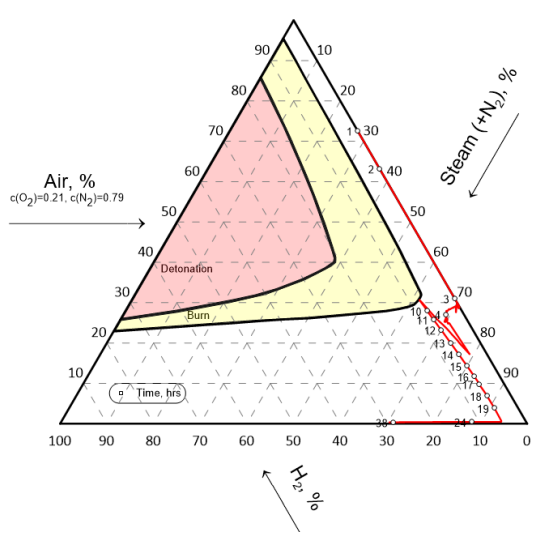
Scenario 3 – SBO without PARs, sprays activation ex-vessel



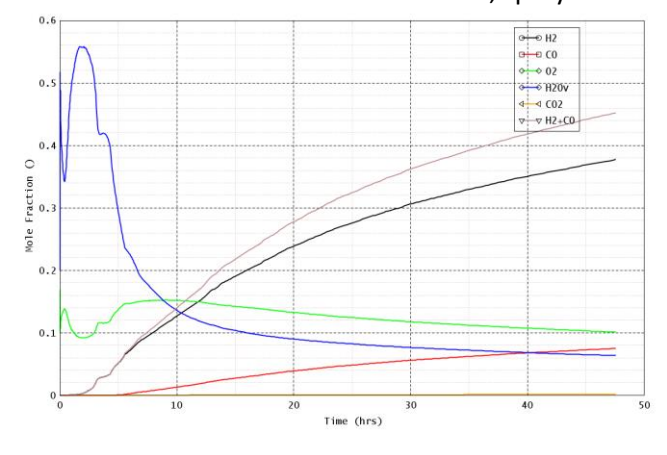


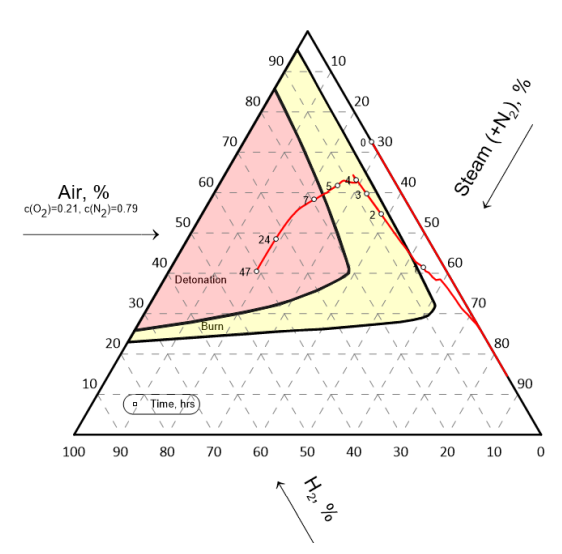
Scenario 4 – SBO with PARs, sprays activation ex-vessel



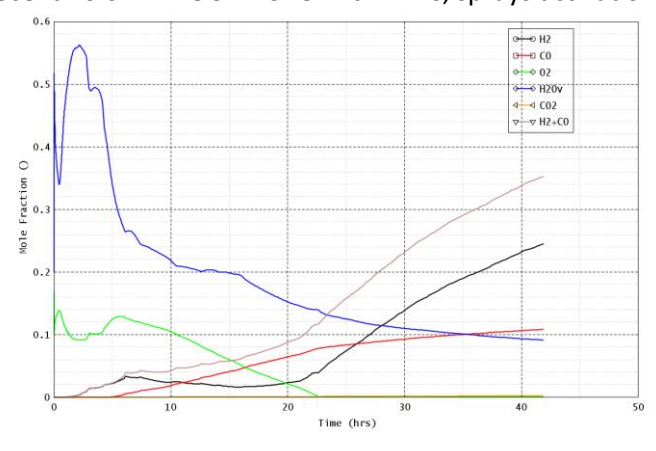


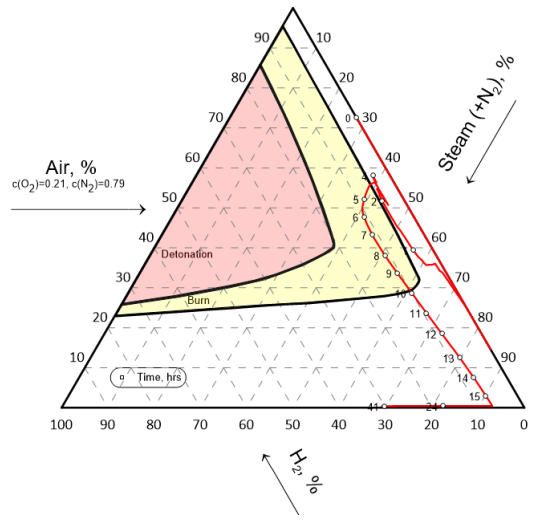
Scenario 5 – LBLOCA + SBO without PARs, sprays activation in-vessel



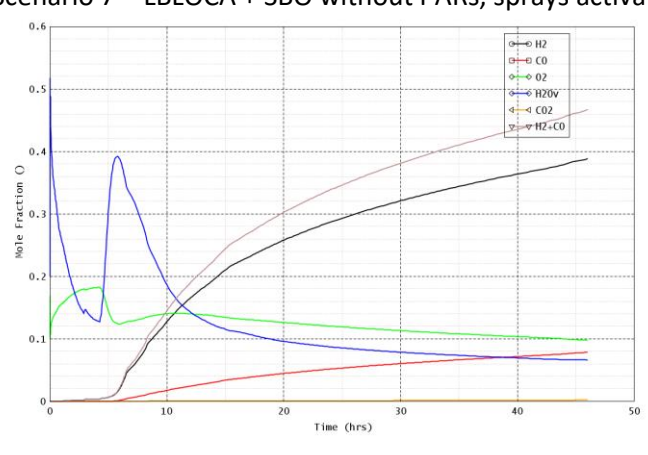


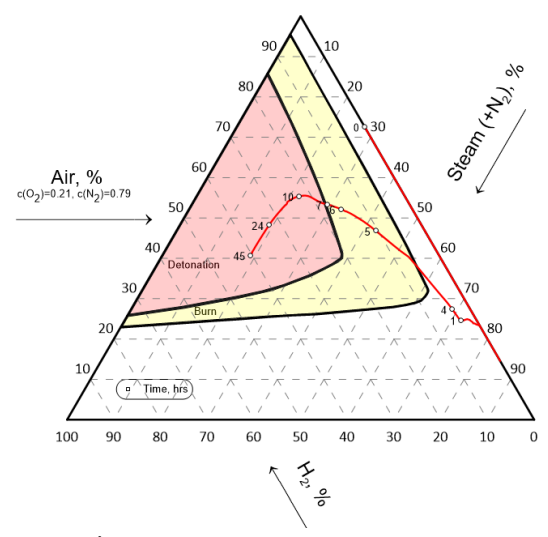
Scenario 6 – LBLOCA + SBO with PARs, sprays activation in-vessel



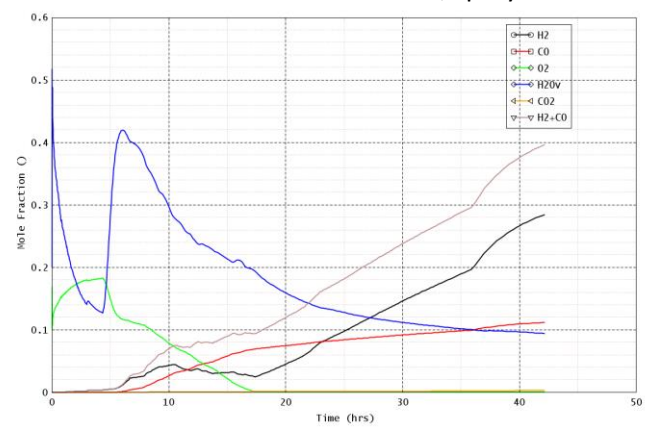


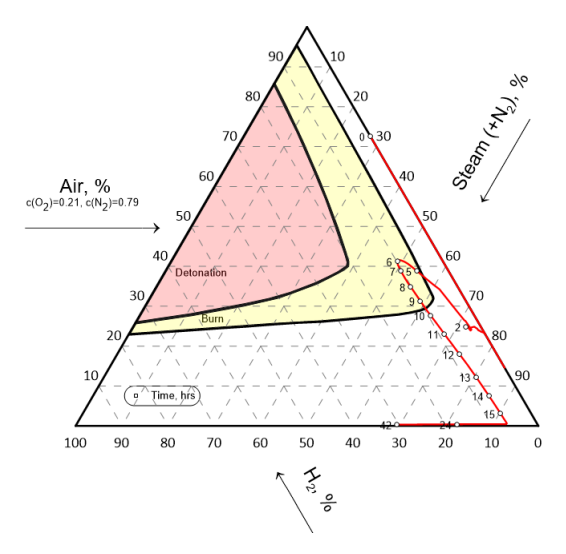
Scenario 7 – LBLOCA + SBO without PARs, sprays activation ex-vessel



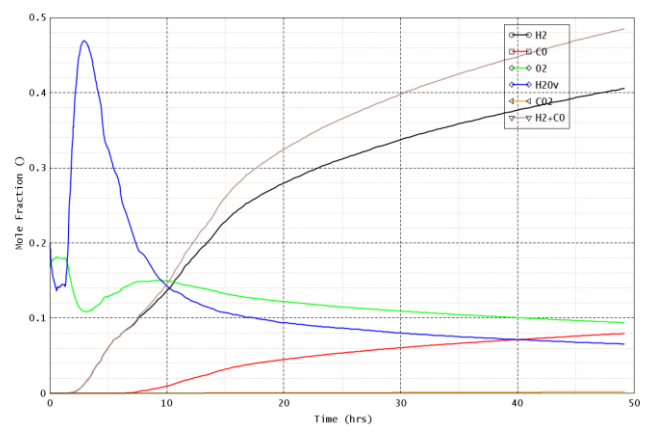


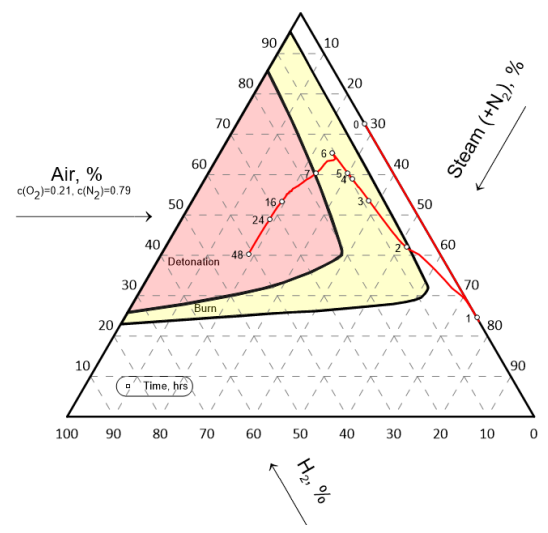
Scenario 8 – LBLOCA + SBO with PARs, sprays activation ex-vessel



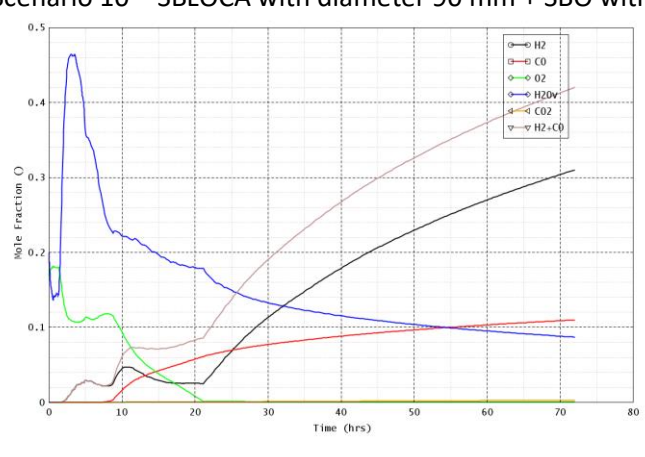


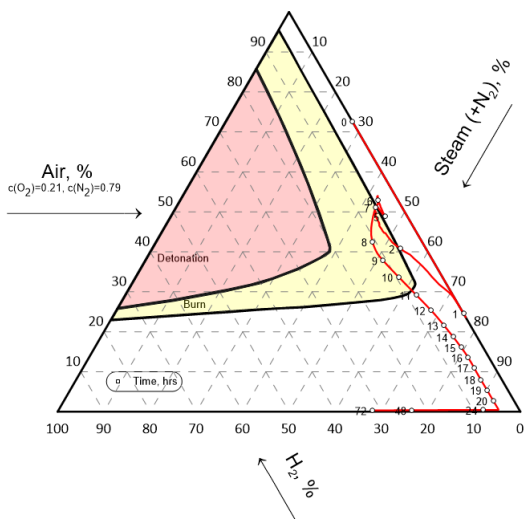
Scenario 9 – SBLOCA with diameter 90 mm + SBO without PARs, sprays activation in-vessel



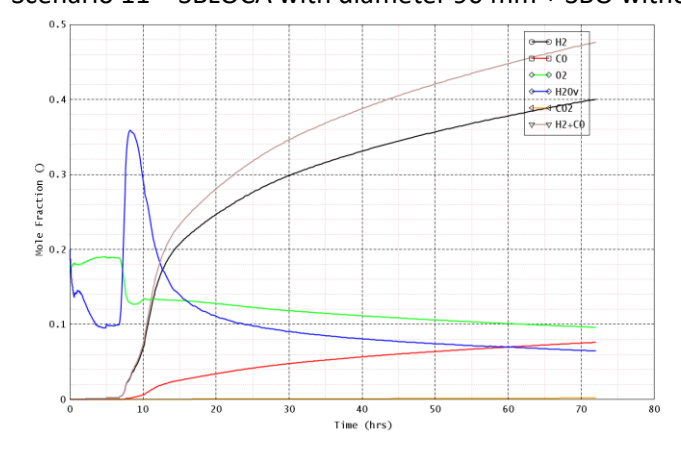


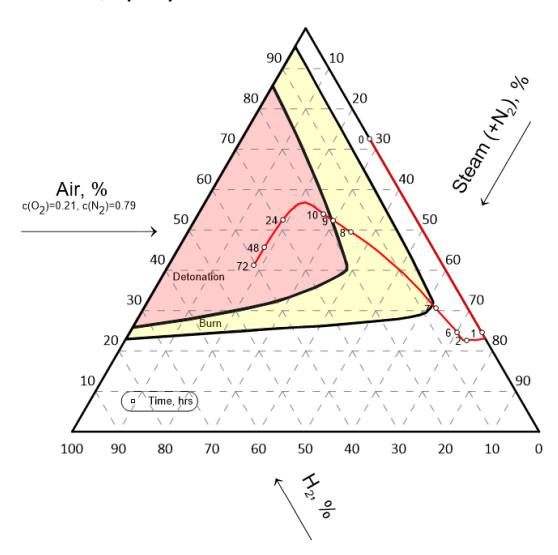
Scenario 10 – SBLOCA with diameter 90 mm + SBO with PARs, sprays activation in-vessel





Scenario 11 – SBLOCA with diameter 90 mm + SBO without PARs, sprays activation ex-vessel





Scenario 12 – SBLOCA with diameter 90 mm + SBO with PARs, sprays activation ex-vessel

